



HAL
open science

Membrane binding properties of RAB GTPases

Guillaume Kulakowski

► **To cite this version:**

Guillaume Kulakowski. Membrane binding properties of RAB GTPases. Biophysics. Université Pierre et Marie Curie - Paris VI, 2017. English. NNT : 2017PA066358 . tel-01816178

HAL Id: tel-01816178

<https://theses.hal.science/tel-01816178>

Submitted on 15 Jun 2018

HAL is a multi-disciplinary open access archive for the deposit and dissemination of scientific research documents, whether they are published or not. The documents may come from teaching and research institutions in France or abroad, or from public or private research centers.

L'archive ouverte pluridisciplinaire **HAL**, est destinée au dépôt et à la diffusion de documents scientifiques de niveau recherche, publiés ou non, émanant des établissements d'enseignement et de recherche français ou étrangers, des laboratoires publics ou privés.

Thèse de Doctorat de l'Université Pierre et Marie Curie

Ecole Doctorale Complexité du Vivant – ED515

Spécialité : Interface biologie-physique

Compartmentation et Dynamique Cellulaire – UMRI44

Laboratoire: Mécanismes Moléculaires du Transport Intracellulaire

Membrane binding properties of RAB GTPases

Présentée par

Guillaume KULAKOWSKI

Dirigée par Dr. Bruno GOUD

Présentée et soutenue publiquement le 13 Décembre 2017

Devant un jury composé de :

Joëlle SOBCZACK-THEPOT

Professeur, UPMC, Paris

Présidente

Jacqueline Cherfils

Directrice de Recherche CNRS, LBPA-ENS, Cachan

Rapporteuse

Aurélien Roux

Assistant Professeur, University of Geneva, Switzerland

Rapporteur

Cathy Jackson

Directrice de Recherche CNRS, Institut Jacques Monod, Paris

Examinatrice

Bruno Antonny

Directeur de Recherche CNRS, IPMC, Sophia Antipolis

Examineur

Bruno Goud

Directeur de Recherche CNRS, Institut Curie, Paris

Directeur de thèse



Thèse de Doctorat de l'Université Pierre et Marie Curie

Ecole Doctorale Complexité du Vivant – ED515

Spécialité : Interface biologie-physique

Compartmentation et Dynamique Cellulaire – UMRI44

Laboratoire: Mécanismes Moléculaires du Transport Intracellulaire

Membrane binding properties of RAB GTPases

Présentée par

Guillaume KULAKOWSKI

Dirigée par Dr. Bruno GOUD

Présentée et soutenue publiquement le 13 Décembre 2017

Devant un jury composé de :

Joëlle SOBCZACK-THEPOT

Professeur, UPMC, Paris

Présidente

Jacqueline Cherfils

Directrice de Recherche CNRS, LBPA-ENS, Cachan

Rapporteuse

Aurélien Roux

Assistant Professeur, University of Geneva, Switzerland

Rapporteur

Cathy Jackson

Directrice de Recherche CNRS, Institut Jacques Monod, Paris

Examinatrice

Bruno Antonny

Directeur de Recherche CNRS, IPMC, Sophia Antipolis

Examinateur

Bruno Goud

Directeur de Recherche CNRS, Institut Curie, Paris

Directeur de thèse

Table of contents

Acknowledgements	1
Abbreviations	5
List of figures	II
From cell discovery to membrane binding properties of RAB GTPases.....	15
1 Biology and physics of membranes	19
1.1 The Lipid bilayer	20
1.1.1 From a lipid molecule to a bilayer.....	20
1.1.2 Different classes of lipids.....	21
1.1.3 Lipid synthesis and distribution in cells	23
1.2 Membrane domain formation	26
1.2.1 Different states of membranes	26
1.2.2 Phase state of cellular membranes.....	28
1.3 Membrane deformations	29
1.3.1 Membrane curvature in cells.....	29
1.3.2 Mechanisms of membrane deformation.....	32
1.3.3 Protein curvature sensing.....	39
1.4 <i>In vitro</i> experimental approaches	43
1.4.1 Model membranes for <i>in vitro</i> experiments	43
1.4.2 Phase separation from living cells to model membranes.....	45
1.4.3 Curvature sensing on model membranes	48

Table of contents

2	RAB GTPases	53
2.1	RAB discovery and evolution.....	54
2.2	RAB sequence and structure.....	55
2.2.1	G-domain	56
2.2.2	RAB specific sequence motifs.....	57
2.2.3	RAB C-terminal region	57
2.3	RAB posttranslational modifications.....	58
2.3.1	RAB activation cycle	58
2.3.2	RAB membrane insertion and extraction	61
2.4	Membrane targeting of RAB GTPases	64
2.5	RAB GTPases and vesicular transport	68
2.5.1	General mechanism of intracellular transport	68
2.5.2	RABs and membrane tethering.....	71
2.6	Focus on the RAB proteins used in this study	75
2.6.1	RAB1 and the ER-Golgi intermediate compartment	75
2.6.2	RAB6 and the Golgi	76
2.6.3	RAB4 / RAB5 / RAB11 and the endosomal system.....	77
2.6.4	RAB35 and the plasma membrane	80
3	Materials and Methods	81
3.1	Protein synthesis and modification.....	81
3.1.1	Protein expression and purification.....	81
3.1.2	<i>In vitro</i> modifications of RAB and GST proteins	84
3.2	Experimental studies with GUVs.....	90
3.2.1	Synthesis of giant unilamellar vesicles.....	90
3.2.2	Generalities of the experimental approach.....	93
3.2.3	Curvature sensing experiments with GUVs.....	98

3.3	Experimental studies with purified Golgi membranes	104
3.3.1	Purification of Rat Liver Golgi stacks.....	104
3.3.2	Experimental chamber.....	104
3.3.3	Pulling tubes with kinesins.....	105
3.3.4	Immunofluorescence on Golgi membranes.....	107
4	Article: RAB proteins bind lipid packing defects	109
5	RAB4 and RAB11 binding requirements	135
5.1	Description of the <i>in vitro</i> approach.....	136
5.2	RAB4 and RAB11 recruitment to GUV membranes.....	137
5.2.1	RAB4 and RAB11 are not recruited to PC-containing membranes.....	137
5.2.2	RAB4 and RAB11 are not recruited to GUVs of various lipid composition.....	138
5.2.3	Membrane curvature has no effect on the recruitment of RAB4 and RAB11.....	140
5.3	RAB4 and RAB11 recruitment to purified Golgi fractions.....	141
5.3.1	RAB4 and RAB11 are positively recruited through their prenyl group	141
5.3.2	RAB4/RAB11 membrane recruitment does not depend on the presence of effector proteins.....	144
5.4	Monoprenylated RAB proteins are mislocalized to the same membrane structures.....	144
5.4.1	Monoprenylated RAB proteins localize to the same membrane structures.....	144
5.4.2	Monoprenylated RAB proteins do not localize to Golgi or recycling endosomal structures.....	146
5.5	Discussion.....	150
6	RAB6-induced membrane tethering	157
6.1	Specificities of RAB6-induced membrane tethering	158
6.1.1	Vesicle tethering is a RAB6-specific effect.....	158
6.1.2	Vesicle tethering is nucleotide and concentration dependent	158

Table of contents

6.1.3	RAB6-induced vesicle tethering is mediated by a RAB-RAB dimerization in <i>trans</i>	161
6.1.4	The RAB-RAB interaction is dynamic	163
6.2	Involvement of the Switch regions.....	165
6.2.1	RAB6A mutant induces vesicle tethering	165
6.2.2	Unprenylated RAB6A does not interact with membrane-bound RAB6A	166
6.2.3	Bivalent α RAB:GTP antibodies promote vesicle tethering	168
6.2.4	Effect of monovalent RAB6 effector proteins	170
6.3	Discussion.....	174
Concluding remarks		179
References		181

Acknowledgements

When I first encountered Bruno Goud, it was to start as an engineer, and eventually start a few months later a PhD. At the same time, I had a very interesting offer for a 2 year-position in a famous pharmaceutical company (my initials might help to figure out which one it is...). It was not an easy decision to make. I made this famous list of pros and cons, discussed with many people, but I was still not able to make up my mind. One conversation that I will never forget is the one that I had with my parents. They made me realize that I had been talking about doing a PhD for months, even years, and that when hesitating between two alternatives, it is often better to go with the first one. I did not have the feeling that my parents were pushing me into doing anything, they would've been happy for me either way. But these words made all the difference and on the 3rd of March 2014 I started in Bruno's lab as an engineer, and a couple months later started my PhD.

First, I would like to thank Bruno Goud for welcoming me in his lab and for his supervision during the last three years and a half. Bruno was always available to answer my questions, to discuss about the project and to share his knowledge. He greatly contributed to the improvement of my scientific skills and made me (I think) a better scientist.

I also greatly acknowledge Lena Oesterlin for her supervision and support. In the past years we had our differences, did not always agree on everything, but I am confident that it made me stronger as a scientist and as a person. In the end, I think we can agree that what we accomplished was very exciting and successful.

I would like to deeply acknowledge the members of my thesis committee Sandrine Etienne-Manneville, Aymelt Itzen and Jean-Claude Guillemot for fruitful discussions and great guidance. Many thanks to my thesis Jury, Joelle Sobczack-Thepot, Jacqueline Cherfils, Cathy Jackson, Bruno Antonny and Aurélien Roux for the time they have spent reading my manuscript and for the very interesting discussion that (I hope) we will have on December 13th.

Doing a PhD is a very rewarding experience not only because you learn a lot as a scientist but also because you get to meet and interact with many people. I would like to thank Jean-Baptiste M., for all the help over the past years. I learned a lot from him concerning membranes, microscopy

Acknowledgements

and many other things. He was always available to answer my many questions, to have a look at the thesis manuscript and to help with the scientific article.

I would also like to thank Stephanie (do not call her “Steph”, she hates it), not only for the critical reading of this manuscript, but also for being who she is. Stephanie and I have had many scientific and less scientific discussions. Surprisingly, Star wars and Game of thrones were recurrent subjects. I hope I will find someone up to the task to debrief the last season (damn need to wait until 2019!).

Great thanks to Sabine, the pillar of the lab (what am I saying, of the whole floor!), the one person that makes everything hold. I do not even know where to start... Thank you for all your advices, your support, for being here in good but also bad moments. You are a great person, full of humanity and respect.

All the other members of the Goud team have had such a good and positive influence on me. Thank you all Kristine, Anahi, Samuel, Surya, Charlotte, Azumi and all the members of the Coudrier team for the nice atmosphere, and great exchanges especially during lab meetings.

I would like to take some time to point out some unexpected encounters with people who were colleagues in the beginning and now so much more. Bruno and Hugo, my buddies, thank you both for all the amazing moments playing shuffleboard and belote; and also for other let's say less serious moments... I think we can agree that shuffleboard is not my thing and that Bruno might need to improve his belote skills (maybe stop drinking while playing?). Hugo on the other hand will tell you that he is the 1992 world champion; still trying to figure out if this is true... Thanks to Hugo for all the protein purifications, none of this work would've been possible without your involvement. Thanks to Bruno and Laure for taking care of Tomy (it's my cat) when I was away, I am sure he will miss you guys!

When arriving to this point, I can bet that some people will complain because I still did not acknowledge them. Girls, you brought me so much during the past years that it would just be impossible to not mention you! Imene, Alex, Melissa, Camilla and Lea, thank you all for your friendship and for supporting me during these last years. I still remember when I arrived at Curie and I would see Melissa and Lea taking a break, I did not know them but still thought “wow they look cool”. It is only a couple months later, at the young scientist retreat in Aachen (thanks ADIC), that we really started talking and that I realized that the two of them would play an important role during my curie experience. I can now say that it has indeed been the case, especially Melissa who has been such a great and important support during good but also bad moments. Camilla was already in the lab when I arrived and it did not take me much time to

realize what a great, selfless and strong person she is, always smiling and joyful. I am pretty sure she will always think about me as long as the “Dyson” brand exists and when going to the Spa... When I arrived in the lab, I was appointed an office which was supposed to be provisional. What I did not know at this time is that I would never leave it. I met Imene (aka “the dragon”), my break companion, with whom the vibe felt right straight from the beginning. You taught me so much and always pushed me to go further so thank you! People came and went through the office, and it will be difficult to acknowledge them all. I will, however, remember the 18th of January 2016, the day when Alexandra arrived and sat on the desk just next to mine. This date marks the beginning of a very intense (maybe a bit unhealthy?) relationship. My grandmother often tells me “qui aime bien châtie bien” and I think this sentence is in this case very appropriate. Alexandra has a very honest and definite opinion about things, and this is a quality that I admire. Thanks Alex for all your advices, your help and for being so patient with me while I was writing this manuscript. Again, thank you girls for all the awesome moments that we shared together, weekends, parties and all the ADIC (association des doctorants, post-doctorants et jeunes chercheurs de l’institut Curie) events. It’s been great!

Many other people greatly contributed to the good and effective working environment. Thanks to all the Tran/Paoletti team and especially those with whom I shared the office. Ana and Lara, thank you for all the laughter, helping me with the abstract shortening, making sure that I drink enough water and for always offering food.

I am also grateful to Aurelie and Edwige for all their help with administrative matters and their kindness. I would also like to thank the laverie, and especially Chedly for his good mood and for making sure the lab functioned properly.

Over my time at Curie, I had the opportunity and the pleasure to meet many people from other departments. I spent a great amount of time in the Bassereau lab mostly preparing vesicles; and this allowed me to exchange a lot with them scientifically but also personally. I would like to thank Patricia Bassereau for welcoming me in her lab, for stimulating discussions and for inviting me to her legendary parties; it made me feel like a true member of the Bassereau team. Big thanks to Julien, Ajay, Thibaut, Nicola, Alex, Kodjo, Stephanie and Alicia for the great atmosphere and laughter. I would especially like to acknowledge Maryam and Feng. I don’t even know how many times I annoyed you with my questions, but you were always inclined to help me and to teach me everything there is to know about tube pulling. As I like to tell them, “physicists rock!!”.

Acknowledgements

It would not have been possible to keep a sane mind throughout this PhD, without the presence of let's say non-scientific friends. I would like to thank my high school friends the "Croustibat" crew, Mike, François, Simon, Romain, Samy, Lucas and Dimitry; and also the girls, Laura, Cha, Alex, Camille and Loulou. I feel so lucky to have such amazing and lasting friends. It is great to see that things don't change and that the distance does not prevent us from regularly seeing each other.

One other thing that hasn't changed in the past years is that I still am a bad loser. I am sure Fanny and Thibaut will agree with this! Thank you both for the great times that we spent together, playing board games, the treasure hunts in Paris and going out. I will definitely miss you once I leave Paris.

Over the years, I realized that work is not all (I think most people will agree with me), and that it is important to get involved in other activities. Thursday night was football night with A Pucchiacca international and it was a bad idea to miss it unless you wanted to suffer Jean-Baptiste's wrath! Thank you guys, even though we have lost many games (probably more losses than victories), we never gave up. Sweat, blood and eternal glory!

My involvement in the ADIC also represented an important part of my life as a PhD student. I would like to acknowledge all the past and current members of the association for the great and sometimes complicated times that we spent trying to make things work!

Great thanks to my family, and especially my parents. They have been so supportive not only throughout this PhD, but during my whole life. Big up to my two brothers Matthieu and François and their respective wives (Flore do not freak out) just because they are the best. Particular thoughts for my goddaughter who is the cutest child ever! I would also like to address special thanks to my godfather and godmother for inviting us over for dinner so many times.

Finally, it is said that behind every (great) man there is a woman, and I am no exception. I am sure that Louise will want to read what I wrote and for this reason I will continue in French. En 2014, lorsqu'il a fallu que je déménage à Paris tu n'as pas hésité à me suivre. Tu travaillais depuis à peine trois mois, nous n'avions jamais habité ensemble et pourtant, sans aucun doute, tu as foncé. Comme j'aime te le dire tu as été mon roc pendant ces dernières années, un soutien crucial dans des moments de stress et de doutes, et d'une grande patience surtout lors de l'écriture de ce manuscrit. Pour tout cela je te remercie.

Abbreviations

AC: Alternating current

ADP: Adenosine 5'-diphosphate

AH: Amphipathic helix

Alexa488 5-SDP ester: Alexa Fluor™ 488 Sulfodichlorophenol ester

ALPS: Amphipathic lipid packing sensor

AnkX: Ankyrin repeat-containing protein X

ARF: ADP-ribosylation factor

ATP: Adenosine-5'-triphosphate

BAR: Bin/Amphiphysin/Rvs

BCCP: Biotin carboxyl carrier protein

BMP: Bis(monoacylglycero)phosphate

BodipyFL-C5-HPC: 2-(4,4-Difluoro-5,7-Dimethyl-4-Bora-3a,4a-Diaza-s-Indacene-3-Pentanoyl)1-Hexadecanoyl-sn-Glycero-3-Phosphocholine

BSM: Brain sphingomyelin

C₀: Spontaneous curvature

CDR: Complementary determining region

Cer: Ceramide

COG: Conserved oligomeric Golgi

COP: Coat protein

CORVET: Class C core vacuole/endosome tethering

C_p: Protein spontaneous curvature

DAG: Diacylglycerol

DENN: Differentially expressed in normal and neoplastic cells

DHPE: 1,2-Dihexadecanoyl-sn-glycero-3-phosphoethanolamine (triethylammonium salt)

DIC: Differential interference contrast

DOG: 1,2-dioleoyl-sn-glycerol

DOPC: 1,2-dioleoyl-sn-glycero-3-phosphocholine

DPPE: 1,2-dipalmitoyl-sn-glycero-3-phosphoethanolamine

Abbreviations

DrrA/SidM: Defects in RAB1 recruitment protein A

DslI: Dependence on SLY1-20 protein 1

DSPE-PEG(2000)-Biotin: 1,2-distearoyl-*sn*-glycero-3-phosphoethanolamine-N-[biotinyl (poly-ethyleneglycol)-2000] (ammonium salt)

EE: Early endosome

EEA1: Early endosome antigen 1

EF: Electroformation

EggPC: L- α -phosphatidylcholine (Egg, Chicken)

EM: Electron microscopy

ENTH: Epsin N-terminal homology

ER: Endoplasmic Reticulum

ERC: Endosomal recycling compartment

FFAT: Two phenylalanines in an acidic tract

Fpp: Farnesylpyrophosphate

FTase: Farnesyl transferase

FYVE: FABI YOTB VAC1 and EEA1

G-actin: Globular actin

GAP: GTPase-activating protein

GARP: Golgi associated retrograde protein

GBFI: Golgi-specific brefeldin A-resistance guanine nucleotide exchange factor 1

GCCI85: 185 kDa Golgi coiled-coil protein

GDF: GDI dissociation factor

GDI: GDP dissociation inhibitor

GDP: Guanosine 5'-diphosphate

GEF: Guanine nucleotide exchange factor

GFP: green fluorescent protein

GGpp: Geranylgeranyl pyrophosphate

GGTaseI: Geranylgeranyl transferase type I

GlcCer: Glucosylceramide

GLUT4: Glucose transporter type 4

GMI: Monosialotetrahexosylganglioside

GMI30: Golgi matrix protein 130
GPMV: Giant plasma membrane vesicle
GppNHp: Guanosine-5'-[(β,γ)-imido]triphosphate
GSL: Glycosphingolipid
GST: Glutathione S-transferase
GTP: Guanosine-5'-triphosphate
GUV: Giant unilamellar vesicle
GYP: GAP for YPT/RAB proteins

His: Histidine
HOPS: Homotypic fusion and protein sorting
HPLC: High-performance liquid chromatography

IPTG: Isopropyl β -D-1-thiogalactopyranoside
ITO: Indium tin oxide

Ld: Liquid-disordered
Lo: Liquid-ordered
LPA: Lysophosphatidic acid
LUV: Large unilamellar vesicle

MBP: Maltose-binding protein
MCS: Membrane contact site
MLV: Multilamellar vesicle
MVB: Multivesicular body

NBD: Nitrobenzoxadiazole
Ni-NTA: Nickel-nitrilotriacetic acid

OCRL: Oculo-cerebro-renal syndrome of Lowe
OSBP: Oxysterol-binding protein

PA: Phosphatidic acid
PC: Phosphatidylcholine

Abbreviations

PDMS: Polydimethylsiloxane

PE: Phosphatidylethanolamine

PEG: Polyethylene glycol

PFA: Paraformaldehyde

PH: Pleckstrin homology

PI(3)P: Phosphatidylinositol 3-phosphate

PI(3,4)P₂: Phosphatidylinositol 3,4-biphosphate

PI(3,4,5)P₃: Phosphatidylinositol 3,4,5-triphosphate

PI(4)P: Phosphatidylinositol 4-phosphate

PI(4,5)P₂: Phosphatidylinositol 4,5-biphosphate

PI: Phosphatidylinositol

PLA: Phospholipase A

PLC: Phospholipase C

PLD: Phospholipase D

PLIF: Protein-lipid interaction by fluorescence

PMSF: Phenylmethylsulfonyl fluoride

PMT: Photomultiplier tube

POPE: 1-palmitoyl-2-oleoyl-sn-glycero-3-phosphoethanolamine

PRA: Prenylated RAB acceptor protein

PS: Phosphatidylserine

PTEN: Phosphatase and tensin homolog

PUFA PE: 1-stearoyl-2-docosaheptaenoyl-sn-glycero-3-phosphoethanolamine

PUFA: Polyunsaturated fatty acid

RAB: RAS-related in brain

RABF: RAB family region

RABGGTase: RAB geranylgeranyl transferase

RABSF: RAB subfamily region

RAC: RAS-related C3 botulinum toxin substrate

RAN: RAS-related nuclear protein

RAS: Rat Sarcoma

REP: RAB escort protein

RHO: RAS homology

RILP: RAB-interacting lysosomal protein

RND3: RHO family GTPase 3

SAR: Secretion-associated RAS-related protein

scFv: Single-chain variable fragment

SDS-PAGE: Sodium dodecyl sulfate polyacrylamide gel electrophoresis

SLB: Supported planar lipid bilayer

SLiC: Single liposome curvature assay

SM: Sphingomyelin

SNARE: Soluble N-ethylmaleimide-sensitive factor attachment protein receptor

So: Solid-ordered

SUV: Small unilamellar vesicle

TBC: Tre2/Bub2/Cdc16

TEV: Tobacco etch virus

TGF: Transforming growth factor

TGN: *Trans*-Golgi network

TIP47: 47-kDa tail-interacting protein

T_m: Melting temperature

TRAPP: Transport protein particle

t-SNARE: Target-SNARE

VAP-A: Vesicle-associated membrane protein-associated protein A

VPS: Vacuolar protein sorting

v-SNARE: Vesicle-SNARE

WGA: Wheat germ agglutinin

WT: Wild-type

YIP: YPT-interacting protein

YPT: Yeast proximal tubulin

List of figures

Figure 1.1: Lipids can self-assemble into different structures depending on their molecular shapes.....	21
Figure 1.2: Membrane lipids.....	22
Figure 1.3: Lipid synthesis and distribution in cells.....	24
Figure 1.4: Mechanism of lipid domain formation.....	27
Figure 1.5: Membrane shapes and related curvatures.....	30
Figure 1.6: Membrane curvature in cells.....	31
Figure 1.7: Mechanisms of membrane deformation.....	33
Figure 1.8: Deformation induced by changes in lipid composition.....	34
Figure 1.9: Mechanisms of membrane deformation by the cytoskeleton.....	36
Figure 1.10: Mechanisms of curvature sensing.....	41
Figure 1.11: Schematic of the different available methods to produce model membranes.....	44
Figure 1.12: Phase separation in model membranes.....	47
Figure 1.13: <i>In vitro</i> experimental setups for the study of curvature sensing.....	49
Figure 1.14: Description of the gradient force.....	51
Figure 2.1: Alignment of all YPTs (in red) and their human RAB homologues (in black).....	55
Figure 2.2: Structural representation of the different members of the RAB family.....	56
Figure 2.3: Schematic representation of RAB protein motifs.....	57
Figure 2.4: RAB prenylation and activation cycle.....	59
Figure 2.5: Mechanisms of protein prenylation.....	62
Figure 2.6: Subcellular localization of RAB proteins.....	65
Figure 2.7: RAB proteins are involved in all steps of vesicular transport.....	69
Figure 2.8: Mechanisms of vesicle recognition and tethering.....	72
Figure 2.9: RAB proteins can directly drive vesicle tethering <i>in vitro</i>	74
Figure 2.10: RAB6 regulates multiple trafficking pathways to and from the Golgi.....	77
Figure 2.11: Mechanism of cargo endocytosis mediated by specific RAB domains.....	78
Figure 3.1: RAB5A purification on affinity column using the ÄKTA purifier system.....	83
Figure 3.2: Measurement of nucleotide exchange efficiency by HPLC ion-paired reverse phase chromatography using the ÄKTA system.....	87

List of figures

Figure 3.3: Mechanisms of RAB prenylation	88
Figure 3.4: RAB1 and RAB4 prenylation tests.....	89
Figure 3.5: Schematic of GUV electroformation chambers	92
Figure 3.6: Schematic of the microscope experimental setup	94
Figure 3.7: Measurements of fluorescence intensities	95
Figure 3.8: Green fluorescence calibration.....	97
Figure 3.9: Hand-made PDMS chamber in metal insert.....	98
Figure 3.10: Experimental chamber for tube pulling experiments.....	99
Figure 3.11: Tube pulling experimental setup.....	100
Figure 3.12: Determination of the proportionality constant between tube radius and fluorescence	103
Figure 3.13: Experimental chamber for Golgi membranes studies	104
Figure 3.14: Tubulation of Golgi membranes mediated by kinesin motors	105
Figure 5.1: Monoprenylated RAB4A and RAB11A are not recruited to PC-containing vesicles.....	138
Figure 5.2: Monoprenylated RAB4A and RAB11A are not recruited to GUV membranes of various lipid composition.....	139
Figure 5.3: Monoprenylated RAB4A and RAB11A are not recruited to curved membranes.....	141
Figure 5.4: Electron microscopy analyses of the purified Golgi fractions	142
Figure 5.5: Monoprenylated and active RAB6A, RAB4A and RAB11A are recruited to purified Golgi fractions through their prenyl group.....	143
Figure 5.6: Monoprenylated and inactive RAB4A and RAB11A are recruited to purified Golgi fractions through their prenyl group.....	145
Figure 5.7: Monoprenylated RAB4A, RAB11A and RAB6A localize to the same membrane structures	147
Figure 5.8: Monoprenylated RAB4A, RAB11A and RAB6A do not localize to Golgi or recycling endosomal structures	149
Figure 5.9: Study of RAB4A/RAB11A curvature sensing using purified Golgi fractions and kinesin motors	151
Figure 5.10: Description of the PLIF (protein-lipid interaction by fluorescence) assay adapted to my study.....	153
Figure 6.1: Vesicle tethering is a RAB6-specific effect	159
Figure 6.2: Vesicle tethering is nucleotide and concentration dependent	160

Figure 6.3: Vesicle tethering is induced by a RAB6-RAB6 dimerization in <i>trans</i>	162
Figure 6.4: Structure of the YPT1:GDI complex	163
Figure 6.5: The RAB6-RAB6 interaction is dynamic.....	164
Figure 6.6: RAB6 dimer crystal structure	165
Figure 6.7: Vesicle tether in presence of RAB6A-Y35R-D49R.....	166
Figure 6.8: Unprenylated RAB6A does not compete with membrane-bound RAB6A.....	167
Figure 6.9: Bivalent α RAB:GTP antibodies promote vesicle tethering	169
Figure 6.10: α RAB6:GTP (scFv) can access the interaction sites but does not inhibit vesicle tethering.....	171
Figure 6.11: Inhibition of vesicle tethering by LidA ₂₀₁₋₅₈₃	172
Figure 6.12: Effect of OCRL ₅₃₈₋₉₀₁ on vesicle tethering	173

From cell discovery to membrane binding properties of RAB GTPases

The cell is known as the smallest functional unit of all living organisms. It was first discovered in 1665 by Robert Hooke who called it “cell” from the Latin word *cellula*, meaning a small room. It was only in the middle of the 19th century that the “cell theory” was developed by Theodor Schwann, Jakob Schleiden and Rudolf Virchow, stating that all organisms are composed of at least one cell and that cells originate from preexisting ones. In the late 19th century, the discovery of the Golgi apparatus and the endosomes by Camillo Golgi in 1898 and Ilya Metchnikoff in 1887, respectively, led to the finding that cells are divided into sub-cellular compartments. Other intracellular compartments such as lysosomes, mitochondria and the endoplasmic reticulum (ER) were discovered by Christian de Duve, George Palade and Albert Claude in the middle of the 20th century with the emergence and development of new techniques such as ultra-centrifugation and electron microscopy. The isolation of these different compartments demonstrated that they have different lipid and protein compositions, therefore suggesting that they also have different functions. A new view of intracellular architecture had emerged: eukaryotic cells are constituted of multiple intracellular compartments called organelles. These different organelles are delimited by membranes and each of them has a specific and unique composition and function, thereby allowing the compartmentalization of specific reactions and an increased complexity as compared to prokaryotic cells.

Even though cells are well compartmentalized, the different intracellular organelles are not isolated structures fulfilling independent functions. They are, on the contrary, constantly communicating between each other through exchange of intracellular components such as proteins and lipids. The first pathway to be described was the secretory pathway: Proteins are synthesized in the ER, enter the Golgi on its *cis* side and are finally released from the Golgi in secretory vesicles or granules that are then released out of the cell (Duve, 1975; Palade, 1975). Up to date, many other trafficking routes have been identified. Endocytosis was first discovered by Ilya Metchnikoff in 1883 (at the time known as the “phagocytosis theory”), but was only described in more detail decades later as the process by which molecules can get internalized into the cell (see (Schmid *et al.*, 2014) for extensive review). Other retrograde pathways from the plasma membrane to the Golgi and to the ER have been described as well (Johannes and Popoff, 2008).

From cell discovery to membrane binding properties of RAB GTPases

Intracellular trafficking was proposed, based on electron microscopy studies (Palade, 1975; Roth and Porter, 1964) to occur by encapsulation of secretory proteins into small vesicles and their transport from a donor compartment (fission process) to an acceptor compartment (fusion process).

Among others, James Rothman, Randy Sheckman and Thomas Südhof, who were awarded the 2013 Nobel Prize in Physiology or Medicine, spent decades trying to unravel the molecular mechanisms of intracellular transport. Their studies led to a deep understanding of vesicular transport with the identification of coat proteins involved in vesicle budding and specific selection of cargos and the discovery of SNARE proteins that allow vesicle fusion with the acceptor compartment and the following release of the cargos (Bonifacino, 2014).

Intracellular trafficking consists in the sequential action of multiple sets of proteins to allow the exchange of molecules from one compartment to another. Small GTPases such as RAB proteins are key components of this process. The first *RAB* gene *YPT1* (in *Saccharomyces cerevisiae*) was discovered in 1983 by Gallwitz and coworkers (Gallwitz *et al.*, 1983), and many other *RAB* genes were identified in the following decade with the completion of the yeast and human genomes-sequencing projects. The RAB family of proteins is now composed of over 60 members. RAB proteins were rapidly described to localize to the cytosolic face of most intracellular organelles (compartmental membranes but also transport vesicles) and to be implicated in the secretory and endocytic vesicular transport pathways (Martinez and Goud, 1998). RABs were shown to be physically attached to intracellular compartments through the insertion of their prenyl group, a lipid moiety at their C-terminus consisting of one or two geranylgeranyl groups (Casey and Seabra, 1996).

RAB proteins have been shown to localize to specific compartments, thereby defining organelle identity (Zerial and McBride, 2001; Zhen and Stenmark, 2015); and this is thought to be crucial for the control and directionality of vesicular trafficking. The mechanisms regulating specific RAB membrane targeting and localization are thus of great interest to understand intracellular transport events. The question of RAB protein targeting to specific membranes was first addressed 25 years ago and many teams have tried to answer this question. Originally, the C-terminal hypervariable region of RAB proteins was suggested to contain specific targeting information (Chavrier *et al.*, 1991). Other studies later revised this statement by suggesting that multiple sequence motifs of RAB proteins, including this hypervariable region, can contribute to their specific membrane targeting (Ali *et al.*, 2004; Beranger *et al.*, 1994). These motifs were

mostly described to mediate RAB specific membrane localization via their interaction with RAB interacting proteins such as RAB GEFs (Blumer *et al.*, 2013) or effector proteins (Aivazian *et al.*, 2006; Wu *et al.*, 2005).

Most studies so far have focused on the role of RAB interacting proteins in the mechanisms allowing the targeting of RAB proteins to specific membranes; but the role of the physicochemical properties of the membranes themselves has remained largely unexplored. It is however now well established that intracellular membranes are fluid environments that display different compositions and structures. These divergent properties can be exemplified by the formation of nanodomains of lipids or by membrane curvature, important features for the recruitment of some peripheral membrane proteins. Membrane charge, which is specific of endocytic compartments and the plasma membrane, is also a key feature regulating the specific recruitment of C-terminally positively charged proteins (Heo *et al.*, 2006).

I thus focused my study on the physicochemical membrane properties regulating the recruitment of RAB proteins. This issue being difficult to assess inside the cell, I have used an *in vitro* approach consisting of purified and prenylated RAB proteins and giant unilamellar vesicles (GUVs) as model membranes.

I started my study with RAB1 and RAB6 which associate with pre-Golgi and Golgi/trans Golgi network membranes respectively, RAB5 which is present on early endosomes and RAB35 which localizes to recycling endosomes and to the plasma membrane (Chapter 4).

RAB4 and RAB11 were shown to localize to tubular structures on endosomes (Sonnichsen *et al.*, 2000) suggesting that curvature might play an important role in their specific localization. Their specific membrane recruitment however proved to be more complex and this will be addressed in Chapter 5.

Finally, previous studies in the lab had led to the unexpected observation that RAB6 incorporation into GUVs can induce membrane tethering. I also got to investigate this process during my PhD and detailed information about the possible mechanism behind this effect will be found in Chapter 6.

1 Biology and physics of membranes

1.1	The Lipid bilayer	20
1.1.1	From a lipid molecule to a bilayer.....	20
1.1.2	Different classes of lipids.....	21
1.1.3	Lipid synthesis and distribution in cells	23
1.2	Membrane domain formation	26
1.2.1	Different states of membranes	26
1.2.2	Phase state of cellular membranes.....	28
1.3	Membrane deformations	29
1.3.1	Membrane curvature in cells.....	29
1.3.2	Mechanisms of membrane deformation.....	32
1.3.3	Protein curvature sensing.....	39
1.4	<i>In vitro</i> experimental approaches	43
1.4.1	Model membranes for <i>in vitro</i> experiments	43
1.4.2	Phase separation from living cells to model membranes.....	45
1.4.3	Curvature sensing on model membranes	48

The first part of this chapter will focus on presenting membranes, how they are formed and how the very heterogeneous compositions of cellular membranes can lead to differences in their physicochemical properties. Because membranes are complex systems composed of many different molecules (proteins, lipids), their study in cells remains very challenging. Thus, in the second part of this chapter I will present multiple *in vitro* experimental model membranes that can be used to mimic in a more simplistic way the different properties of membranes.

1.1 The Lipid bilayer

Eukaryotic cells are divided into compartments. These compartments, as well as cells themselves, are delimited by membranes. In the middle of the 20th century, the membrane was described as a two dimensional fluid structure (the lipid bilayer) which led to the fluid mosaic model (Singer and Nicolson, 1972). In this model, the membrane is a fluid matrix of lipids in which peripheral and integral proteins diffuse. Since then, this model has been refined and it appears that lipids are not immobile structures holding proteins together. Membranes are crowded and heterogeneous environments with lipids and proteins diffusing laterally allowing the formation of regions which vary in thickness and composition (Engelman, 2005).

1.1.1 From a lipid molecule to a bilayer

The basic components of membranes are lipids. Lipid molecules are amphiphilic and are thus composed of a hydrophilic part, the head, and a hydrophobic part, the tail. The hydrophilic head of the lipid defines the lipid type and can be neutral or charged. The hydrophobic tail is most often made of two aliphatic chains (can vary from 1 to 4 chains) of various length and degree of unsaturation. Due to their amphiphilic structure, lipids have the property to self-assemble in such a way that the heads are accessible to the solvent, whereas the tails (more hydrophobic) are buried in the core of the membrane. This spontaneous rearrangement of the lipids is of entropic origin and the result of a competition between the hydrophobic attraction (also called hydrophobic effect), which tends to aggregate the molecules together therefore reducing the interfacial area; and the repulsion of the hydrophilic head groups which tends to increase the interfacial area (Israelachvili, 1992).

This competition between hydrophobic attraction and headgroup repulsion results in a constant area per lipid. Depending on this parameter as well as on the geometrical shapes of lipids, lipid assemblies will exhibit different morphologies (**Figure 1.1**). Most common lipid assemblies in water are micelles (also called hexagonal phase) (**Figure 1.1A**) and bilayers (lamellar phase) (**Figure 1.1B**), which are respectively mainly composed of inverted cone-shaped and cylinder-shaped lipids. Micelles are globular structures where the lipid head groups form a spherical shell protecting the lipid tails (**Figure 1.1A**). Bilayers are composed of two monolayers in which the lipids are parallel to each other and the tails of each monolayer are facing each other in the core of the membrane (**Figure 1.1B**). On average bilayers have a thickness of around 5 nm with an area

per lipid of around 0.7 nm^2 (this will of course depend on the type of lipid). Lipids with a conical shape have the possibility to self-assemble into an inverted micelle structure (also called inverted hexagonal phase) (**Figure 1.1C**).

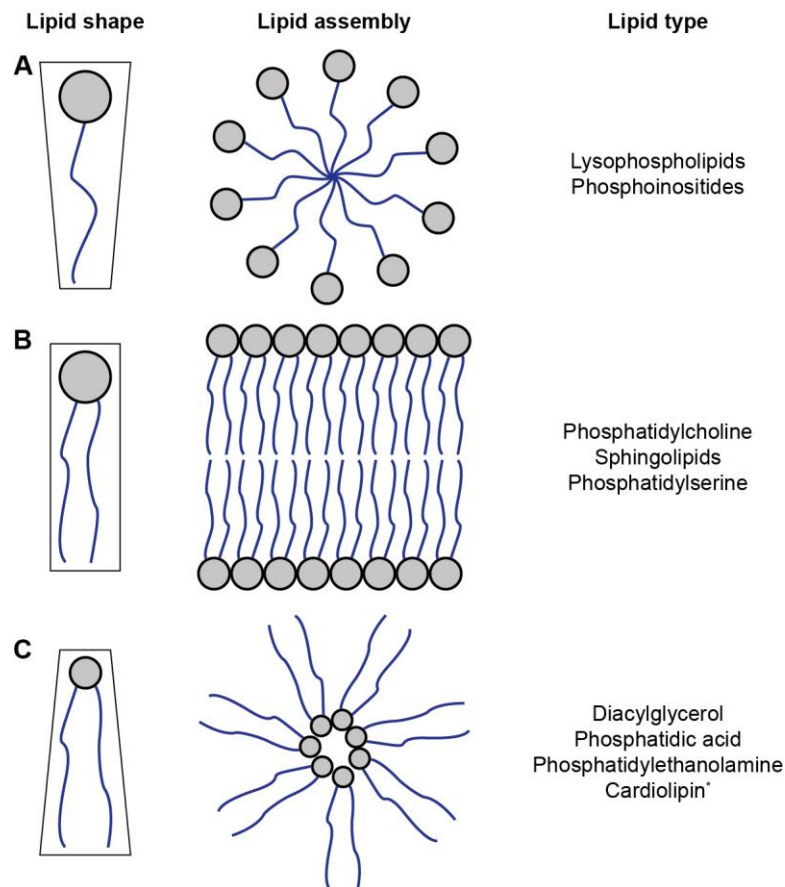


Figure 1.1: Lipids can self-assemble into different structures depending on their molecular shapes. (A) Inverted-conical lipids will tend to self-assemble into micelles, (B) cylinder-shaped lipids into bilayers and (C) cone-shaped lipids into inverted micelles. *Cardiolipins (or Diphosphatidylglycerol) contain 4 acyl chains and consequently display a high conical shape.

It is important to mention that the shape (also called packing parameter) of a particular lipid is not fixed. External parameters such as hydration, temperature and pH can modulate the headgroup effective area as well as the apparent chain volume (Pomorski *et al.*, 2014).

1.1.2 Different classes of lipids

The most abundant membrane lipids in eukaryotic cells are phospholipids. They are usually composed of two fatty acids (their hydrophobic tails) which are linked to the headgroup, made of a phosphate group and another group such as choline. The two major classes of phospholipids are glycerophospholipids and sphingolipids (**Figure 1.2**).

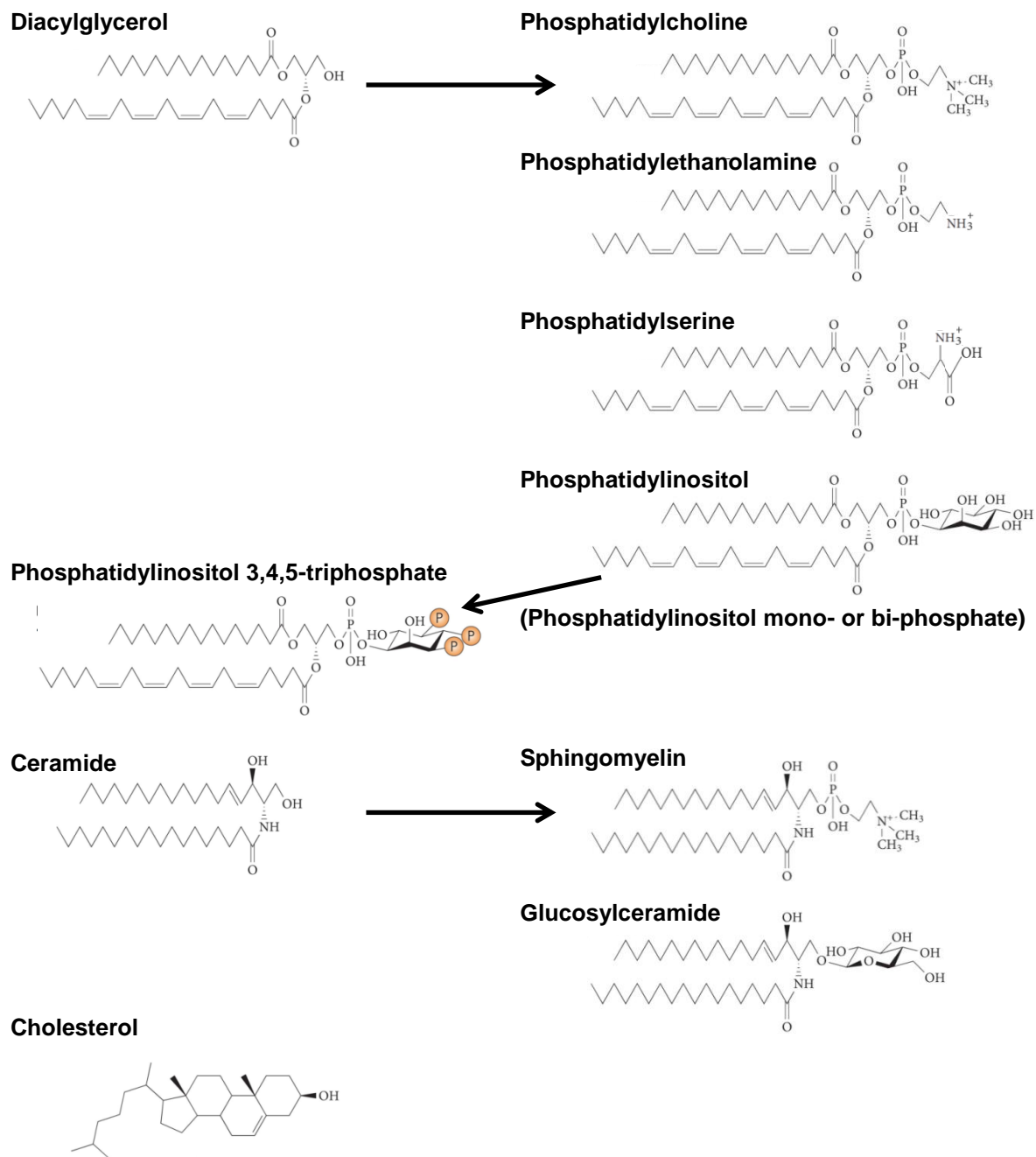


Figure 1.2: Membrane lipids. Phospholipids comprise two subclasses of lipids: glycerophospholipids containing a diacylglycerol backbone and sphingolipids which contain a ceramide backbone. These subclasses are further divided into lipid species that display different headgroups. Here we show the four types of glycerophospholipids (Phosphatidylcholine, Phosphatidylethanolamine, Phosphatidylserine, Phosphatidylinositol), and one type of sphingolipid (Sphingomyelin) used in the study. Glucosylceramide contains a ceramide backbone and is the key precursor for most Glycosphingolipids. Cholesterol is the major sterol found in eukaryotic cells. Of note glycerophospholipids are mostly composed of unsaturated acyl chains whereas sphingolipids mostly exhibit saturated tails. Adapted from (van Meer et al., 2008).

Polar lipids from the glycerophospholipid family are the main eukaryotic membrane lipids. They are based on a diacylglycerol backbone supplemented by a phosphate group (cone-shaped phosphatidic acid, PA) (**Figure 1.2**). Phosphatidylcholine (PC), the major species of this family is formed by the addition of a choline on top of the PA. PC lipids are zwitterionic (contain both a positive and a negative charge at physiological conditions) and usually have a rather cylindrical shape. Other groups can be added instead of the choline to form a phosphatidylethanolamine (PE), a species with a conical shape due to the small size of its headgroup. Phosphatidylserine (PS) is a negatively charged and cylinder-shaped phospholipid mainly concentrated in the inner (cytosolic) leaflet of the plasma membrane. Phosphatidylinositol lipids (PI) are present in smaller amounts and bear a negative charge. PI lipids are known to be phosphorylated by several different kinases and their derivatives are known to be involved in a multitude of signaling processes, mainly at the plasma membrane and at the endocytic compartments (Di Paolo and De Camilli, 2006; van Meer *et al.*, 2008).

Sphingolipids have a ceramide (Cer) backbone (sphingosine base amid-linked to a fatty acid) (**Figure 1.2**). Sphingomyelin (SM) is the most abundant species of this family of lipids, and is composed of a phosphate-choline headgroup. Another important class of ceramide based lipids is the Glycosphingolipids (GSLs), consisting of a ceramide molecule attached to monosaccharides or polysaccharides. SM and GSL are found on the non-cytosolic (extracellular or luminal) leaflet of the plasma membrane (van Meer *et al.*, 2008).

Sterols constitute another major class of lipids present in cellular membranes. The presence of the OH group on the lipid headgroup suggests that they are slightly polar and their specific structure suggests that they are non-bilayer forming molecules (even though they are able to insert in membranes). Cholesterol (**Figure 1.2**) is the major sterol present in mammalian cells and its level increases from the ER to the plasma membrane (Ikonen, 2008; Mesmin and Maxfield, 2009).

1.1.3 Lipid synthesis and distribution in cells

Lipids are not homogeneously distributed across cellular membranes (**Figure 1.3**). Additionally, the two leaflets of the Golgi, endosomal and plasma membranes all exhibit asymmetric lipid compositions (Devaux, 1991; Verkleij *et al.*, 1973; Wood *et al.*, 2011).

Chapter 1: Biology and physics of membranes

The **endoplasmic reticulum** (ER) is the main lipid and protein biosynthetic organelle (Bell *et al.*, 1981). The presence of ribosome complexes, which gives its rough aspect to the ER, is responsible for protein synthesis. This compartment is mostly composed of Glycerophospholipids (PC and PE). The ER produces the bulk of structural phospholipids and cholesterol. Ceramide, the precursor of complex sphingolipids is also produced at the ER. Even though sterols and complex sphingolipid precursors are synthesized in the ER, these products are rapidly leaving this compartment and are transported to other organelles via vesicular transport but also via a non-vesicular route involving membrane contact sites (Jackson *et al.*, 2016) (also discussed in chapter 2).

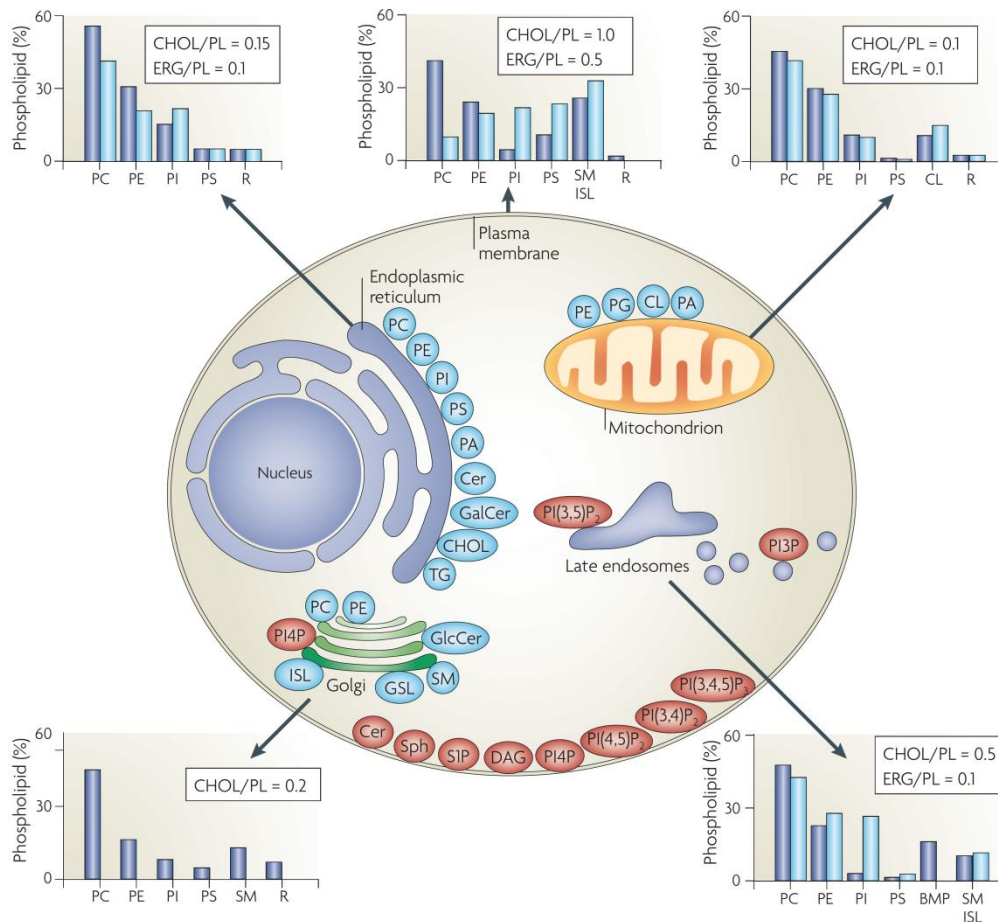


Figure 1.3: Lipid synthesis and distribution in cells. Lipid composition is shown as graphs and expressed as the percentage of total phospholipid content (blue for mammals and light blue for yeast). The figure shows the sites of synthesis of the major phospholipids (in blue) and that of signaling lipids involved in membrane recognition (in red). From (van Meer *et al.*, 2008).

The **Golgi apparatus** is a lipid-based sorting station. It is composed of several compartments called cisternae. The cisterna on the ER side is called the *cis*-Golgi and the cisterna on the plasma membrane side is called the *trans*-Golgi. The main processes that take place at the Golgi

apparatus are the post-translational modifications of newly synthesized proteins coming from the ER (known as protein maturation). The Golgi is the place where significant level of lipid synthesis occurs. This compartment is specialized in the synthesis of complex sphingolipids (SM, GSLs) (Futerman and Riezman, 2005). PC and PE synthesis can also take place at the Golgi apparatus. Cholesterol levels are higher as compared to the ER membrane. The PI derivative PI(4)P, which acts as a signaling lipid, is enriched at the *trans*-Golgi network.

The **plasma membrane** has very different lipid content as compared to the other intracellular membranes (**Figure 1.3**). It is enriched in sphingolipids and sterols which are packed at higher density than glycerophospholipids and can resist mechanical stress. The plasma membrane bilayer is highly asymmetric as the outer leaflet mainly contains SM and PC while the inner leaflet contains mostly PE, PS but also the PI derivative PI(4,5)P₂ (van Meer *et al.*, 2008). The inner leaflet is thus highly negatively charged.

The plasma membrane is not involved in the autonomous synthesis of structural lipids but numerous PI lipid derivatives (PI(3,4)P₂, PI(4,5)P₂, PI(3,4,5)P₃, PI(4)P), involved in signaling cascades, were shown to be synthesized or degraded there (Di Paolo and De Camilli, 2006). SM synthesis was also shown to take place at the plasma membrane (Tafesse *et al.*, 2007).

While the composition of early endosomes is very similar to that of the plasma membrane, late endosomes have a quite different composition as the amounts of sterols and PS decrease whereas the levels of bis(monoacylglycero)phosphate (BMP) increase (Kobayashi *et al.*, 2002). BMP is a cone-shaped and negatively charged lipid which was shown to act in multivesicular body generation (endosome containing internal vesicles that originate from inward budding), fusion processes and sphingolipid hydrolysis (Gallala and Sandhoff, 2011; Matsuo *et al.*, 2004). The endocytic compartments recruit specific sets of kinases and phosphatases that allow the regulation of phosphoinositide content (Di Paolo and De Camilli, 2006). Thus, early endosomes are composed of PI(3)P, whereas PI(3,5)P₂ is mainly found on late endosomes.

As a general important comment, the PI lipid derivatives previously mentioned act as signaling lipids which allow membrane identification and subsequently the recruitment of cytosolic proteins involved in vesicular transport (Di Paolo and De Camilli, 2006).

1.2 Membrane domain formation

1.2.1 Different states of membranes

As previously mentioned, cellular membranes are composed of mixtures of many different lipid species which display various geometrical shapes. This lipid structure is dependent on their physical properties (size of the headgroup, degree of unsaturation, aliphatic chain length) but also on external parameters such as temperature or hydration (Pomorski *et al.*, 2014). As any physical system, lipid bilayers can exist in different phases depending on the overall structures of their lipid content.

The membrane is fluid at high temperature and in different liquid-crystal phases at lower temperatures (Los and Murata, 2004). The two most extreme phases are the gel or solid ordered phase (So) and the liquid disordered phase (Ld) (**Figure 1.4**). In the So phase, the lipid acyl chains can undergo trans-isomerization which leads to their extension and more Van der Waals interactions. Stronger interactions lead to more ordered lipid packing which prevents any lateral lipid diffusion (Seu *et al.*, 2006). The Ld phase is usually characterized by the presence of unsaturated lipids (one or more double bonds in the acyl chain) and their irregular packing. Unsaturation of the acyl chains leads to kinks in their structure which reduces the surface area accessible to other lipids and thus weakens Van der Waals interactions. Consequently, the Ld phase is a highly fluid state in which individual lipids can freely diffuse (Seu *et al.*, 2006).

Under physiological conditions, intracellular bilayers tend to exist in a fluid phase and can undergo phase transition under correct environmental conditions. The temperature at which a membrane lipid can undergo phase transition from the gel to the liquid state is the melting temperature (T_m). The T_m can vary between lipids due to their different structural properties (acyl chain length and degree of unsaturation) (Cevc, 1991). Lipids that exhibit longer acyl chains will have higher surface areas as compared to lipids exhibiting smaller chain length, resulting in stronger Van der Waals interactions between aliphatic chains and thus increased T_m . As previously mentioned, increasing unsaturation leads to weaker Van der Waals interactions and thus to lower T_m of the lipid. As the T_m strongly depends on the amount of unsaturation and on the length of the acyl chains, one can thus make the distinction between high T_m lipids that will be in a solid state at physiological conditions, and low T_m lipids that will be in a liquid state under the same conditions.

As an example, sphingolipids usually carry saturated or trans-unsaturated (linear) aliphatic chains whereas the acyl chains of glycerophospholipids are often unsaturated. Membranes composed of sphingolipids therefore adopt a more tightly packed structure (solid-like phase) as compared to glycerophospholipids containing membranes that form less ordered domains (L_d phase).

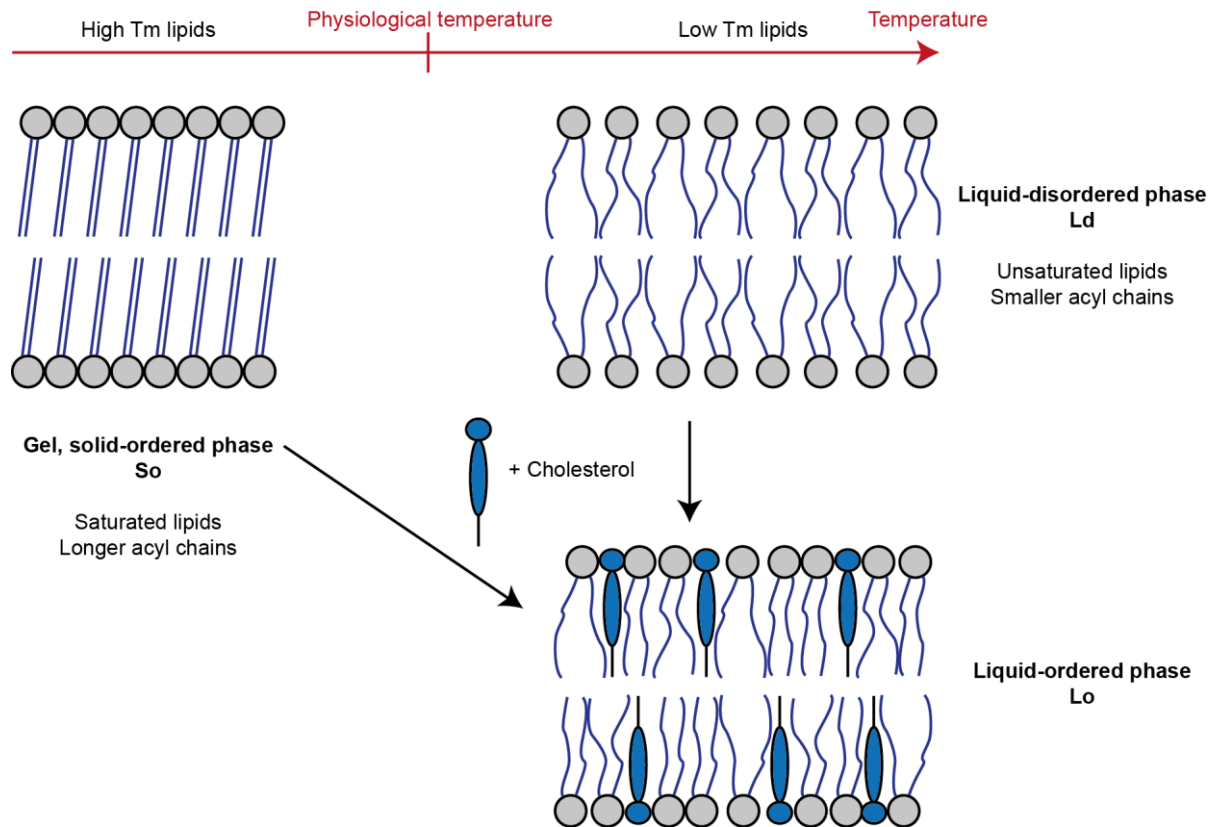


Figure 1.4: Mechanism of lipid domain formation. Membranes can exist as a fluid state or as a solid state at high and low temperature, respectively. The temperature at which a lipid can transition from one phase to another is the melting temperature (T_m). The T_m is dependent of the specific structure of the lipid (acyl chain length, degree of unsaturation). At physiological conditions, high T_m lipids (long saturated acyl chains) will localize to the solid phase whereas low T_m lipids (short unsaturated acyl chains) will transition to the liquid-disordered state (L_d). Cholesterol can induce the formation of an intermediate liquid-ordered phase (L_o).

Cholesterol is another key component of eukaryotic cellular membranes and was shown to drastically affect the physical properties of membranes, through lateral order disruption of the gel phase and ordering of the L_d phase (Henriksen *et al.*, 2006; Ipsen *et al.*, 1987). The presence of cholesterol in membranes can lead to the appearance of an intermediate state between gel phase and L_d , the liquid ordered (L_o) phase (**Figure 1.4**). This L_o phase is characterized by a tight lipid packing, as in the gel solid-ordered phase, but also by a rapid lateral diffusion rate, as in L_d

membranes (London, 2002; M'Baye *et al.*, 2008). Lo membranes are usually thicker, stiffer and less permeable than Ld membranes (Rawicz *et al.*, 2008). The lateral diffusion coefficient is 2-3 fold less in the Lo phase as compared to the Ld phase (Veatch and Keller, 2005).

1.2.2 Phase state of cellular membranes

Cellular membranes display inhomogeneous lipid distribution at different levels (van Meer *et al.*, 2008). The lateral heterogeneity in cellular membranes can be described by the lipid raft hypothesis (Simons and Ikonen, 1997) which has been a matter of great debate in the last 20 years. In biomembranes, lipid rafts, which are characterized by a tight packing of saturated lipids and cholesterol, likely exist in a Lo state and behave like islands floating in a sea of loosely-packed Ld domains of unsaturated glycerophospholipids (M'Baye *et al.*, 2008). Lipid rafts have received a huge attention as they are believed to be involved in many cellular processes such as signal transduction, lipid trafficking and regulation of membrane protein activity (Jacobson *et al.*, 2007; Lingwood and Simons, 2010; Owen *et al.*, 2012).

Another less described heterogeneity is related to the differential composition and organization of the plasma membrane as compared to intracellular membranes. Cholesterol and sphingolipid levels were found to be increased from the ER to the plasma membrane and this seems to be due to the directed anterograde transport and the absence of retrograde transport of these lipids (Brugger *et al.*, 2000; Klemm *et al.*, 2009). As previously mentioned, even though raft components are synthesized in the ER and the Golgi complex, they are quickly leaving these compartments and are transported towards the plasma membrane. As an example, sphingomyelin is mainly found at the plasma membrane even though ceramide, the hydrophobic backbone of sphingolipids, is synthesized in the ER and the assembly of the sphingolipids headgroups to ceramide takes place at the Golgi complex (van Meer and Lisman, 2002).

Thus, lipid raft components are moved toward the plasma membrane where they concentrate but also spread into the endocytic recycling pathways (Mukherjee and Maxfield, 2000). This seems to be consistent with studies showing that more than 60% of all cellular cholesterol is located to the plasma membrane whereas intracellular membranes such as the ER or the Golgi membranes exhibit low levels of cholesterol (Ikonen, 2008; Mesmin and Maxfield, 2009).

As cholesterol is known to promote phase separation (Ohvo-Rekila *et al.*, 2002; Silvius *et al.*, 1996), this process is thought to mainly occur at the cholesterol-rich plasma membrane. Multiple

studies, in particular the ones using fluorescent probes such as Laurdan (Bagatolli, 2006; Owen *et al.*, 2012) and its derivatives (Kim *et al.*, 2008; Sezgin *et al.*, 2014) have focused on lipid raft organization in model and cell membranes. These probes have the ability to change fluorescence color and intensity in response to changes in membrane hydration and solvent relaxation (Demchenko *et al.*, 2009), two parameters linked to lipid order.

Niko and coworkers recently developed a new probe based on pyrene which demonstrates enhanced photophysical properties over Laurdan (Niko *et al.*, 2016). Their study confirms clear differences in lipid order among the different cellular membranes with the plasma membrane mainly composed of Lo domains while intracellular membranes are much closer to Ld phases. This is consistent with the higher amount of sphingomyelin and cholesterol, both responsible for the formation of lipid rafts, at the plasma membrane.

1.3 Membrane deformations

Biological membranes are two-dimensional surfaces with two principal curvatures $C_1 = 1/R_1$ and $C_2 = 1/R_2$ (with R_1 and R_2 referred to as the principal radii of curvature) along two perpendicular directions (Zimmerberg and Kozlov, 2006) (**Figure 1.5**). The total curvature of the membrane is $C = C_1 + C_2$. In the case of a spherical vesicle of radius R , the membrane deforms equally in both directions leading to $C_1 = C_2 = 1/R$ and a total curvature $C_v = 2/R$. In the case of a cylindrical tube of radius R , which is curved only in one direction and flat in the other, $C_1 > 0$ and $C_2 = 0$ yielding a total curvature $C_t = 1/R$. When proteins interact with the membrane, it is said that a protein can sense positive curvature if it senses the convex side of the membrane whereas the curvature is negative if it senses its concave side.

Lipid bilayers have an average thickness in the order of 4-5 nm (Marquardt *et al.*, 2016). Logically enough, this value also corresponds to the lower limit of radii to which a bilayer can be bent. Thus, in the perspective of a protein, if a membrane has a curvature radius in the same range (10-50 nm) it will be considered as highly curved whereas if the radius is superior to 50 nm it will be considered as weakly curved.

1.3.1 Membrane curvature in cells

Due to their heterogeneous lipid and protein compositions, intracellular compartments exhibit membrane regions with both high and low curvature (**Figure 1.6**). For example, the ER and the

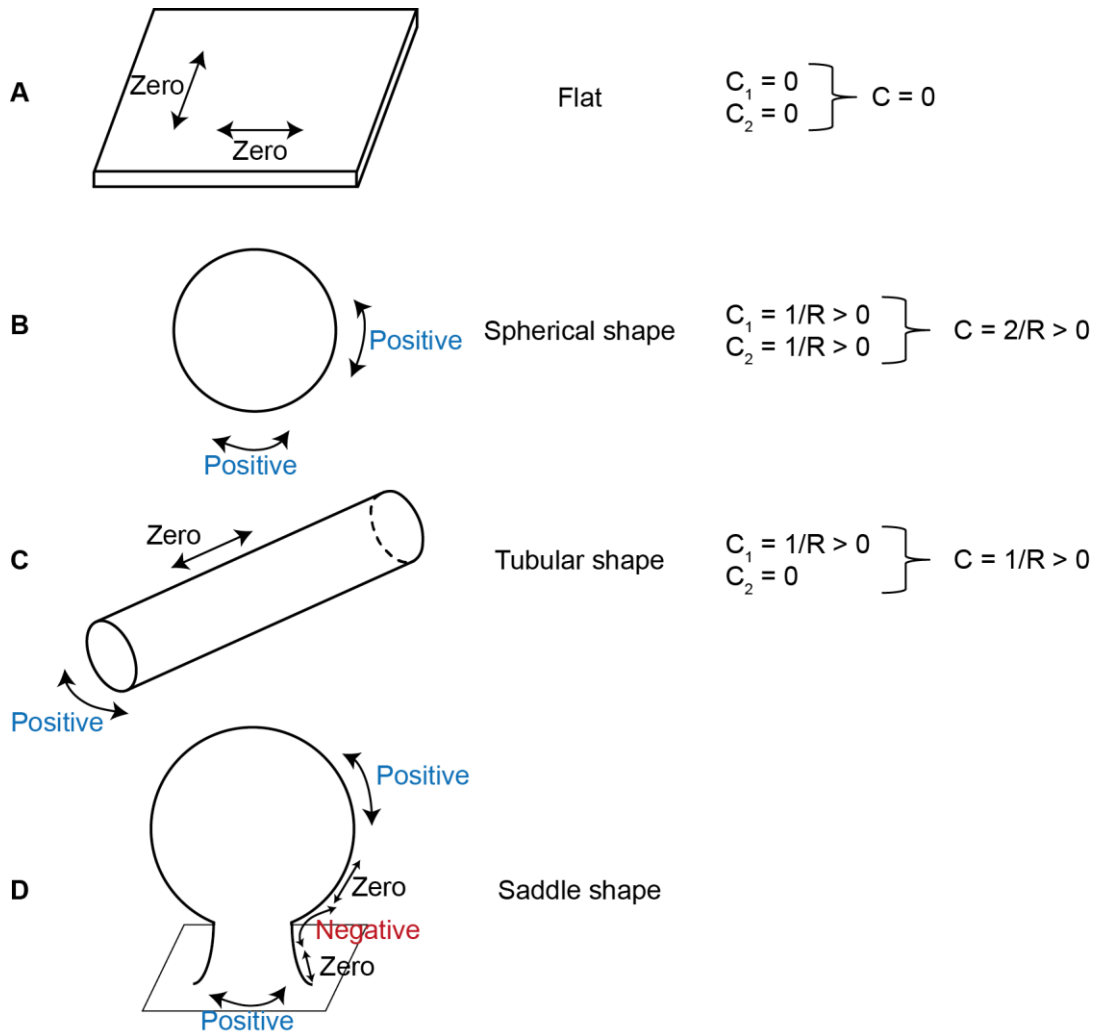


Figure 1.5: Membrane shapes and related curvatures. Cellular membranes can be found harboring different shapes. (A) A flat or plane shape, such as basic compartmental membranes, which displays no curvature ($C_1 = C_2 = 0$). (B) A spherical shape, like intracellular vesicles, which is similarly positively curved in two directions ($C_1 = C_2 > 0$). (C) A tubular shape, such as tubules emanating from the Golgi, which is only deformed in one direction ($C_1 > 0$, $C_2 = 0$). (D) A saddle shape, which can be observed during vesicle budding processes, which displays two positive curvatures on the spherical vesicle part but also a negative curvature at the neck of the membrane bud. Adapted from (Zimmerberg and Kozlov, 2006).

Golgi form complex networks of interconnected flat sheets and highly curved tubules (30-60 nm diameter) (Shibata *et al.*, 2009; Voeltz and Prinz, 2007). Mitochondria also display many curved invaginations (30 nm in diameter), called cristae, which are directed towards the mitochondrial matrix and thus greatly increase the total surface area necessary for chemical reactions (Voeltz and Prinz, 2007). Endosomes were also shown to exhibit tubular regions of high curvature and globular regions of low curvature (Sonnichsen *et al.*, 2000).

These tubular structures are often highly dynamic. They can undergo continuous fission and fusion events and get continuously rearranged by moving along the actin or microtubule cytoskeleton.

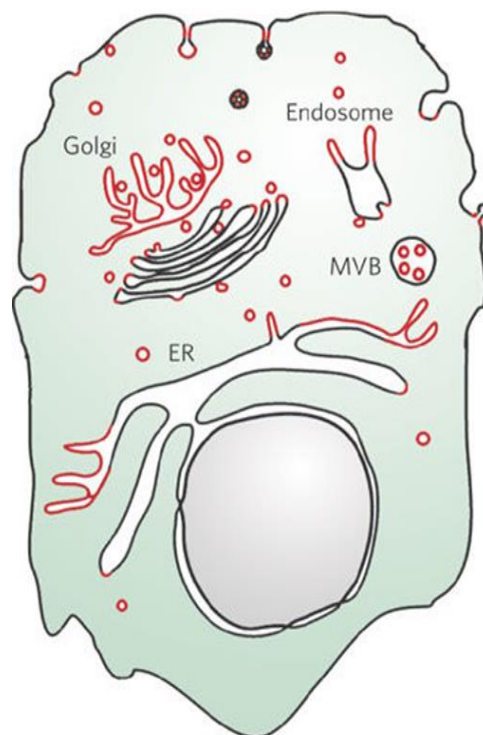


Figure 1.6: Membrane curvature in cells. Almost all cellular membranes display regions of high curvature. Regions of high positive curvature are highlighted in red. From (McMahon and Gallop, 2005).

Particular membrane budding can also take place during the formation of multivesicular bodies (MVBs) (Hurley *et al.*, 2010) (**Figure 1.6**). MVBs are late endosomes containing internal vesicles that sort membrane proteins destined for degradation into these vesicles. These internal vesicles are formed by invagination of the endosomal membrane followed by scission of the buds. In contrast to clathrin and COP-coated vesicles formation which consists in budding towards the cytosol (implying positive curvature for cytosolic proteins), the generation of MVBs consists in the membrane budding away from the cytosol which thus has an opposite negative curvature. Enveloped viruses release is also occurring away from the cytosol which also implies negative

curvature. ESCRT (endosomal sorting complexes required for transport) proteins were described to be deeply involved in both MVB formation and virus budding processes (Babst, 2011; Votteler and Sundquist, 2013).

Intracellular trafficking also involves curved membranes (**Figure 1.6**) as it consists in the transport of highly curved transport vesicles of 40-80 nm in diameter but also in membrane deformation events allowing fission of these vesicles from the donor compartment and their subsequent fusion with the acceptor compartment (Takamori, 2006, Bonifacino, 2004). This vesicle transport process will be further discussed in Chapter 2.

1.3.2 Mechanisms of membrane deformation

Membrane deformation can be achieved through the alteration of membrane properties in an asymmetric manner or by applying unilateral constraints to it. In other words, membrane curvature can be dynamically regulated not only by changes in lipid composition but also through the action of external factors such as the cytoskeleton or proteins that can directly get inserted in membranes and act as wedges or that can form scaffolds around the membrane (McMahon and Gallop, 2005). **Figure 1.7** gives an overview of biologically relevant ways to deform membranes and each of them will be further discussed in the next sections.

1.3.2.1 Lipid dependent membrane deformations

As a general mechanism, bilayers that have symmetrical lipid content between the two leaflets and similar interacting environments should remain flat. However, if some degree of asymmetry is introduced into the system (a difference in composition between the leaflets), the bilayer acquires a spontaneous curvature.

As previously mentioned, depending on their geometrical properties, lipids will self-assemble into different structures. Even if they cannot form bilayers on their own, non-cylinder shaped lipids (conical or inverted-conical) can still be incorporated in these structures. In this case they will induce a spontaneous curvature of the monolayer they are embedded in (**Figure 1.8**). However, if these lipids are homogeneously distributed between the two monolayers (symmetrical bilayer) the spontaneous curvature of both leaflets will cancel each other (Zimmerberg and Kozlov, 2006). In order for spontaneous curvature to actually happen, the enrichment of a specific lipid in one of the monolayers is required.

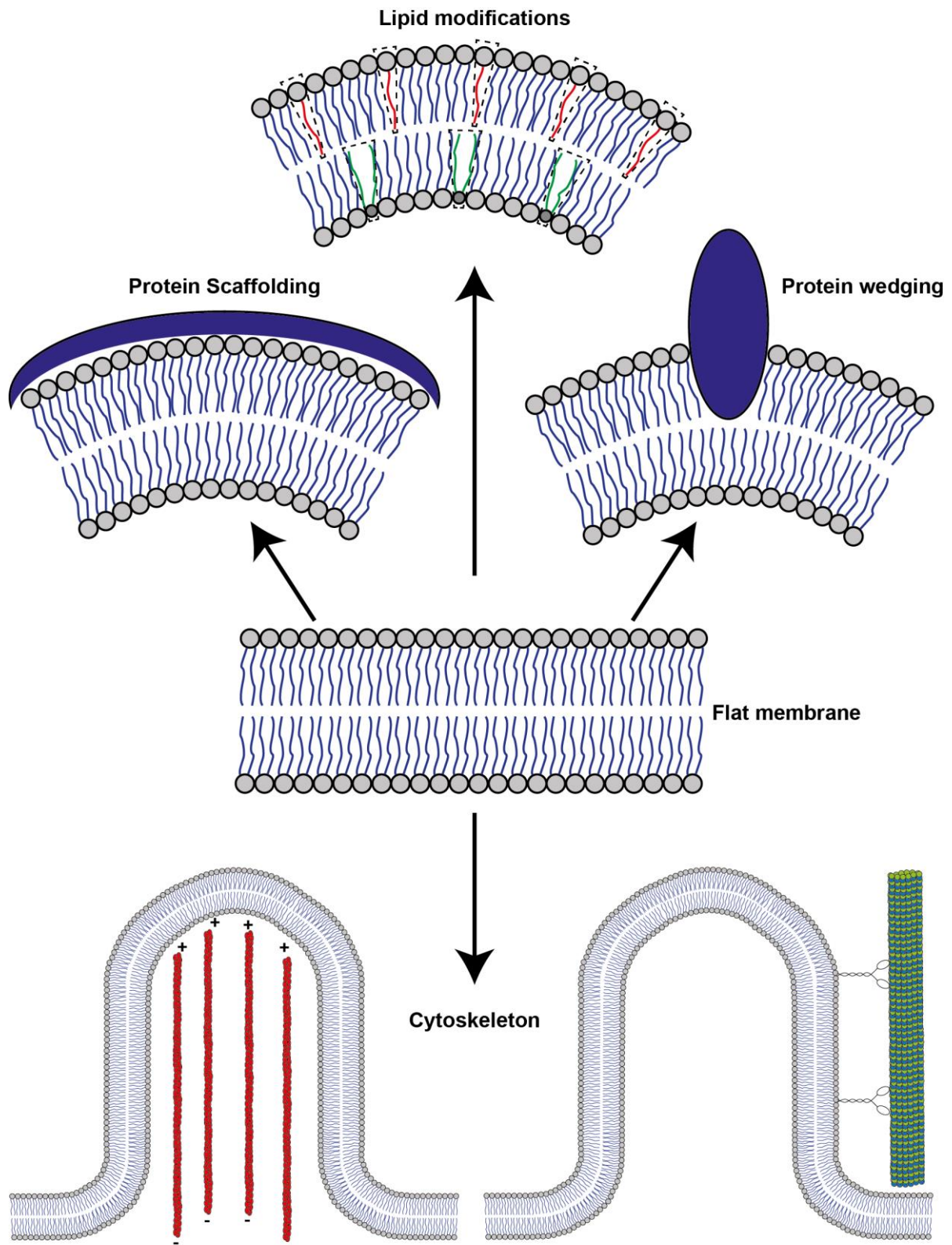


Figure 1.7: Mechanisms of membrane deformation. Membranes can be deformed by internal (changes in lipid composition) but also external constraints (protein scaffolding, insertion of hydrophobic domains in one monolayer, cytoskeleton polymerization and movement of motor proteins on cytoskeletal tracks). Adapted from (McMahon and Gallop, 2005).

Membrane asymmetry can be caused by a directional transfer of lipids between the two membrane leaflets (also called transbilayer flip-flop) or by lipid modifying enzymes that can modify the chemical properties of lipids.

Lipid transfer between two monolayers can be spontaneous in the case of cholesterol or lipids exhibiting either a small or a non-polar headgroup such as DAG and PA (Sprong *et al.*, 2001); and can also be assisted by proteins such as flippases (Devaux *et al.*, 2008).

Phospholipid flippases, such as Type IV-type ATPases (P4-ATPase), control the translocation of phospholipid molecules across the membrane (Muthusamy *et al.*, 2009). More specifically, they have been shown to establish and maintain plasma membrane asymmetry by transferring PS and PE from the external leaflet to the cytosolic leaflet of the bilayer and to be involved in sterol trafficking and metabolism, and in vesicle-mediated protein transport (Muthusamy *et al.*, 2009).

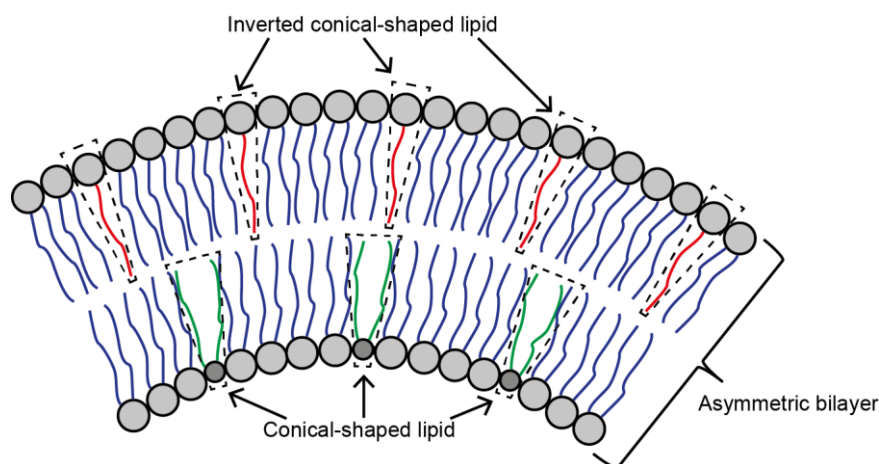


Figure 1.8: Deformation induced by changes in lipid composition. Asymmetric bilayers can undergo some deformations. Inverted cone-shaped lipids such as lysophospholipids (in red) tend to induce positive curvature whereas cone-shaped lipids (in green) induce negative curvature.

Lipid modifying enzymes also have the ability to asymmetrically change the lipid composition of one monolayer and induce membrane curvature. Phospholipase A (PLA) hydrolyses the acyl chain of a phospholipid to produce lysophospholipid (**Figure 1.8**: red lipids) known to build positively curved membranes. PLA₂ for example has been shown to be involved in the formation of tubules from the Golgi and endosomes (Brown *et al.*, 2003). Sphingomyelinases release the phosphocholine headgroup of sphingomyelin (known to have no spontaneous curvature) and produce the ceramide lipid known to build negative curvature. This process was suggested to be used by cells to mediate exosome formation (Trajkovic *et al.*, 2008). In contrast, phospholipase D (PLD) modifies the polar headgroup to yield cone-shaped PA, while phospholipase C (PLC)

produces cone-shaped DAG (**Figure 1.8**: green lipids). These phospholipases were also shown to induce membrane deformations (Holopainen *et al.*, 2002; Inaba *et al.*, 2016).

However even though spontaneous curvature is known to exist in cells, it is not believed to play a major role in the generation of membrane curvature (Kozlov *et al.*, 2014; Shibata *et al.*, 2009). Flippases for example are more effective if they localize to a small membrane area. If they act only on a small portion of a larger surface, such as the plasma membrane, their effect will be equilibrated on the entire surface and the resulting influence on membrane curvature would be negligible.

Membrane deformation was also observed in artificial membranes exhibiting distinct lipid domains (such as Lo and Ld). The boundary separating these domains has an energy cost, due to line tension, that the system would like to minimize. This is achieved with the Ostwald ripening (Lifshitz and Slyozov, 1961), a process by which the size and shape of membrane domains is adjusted to minimize the energy associated to the surface tension. Over time, lipids diffuse and domains coalesce so that the number of domains constantly decreases whereas the average domain size constantly increases, ultimately resulting in a more energetically favorable complete phase separation (fully separated vesicle with two domains). The shape of such a vesicle is no longer spherical but is the result of a competition the bending energy and the line tension of the boundary separating the two domains. This effect was shown to lead to domain budding (Baumgart *et al.*, 2003) and even to membrane fission (Roux *et al.*, 2005).

1.3.2.2 Deformation induced by external objects

In the previous section, I focused on models where the membrane shape is determined by its lipid composition. However, other types of deformations exist in a biological context and consist in the interaction of membranes with external objects. For example, the generation of membrane carriers requires close and independent collaboration between the membrane itself and the cytoskeleton (filament polymerization), motor proteins and membrane shaping proteins (coat proteins for example) (Anitei and Hoflack, 2011).

Cytoskeleton

The cytoskeleton is composed of networks of polymers and filaments involved in various biological processes. The actin and microtubule filaments, which are the best characterized, can

generate pushing forces on cellular membranes (**Figure 1.9A**). It is well described that cell membranes can exhibit very thin extensions called filopodia or extended flat lamellipodia which are formed by different modes of actin polymerization and play a major role in cell migration. The formation of these structures requires multiple proteins such as proteins nucleating and elongating the filaments, protecting them from capping, and bundling them together (Mattila and Lappalainen, 2008). It has been shown *in vitro* that actin filament and microtubule polymerization forces are able to tubulate membranes (Limozin *et al.*, 2003; Nomura *et al.*, 2002), and actin polymerization has been suggested to be involved in the generation of tubular transport intermediates in the secretory and endocytic pathways (Anitei and Hoflack, 2011).

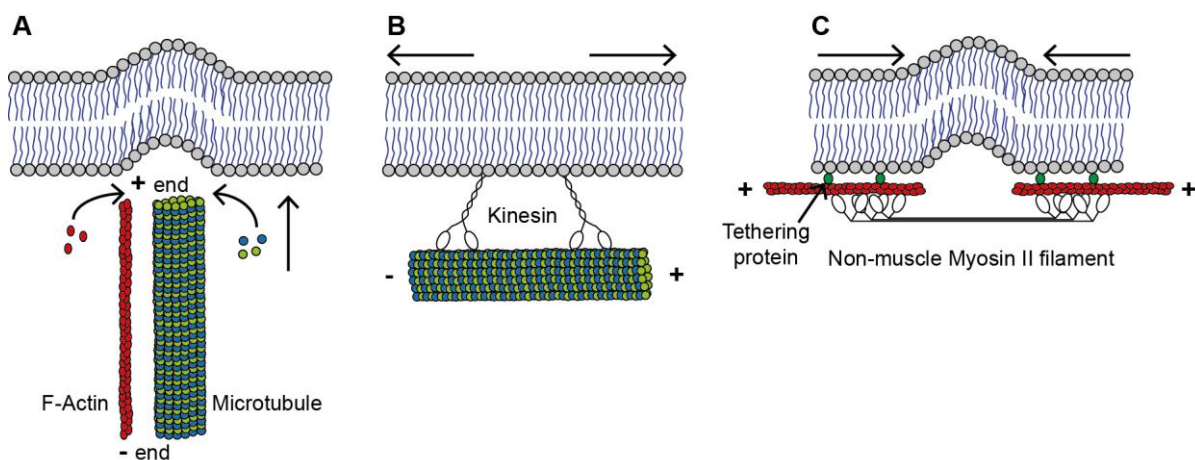


Figure 1.9: Mechanisms of membrane deformation by the cytoskeleton. (A) Membranes can be pushed by the addition of new G-actin or α - β -tubulin subunits at the + end of actin filaments and microtubules, respectively. (B) Membranes can be pulled via the movement of motor proteins on cytoskeletal tracks. Kinesin and Dynein motors move on microtubules (mostly towards the + and - end, respectively); and Myosins move on actin filaments (mostly towards the barbed (or +) end). (C) Motor proteins such as non-muscle Myosin II can induce the constriction of membranes attached to actin filaments. Adapted from (Gurel *et al.*, 2014).

Motor proteins that have the ability to “walk” on these filaments (myosins on actin filaments; and kinesins and dyneins on microtubules) can also play a role in the biogenesis of intracellular carriers at the ER or at the Golgi (Gurel *et al.*, 2014). Membrane-bound motor proteins have the possibility to induce membrane deformations by moving along the cytoskeleton tracks (**Figure 1.9B** and **Figure 1.9C**).

In vitro studies have also shown that microtubule-associated kinesins (Koster *et al.*, 2003; Leduc *et al.*, 2004; Roux *et al.*, 2002) and actin-associated Myosin II (Carvalho *et al.*, 2013) have the ability to deform liposomes by applying a pulling force on them.

Hydrophobic insertion or wedging

Certain peripheral or transmembrane proteins also have the ability to mold biological membranes through the insertion of hydrophobic or amphipathic domains. These protein insertions can be separated in two classes: shallow insertions, which are only incorporated in the external part of a monolayer and integral insertions that occupy the whole membrane space. Shallow insertions have been demonstrated to be much more powerful generators of membrane curvature (Campelo *et al.*, 2008). These proteins can generate membrane asymmetry through the hydrophobic insertion of hydrophobic or amphipathic domains (helix) into one monolayer. This process known as “wedging” was mostly described as the incorporation of a helix to about 30-40% of the monolayer thickness (Campelo *et al.*, 2008). The region of the lipid headgroups is expanded while the region of the acyl chains remains undisturbed. This leads to a strong membrane asymmetry and thus to the generation of positive membrane curvature.

To this class belong the amphipathic helices (AH) of the N-BAR domains of various proteins (Frost *et al.*, 2009; Gallop *et al.*, 2006), of epsin N-terminal homology (ENTH) domains (Ford *et al.*, 2002) and of small G-proteins such as ARF1 and SARI (Lee *et al.*, 2005; Lundmark *et al.*, 2008).

N-BAR domain proteins such as amphiphysin or endophilin possess an AH at their N-terminal extremity and have been shown to be involved in membrane tubulation (Gallop *et al.*, 2006; Masuda *et al.*, 2006).

The ENTH domain of Epsin folds into an AH upon binding to PI(4,5)P₂ and was shown to tubulate synthetic vesicles (Ford *et al.*, 2002). It is also known to play a role in clathrin-dependent endocytosis (Boucrot *et al.*, 2012; Itoh and De Camilli, 2006).

The small GTPases ARF1 and SARI are recruited to the cytosolic leaflet of membranes through the exposure of an AH. This process, induced by GTP binding, consists in the displacement of the N-terminal domain from the core of the protein and the subsequent availability of the AH for membrane binding. AHs of SARI and ARF1 were suggested to be important for vesicle budding, through the respective induction of COPII (Lee *et al.*, 2005) and COPI-coated vesicle curvature (Beck *et al.*, 2008).

Interestingly, a study from Stachowiak and coworkers demonstrates that membrane bending and tubulation can still occur when the AH of the ENTH domain of Epsin is removed and that moderate protein coverage is able to induce membrane bending independently of the wedge mechanism (Stachowiak *et al.*, 2012). Membrane curvature was thus suggested to be induced by

hydrophilic proteins through a crowding mechanism. This process consists in the thermally induced lateral diffusion of proteins which collide with each other. The generated steric effect leads to a lateral pressure on the membrane which can be released through the formation of tubules.

Scaffolding

The binding of hydrophilic protein domains to the surface of one monolayer can also lead to membrane asymmetry and subsequently to membrane curvature.

The scaffolding mechanism consists in the transfer of curvature from the intrinsically curved interaction site of the protein to the underlying membrane. This curved interface can be pre-existing in one protein monomer or be the result of protein oligomerization. Protein scaffolds can impose their curvature on membranes only if they can overcome the rigidity of the bilayer. Coat proteins such as COPI, COPII and clathrin are well documented protein coats that polymerize around nascent vesicles into a cage-like shell and induce membrane curvature (Faini *et al.*, 2013). COPII and COPI coats are respectively implicated in the anterograde pathway (export from the ER) and in the intra-Golgi and retrograde (Golgi to ER) pathways. Clathrin-mediated membrane deformations were shown to be involved in endocytosis (McMahon and Boucrot, 2011) but also in trafficking events at the TGN (Antonny, 2006).

Reticulons and Caveolins are membrane-embedded proteins that were described to generate curvature through the formation of wedge-shaped insertions and oligomeric scaffolds (Shibata *et al.*, 2008; Walser *et al.*, 2012). Reticulons and Caveolins were respectively shown to be involved in the formation of tubules at the ER (Voeltz *et al.*, 2006) and the creation of plasma membrane invaginations (Walser *et al.*, 2012). ESCRT proteins were also described to drive membrane deformation during MVB generation by polymerizing at the neck of budding vesicles (McCullough *et al.*, 2015; Wollert and Hurley, 2010). Dynamin (Ferguson and De Camilli, 2012) and BAR domain proteins (Masuda and Mochizuki, 2010) also have the ability to deform membranes into tubules by acting as cylindrical oligomeric scaffolds.

Finally, shallow hydrophobic insertion and intrinsically curved protein scaffolds appear as the most effective generators of membrane curvature. However, even though these two mechanisms are different in their way to generate curvature, it is thought that they can still be complementary to each other. Indeed, as certain proteins, such as N-BAR, Reticulons or Caveolins, are involved in both scaffolding mechanism and hydrophobic insertion, membrane curvature generation could

very well be the result of a combination of these two effects. Studies show that mutation of the SAR1 AH compromises COPII vesicle budding even though COPII was still able to deform liposomes (Lee *et al.*, 2005). This suggests that the COPII mediated scaffolding mechanism is not sufficient to drive vesicle budding. Similar studies about ARF and its involvement in COPI-coated vesicle budding (Beck *et al.*, 2008; Krauss *et al.*, 2008) show that inhibition of ARF1 dimerization prevents vesicle budding without disrupting COPI membrane interaction. Therefore, the intracellular generation of membrane curvature is probably the result of a concerted action of several protein-based mechanisms.

1.3.3 Protein curvature sensing

Membrane curvature is not only a consequence of the mechanical or enzymatic actions of some proteins; it can also serve as spatial information for the recruitment and docking of proteins. Curvature sensing is thought to be important for vesicular trafficking processes (Antonny, 2011; Liu *et al.*, 2010).

The regulation of protein membrane binding by curvature was first suggested for ARFGAP1 which is involved in the uncoating of COPI vesicles (Bigay *et al.*, 2003). Vesicle budding from the Golgi membrane is mediated by the assembly of COPI coat proteins that are attached to the membrane via the activated (GTP-bound) adaptor protein ARF1. Subsequent disassembly of the coat requires ARF1 inactivation by ARFGAP1. Bigay and coworkers demonstrated that ARF1 inactivation and subsequent release of coat proteins was faster at the surface of small liposomes suggesting that ARFGAP1 recruitment was enhanced in presence of curved membranes (Bigay *et al.*, 2003).

Logically enough all mentioned curvature generators are also able to detect membrane curvature. This was mostly described for BAR domain proteins (Bhatia *et al.*, 2009; Gallop *et al.*, 2006; Peter *et al.*, 2004), Epsin (Capraro *et al.*, 2010) and Dynamin (Roux *et al.*, 2010). This double function is thought to be dependent on their membrane-bound density (Antonny, 2011; Sorre *et al.*, 2012) with curvature generation and sensing respectively representing the high and low density behavior of the same protein.

Because the observed curvature generation activity of these proteins was assessed either by overexpression in cells or by high concentration on liposomes, it might not be physiologically relevant *in vivo*. The curvature generation and sensing activities can however be related in the

way that if a protein accumulates on a curved surface in the cell, it might reach a high enough concentration which is sufficient to induce further deformations.

Two major mechanisms of curvature sensing have been described: the sensing of surface geometry and the sensing of lipid packing defects (**Figure 1.10**). N-BAR domain proteins such as Amphiphysin or Endophilin are curvature sensors that have been suggested to use both mechanisms.

Sensing of surface geometry and charge

BAR domains are extended dimers containing cationic residues and exhibiting an arc-shaped structure that will preferentially bind curved and negatively charged membranes (Peter *et al.*, 2004) (**Figure 1.10A**). In the case of BAR domain curvature sensing appears intuitive. If the membrane displays a curvature that is closer to that of the BAR domain, this will lead to more electrostatic interactions between the negatively charged membrane and the positively charged domain, thus leading to a higher gain of energy. Of note, classical BAR domains preferentially sense highly positively curved membranes whereas F-BAR (extended FCH domain) domains sense low positive curvature and I-BAR (Inverse BAR) domains bind to negatively curved membrane surfaces (Mim and Unger, 2012).

Dynamin is a curvature sensor that, contrary to BAR domain proteins, does not display a curved interface (Ferguson and De Camilli, 2012). It was shown to be preferentially recruited to highly curved tubes and this was suggested to be related to its polymerization activity (formation of a curved dynamin coat) on curved membranes (Roux *et al.*, 2010). Dynamin also possess a hydrophobic loop, emerging from its pleckstrin homology domain, which displays curvature sensing activity (Vallis *et al.*, 1999), possibly by the second curvature sensing mechanism: the sensing of lipid packing defects.

Hydrophobic insertion into lipid packing defects

Proteins can also sense curvature, not through the sensing of membrane surface geometry but through the sensing of lipid packing defects induced by membrane curvature (Bigay *et al.*, 2005; Drin *et al.*, 2007). When a membrane is curved, the surface area of the lipid headgroup region of one monolayer is expanded whereas the hydrophobic region remains undisturbed thus leading to the formation of lipid packing defects (**Figure 1.10B**). Of note, defects in the arrangement of lipids can also be related to the specific membrane compositions and consequently to membrane

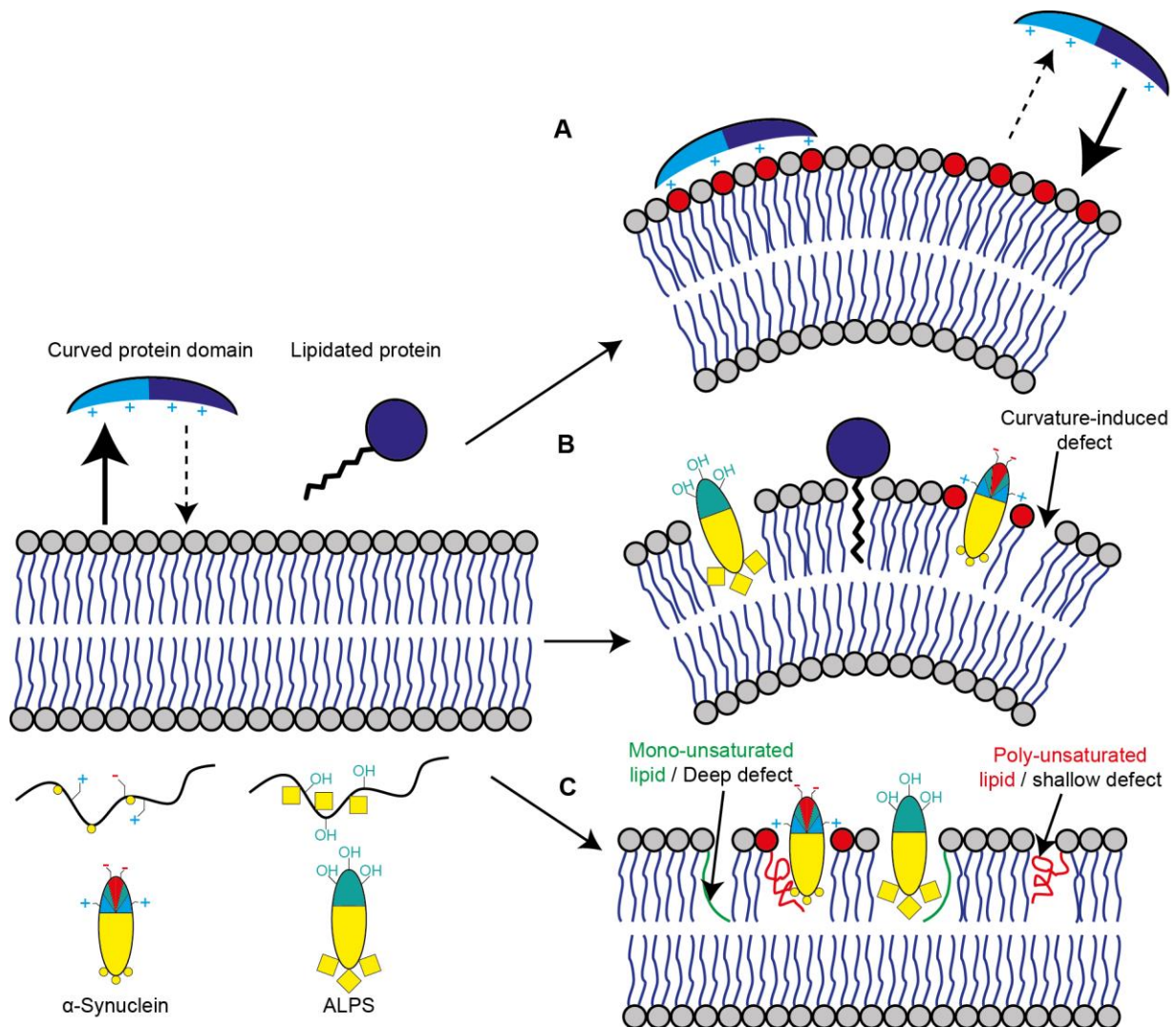


Figure 1.10: Mechanisms of curvature sensing. (A) Proteins, such as BAR domain proteins, can sense the geometry of curved membranes through their curved BAR domain and electrostatic interactions with negatively charged lipids (red lipid headgroups). (B) Membrane curvature induces the formation of lipid packing defects (expansion of the headgroup region of one monolayer) which allows the preferential insertion of protein hydrophobic domains (amphipathic helices or lipidated groups). The ALPS motif binds only to curved membranes via the insertion of hydrophobic residues (yellow squares). In contrast, α -Synuclein has small and poorly hydrophobic residues (yellow circles) and a zwitterionic polar face (positive and negative charges) and will bind only to curved and negatively charged (red lipid headgroups) membranes. (C) Specific lipid compositions (conical-shaped lipids) can also lead to the formation of lipid packing defects. Mono-unsaturated lipids promote the formation of deep defects, which are preferential binding sites for ALPS motifs, whereas poly-unsaturated lipids promote the formation of shallow defects which allow α -Synuclein membrane insertion. Adapted from (Drin and Antony, 2010).

order (Antonny, 2011). Indeed, cone-shaped lipids can promote the formation of packing defects (**Figure 1.10C**), and consequently the formation of a liquid-disordered phase.

This type of curvature sensing is mediated by the insertion of hydrophobic or amphipathic protein domains.

Amphipathic helix (AH) membrane insertion into curved membranes was shown to be dependent on the presence of higher amounts of lipid packing defects as compared to flat membranes (Vanni *et al.*, 2013). AHs are well described curvature sensors that can be found in many different proteins, involved for example in vesicular trafficking processes. Proteins such as Epsin are involved in coat assembly (Ford *et al.*, 2002) whereas ARFGAP1 is involved in coat disassembly (Bigay *et al.*, 2003). AHs are thought to fold upon contact with membranes and insert their hydrophobic face in the lipid bilayer in contact with the lipid hydrophobic tails often with the help of positively charged residues on the helix that will interact with the lipid polar head group (Drin and Antonny, 2010).

More recently, lipidated proteins such as trimeric G proteins (Hatzakis *et al.*, 2009) or RAS proteins (Larsen *et al.*, 2015; Larsen *et al.*, 2017) were also shown to sense curvature. The membrane recruitment of N-RAS proteins, which bear a palmitoyl and a farnesyl lipid group, was enhanced on highly curved liposomes and an increase in membrane curvature was shown to shift the preferential N-RAS recruitment from Ld membranes to Lo membranes (Larsen *et al.*, 2015). N-RAS membrane binding was subsequently shown to be dependent on the amount of lipid packing defects induced by curvature and lipid geometrical shape (Larsen *et al.*, 2017).

Due to the fact that, not only AHs, but also alkyl hydrophobic chain motifs can sense lipid packing defects induced by curvature, it was suggested that this type of membrane curvature sensing is not dependent on the affinity of the hydrophobic domain for the membrane but simply on the ability of a curved membrane to host more proteins (Hatzakis *et al.*, 2009).

However, the “Velcro model” (Antonny, 2011) suggests that the AH’s global and effective interaction with curved membranes is a result of many weak and identical interactions of different AH hydrophobic regions with the membrane. Thus, the binding of shorter AHs displaying a good balance between polar and non-polar faces will require less packing defects as compared to longer and strongly imbalanced (larger hydrophobic side) AHs.

Because of these variations in their chemical properties, AH motifs can be recruited to different cellular and curved membranes (Antonny, 2011; Bigay and Antonny, 2012). For example,

membranes of the early secretory pathway display loose packing and low surface charges which will favor curvature recognition by AHs composed of a larger hydrophobic side and a small polar face, such as the ALPS motif found in ARFGAPI (**Figure 1.10B**) (Mesmin *et al.*, 2007). In contrast to this, α -Synuclein, which displays a smaller hydrophobic side and more charged residues, will preferentially recognize membrane curvature in bilayers exhibiting tighter lipid packing and higher amounts of negatively charged lipids (**Figure 1.10B**), mainly found in the late secretory pathway (Jao *et al.*, 2008).

Thus, one can differentiate between deep lipid packing defects, preferentially recognized by the ALPS motif and shallow lipid packing defects sensed by α -Synuclein (Pranke *et al.*, 2011) (**Figure 1.10C**).

1.4 *In vitro* experimental approaches

1.4.1 Model membranes for *in vitro* experiments

Due to the high complexity of cellular membranes, their study remains very challenging. Thus, many model membrane systems of controlled lipid composition are now available to study membrane related events *in vitro* (Bagatolli and Sunil Kumar, 2009; Sezgin and Schwille, 2012). Depending on the study and more specifically on the relevant membrane physical parameters, model membranes with various geometries can be used (**Figure 1.11**): planar shape bilayers like supported lipid bilayers or spherical shape bilayers like vesicles. Spherical vesicles with different sizes can be obtained; from the nanometer range (small unilamellar vesicles, SUVs) to the micrometer range (giant unilamellar vesicles, GUVs). Some of the existing model membrane systems are summarized in **Figure 1.11** as well as the methods to produce them.

Multilamellar vesicles can be synthesized through the hydration of dry lipid films. Subsequent sonication of these vesicles leads to the formation of SUVs (30 to 50 nm in diameter) whereas their extrusion through polycarbonate membranes of varying pore sizes leads to the formation of large unilamellar vesicles (LUVs) with diameters ranging between 100 nm and 1 μ m (**Figure 1.11**). GUVs are unilamellar vesicles of larger sizes (1 to 100 μ m in diameter) that are produced by the hydration of dry lipid films and subsequent electroformation under an alternating current (AC) electric field (Angelova *et al.*, 1992).

Unilamellar vesicles with asymmetric membranes can also be obtained using the inverted emulsion technique (Pautot *et al.*, 2003), which consists in the transfer of inverted emulsion

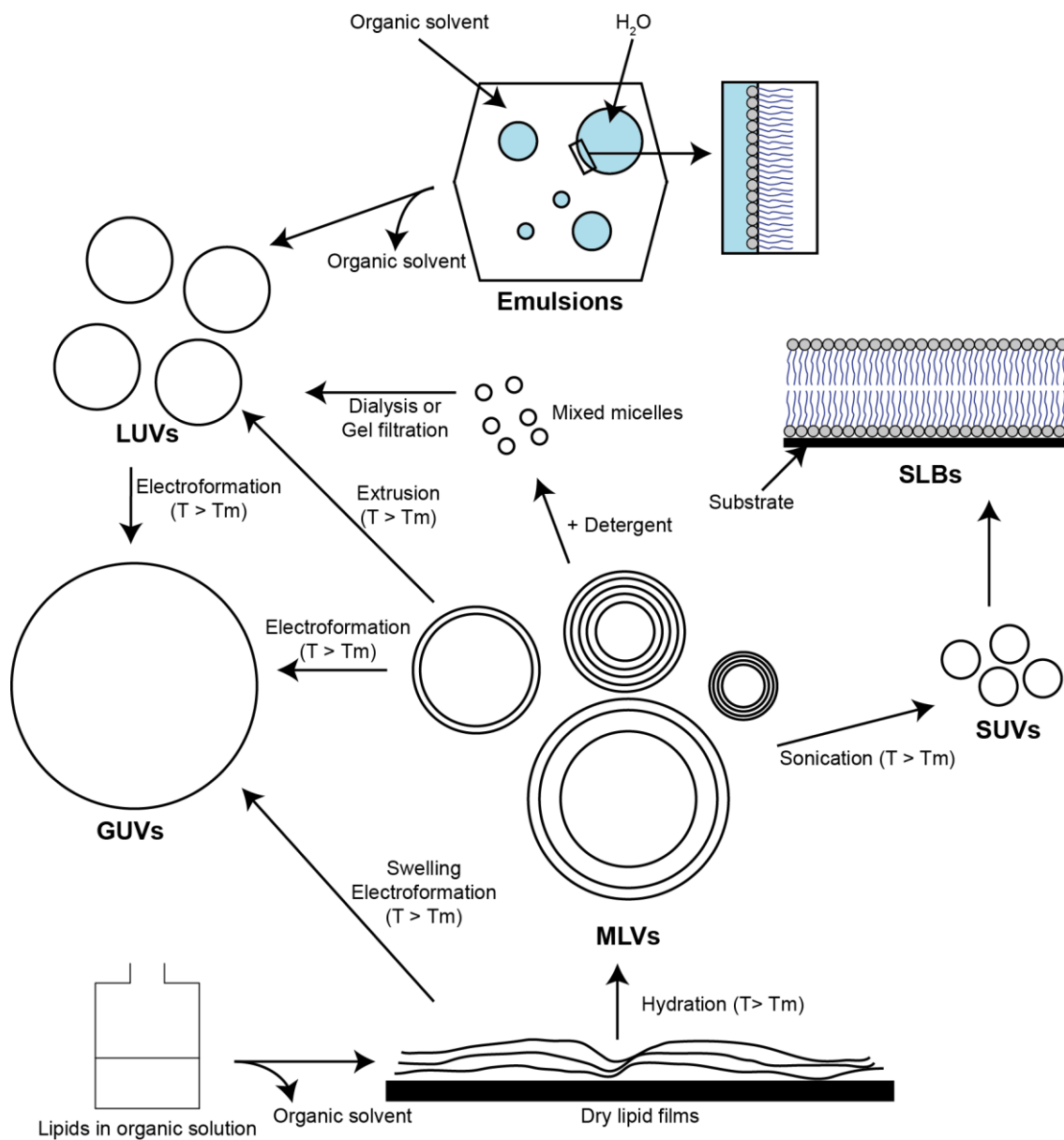


Figure 1.II: Schematic of the different available methods to produce model membranes. MLVs: multilamellar vesicles, SUVs: small unilamellar vesicles, GUVs: giant unilamellar vesicles, LUVs: large unilamellar vesicles, SLBs: supported-planar lipid bilayers. Adapted from (Bagatolli and Sunil Kumar, 2009).

droplets covered with a lipid monolayer through a second monolayer at an oil-water interface. This method can also be used to encapsulate proteins inside GUVs (Pontani *et al.*, 2009). Vesicles, called giant plasma membrane vesicles (GPMVs), can also be obtained from the cell plasma membrane by inducing cell blebbing (Levental and Levental, 2015).

The study that is being presented in this manuscript mostly focuses on the use of GUVs as their micrometer size allowed suitable visualization under a light microscope. They can also be deformed and their tension can be adjusted using micromanipulation techniques thereby allowing the study of the membrane mechanical properties (Henriksen and Ipsen, 2004; Rawicz *et al.*, 2000; Rawicz *et al.*, 2008; Tierney *et al.*, 2005). GUVs have also been widely used to study demixing behaviors of lipid mixtures (Scherfeld *et al.*, 2003; Veatch and Keller, 2003; Wesolowska *et al.*, 2009) and protein interaction and sorting (Ambroggio *et al.*, 2010; Saarikangas *et al.*, 2009; Sorre *et al.*, 2012). A detailed description of giant vesicle applications can be found in (Walde *et al.*, 2010).

One particular disadvantage of using the electroformation method is that only growth buffers containing low levels of salt can be used (Bucher *et al.*, 1998; Dimova *et al.*, 2006). This problem can be circumvented using an optimized electroformation method consisting of platinum electrodes (Meleard *et al.*, 2009).

Another new method, exhibiting higher yield of GUV unilamellarity and faster GUV growth, has more recently been proposed. As compared to the original swelling method where lipids were spread onto glass, lipids are in this case spread on top of a polymer gel consisting of either agarose (Horger *et al.*, 2009) or polyvinyl alcohol (Weinberger *et al.*, 2013). This method also allows the use of aqueous buffer of physiological ionic strength.

1.4.2 Phase separation from living cells to model membranes

The most famous method used to study lipid rafts and their association with membrane proteins consists in the observation of detergent-resistant membranes. However, this method was shown not to be optimal as the use of detergents is thought to potentially induce phase separation and to affect the partitioning of membrane proteins to a specific phase (Heerklotz, 2002; Lichtenberg *et al.*, 2005). Other techniques have thus been developed in order to study native membranes *in situ* (Klymchenko and Kreder, 2014), such as mass spectrometry to monitor the chemical composition

of cell membranes (Lozano *et al.*, 2013) or atomic force microscopy (AFM) which allows nanoscopic resolution and clear distinction between Lo and Ld domains (Goksu *et al.*, 2009).

Lipid rafts in live cells can only be studied and visualized using optical techniques and fluorescent probes. However, even though optical microscopy improved in the last decades now allowing imaging at tens of nanometers resolution, the study of lipid rafts in cells is still very limited considering their small size, thought to be in the nanometer range (Pike, 2006). Additionally, due to their high complexity in composition and structure, the study of membrane rafts in live cells is very challenging. Biophysicists have thus been trying in the last decades to reproduce the complexity of rafts with model systems exhibiting phase separation, such as planar supported lipid bilayers (Longo *et al.*, 2009; Mulligan *et al.*, 2010; Szmodis *et al.*, 2010) and GUVs (Roux *et al.*, 2005; Veatch and Keller, 2003), whose physical properties can be controlled and varied.

In single component systems, the transition to a certain phase occurs at a well-defined melting temperature. Coexistence between the So and Ld phases can be achieved in a 2-component system of high and low T_m lipids. As previously mentioned, cholesterol is key to the formation of the Lo phase. Thus, Lo and Ld domains can coexist in ternary lipid mixtures consisting of high and low T_m lipids and cholesterol. At equilibrium conditions and at a given temperature and composition, the nature of the thermodynamic phases can be predicted and referenced with phase diagrams (**Figure 1.12A**). These representations can be obtained using the Gibbs triangle (Veatch and Keller, 2005) and many can be found in the literature (Feigenson, 2006; Goni *et al.*, 2008). **Figure 1.12A** shows typical phase diagrams for binary (high and low T_m lipids) and ternary lipid mixtures system (high T_m lipid (A)/Cholesterol (C)/low T_m lipid (B)).

Many different phases can be distinguished with ternary lipid mixtures.

- Pure homogeneous Ld phase when the low T_m lipid (**Figure 1.12A (B)**) is in excess.
- Pure homogeneous Lo phase when the high T_m lipid (**Figure 1.12A (A)**) is in excess with moderate cholesterol (**Figure 1.12A (C)**) amount.
- Coexistence of multiple phases: the three components are in comparable amounts (central area of the phase diagram). Two specific regions can be distinguished: (1) Lo/Ld and (2) So/Lo/Ld phase coexistence.

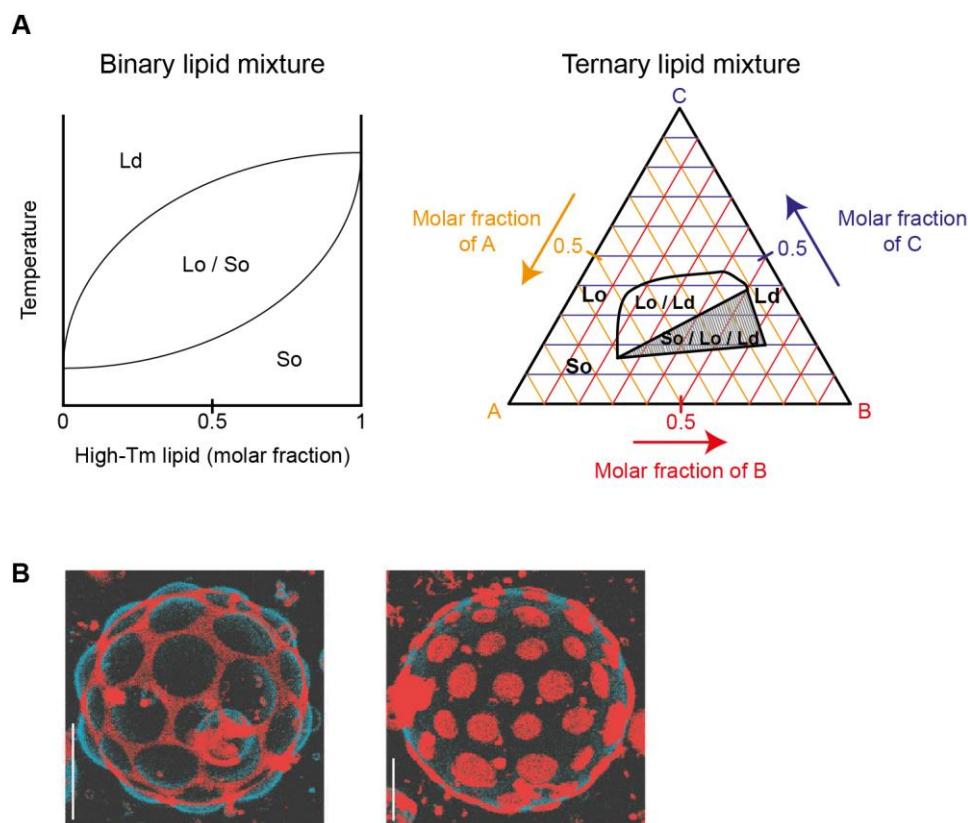


Figure 1.12: Phase separation in model membranes. (A) Representation of the phase behavior of lipid mixtures using phase diagrams. Phase coexistence can be observed with binary lipid mixtures of different T_m (left diagram) and also with ternary lipid mixtures containing additional cholesterol (right diagram). A: High T_m lipid, B: Low T_m lipid, C: Cholesterol. Adapted from (Bagatolli and Sunil Kumar, 2009). (B) Phase separation on giant vesicles visualized using a rhodamine - 1,2-Bis(diphenyl-phosphino)ethane red fluorescent probe for Ld domains and perylene to mark the Lo phase (blue). From (Baumgart *et al.*, 2003).

It is important to note that this description of ternary mixture phase behavior is very general and details will vary from one system to another depending on the lipids used and their physical properties (acyl chain length, degree of unsaturation, charge). Lipid and protein interactions have also been shown to have an influence on phase diagrams. One of the best characterized examples is the interaction between Cholera toxin and GM1 lipids. Cholera toxin interacts with GM1 lipids and induces lipid clustering which thus leads to phase separation (Hammond *et al.*, 2005).

In the case of Lo/Ld phase separation (that was used in this study), model membranes exhibit areas having Lo properties which are connected to Ld domains. It is possible to identify the different phases by using fluorescent lipids or lipophilic probes that will preferentially sort into one of the two phases (Baumgart *et al.*, 2007; Klymchenko and Kreder, 2014) (Figure 1.12B).

1.4.3 Curvature sensing on model membranes

Different model membrane systems and protocols exist to detect protein curvature sensing (**Figure 1.1B**).

Wavy supported lipid bilayers are a very interesting system as they display a continuum of positively and negatively curved regions (Cheney *et al.*, 2017; Hsieh *et al.*, 2012). However this method is very limited as the displayed curvature values are relatively small (radius in the few hundred nanometer range) (**Figure 1.1BA**). A good alternative system that has been recently described is the use of supported membrane tubes (Dar *et al.*, 2017). This system has the advantage, contrary to the previously mentioned system, to display highly curved regions (between 10 and 40 nm tube radii) (**Figure 1.1BB**).

Curvature sensing can also be assessed by using liposomes of decreasing diameters, which can, as previously mentioned, be generated by vesicle extrusion through pores of decreasing sizes (**Figure 1.1BC**). Vesicles are incubated with the proteins and centrifuged. Subsequent SDS PAGE analysis of the pellet and the supernatant fractions will allow the assessment of protein binding (Peter *et al.*, 2004). An alternative and more effective way to study liposome-protein interactions is by flotation assay, where vesicles are centrifuged in a sucrose gradient of higher density than the liposome preparation buffer. Vesicles are thus always recovered in the top fraction. All fractions are analyzed by SDS PAGE to assess membrane localization (Bigay *et al.*, 2005). The efficiency of protein binding to vesicles can also be studied using a lipid-sensitive probe covalently attached to the protein (Pranke *et al.*, 2011).

The single liposome curvature assay (SLiC) is another method used to assess liposome curvature sensing and, in contrast to the previous mentioned methods, allows the assessment of protein binding to individual vesicles with diameters ranging from 30 nm to 1 μm (Jensen *et al.*, 2011; Larsen *et al.*, 2015). Liposomes are immobilized on a passivated glass surface through biotin-streptavidin interactions (**Figure 1.1BD**). Binding of fluorescent proteins as well as fluorescent liposome signal are then assessed by confocal microscopy. The great advantage of this method is that because SLiC works at the single-liposome level, and each frame is comprised of hundreds of vesicles exhibiting various curvatures, it thus permits to probe a wide range of curvatures in the same experiment (Larsen *et al.*, 2015).

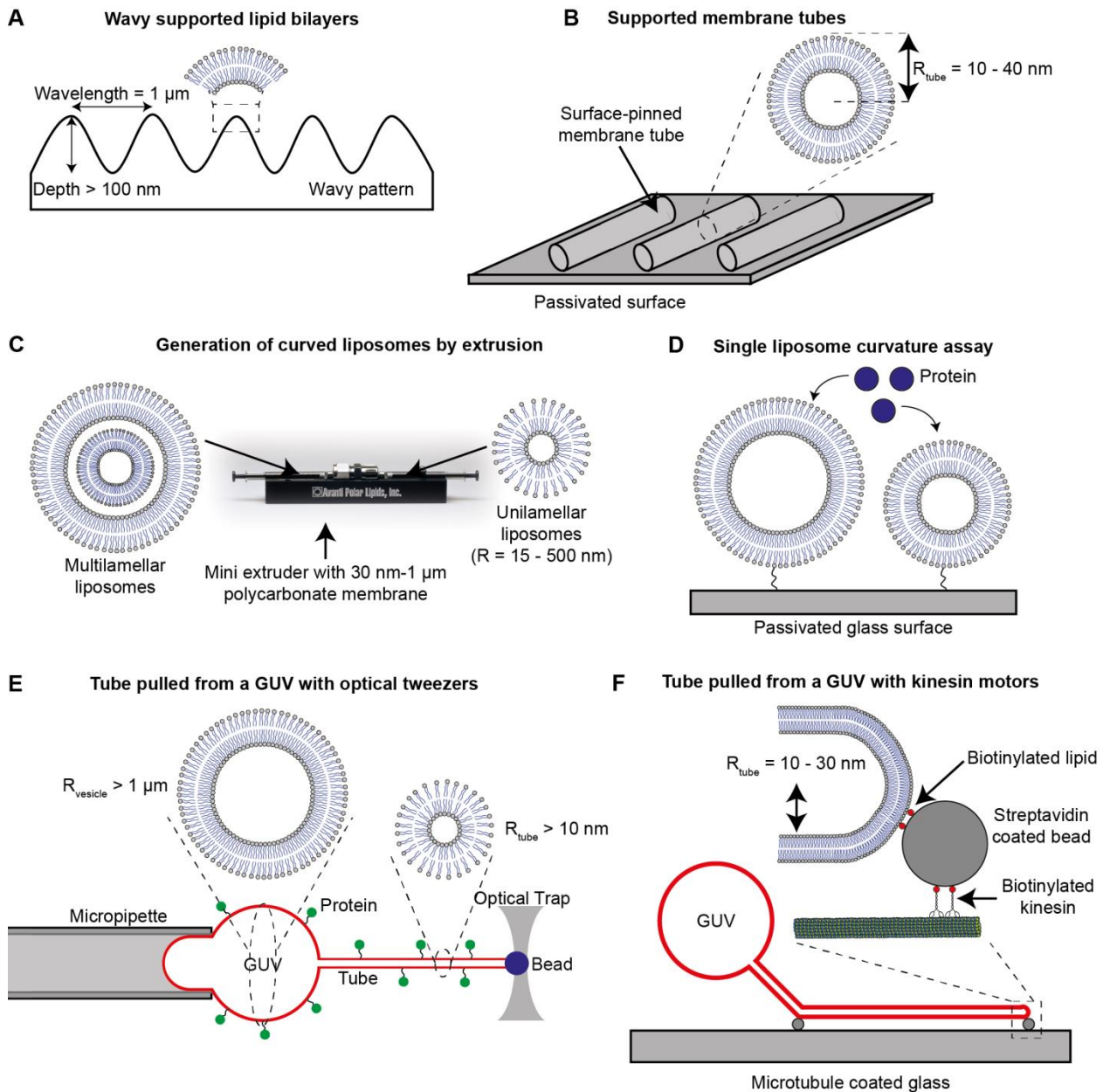


Figure 1.B: *In vitro* experimental setups for the study of curvature sensing. (A) Wavy supported lipid bilayers. Adapted from (Hsieh *et al.*, 2012). (B) Supported membrane tubes. Adapted from (Dar *et al.*, 2017). (C) Generation of curved liposomes by extrusion. Extruder image from Avanti polar lipids. (D) Single liposome curvature assay. Adapted from (Jensen *et al.*, 2011). (E) Tube pulled from a GUV with optical tweezers. (F) Tube pulled from a GUV with kinesin motors. Adapted from (van Meer and Vaz, 2005).

Finally, the setup that has been used in this study consists in the pulling of membrane nanotubes from GUVs (**Figure 1.13E**). Tube formation occurs through the aspiration of the GUV with a micropipette on one side and the trapping (using an optical tweezer setup) of a bead tethered to the vesicle on the other side. This technique allows the quantitative study of protein enrichment on a highly curved membrane region (the tube) as compared to a flat membrane region (the GUV) (Ambroggio *et al.*, 2010; Prevost *et al.*, 2015; Sorre *et al.*, 2012).

The micropipette aspiration technique, which was first introduced by Evans on red blood cells (Waugh and Evans, 1979) and later on large vesicles (Kwok and Evans, 1981), allows the control of membrane tension and was thus originally meant to assess elastic properties of membranes. I used it for two purposes: holding the GUV and controlling membrane tension (and consequently tube curvature).

Tube extraction was first achieved by applying a flow on red blood cells attached to a glass surface (Hochmuth *et al.*, 1973). Later on, cells were held with a micropipette and tubes were pulled using a bead immobilized with a second micropipette (Hochmuth *et al.*, 1982).

Finally, tubes were extracted using optically or magnetically trapped beads. While holding the vesicle with a micropipette, these trapped beads are used to apply a point force on the membrane and consequently extract the tubes (Cuvelier *et al.*, 2005; Heinrich and Waugh, 1996) (**Figure 1.13E**).

Optical tweezers allow the micromanipulation of micron-size particles. The optical trap is created by tightly focusing a laser beam with an objective of high numerical opening. The dielectric and trapped particle experiences two forces: a scattering force which tends to push the particle in the direction of the propagation of light; and a gradient force, which acts in the direction of the intensity gradient and will thus tend to bring the particle back to the focus (**Figure 1.14**) (Neuman and Block, 2004). Thus, for an object to be efficiently trapped, the gradient force must exceed the scattering force. This is the reason why the laser beam must be tightly focused (higher focusing results in a greater intensity gradient).

Of note, other similar tube-pulling methods have been developed, such as the use of forces generated by kinesin motors walking on microtubules (Roux *et al.*, 2002) (**Figure 1.13F**). Briefly, biotinylated kinesins interact with membranes composed of biotinylated lipids, in presence of streptavidin beads. Subsequent ATP addition will activate the kinesins and allow them to walk on

the polymerized microtubules and consequently to pull membrane tubes. A detailed experimental protocol will be described in Chapter 3.

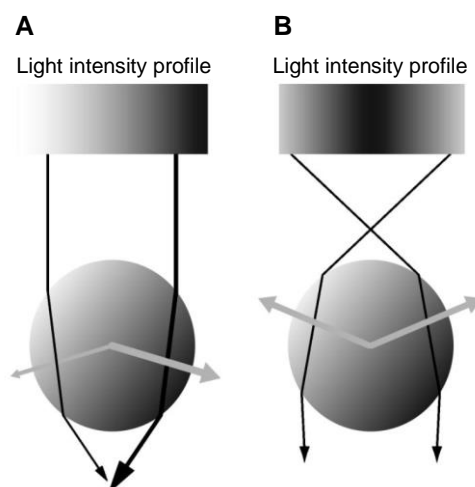


Figure 1.14: Description of the gradient force. A: a micrometric transparent bead is illuminated by a parallel beam of light with an intensity gradient increasing from left to right (represented by a white (low intensity) to black (high intensity) gradient). Two example rays of different intensities are shown in black (black lines of different thickness). These rays are refracted, and thus change direction, when entering and exiting the bead, resulting in a similar directional change of the momentum of the photons. A momentum of same intensity and opposite direction is then imparted to the bead, resulting in the force depicted by the gray arrows. The thicker ray carries more intensity and therefore transmits a greater momentum to the bead. As a result, the net force on the bead is towards the high intensity (and slightly downward). B: To form a stable trap, the light has to be focused. To do so, the bead is illuminated by a focused beam of light with a radial intensity gradient (highest intensity is depicted in black). In this case, the two lateral rays have the same intensity and their refraction leads to a transfer of momentum resulting in lateral forces that balance each other. Therefore only the axial force remains. This axial force is balanced by the scattering force (not shown), resulting in the axial stability of the bead. If the bead is moved away from the center of the beam, the radial gradient force will bring it back to the equilibrium position. From (Neuman and Block, 2004).

Chapter 2

2 RAB GTPases

2.1	RAB discovery and evolution	54
2.2	RAB sequence and structure	55
2.2.1	G-domain.....	56
2.2.2	RAB specific sequence motifs.....	57
2.2.3	RAB C-terminal region	57
2.3	RAB posttranslational modifications.....	58
2.3.1	RAB activation cycle	58
2.3.2	RAB membrane insertion and extraction	61
2.4	Membrane targeting of RAB GTPases	64
2.5	RAB GTPases and vesicular transport	68
2.5.1	General mechanism of intracellular transport	68
2.5.2	RABs and membrane tethering.....	71
2.6	Focus on the RAB proteins used in this study	75
2.6.1	RAB1 and the ER-Golgi intermediate compartment	75
2.6.2	RAB6 and the Golgi.....	76
2.6.3	RAB4 / RAB5 / RAB11 and the endosomal system.....	77
2.6.4	RAB35 and the plasma membrane	80

RAB (Ras-like in brain) proteins are members of the RAS (Rat Sarcoma) superfamily of small GTPases. This superfamily is comprised of more than 160 members and is divided into five major families (Rojas *et al.*, 2012). RAS proteins couple extracellular signals to intracellular pathways and thus play a critical role in cellular processes such as proliferation, apoptosis, differentiation, motility and transcription (Karnoub and Weinberg, 2008). The RHO (RAS homology) family of proteins regulates various cellular processes including cell polarity, cytoskeletal organization, cell

cycle and transcriptomal dynamics (Bustelo *et al.*, 2007) and the RAN (RAS-related nuclear protein) family mediates nuclear transport processes and mitosis (Melchior, 2001). The members of the ARF (ADP-ribosylation factor) family of proteins are involved in the recruitment of coat proteins, the regulation of phospholipid metabolism and in the modulation of actin structure at the surface of membranes; and thereby regulate membrane trafficking events and organelle structure (Donaldson and Jackson, 2011; Jackson and Bouvet, 2014). Finally, RAB proteins represent the largest family of small GTPases with over 60 *RAB* genes identified in humans. These proteins actively regulate membrane trafficking events in the cell and localize to distinct compartments, thereby defining organelle identity (Zhen and Stenmark, 2015).

As this study focuses on the membrane binding properties of RAB proteins, a detailed description of RAB structure, localization and function will be provided in this second chapter and a particular attention will be set on the different RAB proteins used in this study.

2.1 RAB discovery and evolution

The first two *RAB* genes, *YPT1* and *SEC4*, were discovered in yeast (Gallwitz *et al.*, 1983; Salminen and Novick, 1987). At this time, these RAS-like proteins were thought, like all G proteins, to act in the transduction of signals through the plasma membrane (Barbacid, 1987; Gilman, 1987). The observation that *SEC4* mutations confer late secretory defects suggested a role for *SEC4* in intracellular trafficking (Salminen and Novick, 1987). A year later, *YPT1* was shown to localize to the yeast Golgi and *YPT1* mutant cells were shown to exhibit defects in the transfer of material between the ER and the Golgi (Segev *et al.*, 1988). *YPT1* became the first GTPase shown to function inside cells and to regulate intracellular trafficking. The term RAB for RAS-related in Brain came from the isolation of four *RAS* genes, homologous to the yeast YPT proteins, using a screen of a rat brain cDNA library (Touchot *et al.*, 1987).

The conservation of YPTs in evolution was first shown for *YPT1*. Its closest human homolog, *RAB1* was shown to not only share 71% amino acid sequence identity (Touchot *et al.*, 1987) but also to localize to the Golgi (Segev *et al.*, 1988). The subsequent discovery that mouse *RAB1* could functionally replace *YPT1* in yeast led to the assumption that membrane trafficking events were regulated by conserved machineries (Haubruck *et al.*, 1989). More YPTs and RABs were then discovered by searching for homologs of *YPT1* and *SEC4* (Zahraoui *et al.*, 1989) and even more were identified when the yeast and human genome-sequencing projects were completed (Bock *et al.*, 2001; Lazar *et al.*, 1997). Currently, eleven yeast YPTs and more than 60 human RABs have been identified; and *YPT1*, *YPT51*, *YPT6*, *YPT7*, *SEC4* and *YPT31/YPT32* have proved to be very

homologous to RAB1, RAB5, RAB6, RAB7, RAB8 and RAB11 respectively in mammalian cells (**Figure 2.1**). Interestingly, the YPT/RAB family expanded significantly from yeast to multicellular organisms, such as worms and flies, and then to mammals (Bock *et al.*, 2001), implying that trafficking pathways in mammals are much more tightly regulated, but also tissue specific (some RAB proteins are not ubiquitously expressed).

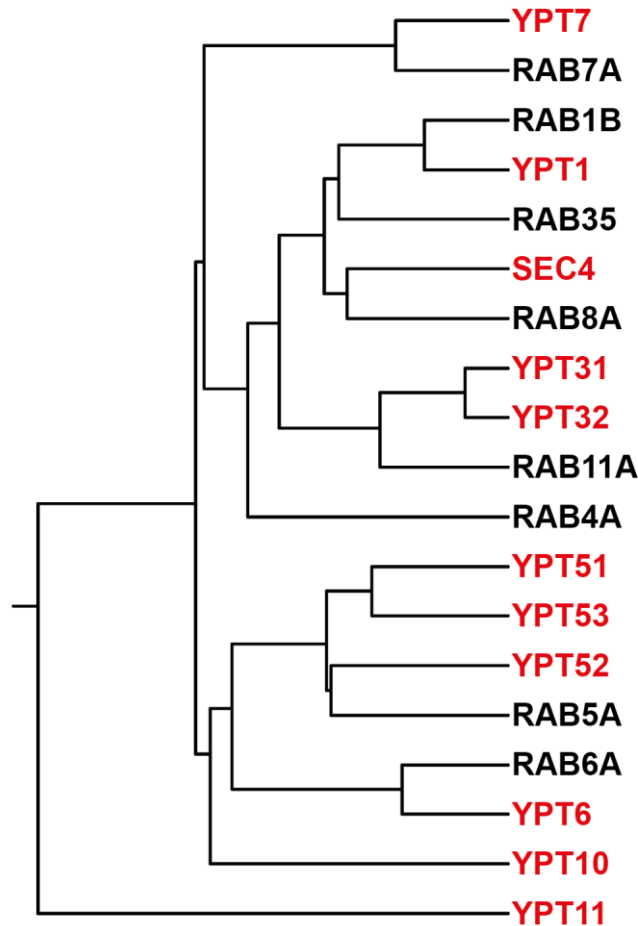


Figure 2.1: Alignment of all YPTs (in red) and their human RAB homologues (in black). The YPT/RAB family has significantly expanded from unicellular to multicellular organisms and is now composed of more than 60 members in humans (see (Hutagalung and Novick, 2011) for detailed review about existing RAB proteins). Sequences were retrieved from UniProt and aligned using ClustalW.

2.2 RAB sequence and structure

Extensive sequence analysis and crystallographic studies led to the identification of several RAB sequence regions and motifs which are critical for function and specific membrane recruitment.

2.2.1 G-domain

RAB proteins are composed of only one structural domain, common to all members of the RAS superfamily, called the G domain. This domain, which structurally consists of a central β -sheet with six strands that is flanked by five α -helices on both sides, serves as the binding and hydrolysis site of guanine nucleotides, and switches conformation upon GTP or GDP binding (**Figure 2.2A**) (Dumas *et al.*, 1999; Ostermeier and Brunger, 1999).

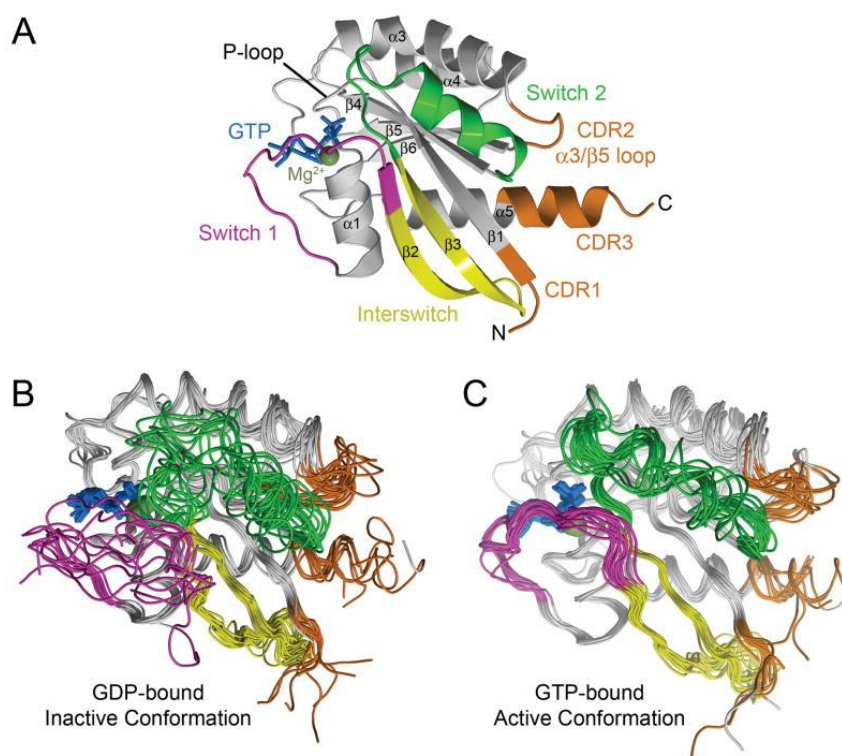


Figure 2.2: Structural representation of the different members of the RAB family. (A) Structural representation of RAB3 with its different functional regions. (B) Comparison of inactivated GDP-bound RAB proteins. The switch regions display a poorly ordered structure. (C) Superposition of GTP-bound RABs. Switch regions are more ordered than with GDP-bound RABs and Switch II displays great conformational differences between RABs. From (Lee *et al.*, 2009).

The specific regions that can sense the nature of the bound nucleotides and are involved in GTP hydrolysis are the switch I and switch II regions. The respective contributions of these two regions vary among the members of the RAS superfamily. Both switch regions were shown to interact with the γ -phosphate of GTP whereas GDP interaction (through its guanine base) is only mediated by the Switch I region (Cherfils and Zeghouf, 2013; Vetter and Wittinghofer, 2001). Both tend to be disordered in the GDP-bound form and undergo major changes to adopt a

structurally ordered state upon GTP binding (**Figure 2.2B** and **Figure 2.2C**) (Lee *et al.*, 2009). When comparing the switch region crystal structures of several GTP-bound RAB proteins, significant resemblance can be observed in terms of overall length and boundaries but structural differences between RAB subfamilies can also be detected (**Figure 2.2C**), specifically in their switch and complementary determining (CDRs) regions (Pfeffer, 2005).

2.2.2 RAB specific sequence motifs

Extensive sequence analyses of different RAB proteins have shown the existence of specific motifs (**Figure 2.3**). Pereira-Leal and Seabra (Pereira-Leal and Seabra, 2000) have identified five RAB family regions (RABF) that distinguish RAB proteins from the other members of the RAS superfamily and four subfamily regions (RABSF) that stand to differentiate each RAB subfamily (RAB1 from RAB6 for example). To note, the previously mentioned CDRs correspond approximately to the RABSF motifs (RABSF1, RABSF3, RABSF4) (Pfeffer, 2005). Different combinations of mutations of these motifs led to mislocalization of the RAB proteins suggesting that membrane specificity is also determined by these specific RAB sequence domains (Ali *et al.*, 2004).

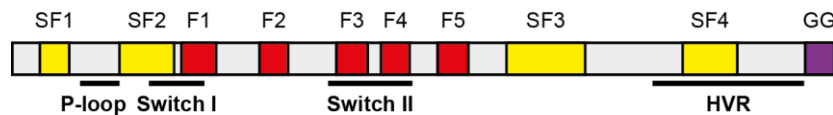


Figure 2.3: Schematic representation of RAB protein motifs. RAB family motifs (F1 to F5) differentiate the RAB proteins from the other members of the RAS superfamily while RAB subfamily motifs (SF1 to SF4) are variable among RAB proteins. The C-terminus of most small GTPases, including RAB proteins, is composed of a hypervariable region (suggested to be important for RAB specific membrane targeting) and a mono or di-cysteine motif on which can be added one or two geranylgeranyl groups. The black bars show the location of the phosphate-loop, the switch regions and the hypervariable domain. Adapted from (Ali and Seabra, 2005).

2.2.3 RAB C-terminal region

The C-terminal extremity of RAB proteins, and more specifically the last 35 to 40 amino acid region, is unstructured and highly variable among the different RAB proteins. It was initially proposed that RAB specific membrane targeting was only dependent on the RAB hypervariable C-terminal sequence (Chavrier *et al.*, 1991). This hypothesis was however later questioned when the

specific localization of RAB proteins was shown to not always be dependent on their C-terminal region but instead to be dependent on motifs distributed throughout their primary sequence (Ali *et al.*, 2004; Beranger *et al.*, 1994). An even more recent study demonstrated that when most of the hypervariable region was replaced with a polyethylene glycol linker, RAB1 and RAB5 were still found to localize to the correct intracellular compartment (Li *et al.*, 2014); thus also going against the prediction that the C-terminus of RAB proteins is critical for RAB targeting.

Some RAB proteins however do possess C-terminal residues involved in specific membrane targeting. It was shown that the replacement of the polybasic C-terminal sequence of RAB35 with uncharged elements led to the absence of proper plasma membrane localization (Li *et al.*, 2014). It was thus suggested that the specific recruitment of RAB35 to the plasma membrane (which is negatively charged) is mediated by electrostatic interactions. RAB7 specific localization to late endosomes / lysosomes was also described to be dependent on its hypervariable region and more specifically on the C-terminal region involved in the binding with the RAB-interacting lysosomal protein (RILP) (Li *et al.*, 2014).

The C-terminal extremity of RAB proteins is also composed of a mono or di-cysteine motif which allows the covalent attachment of respectively one or two geranylgeranyl lipid moieties necessary for RAB membrane insertion (Desnoyers *et al.*, 1996). This will be further discussed in the next section.

2.3 RAB posttranslational modifications

2.3.1 RAB activation cycle

Like all GTPases, YPTs/RABs cycle between an active GTP-bound form and an inactive GDP-bound form (**Figure 2.4**). Upon membrane incorporation, RAB proteins are activated by a guanine nucleotide exchange factor (GEF) and bound GDP is replaced by the approximately 10-fold more abundant GTP (Barr and Lambright, 2010; Cherfils and Zeghouf, 2013). It is important to note that GEF proteins can catalyze the exchange reaction in both directions but directionality is dictated by the higher concentration of GTP over GDP (Goody and Hofmann-Goody, 2002). In such a conformation, RABs can fulfill their functions in the trafficking processes through their interaction with effector proteins. RABs then undergo an inactivation process which is mediated by GTPase-activating proteins (GAPs) and consists in the hydrolysis of GTP to GDP (Barr and Lambright, 2010; Cherfils and Zeghouf, 2013).

GEFs and GAPs regulate RAB activation in a spatiotemporally controlled manner. So far, many RABGEFs have been identified including the two large families Vps9-domain containing proteins (specific for the RAB5 family) (Carney *et al.*, 2006; Horiuchi *et al.*, 1997) and DENN domain GEFs which act on several different RABs (Marat *et al.*, 2011). Many other structurally different GEFs, that are not part of these two families, have also been identified (see (Muller and Goody, 2017) for extensive review). These different RABGEF proteins exhibit very low structural and sequence homology to each other, which explains why the corresponding GEFs of some RABs are yet to be identified.

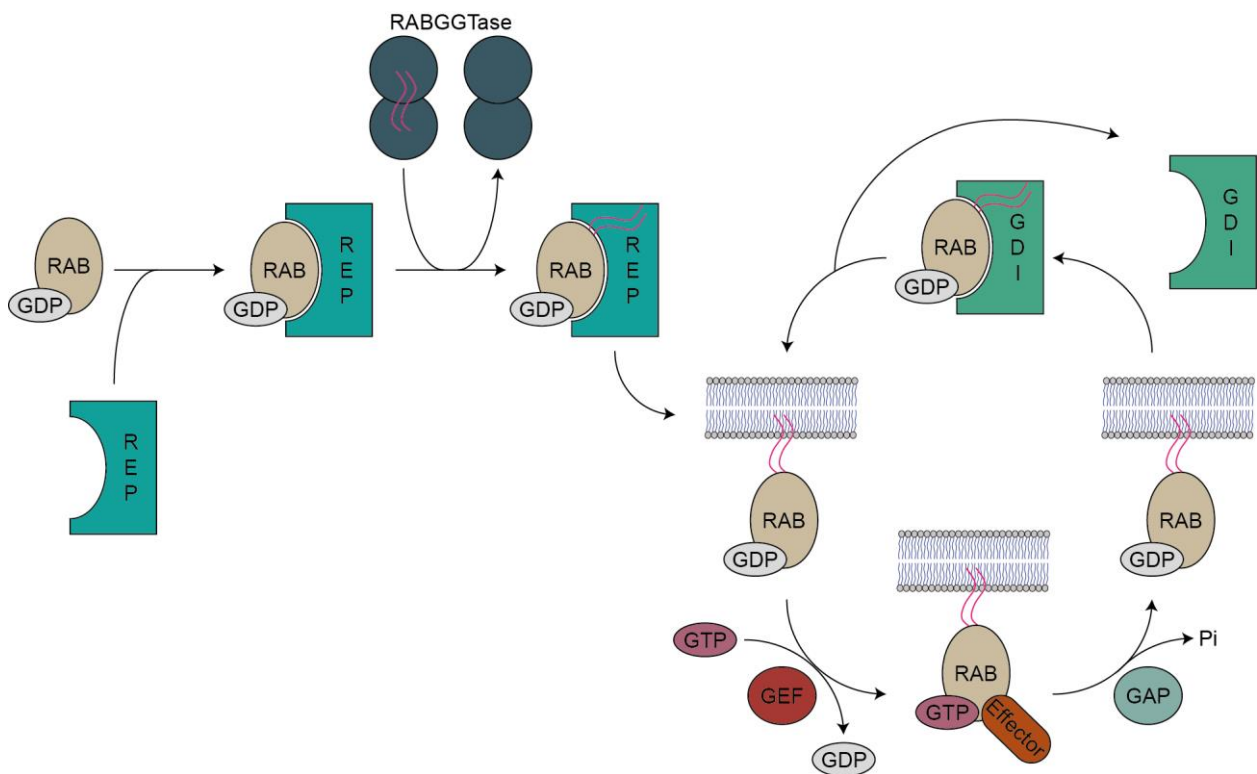


Figure 2.4: RAB prenylation and activation cycle. The RAB escort protein (REP) interacts with the GDP-bound RAB protein and directs it towards the RAB geranylgeranyltransferase (RABGGTase) which catalyzes the transfer of one or two (mostly two) prenyl groups (geranylgeranyl moieties) onto the C-terminal mono- or di-cysteine motif of the RAB protein. Once they are prenylated, RAB proteins can bind to membranes and get subsequently activated (GDP to GTP exchange) by guanine nucleotide exchange factors (GEF) which allows their interaction with effector proteins. RABs subsequently interact with GTPase activating proteins (GAPs) which catalyze GTP to GDP hydrolysis and GDP-bound RABs can get recycled back to the donor compartment by the GDP dissociation inhibitor (GDI). Adapted from (Hutagalung and Novick, 2011).

Chapter 2: RAB GTPases

Several GEFs of small GTPases, such as RASGEFs SOS and ARFGEFs Cytohesins, have been reported to be controlled by feedback loops, in which the GTP-bound GTPases or their effectors bind to their cognate GEFs and modify their basal nucleotide exchange rate (Cherfils and Zeghouf, 2013). Interestingly, some RABGEFs have been suggested to be regulated by similar feedback loops.

RAB5GEF Rabex-5 is the best characterized example as it was described to interact with Rabaptin-5, a RAB5 effector (Horiuchi *et al.*, 1997). Briefly, RAB5 is activated by Rabex-5 upon membrane recruitment and is then able to interact with its various effectors, including Rabaptin-5. Rabaptin-5 then interacts with Rabex-5 and allows the increase of nucleotide exchange activity of Rabex-5 towards RAB5 (feedback effect). These interactions generate a feedback loop which prevents RAB5 inactivation by its cognate GAP, and GDI-mediated membrane extraction (Lippe *et al.*, 2001). This feedback mechanism was however recently challenged with the finding that Rabaptin-5 recruitment to early endosomes is independent of RAB5 and relies on its interaction with Rabex-5 and RAB4 (Kalin *et al.*, 2015). A similar feedback mechanism was suggested to occur in yeast where SEC4 and its cognate GEF SEC2 both interact with SEC15, a subunit of the exocyst complex (Medkova *et al.*, 2006).

A key feature of small GTPases is their ability to intrinsically hydrolyze GTP, but this activity is very low. Thus, as mentioned above, RAB proteins get more rapidly inactivated through GAP mediated GTP hydrolysis. In contrast to RAB GEFs, human RAB GAPs consist of one major family, the TBC domain containing proteins with more than 40 members in humans (Fukuda, 2011). An exception to this is found with the RAB3 subfamily-specific GAP complex which consists of 2 different proteins (Nagano *et al.*, 1998).

GAP proteins but also GEFs were shown to be involved in RAB cascades, where RABs recruit effectors that act as GAPs for upstream RAB protein or as GEFs for RABs acting further down the pathway. YPT32 was shown to recruit SEC2, the GEF of the later acting SEC4 (Ortiz *et al.*, 2002), and also to recruit GYP1 and GYP6, the two respective GAPs of the previous acting YPT1 and YPT6 (Rivera-Molina and Novick, 2009; Suda *et al.*, 2013). A similar cascade was described for endocytic RABs; RAB5 recruits the class C VPS/HOPS complex, a known GEF for RAB7 (Rink *et al.*, 2005). These RAB cascades were suggested to keep RAB domains distinct through the removal of a RAB from a domain in which it does not belong (Nottingham and Pfeffer, 2009).

2.3.2 RAB membrane insertion and extraction

RAB proteins cycle between a cytosolic and a membrane bound form (**Figure 2.4**). In order to reversibly bind to membranes, RABs, but also RAS and RHO/RAC proteins, need to be prenylated at their C-terminal cysteine residues (**Figure 2.5**) (Zhang and Casey, 1996). Prenylation is a posttranslational modification that was discovered in the late 1970s but was only described for RABs more than 10 years later (Farnsworth *et al.*, 1991; Khosravi-Far *et al.*, 1992).

Prenylation consists in the addition of either a farnesyl (**Figure 2.5A**) or geranylgeranyl group (**Figure 2.5B**) at the C-terminus of target proteins and is catalyzed by 3 different enzymes. Farnesyltransferase (FTase) and geranylgeranyltransferase I (GGTase I) both recognize C-terminal CAAX motifs (C is a Cysteine, A is an aliphatic amino acid and X is any amino acid) and attach a single farnesyl or geranylgeranyl group to the cysteine via a thioester linkage (Seabra *et al.*, 1991). If X is a methionine, serine, glutamine, or alanine, the substrate is farnesylated whereas if it is a leucine or phenylalanine, the protein is geranylgeranylated. Conversely, RAB geranylgeranyl transferase (RABGGTase, also called GGTase II) catalyzes the addition of usually two geranylgeranyl groups on a di-cysteine motif (CC, CXC or CCXX) at the C-terminal extremity of RAB proteins (**Figure 2.5B**) (Seabra *et al.*, 1992).

After their synthesis, RAB proteins first bind the RAB escort protein (REP) which then presents the RAB to the RABGGTase for geranylgeranylation (**Figure 2.4**) (Alexandrov *et al.*, 1999; Andres *et al.*, 1993). The subsequent binding of a new geranylgeranylpyrophosphate (GGpp) substrate molecule to the active site of the RABGGTase leads to RAB dissociation from the REP and delivery to the target membrane (Thoma *et al.*, 2001a; Thoma *et al.*, 2001b). It is important to note that some RABs, such as RAB8 and RAB13, display a mono-cysteine CAAX motif at their C-terminus and are modified by a single geranylgeranyl moiety (Joberty *et al.*, 1993). This monoprenylation reaction seems to still be mediated by REP and RABGGTase (Gomes *et al.*, 2003; Wilson *et al.*, 1998). It has also been suggested that the mono- and diprenylation motifs are important for RAB specific membrane targeting possibly because of the higher hydrophobicity of the double lipid modification or the preferential recognition of double prenylated RABs by regulatory proteins (Calero *et al.*, 2003; Gomes *et al.*, 2003).

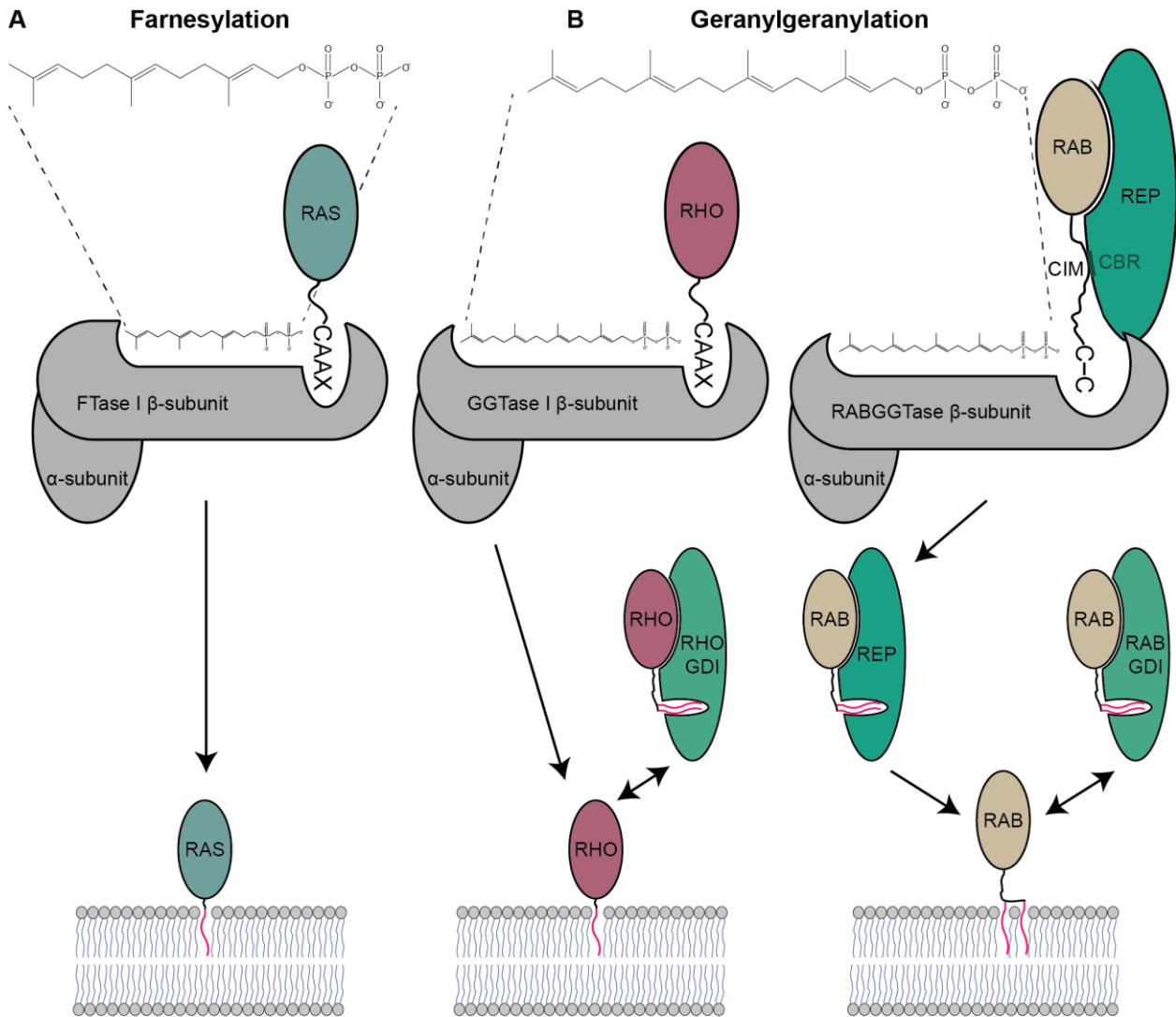


Figure 2.5: Mechanisms of protein prenylation. Most members of the RAS superfamily (RAS, RHO and RAB proteins) are prenylated, at their C-terminus, by prenyl transferases. Prenylation consists in the addition of a (A) farnesyl group (substrate is farnesylpyrophosphate) by a farnesyl transferase, specific to RAS proteins, or in the addition of (B) one or two geranylgeranyl groups (substrate is geranylgeranylpyrophosphate) by geranylgeranyl transferases for RHO and RAB proteins. Farnesyl transferase (FTase) and geranylgeranyl transferase I (GGTase I) recognize the CAAX (C is a cysteine, A is an aliphatic amino acid and X is any amino acid) motif at the protein C-terminus. In contrast, the RAB geranylgeranyl transferase (RABGGTase) does not recognize any specific motif. RAB proteins interact with the RAB escort protein (REP) by forming two binding interfaces: the first is between the RAB-binding platform and effectors loops of the RAB protein; and the second is between the C-terminal-binding region (CBR) and the CBR interacting motif (CIM). The REP then recruits the RABGGTase for prenylation and subsequently directs the RAB to the target membrane. GDP-bound RHO and RAB proteins can get extracted from membranes and recycled back to their original compartment by GDP dissociation inhibitors (RHOGDI and RABGDI respectively). Adapted from (Guo *et al.*, 2008).

Once membrane bound RAB proteins have fulfilled their functions, they need to be extracted from membranes and recycled back to the donor compartment (**Figure 2.4**). The protein responsible for this was originally identified as a RAB3 interacting protein that inhibited the dissociation of GDP and was thus named GDP dissociation inhibitor (GDI) (Sasaki *et al.*, 1990). Interestingly, RABGDI and REP were shown to be structurally very homologous to each other (Alory and Balch, 2001). However, even though both REP and GDI were shown to bind GDP-bound RABs with higher affinity as compared to GTP (Wu *et al.*, 2010), REP displayed higher affinity for unprenylated RABs whereas GDI displayed higher affinity for the prenylated form (Wu *et al.*, 2007). This ensures that RAB interaction with GDI only occurs once their trafficking cycle is completed and they have been inactivated.

Due to the high affinity of the RAB:GDI complex, the intrinsic rate of GDI dissociation is very low which hence limits the rate of RAB recycling and consequently of active RAB generation (Shapiro and Pfeffer, 1995). This led to the assumption that possible mechanisms exist to accelerate this process.

Some studies suggested that the YIP3/PRA1 protein might function as a GDI dissociation factor (GDF) that is able to dissociate RAB proteins from high affinity RAB:GDI complexes to catalyze the final step of their recycling to the donor compartment (Dirac-Svejstrup *et al.*, 1997; Sivars *et al.*, 2003). YIP proteins have consequently been considered as potential GDFs for various RAB proteins (Barrowman and Novick, 2003). The absolute requirement for GDFs has however been disputed as the GEF activity of the *Legionella pneumophila* DrrA/SidM was shown to be sufficient to displace GDI from the RAB:GDI complex (Schoebel *et al.*, 2009). Additional studies demonstrated that deletion of YIP proteins did not alter the localization of YPT7 (Cabrera and Ungermann, 2013), again arguing against the role of YIP proteins as potential GDFs.

Other studies showed that, after spontaneous dissociation of RAB:GDI complexes, phosphocholination and adenylation respectively mediated by AnkX and DrrA/SidM from *Legionella pneumophila*, can inhibit the reformation of the RAB:GDI complexes (Oesterlin *et al.*, 2012). It was at that time thought that human cells could naturally use similar mechanisms to displace RABs from GDI. This was recently confirmed when phosphorylation of RAB1 at the switch II region by TGF- β activated kinase I was shown to preferentially occur when RAB1 is GDP-bound, and to consequently disrupt RAB-GDI interaction (but not interactions with GEF or GAP proteins) (Levin *et al.*, 2016).

Other RAB phosphorylations at different positions of their primary sequence have been reported. RAB4 was shown to be phosphorylated at Ser₂₀₄ near to the C-terminal cysteines and this was described to regulate its localization during cell cycle progression (Bailly *et al.*, 1991; van der Sluijs *et al.*, 1992a). RAB8 and RAB13 were also shown to be phosphorylated at Ser_{III} by PTEN-induced kinase 1. Phosphorylation of RAB8 was at the same time shown to negatively regulate its activation by its cognate GEF Rabin8 (Lai *et al.*, 2015). Interestingly, phosphorylation events seem to rather negatively regulate the membrane insertion of some RAB proteins.

Some RAB proteins can undergo additional C-terminal modifications following geranylgeranylation, such as proteolysis and/or carboxyl methylation, depending on their prenylation motif. Similarly to RAS and RHO GTPases, CAAX motifs-containing RAB proteins undergo proteolytic cleavage of the AAX tripeptide which allows the exposure of the C-terminal cysteine (Leung *et al.*, 2007). Following proteolysis, RAB proteins exhibiting CAAX but also CXC motifs at their C-terminal extremity are methylated (Leung *et al.*, 2007; Smeland *et al.*, 1994). RAB carboxyl methylation, which consists in the addition of a carboxyl group to the exposed prenylated cysteine, was shown to enhance the hydrophobicity of the C-terminus and subsequently to increase membrane affinity (Michaelson *et al.*, 2005; Silvius and l'Heureux, 1994). Methylation was subsequently shown to be required for RAS (Michaelson *et al.*, 2005) but not for RAB (Leung *et al.*, 2007) proper localization. Both studies also observed an increase of protein cytosolic pool in the absence of methylation, which appears to be related to increased RHO/RAC:GDI and RAB:GDI affinities.

2.4 Membrane targeting of RAB GTPases

RAB proteins have been shown to localize to specific compartments, thereby defining organelle identity (Zerial and McBride, 2001; Zhen and Stenmark, 2015) (**Figure 2.6**); and this is thought to be crucial for the control and directionality of vesicular trafficking. The mechanisms regulating specific RAB membrane targeting and localization are thus of great interest to understand intracellular transport events. The question of RAB protein targeting to specific membranes was initially probed 25 years ago and many have tried to answer this question. Originally, RAB membrane targeting was thought to be mediated by the RAB hypervariable C-terminal domain (Chavrier *et al.*, 1991). Although this region was confirmed to be important for the specific localization of some RAB proteins (Li *et al.*, 2014), other studies demonstrated that this is not

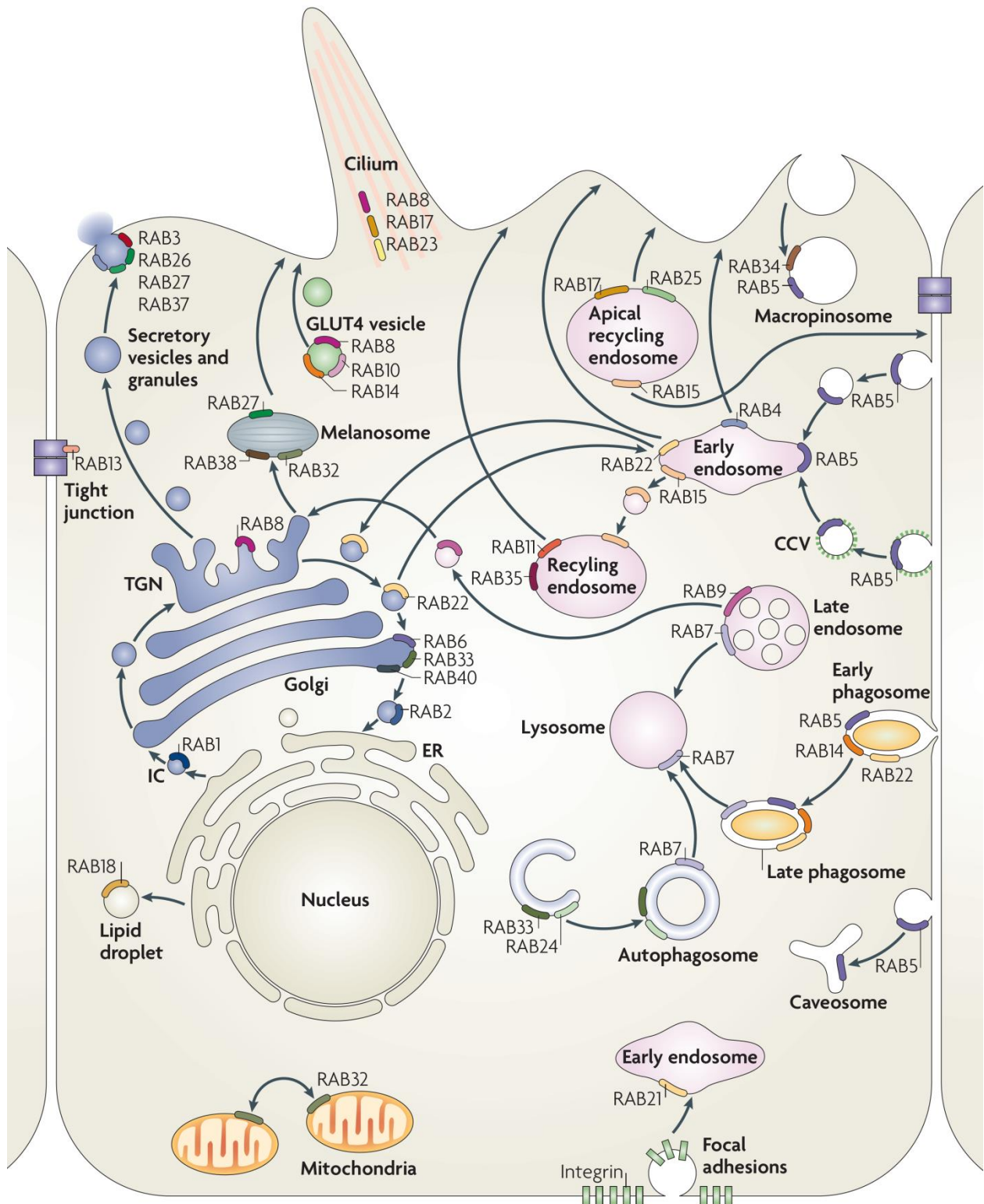


Figure 2.6: Subcellular localization of RAB proteins. All RAB GTPases localize to specific membranes and are involved in specific transport pathways. Detailed information about the different RAB proteins used in this study (RAB1, RAB4, RAB5, RAB6, RAB11 and RAB35) can be found in the last part of this chapter. Specific localization and function of the other RABs will be detailed here. RAB2 localizes to the ER-Golgi intermediate compartment and is involved in Golgi-ER trafficking. RAB33 and RAB40 localize to the Golgi

Chapter 2: RAB GTPases

and regulate intra-Golgi transport (RAB33 also involved in autophagosome formation with RAB24). RAB8 is found on the plasma membrane and mediates *trans*-Golgi network to plasma membrane transport, ciliogenesis (together with RAB17 and RAB23) and GLUT4 vesicle translocation (together with RAB10 and RAB14). RAB3 (secretory vesicles, plasma membrane), RAB26 (secretory granules), RAB27 (melanosomes) and RAB37 (secretory granules) are all involved in exocytic events. RAB32 and RAB38 both localize to melanosomes and are involved in their biogenesis; RAB32 is also found on mitochondria and was shown to play a role in mitochondria fission. RAB13 is involved in tight junction assembly between cells. RAB18 regulates lipid droplet formation. RAB21 and RAB22 are both found on early endosomes; and respectively mediate integrin endocytosis and TGN-early endosomes transport / early phagosome maturation (together with RAB5 and RAB14). RAB15 localizes to early and recycling endosomes and is involved in trafficking between these two compartments and to the plasma membrane. RAB17 mediates the transport between recycling endosomes and the plasma membrane. RAB7 mostly localizes to late endosomes and lysosomes and is involved in late endosome / phagosome maturation. From (Stenmark, 2009).

always the case and that additional sequence motifs of RAB proteins also play a key role (Ali *et al.*, 2004; Beranger *et al.*, 1994).

In relation to this, studies suggested that RAB protein interaction with some effectors could also mediate RAB specific localization. As an example, mutations of RAB7 specific RABSF1 and RABSF4 domains led to RAB7 mislocalization. This was suggested to be due to the absence of interaction with the effector RILP, which is known to partially interact with these parts of the RAB7 sequence (Wu *et al.*, 2005). Another study has shown that a chimeric construct consisting of RAB5 with the C-terminal hypervariable domain of RAB9 was re-localized to late endosomes (where RAB9 is originally found) (Aivazian *et al.*, 2006). This has been suggested to be due to the interaction of the RAB9 C-terminus with its effector TIP47, and was confirmed when the abrogation of RAB9-TIP47 interaction (through TIP47 mutation) failed to localize the chimeric RAB5/RAB9 protein to late endosomes (Aivazian *et al.*, 2006).

A role in membrane targeting was also suggested for GEFs, since they can catalyze the activation of RAB proteins and consequently stabilize them on membranes (Blumer *et al.*, 2013; Schoebel *et al.*, 2009). Indeed, the *Legionella pneumophila* protein DrrA, a GEF for RAB1 was shown to displace GDI from RAB1:GDI complexes and to subsequently activate RAB1 (Schoebel *et al.*, 2009); and mistargeting of DrrA, Rabex-5 and Rabin-8 (known GEFs for RAB1, RAB5 and RAB8 respectively) to mitochondria led to RAB1A, RAB5A and RAB8A mislocalization to the same compartment (Blumer *et al.*, 2013).

As already mentioned, membrane localized GDFs are thought to allow the dissociation of GDIs from RABs and thus to contribute to membrane specific localization (Dirac-Svejstrup *et al.*, 1997; Sivars *et al.*, 2003) but this matter is still debated as it was later suggested that GDFs are not absolutely required for RAB membrane targeting (Cabrera and Ungermann, 2013; Schoebel *et al.*, 2009).

In conclusion, RAB specific membrane targeting seems to be mediated by a plethora of factors, such as GDFs, GEFs, effector proteins and RAB C-terminal hypervariable region.

Most studies so far have focused on protein factors, but one cannot forget that RAB proteins are peripheral membrane-bound proteins that localize to specific membranes exhibiting specific composition and physical properties. In relation to this, there is strong evidence that membrane-bound molecules are not randomly distributed in the membrane bilayer but are enriched in membrane domains of varying lipid compositions (Mukherjee and Maxfield, 2000). Good examples are the glycosylphosphatidyl-inositol anchor proteins which were shown to preferentially localize to lipid rafts at the plasma membrane (Paulick and Bertozzi, 2008) but also other lipidated proteins such as N-RAS, H-RAS and K-RAS that were respectively described to preferentially bind to lipid packing defects (Larsen *et al.*, 2015; Larsen *et al.*, 2017), lipid rafts and disordered membranes in a GTP-dependent manner (Prior *et al.*, 2001); and negatively charged membranes (Gulyas *et al.*, 2017; Jang *et al.*, 2015).

Interestingly, clear compartmentalization of RAB5, RAB4 and RAB11 within the endosomal membrane has also been observed (Sonnichsen *et al.*, 2000). In this study, three main populations of endosomes could be distinguished: one that is only composed of RAB5, another one that contains both RAB5 and RAB4 and a third one that harbours RAB4 and RAB11. Although it was proposed that effector protein recruitment and clustering might mediate the formation of RAB membrane domains through simultaneous effector interaction with RABs and specific lipids (Zerial and McBride, 2001), another possible explanation could consist in the direct binding of RAB proteins to membrane domains exhibiting differential geometry and physicochemical properties (curvature, order, charge). The study from Sonnichsen also demonstrates that on the same endosomal membrane, RAB5 localizes to globular structures whereas RAB4 is found on tubular (and thus more curved) structures (Sonnichsen *et al.*, 2000), thus suggesting that some RAB proteins might preferentially bind to curved membranes.

2.5 RAB GTPases and vesicular transport

2.5.1 General mechanism of intracellular transport

Intracellular membrane trafficking, which allows the exchange of material between the different cellular organelles, can broadly be divided into two distinct pathways. The secretion pathway, which was the first one to be described (Duve, 1975; Palade, 1975), consists in the transport of newly synthesized secretory proteins from the endoplasmic reticulum (ER) to and through the Golgi complex, release from the Golgi to secretory vesicles and final delivery to the extracellular space (Bonifacino and Glick, 2004). In contrast to this directed transport toward the cell exterior, the endocytic pathway can be described as an inward-bound pathway from the cell exterior to the endosomal and lysosomal compartments. The transport of proteins or lipids from the ER towards the plasma membrane, endosomes or lysosomes is referred to as the anterograde pathway. In contrast to this, proteins and lipids can also be recycled from the cell surface/endosomes back to intracellular compartments through the retrograde pathway (Bonifacino and Rojas, 2006; Johannes and Popoff, 2008). Intracellular membrane transport has been extensively studied in the last decades and led to the identification of a complex variety of lipids and proteins, including RABs, involved in the regulation of this process (Cai *et al.*, 2007a; Hutagalung and Novick, 2011; Stenmark, 2009).

The transport of vesicles from one compartment to the other occurs through different steps, all of which are to some extent regulated by RAB GTPases (**Figure 2.7**).

The recruitment and assembly of coat proteins (Clathrin, COPI, COPII) leads to membrane distortion and consequently to vesicle budding from the donor compartment. The selective incorporation of cargoes into the forming vesicles is mediated by adaptor proteins and their activation can be mediated by RAB proteins (**Figure 2.7A**). As an example, in the recycling of mannose-6-phosphate receptors from late endosomes to the *trans*-Golgi network, the cytosolic tail of the receptor is recognized by the sorting adaptor TIP47, a known RAB9 effector (Carroll *et al.*, 2001).

After vesicle budding, partial vesicle uncoating occurs. Membrane dissociation of COPI coats is thought to mostly be mediated by ARFI GTP hydrolysis (Bigay *et al.*, 2003; Tanigawa *et al.*, 1993) whereas COPII dissociation is achieved through SARI GTP hydrolysis (Aridor *et al.*, 1995; Yoshihisa *et al.*, 1993). RAB proteins have also been proposed to play a role in this process

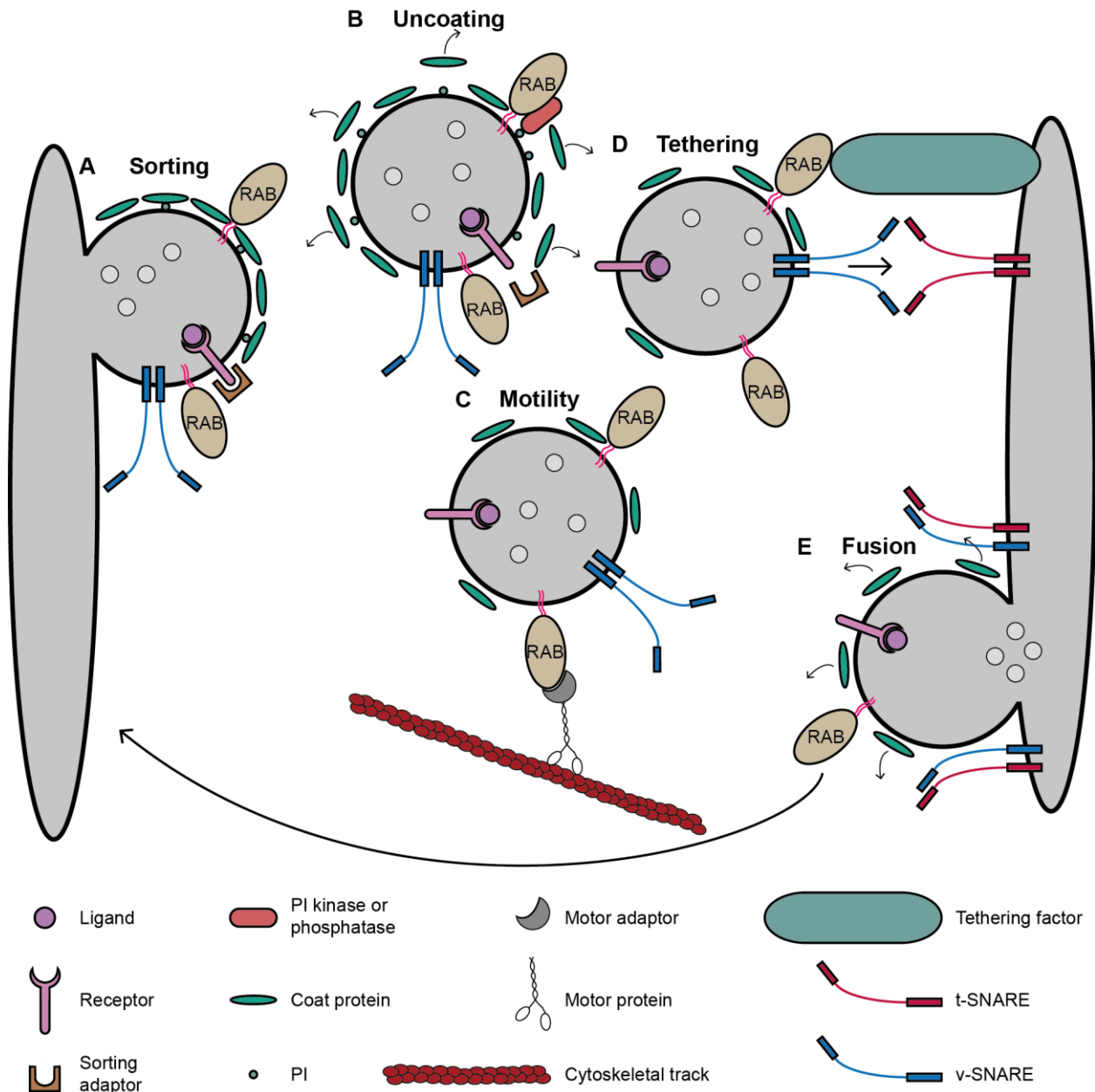


Figure 2.7: RAB proteins are involved in all steps of vesicular transport. (A) During vesicle budding, RAB proteins can activate sorting adaptors to selectively incorporate cargoes into the vesicle. (B) After vesicle fission, coat proteins are partially dissociated from the vesicle. RAB proteins can recruit phosphoinositide (PI) kinases or phosphatases leading to the dissociation of PI binding coat proteins. (C) RAB proteins can mediate vesicle movement on cytoskeletal tracks either by interacting with motor adaptors or directly with motor proteins. (D) Membrane recognition and vesicle tethering can be mediated by RAB proteins through their interaction with tethering factors. (E) These tethering factors can simultaneously recruit SNARE proteins (soluble N-ethylmaleimide-sensitive factor attachment protein receptor) and allow SNARE complex assembly and subsequent vesicle fusion with the acceptor compartment. Adapted from (Stenmark, 2009).

(**Figure 2.7B**) through the recruitment of PI kinases or phosphatases (Christoforidis *et al.*, 1999; Shin *et al.*, 2005) which alter the vesicle composition and can consequently cause the dissociation of PI-binding protein coats (Haucke, 2005).

Cargo containing vesicles are then transported to their final destination by diffusion or by motor-mediated transport along cytoskeletal tracks. RAB proteins are also involved in this process through recruitment of motor adaptor proteins or direct interaction with motors (**Figure 2.7C**) (Hammer and Wu, 2002; Seabra and Coudrier, 2004).

Dyneins and kinesins are microtubule-based motors which move towards the minus end and either the plus or minus end of microtubules, respectively. The best described example of RAB-kinesin direct interaction is between RAB6 and KIF20A (originally called Rabkinesin-6) (Echard *et al.*, 1998) which mediates transport from the Golgi and was shown to be required for successful cleavage furrow and cytokinesis (Hill *et al.*, 2000). Many studies however indicate that RAB proteins, such as RAB 3, 6, 9, 11 and 27 mostly interact indirectly with motors via adaptor proteins (Horgan and McCaffrey, 2011). Another type of indirect interaction can be illustrated with RAB5 and KIF16B. RAB5 recruits VPS34, a phosphoinositide 3-kinase, to early endosomes. VPS34 locally synthesizes PI(3)P and consequently recruits KIF16B (Hoepfner *et al.*, 2005).

While some RAB proteins, such as endosomal RAB4, were shown to directly interact with dynein motors (Bielli *et al.*, 2001), most RAB-dynein interactions are indirect. RAB11 associates with dynein-I through the binding of its effector FIP3 to the LIC1 and LIC2 (light intermediate chain) subunits (Horgan *et al.*, 2010). RAB7 associates with the cytoplasmic dynein-I-dynactin motor complex through the binding of its effector RILP to the dynactin p150^{Glued} subunit (Jordens *et al.*, 2001). RAB6 was also shown to interact with the p150^{Glued} subunit of the dynactin complex and with the dynactin-interacting protein Bicaudal D2 (Short *et al.*, 2002).

Myosins are actin-based motors which, with the exception of Myosin VI, move towards the barbed (+) end of actin filaments. The best characterized RAB-Myosin interactions involve mainly class V myosins. RAB27 and Myosin Va interact with each other through Melanophilin and MyRIP (Myosin and RAB interacting protein), which allows the regulation of melanosome transport in melanocytes (El-Amraoui *et al.*, 2002; Matesic *et al.*, 2001). Later on, Myosin Va was shown to directly associate with RAB3A (Wollert *et al.*, 2011), RAB8A/RAB10 (Roland *et al.*, 2009), and to multiple other RABs, including RAB6, RAB14 and RAB39B, via three distinct RAB-binding domains (Lindsay *et al.*, 2013). Additionally, RAB6 regulates the fission of transport vesicles from the Golgi through its direct interaction with Myosin II (Miserey-Lenkei *et al.*, 2010).

Finally, vesicle fusion with the acceptor compartment is mediated by the pairing of SNAREs (soluble N-ethylmaleimide-sensitive factor attachment protein receptor) (**Figure 2.7E**) (see (Jahn and Scheller, 2006) for extensive review about SNAREs). A SNARE on a transport vesicle (v-SNARE) interacts with its cognate SNARE-binding partner (t-SNARE) and forms a complex. The free energy release, derived from the SNARE complex assembly, is able to overcome the repulsive forces between opposing bilayers and to subsequently drive the fusion of the two opposite membranes (Hanson *et al.*, 1997; Jena, 2008). RAB proteins are also involved in this process through interaction with proteins that regulate SNARE function (Novick *et al.*, 2006; Ohya *et al.*, 2009). As an example, two RAB5 effector proteins EEA1 (early endosome antigen 1) and Rabenosyn-5 respectively interact with the SNARE proteins Syntaxin-6 and Syntaxin-13 (McBride *et al.*, 1999; Simonsen *et al.*, 1999), and VPS45, a member of the SEC1 family of SNARE regulators (Morrison *et al.*, 2008; Nielsen *et al.*, 2000).

2.5.2 RABs and membrane tethering

Prior to vesicle fusion, the interaction between the vesicle and its target membrane needs to be established and this is referred to as membrane tethering (**Figure 2.7D**). Proteins and protein complexes called tethers or tethering factors are key to this process (Brocker *et al.*, 2010; Sztul and Lupashin, 2006). All tethering factors can broadly be divided into two categories: coiled-coil tethers and multi-subunit tethers. Tethering is mostly achieved through tether interactions with RAB GTPases (Hutagalung and Novick, 2011; Stenmark, 2009) (**Figure 2.8A** and **Figure 2.8B**) and coat proteins (**Figure 2.8C**) (Cai *et al.*, 2007a; Trahey and Hay, 2010). A large number of tethers are RAB effectors and some have been described to also act as RABGEFs.

Most coiled-coil tethers have been found in the Golgi and are now referred to as Golgins (Short *et al.*, 2005). Due to their large size and elongated structure (up to 3000 residues) they are able to bridge distances of more than 200 nm. They also exhibit multiple RAB binding sites in their structure (**Figure 2.8A**). Because of these properties Golgins are thought to potentially serve as scaffolds to recruit RAB containing vesicles to the correct side of the Golgi (Sinka *et al.*, 2008). The previously mentioned RAB5 effectors EEA1 and Rabenosyn-5 involved in SNARE-mediated membrane fusion were also identified as coiled-coil tethering factors (Nielsen *et al.*, 2000; Simonsen *et al.*, 1998). Both effectors possess a FYVE domain that binds PI(3)P which is usually found on early endosomes. Specific RAB effectors can therefore connect membranes and simultaneously recruit specific SNARE proteins that mediate fusion (Dubuke and Munson, 2016).

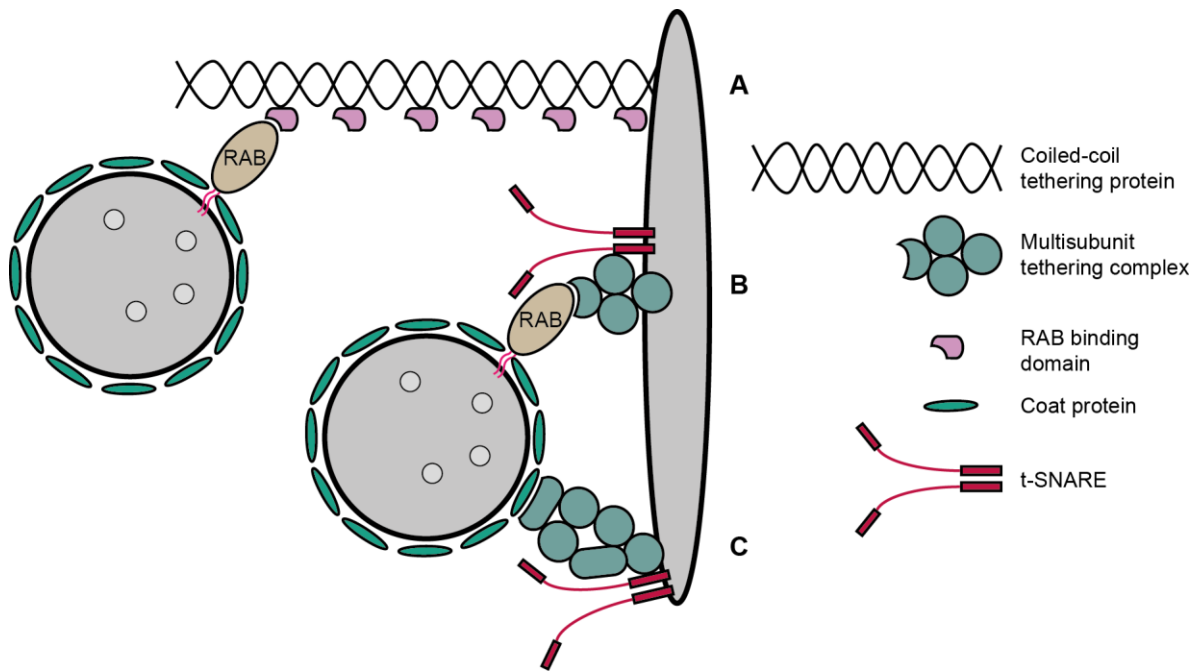


Figure 2.8: Mechanisms of vesicle recognition and tethering. Tethering is mostly achieved through tether interaction with RAB proteins (A and B) or with coat proteins. (C). (A) RAB proteins can recognize coiled coil tethering factors which exhibit multiple RAB binding sites and are able to bridge long distances. Multi-subunit tethering complexes can also mediate vesicle tethering via their interaction with RAB (B) or coat (C) proteins. Some tethering factors might also recruit SNAREs or their regulators and thereby can also regulate vesicle fusion. Adapted from (Brocker *et al.*, 2010).

Multi-subunit tethering complexes can be divided into two general groups: those required for membrane fusion with organelles of the secretory pathway (Dsl1p, COG, GARP, exocyst) and those of the endo-lysosomal pathway (CORVET and HOPS). Each of these protein complexes, except Dsl1p, were shown to act as RAB protein effectors (**Figure 2.8B**) (see (Brocker *et al.*, 2010) for extensive review) and they all seem to couple the recognition of membranes via RAB GTPases with the subsequent SNARE-mediated membrane fusion, again demonstrating that membrane tethering and fusion are closely related processes (Dubuke and Munson, 2016).

The TRAPP complexes, known to act as GEFs for RAB1/YPT1 and YPT31/YPT32 (Jones *et al.*, 2000; Wang *et al.*, 2000) were shown to promote membrane tethering through their interaction with COPII proteins (Cai *et al.*, 2007b; Sacher *et al.*, 2001) and can thus also be referred to as tethering factors.

Thus, abundant evidence indicates that RAB proteins and their effectors promote membrane tethering. However, tethering activity was originally mostly assessed *in vivo*, or by using cell extracts. Due to the large amount of molecules in these systems, it remains very challenging to

identify their precise mode of action; some might directly mediate tethering while others only act as upstream regulators that promote tethering but do not directly mediate it. As a consequence, more and more biological processes were reconstituted *in vitro* using minimal reaction systems of purified components, in order to explore more precisely their mechanisms of action (Cheung *et al.*, 2015; Drin *et al.*, 2008; Lurick *et al.*, 2017; Murray *et al.*, 2016).

Interestingly, by using this type of chemically defined system, the yeast RAB5 ortholog VPS21 as well as other endosomal RAB proteins from *Saccharomyces cerevisiae* (YPT10 and YPT53) were shown to undergo GTP-regulated RAB-RAB interactions that directly drive membrane tethering *in vitro*, without the need of any effectors (**Figure 2.9A** and **Figure 2.9B**) (Lo *et al.*, 2011). VPS21-mediated vesicle tethering could be observed by using a liposome-based *in vitro* system (His-tag VPS21 proteins interact with Nickel-NTA-DOGS-containing liposome and subsequent liposome tethering is observed by quasi-elastic light scattering) (**Figure 2.9A**). This tethering effect could only be observed when VPS21 was preloaded with GTP, and was shown to be positively regulated by VPS9 (GEF for VPS21) and inhibited in presence of GYPI (VPS21 GAP protein). Additionally, by using a bead-liposome assay, vesicle tethering was shown to occur in a symmetric manner, with VPS21 anchored to two opposite membranes and subsequent vesicle tethering mediated by VPS21 dimerization or oligomerization *in trans* (**Figure 2.9B**). Finally, heterotypic vesicle tethering was shown to occur as well through VPS21 interaction with two other endosomal RABs, YPT10 and YPT53.

The VPS21 intrinsic tethering capacity was finally suggested to act in concert with other effector tethers and SNAREs to mediate membrane recognition, tethering and fusion events during endosomal transport.

Furthermore, during the course of my thesis, a study has demonstrated that human RAB5A, but also RAB2A (ER/Golgi localized) and RAB7A (late endosome/lysosome localized) also drive vesicle tethering *in vitro* without the need of any additional components (**Figure 2.9C** and **Figure 2.9D**) (Tamura and Mima, 2014). Vesicle tethering was observed using three different methods consisting of streptavidin-bead assays (**Figure 2.9C**), turbidity assays and fluorescence microscopy (**Figure 2.9D**). The nucleotide dependency of this effect was not extensively assessed using RABs preloaded with GTP or GDP or using specific GEFs and GAPs and thus no conclusion was made on this point.

This additional study also suggests that RAB proteins could potentially directly drive membrane tethering during vesicle transport events, possibly via a RAB-RAB interaction.

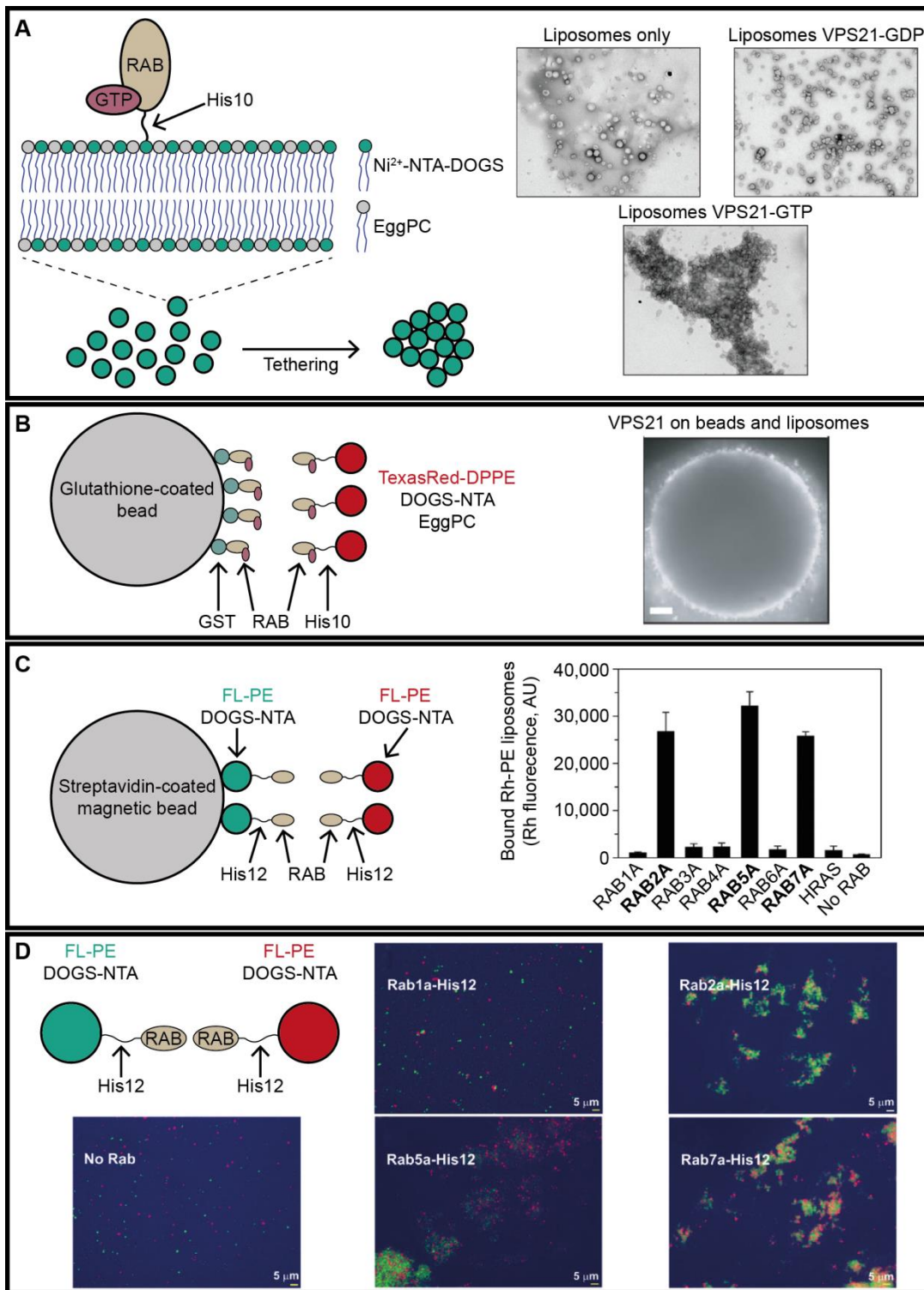


Figure 2.9: RAB proteins can directly drive vesicle tethering *in vitro*. (A) Poly-histidine tagged VPS21 was incorporated into liposomal membranes containing Nickel-NTA-DOGS lipids and liposome tethering was observed by quasi-elastic light scattering in presence of GTP-bound VPS21 only. Adapted from (Lo *et al.*, 2011). (B) Using epifluorescence microscopy, GST tagged VPS21 immobilized on glutathione coated beads were shown to interact with the previously mentioned VPS21 containing liposomes (made fluorescent with TexasRed DPPE) thereby suggesting that vesicle tethering is mediated by VPS21 dimerization/

oligomerization in *trans*. Adapted from (Lo *et al.*, 2011). (C) Using a similar bead-liposome assay (liposomes labeled with Rhodamine PE), RAB2A, RAB5A and RAB7A were shown to induce vesicle tethering. Adapted from (Tamura and Mima, 2014). (D) Using fluorescence microscopy, the same poly-histidine tagged RAB proteins, incorporated into two differently labeled liposome populations (Rhodamine PE and fluorescein PE), were shown to induce liposome aggregation. Adapted from (Tamura and Mima, 2014).

It is important to note that membrane tethering events (with no subsequent fusion) can also mediate transient contact sites mostly between the ER and other organelles such as Golgi, Mitochondria, endosomes, plasma membrane and lipid droplets. These membrane contact sites have been described to be crucial for the exchange of material such as lipids (especially cholesterol) and Ca^{2+} between compartments (see (Jackson *et al.*, 2016; Phillips and Voeltz, 2016) for extensive reviews). RAB7 was shown to promote ER-late endosome contact sites through its interaction with Protrudin, an ER localized protein (Raiborg *et al.*, 2015). It has been suggested that these contact sites may be regulated by activated RAB7 since Protrudin-RAB7 interaction only occurs when RAB7 is GTP-bound and expression of dominant-active RAB7 (RAB7Q67L mutant) leads to an increasing amount of contact sites (Raiborg *et al.*, 2015).

As membrane tethering was also shown to occur *in vitro* in the unique presence of RAB proteins (Lo *et al.*, 2011; Tamura and Mima, 2014), the formation of contact sites between organelles could also be driven by heterotypic interactions of RAB proteins from two opposite membranes.

2.6 Focus on the RAB proteins used in this study

2.6.1 RAB1 and the ER-Golgi intermediate compartment

RAB1 has been highly conserved through evolution. It was shown to be a functional homolog of YPT1 (Haubruck *et al.*, 1989) and exists as two isoforms RAB1A and RAB1B which share 93% amino acid identity. RAB1 was firstly shown to localize to the Golgi (Preuss *et al.*, 1992; Segev *et al.*, 1988) and has also later been shown to localize to the pre-Golgi intermediate compartment (Saraste *et al.*, 1995). RAB1 was first suggested to regulate the anterograde transport of cargoes between the ER and the *cis*-Golgi (Plutner *et al.*, 1991; Tisdale *et al.*, 1992) but subsequent studies have shown that RAB1 is also required for retrograde transport in *Saccharomyces cerevisiae* (Kamena *et al.*, 2008) and seems to play a role in autophagy (Huang *et al.*, 2011; Zoppino *et al.*, 2010). Interestingly, RAB1 is also important for Golgi biogenesis and structure maintenance (Galea *et al.*, 2015), as well as for the extension of the intermediate compartment in the pericentriolar region

(Marie *et al.*, 2009). Most RAB effectors were identified as tethering factors (COG complex, Golgin-84, etc.) (Sato *et al.*, 2003; Suvorova *et al.*, 2002), therefore highly suggesting that RAB is mostly involved in the regulation of vesicle-compartment tethering during transport.

2.6.2 RAB6 and the Golgi

RAB6 is another *RAB* gene conserved from yeast to humans (Pereira-Leal and Seabra, 2001). In human, the *RAB6* subfamily is composed of the splice variants *RAB6A* and *RAB6A'* (Echard *et al.*, 2000) which differ by only 3 amino acids but were shown to play non-overlapping roles (**Figure 2.10**) (Del Nery *et al.*, 2006); and *RAB6B* which displays 91% identity to *RAB6A* (most amino acid differences located at the C-terminal hypervariable region) and is preferentially expressed in neuronal cells (Opdam *et al.*, 2000). A divergent *RAB6* isoform named *RAB6C* has also been identified (Shan *et al.*, 2002; Simpson *et al.*, 2000). *RAB6C*, which is very homologous to *RAB6A'* (97%) but possess an additional C-terminal extension of 46 amino acids, was reported to be a primate-specific retrogene derived from a *RAB6A'* transcript (Young *et al.*, 2010). *RAB6C*, which was shown to localize to the centrosome and was suggested to play a role in cell cycle progression (Young *et al.*, 2010), is less abundant and less stable than *RAB6A'*, does not localize to membranes and exhibits a reduced GTP-binding affinity.

All *RAB6A/A'* and *B* localize to the *medial* and *trans* Golgi cisternae and *trans*-Golgi network (TGN) as well as on dynamic tubulovesicular carriers that move along microtubules (Nizak *et al.*, 2003). *RAB6* was shown to regulate trafficking from endosomes to the Golgi (**Figure 2.10**) (Mallard *et al.*, 2002; Young *et al.*, 2005). This is thought to partially be mediated by the involvement of *RAB6* in the targeting and tethering of endosome derived vesicles to the TGN membrane, through its interaction with the multi-subunit tether GARP (Liewen *et al.*, 2005; Perez-Victoria and Bonifacino, 2009).

The major pool of *RAB6* is located on Golgi membranes and *RAB6* has been suggested to play a key role in intra-Golgi transport and Golgi homeostasis (**Figure 2.10**). *RAB6* associates with several golgins (Short *et al.*, 2005) and other tethering factors such as the COG complex (Fukuda *et al.*, 2008), and thereby drives intra-Golgi membrane tethering.

Finally, *RAB6* was also suggested to be implicated in Golgi-to-ER (White *et al.*, 1999) and Golgi-to-plasma membrane (Grigoriev *et al.*, 2007) transport (**Figure 2.10**) where it can trigger myosin II and actin -dependent fission of transport carriers (Miserey-Lenkei *et al.*, 2010) but also act in cooperation with its effector Bicaudal D2 to recruit the dynamin/dynactin motor complex

necessary for vesicle translocation (Matanis *et al.*, 2002; Short *et al.*, 2002). Finally, RAB6 was also shown to be involved in mitosis and cytokinesis (Bardin *et al.*, 2015; Miserey-Lenkei *et al.*, 2006).

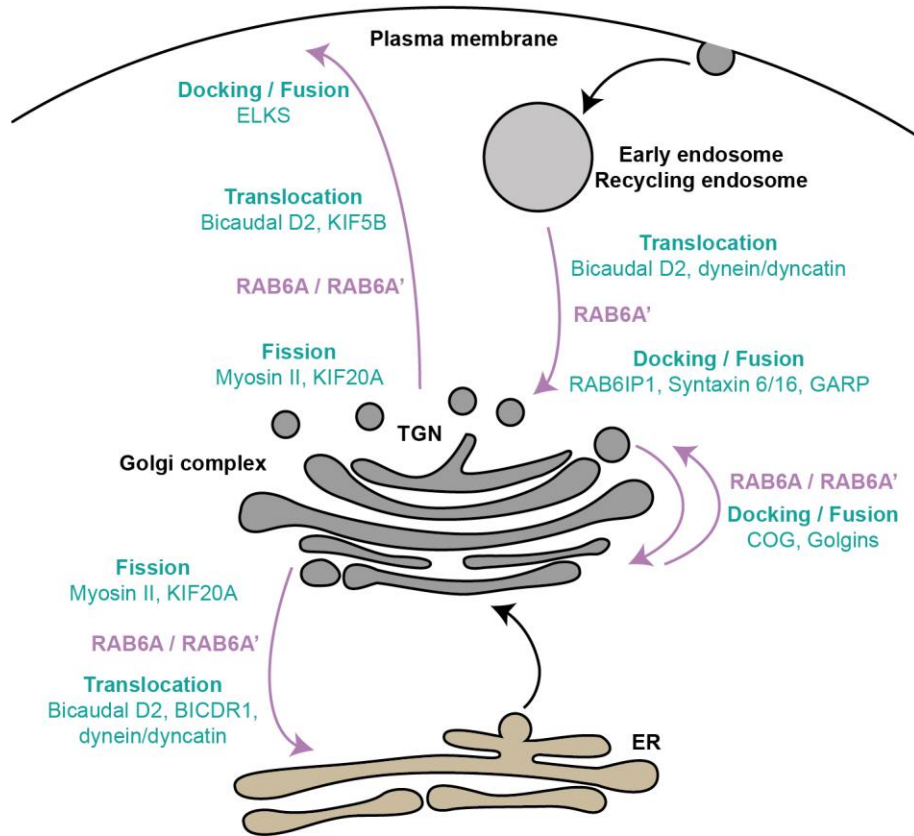


Figure 2.10: RAB6 regulates multiple trafficking pathways to and from the Golgi. RAB6A and RAB6A' are involved in retrograde trafficking from the endosomal compartments to the Golgi and from the Golgi to the ER. RAB6 is also implicated in intra-Golgi transport and Golgi to plasma membrane transport. RAB6 mediates fission of transport carriers through its direct interaction with Myosin II. RAB6 regulates vesicle motility in cooperation with Bicaudal D2 and the dynamin/dynactin complex. Finally, RAB6 also plays a role in vesicle docking and fusion with the acceptor compartment through its interaction with tethering factors (GARP, COG, Golgins) and direct or indirect recruitment of SNARE proteins. Adapted from (Valente *et al.*, 2010).

2.6.3 RAB4 / RAB5 / RAB11 and the endosomal system

As a very general picture, the entry of cargoes from the plasma membrane to early endosomes (EEs) is mediated by RAB5 (**Figure 2.11**). Cargoes can eventually be recycled back to the cell surface by a fast RAB4-mediated pathway and a slow RAB11-mediated process via late recycling endosomes. Of note, RAB5 can also mediate cargo degradation from EEs to multivesicular bodies

and subsequently to lysosomes via RAB7; and RAB9 controls the retrograde transport of cargoes from late endosomes to the TGN. All these endosomal RAB proteins were described to segregate into specific domains on endosomes (**Figure 2.II**) (Barbero *et al.*, 2002; Sonnichsen *et al.*, 2000).

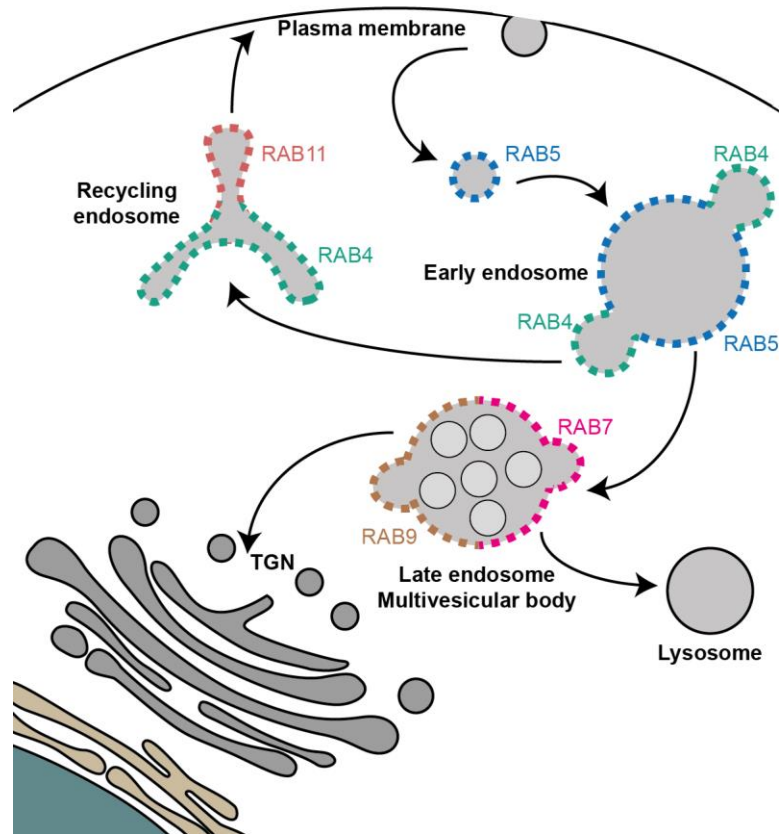


Figure 2.II: Mechanism of cargo endocytosis mediated by specific RAB domains. RAB5 mediates the transfer of cargoes from the plasma membrane to early/sorting endosomes (EEs). EEs display distinct RAB4 and RAB5 domains involved in endocytic recycling and endosome fusion, respectively. RAB4 and RAB11 segregate into specific domains on recycling endosomes and are respectively implicated in vesicular transport from EEs and towards the plasma membrane. Late endosomes, also called multivesicular bodies, are composed of two distinct RAB7 and RAB9 domains which regulate cargo degradation via lysosomes and transport towards the *trans*-Golgi network, respectively. Adapted from (Stenmark, 2009).

RAB5 is a key component of the early endocytic pathway that localizes to the cytosolic side of the plasma membrane, endocytic vesicles and EEs (Chavrier *et al.*, 1990). RAB5 has three ubiquitously expressed isoforms; RAB5A, RAB5B and RAB5C that share over 90% sequence homology (the main differences are located at the N-terminal extremity and the C-terminal hypervariable region). These isoforms appear to be functionally redundant in endocytic trafficking events (Bucci *et al.*, 1995; Gurkan *et al.*, 2005), although RAB5C was recently described to selectively modulate the growth factor-mediated activation of RAC1 and consequently cell motility (Chen *et al.*, 2014).

RAB5 regulates the transport of cargo from the plasma membrane to EEs (Bucci *et al.*, 1992), the generation of PI(3)P lipids on EEs (Christoforidis *et al.*, 1999), EE fusion (Barbieri *et al.*, 1996) and EE motility on cytoskeletal tracks through its interaction with effector proteins and motors (Nielsen *et al.*, 1999). RAB5 was also shown to activate signaling pathways from EEs (Benmerah, 2004; Miaczynska *et al.*, 2004). As previously mentioned, RAB5 can promote the generation of PI(3)P lipids on EEs via its ability to recruit PI(3)P-kinase (Christoforidis *et al.*, 1999), and regulate the levels of PI(4,5)P₂ through the recruitment of 5-phosphatases (Hyvola *et al.*, 2006). This change in membrane composition allows the recruitment of RAB5 effectors, such as EEAI and Rabenosyn-5 that can act as tethering factors, and also mediates the direct or indirect assembly of SNARE proteins, thus enabling EE fusion (Mills *et al.*, 2001; Morrison *et al.*, 2008).

The RAB4 subfamily of proteins is comprised of two isoforms in human RAB4A and RAB4B which display 93% sequence homology and are ubiquitously expressed, even though RAB4A is highly expressed in the brain (Hoogenraad *et al.*, 2010) and RAB4B is the predominant isoform in B cells (Krawczyk *et al.*, 2007). Both isoforms are thought to have redundant functions in recycling (Krawczyk *et al.*, 2007). RAB4 was shown to localize to EEs (Van Der Sluijs *et al.*, 1991), as well as to RAB11-positive recycling endosomes (Trischler *et al.*, 1999). In contrast to RAB5, RAB4 mediates the recycling of cargo from EEs directly back to the plasma membrane (fast recycling route) (Sheff *et al.*, 1999; van der Sluijs *et al.*, 1992b) or directs the sorting of cargoes to the endosomal recycling compartment (ERC) via a “slow recycling” route (Deneka and van der Sluijs, 2002).

RAB4 is also involved in regulating other more specialized trafficking pathways, such as the transport of the glucose transporter GLUT4 in adipocytes (Cormont *et al.*, 1996) or the processing of a receptor-mediated antigen in B lymphocytes (Lazzarino *et al.*, 1998). Interestingly, Rabenosyn-5, in addition to be a RAB5 effector, has also been shown to bind GTP-bound RAB4 and has been proposed to act as a linker between the RAB4-RAB5 domains on EEs and to coordinate the sorting of cargoes from EEs (de Renzis *et al.*, 2002).

Alternatively, cargoes can be recycled back to the plasma membrane via a late endocytic recycling compartment (ERC) on which RAB4 but also RAB11 are present and form distinct domains (**Figure 2.11**) (Sonnichsen *et al.*, 2000). The RAB11 protein family is composed of three isoforms: RAB11A and RAB11B which have redundant functions and are ubiquitously expressed, although RAB11B is more abundant in heart, brain and testes (Lai *et al.*, 1994); and RAB25 (also known as RAB11C) is expressed in polarized epithelial cells derived from colon, lung and kidney tissues

(Goldenring *et al.*, 1993). RAB11A is the best studied and characterized member of this subfamily and has been found to localize to the ERC (Ullrich *et al.*, 1996) and to be implicated in the transport of internalized receptor from ERC to the plasma membrane (Maxfield and McGraw, 2004). The recycling of cargos from the ERC to the plasma membrane was shown to be highly dependent on RAB11 and its effectors, which mediate transport along actin filaments (Hales *et al.*, 2002) and subsequent tethering and fusion (Takahashi *et al.*, 2012).

Additionally, RAB11 and his yeast homolog YPT31/YPT32 were also shown to localize to the TGN (Urbe *et al.*, 1993) and to regulate transport from the Golgi to the plasma membrane (Satoh *et al.*, 2005) and the recycling of plasma membrane proteins back to the Golgi (Chen *et al.*, 2005).

2.6.4 RAB35 and the plasma membrane

RAB35 was initially called RAB1C due to its high sequence similarity with RAB1A and RAB1B and for this reason only started to mobilize attention in the last 10 years. RAB35 was shown to localize to the plasma membrane and to endosomes, and to be involved in endocytic recycling, cytokinesis processes (Dambournet *et al.*, 2011; Kouranti *et al.*, 2006) and exosome secretion (Hsu *et al.*, 2010). RAB35 plasma membrane localization was suggested to be dependent on its highly conserved polybasic C-terminal extremity, through its direct interaction with negatively charged lipids, PI(4,5)P₂ and PI(3,4,5)P₃ (Heo *et al.*, 2006; Li *et al.*, 2014). RAB35 was also described to regulate PI membrane composition through its interaction with OCRL (Oculo-Cerebro-Renal syndrome of Lowe) (Cauvin *et al.*, 2016; Dambournet *et al.*, 2011). OCRL, which is also an effector for RAB5 and RAB6 (Hyvola *et al.*, 2006), was shown to selectively hydrolyze PI(4,5)P₂ into PI(4)P through its phosphatase domain (Lowe, 2005) and to thereby regulate PI(4,5)P₂ levels on endosomes. RAB35 also plays a fundamental role in actin-based events at the plasma membrane leading to its subsequent involvement in a large variety of cellular functions, such as endosomal trafficking, phagocytosis, cell migration and others (Klinkert and Echard, 2016).

3 Materials and Methods

3.1	Protein synthesis and modification	81
3.1.1	Protein expression and purification	81
3.1.2	<i>In vitro</i> modifications of RAB and GST proteins	84
3.2	Experimental studies with GUVs.....	90
3.2.1	Synthesis of giant unilamellar vesicles.....	90
3.2.2	Generalities of the experimental approach.....	93
3.2.3	Curvature sensing experiments with GUVs.....	98
3.3	Experimental studies with purified Golgi membranes	104
3.3.1	Purification of Rat Liver Golgi stacks.....	104
3.3.2	Experimental chamber.....	104
3.3.3	Pulling tubes with kinesins.....	105
3.3.4	Immunofluorescence on Golgi membranes.....	107

3.1 Protein synthesis and modification

3.1.1 Protein expression and purification

This study uses many different proteins. Many DNA constructs were given to us by Roger Goody's lab (Max Planck Institute in Dortmund) and some of the proteins were expressed and purified by them (**Table 3.1**). Others were constructed using standard cloning techniques (amplification, digestion, and ligation). REP-1 was expressed and purified by Ahmed El Marjou (Recombinant Protein Facility, Institut Curie). All monoprenylated proteins were C-terminally modified to contain the CVIL amino acid sequence, a CAAX box recognized by the Geranylgeranyl transferase I. Modifications of the C-terminal recognition site were performed using a simple cloning strategy consisting of oligonucleotides containing the 12 bases coding for the CVIL motif. All constructs

Chapter 3: Materials and Methods

were amplified using OmniMAX competent cells (Invitrogen) and the NucleoSpin Plasmid QuickPure kit (Macherey-Nagel); and sequenced by the Institut Curie sequencing platform.

Proteins, and more specifically RAB5A, were purified using the following method.

Expression: RAB5A expression and purification were performed as previously described (Oesterlin, 2012). RAB5A was expressed as a cleavable His6-MBP-fusion construct. Expression was performed in BL21(DE3) cells (Novagen/Merck) and was induced with 0.2 mM IPTG at 37°C for 5h.

The following protein purification was performed in several steps. First cell lysis was achieved by re-suspending them in 150 mL lysis buffer consisting of 50 mM Hepes pH7.5, 500 mM LiCl, 2 mM β -Mercaptoethanol, 1 mM $MgCl_2$, 10 μ M GDP, 5% Glycerol supplemented with 1 protease inhibitor tablet (complete EDTA free, Roche) per 50 mL lysis buffer, 2 μ g/mL Pepstatin and 1 mM PMSF. The cell suspension was incubated for 30 min on ice under continuous stirring and cells were passed through a cell disruptor (Constant Systems Ltd) at 2.5 kBar. As an alternative to the cell disruptor, cells can also be sonicated. The cell lysate was centrifuged at 20000 rpm at 4°C for 45 minutes and supernatant was filtered with a 0.22 μ m pore size filter (Millipore Express PLUS).

Protein purification / affinity column n°1: RAB5A was then isolated by affinity chromatography using 2 x 5 mL HiTrapTM Chelating HP columns (GE Healthcare) charged with Ni^{2+} mounted on an AKTA purifier system (Amersham Biosciences). As an alternative, Protino Ni-NTA Agarose beads (Macherey-Nagel) packed on an empty column can also be used. Two buffers A and B were used; both the same as the lysis buffer (without protease inhibitors) and buffer B supplemented with 500 mM Imidazole. The cell extract was loaded on the column and sequential washes with buffer A, 2% buffer B and 4 % buffer B were performed to get rid of contaminants which bind unspecifically to the column (**Figure 3.1**). Elution was performed with 200 mL continuous gradient of buffer B (4% to 100%) and 3 mL fractions were collected (**Figure 3.1**). In the case of Ni-NTA Agarose beads, elution was performed with 5%, 10% and 15% buffer B.

Protein purification / digestion: In the case of RAB5A, the protein was expressed using an N-terminal MBP tag that now has to be removed. The MBP tag was followed by a Tobacco etch virus (TEV) protease cleavage site which allows digestion and separation of the MBP tag from the rest of the protein. RAB5A was incubated with TEV protease (1 mg protease for 50 mg protein) and dialyzed overnight at 4°C against 5 L of 50 mM Hepes pH 7.5, 200 mM NaCl, 2 mM β -

Mercaptoethanol, 1 mM MgCl₂, 10 μM GDP in 4 spectra/Por Dialysis membrane (MWCO 12.-14.000, Vol/length: 6.4 mL/cm, Spectrum Laboratories).

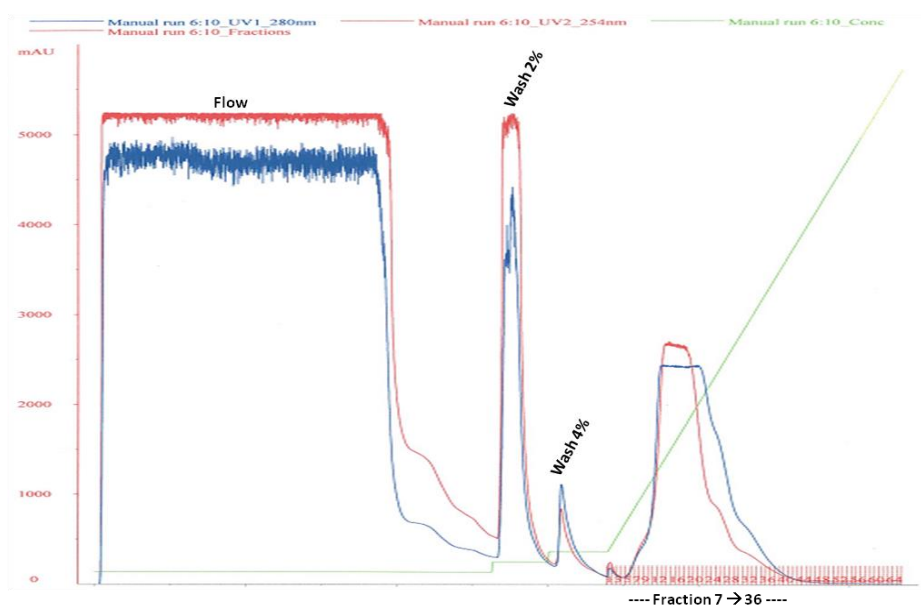


Figure 3.1: RAB5A purification on affinity column using the ÄKTA purifier system. Protein absorbance at 280 nm (blue) and 254 nm (red) at every washing step. The green line represents the percentage of buffer B. His-tag proteins interact with the nickel column and were only eluted with increasing concentrations of Imidazole (when fractionation occurs).

Protein samples at each step were run on a 12% SDS-PAGE gel to identify the RAB5A positive fractions and pool them together. Protein concentration was usually determined at this step using a Bradford protein assay (Bio-Rad).

Protein purification / affinity column n°2: This second protein isolation, meant to separate the His6-MBP tag from the digested RAB5A protein, was performed the same way as before except that washes were only done with buffer A, 4% buffer B and 8% buffer B. At this step, the protein of interest is normally collected in the “flow-through” (when the dialysis product is loaded on the column) while the His6 tag is retained on the column. However, in this particular case, digested RAB5A was found to unspecifically interact with His6-MBP and thus most of it was only collected in the 4% buffer B wash.

The protein was then concentrated to a 3 mL final volume using Amicon Ultra 15 MWCO 10.000 Da concentration tube.

Protein purification / Gel filtration column: To further isolate RAB5A from other protein contaminants, a gel filtration (or size-exclusion) chromatography can be performed using a HiLoad 16/600 Superdex 75 column (GE Healthcare) mounted on the AKTA system with a 4 mL loop. The Gel Filtration column was equilibrated and performed using a buffer consisting of 25 mM Hepes pH7.5, 200 mM NaCl, 1 mM MgCl₂, 2 mM DTE, 10 μM GDP, 5% Glycerol. The first 30 mL were not collected as it corresponds to the dead volume of the column. 60 fractions of 1.5 mL were then collected and loaded on a 12% SDS-PAGE gel. The fractions of interest (23-32 in this case) were then pooled together, the protein concentration was measured by Bradford assay and proteins were aliquoted and stored at -80°C until further use.

Many other proteins were used for this study. Expression and purification of these proteins were performed very similarly to that of RAB5 and varying details can be found in **Table 3.1**.

3.1.2 *In vitro* modifications of RAB and GST proteins

As previously mentioned in chapter 2, following their synthesis RAB proteins undergo posttranslational modifications (addition of the prenyl group) and get activated/deactivated. In our *in vitro* model, purified RAB proteins were also activated/deactivated and prenylated.

3.1.2.1 Nucleotide exchange reaction

During the purification process, most buffers used contain GTP or GDP nucleotides which are required for protein stabilization. However, nucleotide exchange still needs to be performed to make sure that all proteins bind a given nucleotide.

Nucleotide exchange was induced chemically. Briefly, RAB proteins are incubated with a 20 fold molar excess of the desired nucleotide and a 5 fold molar excess of EDTA (over MgCl₂ in buffer), to destabilize the nucleotide binding pocket, for 3 h at 25°C. For protein activation, RAB6 was exchanged to GTP (Sigma Aldrich) and RAB1, RAB4, RAB5, RAB11, RAB35 were exchanged to GppNHp (Jena Bioscience), a non-hydrolysable analog of GTP. Following incubation, a 2 fold molar excess of MgCl₂ (over EDTA) is added to re-stabilize the binding pocket and the protein sample is run on a NAP-5 / NAP-10 size exclusion column (GE Healthcare) to remove the excess of nucleotide.

Table 3.1: List of proteins used in this study and how they were obtained. BL21(DE3) and BL21-CodonPlus(DE3)-RIL cells were respectively obtained from Novagen/Merck and Stratagene/Agilent Technologies. Protino Ni-NTA agarose beads and Protino glutathione agarose 4B beads were both obtained from Macherey-Nagel. The TEV (tobacco etch virus) protease was purified in the lab and the PreScission protease (human rhinovirus 3C protease and GST fusion protein) was purified by Ahmed El Marjou (Recombinant Protein Facility, Institut Curie). * BCCP: Biotin carboxyl carrier protein.

Protein	Tag	Expression	Affinity column / Beads	Digestion	Final Buffer	Previously described in	Construct from
Codon optimized RAB1B-CVIL	His6-MBP	BL21(DE3) 0.2 mM IPTG 20h at 20°C	Ni ²⁺	Yes with TEV	20 mM Hepes pH7.5, 50 mM NaCl, 1 mM MgCl ₂ , 2 mM DTE, 10 μM GDP	Oesterlin 2012	Goody lab, MPI, Dortmund
RAB4A-CVIL	His6-EGFP	BL21(DE3) 0.3 mM IPTG 20h at 20°C	Ni ²⁺	Yes with PreScission	50 mM HEPES pH 7,5, 150 mM NaCl, 2 mM DTE, 5 mM MgCl ₂ , 5% Glycerol		Cloning in a pOPINN vector (Addgene)
RAB5A-CVIL	His6-MBP	BL21(DE3) 0.2 mM IPTG 5h at 37°C	Ni ²⁺	Yes with TEV	25 mM Hepes pH7.5, 200 mM NaCl, 1 mM MgCl ₂ , 2 mM DTE, 10 μM GDP, 5% Glycerol	Oesterlin 2012	Goody lab, MPI, Dortmund
RAB6A-CVIL	His6	BL21-CodonPlus(DE3)-RIL 0.2 mM IPTG 5h at 37°C	Ni ²⁺	Yes with TEV	25 mM Hepes pH 7.5, 50 mM NaCl, 1 mM MgCl ₂ , 2 mM DTE, 10 μM GTP		Modification of RAB6A-WT plasmid via standard cloning strategy
RAB6A-WT	His6	BL21-CodonPlus(DE3)-RIL 0.2 mM IPTG 5h at 37°C	Ni ²⁺	Yes with TEV	20 mM Hepes pH 7.5, 50 mM NaCl, 2 mM DTE, 1 mM MgCl ₂ , 10 μM GTP		Goody lab, MPI, Dortmund
RAB11A-CVIL	His6-EGFP	BL21(DE3) 0.3 mM IPTG 20h at 20°C	Ni ²⁺	Yes with PreScission	25 mM HEPES pH 7,5, 200 mM NaCl, 2 mM DTE, 2 mM MgCl ₂ , 10 μM GDP		Cloning in a pOPINN vector (Addgene)
RAB35-CVIL	His6-EGFP	BL21-CodonPlus(DE3)-RIL 0.2 mM IPTG 20h at 20°C	Ni ²⁺	No	25 mM Hepes pH 7,5, 50 mM NaCl, 2 mM DTE, 1 mM MgCl ₂ , 10 μM GDP		Cloning in a pOPINN vector (Addgene)
GST-CVIL	GST	BL21(DE3) 0.3 mM IPTG 20h at 20°C	Glutathione beads	No	50 mM Hepes pH 7.5, 150 mM NaCl, 1 mM DTE, 5% Glycerol		Cloning in a pGEX-6P1 vector (Addgene)
REP-1	His6	Insect cells (Sf9)	Ni ²⁺	No	25 mM HEPES pH 7.2, 40 mM NaCl, 10 mM DTT	Alexandrov 1999	Goody lab, MPI, Dortmund. Purified by Ahmed El Marjou (Recombinant Protein Facility of Institut Curie)
RABGGTase (α and β subunits)	α : His6-GST β : His6	BL21-CodonPlus(DE3)-RIL electrocompetent 0.1 mM IPTG 20h at 16°C	Ni ²⁺	Yes with TEV	20 mM Hepes pH 7.5, 50 mM NaCl, 2 mM DTE	Dursina 2006	Goody lab, MPI, Dortmund

Chapter 3: Materials and Methods

Protein	Tag	Expression	Affinity column / Beads	Digestion	Final Buffer	Previously described in	Construct from
GGTaseI (α and β subunits)	α : His6-GST β : His6	BL21-CodonPlus(DE3)-RIL electrcompetent 0.2 mM IPTG 20h at 20°C	Ni ²⁺	No	20 mM Hepes pH7.5, 50 mM NaCl, 2 mM DTE	Dursina 2006	Goody lab, MPI, Dortmund
Kinesin-1 ₁₋₄₀₁	C-ter BCCP ⁻ -His6	BL21(DE3) 0.5 mM IPTG 5h at 30°C	Ni ²⁺	No	50 mM Imidazole, 50 mM KCl, 4 mM MgCl ₂ , 2 mM EGTA, 10 mM β -mercaptoethanol, 50 nM ATP, 20% Glycerol	Subramanian 2007	Full construct from Addgene
LidA ₂₀₁₋₅₈₃	His6-mCherry	BL21(DE3) 0.3 mM IPTG 12h at 20°C	Ni ²⁺	No but cleaved after with PreScission	25 mM Hepes pH 8, 50 mM NaCl, 1 mM TCEP	Schoebel 2011	Constructed and purified by Goody lab, MPI, Dortmund
OCRL ₅₃₈₋₉₀₁	His6-mCherry	BL21(DE3) 0.3 mM IPTG 12h at 20°C	Ni ²⁺	No but cleaved after with PreScission	25 mM Hepes pH7.5, 100 mM NaCl, 1 mM TCEP		Constructed and purified by Goody lab, MPI, Dortmund

In order to measure the nucleotide bound state of the protein, an HPLC ion-pair reverse phase chromatography was performed as previously described (Eberth and Ahmadian, 2009) using the ÄKTA purification system. The stationary phase of a Protonsil 120-3-C18 column (Bischoff chromatography) is composed of C18 modified silica. The column is equilibrated with the mobile phase containing 50 mM KPi pH 6.7, 10 mM Tetrabutylammonium bromide, 15-25% (v/v) acetonitrile. 100 μ L of the 50-100 μ M GDP/GTP/GppNHp-bound protein is injected on the column and retention volumes are compared to previously injected GTP/GDP/GppNHp standards (**Figure 3.2A**). Absorption of the nucleotides is measured at 254 nm. If the protein was exchanged to GTP, the nucleotide exchange efficiency can be measured by calculating the ratio of the GTP integrated peak area over the sum of all nucleotide integrated peak areas (**Figure 3.2B**).

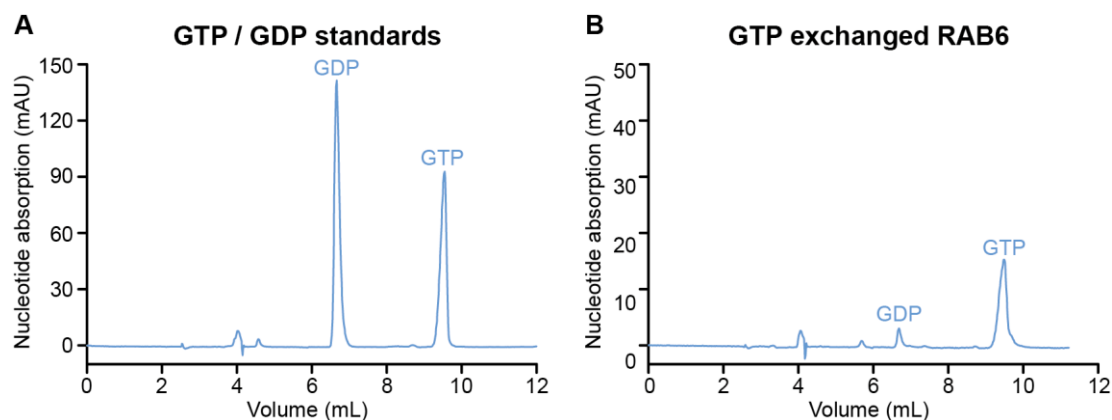


Figure 3.2: Measurement of nucleotide exchange efficiency by HPLC ion-pair reverse phase chromatography using the ÄKTA system. (A) Absorbance and retention volumes of pure 50 μ M GTP and GDP standards at 280 nm (blue) and 254 nm (red). (B) Absorbance and retention volumes of the newly exchanged RAB6 (exchanged to GTP) at 280 nm (blue) and 254 nm (red). The efficiency of nucleotide exchange is measured at 254 nm, by calculating the GTP peak area over the sum of both nucleotide peak areas.

3.1.2.2 Prenylation reaction

The prenylation reaction consists in the addition of one or two C20 geranylgeranyl moieties (Geranylgeranyl pyrophosphate, GGpp, Sigma) to the C-terminal extremity of the proteins (**Figure 3.3A**). Prenylation was achieved either through monoprenylation (addition of one geranylgeranyl group) using purified geranylgeranyl transferase type I (GGTaseI) (**Figure 3.3B**) or diprenylation (addition of two geranylgeranyl groups) using the native prenylation machinery consisting of purified RAB geranylgeranyl transferase (RABGGTase or GGTaseII) and RAB escort

protein (REP-1) (**Figure 3.3C**). Of note, because GGTaseI only recognizes the C-terminal CAAX motif, monoprenylated proteins were mutated to a CVIL motif at their C-terminus.

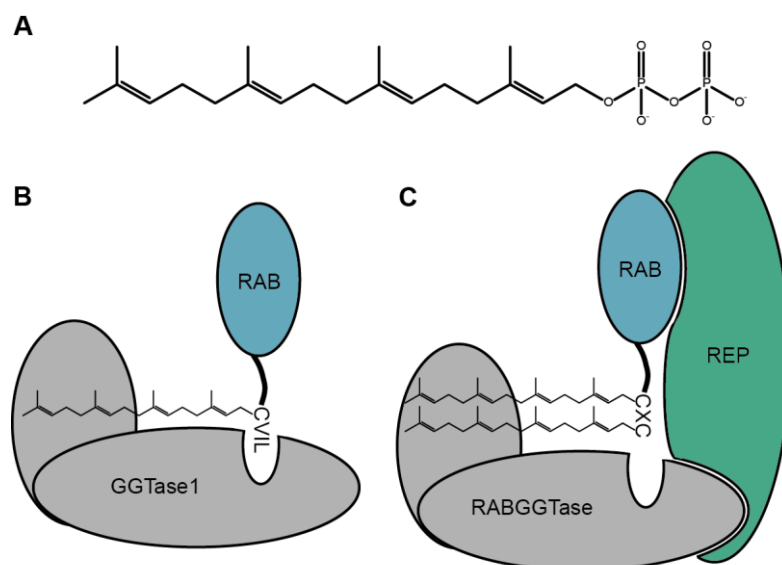


Figure 3.3: Mechanisms of RAB prenylation. (A) Native diprenylation machinery consisting of a GDP-bound RAB protein with a double cysteine motif at its C-terminal extremity, the RAB geranylgeranyl transferase (RABGGTase, with two subunits α and β) and the RAB escort protein (REP). The RABGGTase transfers two geranylgeranyl groups on the double cysteine motif of the RAB protein, with the REP acting as a chaperone. (B) Monoprenylation of a RAB protein mediated by the Geranylgeranyl Transferase type 1 (two subunits α and β). The GGTaseI recognizes the CVIL motif at the C-terminus of the RAB protein (CAAX box) and transfers one geranylgeranyl group on the cysteine.

Monoprenylation reactions were performed at 25°C for 1.5 h with a molar ratio of 0.5:1:5 GGTaseI, RAB and GGpp. Molar ratios for the diprenylation reaction were: 1:5:0.5:0.75 RABGGTase:GGpp:RAB:REP and the reaction was performed at 25°C for 4 h. Of note, diprenylation can only be achieved for GDP-bound RABs (REP only recognizes the GDP-bound form) whereas monoprenylation can be performed with both GTP- and GDP-bound RAB proteins.

To control efficient protein prenylation, NBD-Farnesyl pyrophosphate (NBD-Fpp, Jena Bioscience), a C15 fluorescent analog of GeranylGeranyl pyrophosphate, was used as previously described (Dursina *et al.*, 2006). The prenylation reactions with NBD-Fpp were performed using the same molar ratios as for monoprenylation with GGpp. 15 μ L of each reaction was loaded on a 15% SDS-polyacrylamide gel and gel fluorescence was visualized using the Ethidium Bromide program of a ChemiDoc imaging system (Bio-Rad) (**Figure 3.4**).

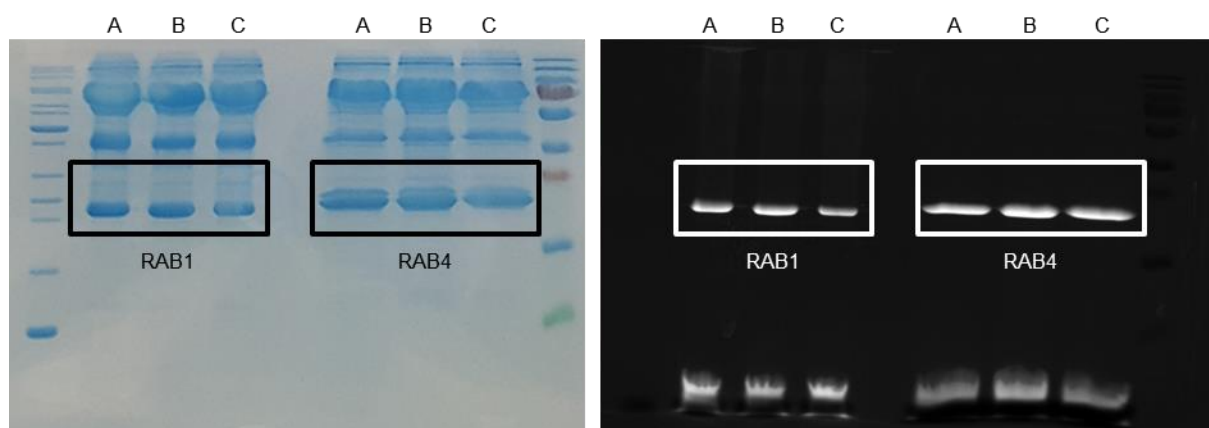


Figure 3.4: RAB1 and RAB4 prenylation tests for (A) 1 h (B) 1 h 45 minutes and (C) 2 h 30 minutes incubation times. The right panel shows the NDB-Fpp fluorescence (detected using a ChemiDoc imaging system) and the left panel shows the coomassie blue staining.

3.1.2.3 Labeling reaction

Prior to prenylation, proteins could be labeled using Alexa FluorTM 488 Sulfodichlorophenol ester (Alexa488 5-SDP ester, Molecular Probes / Life Technologies) or Alexa FluorTM 568 Succinimidyl ester (Alexa568 NHS ester, Molecular Probes / Life Technologies) and by following the associated protocol. To ensure that the label does not interfere with the binding of some effectors or antibodies, proteins were only labeled on their N-terminal amine group. As the pKa of the terminal amine is lower than that of the amine group containing lysines, specific N-terminal labeling could be achieved using a buffer close to neutral pH (in our case proteins are already at pH 7.5).

The protein was incubated with a 4 fold molar excess of Alexa dye for 2 h at 25°C. A 250 fold molar excess of freshly prepared Hydroxylamine was added and the reaction was incubated for 1h at 25°C. A NAP column (GE Healthcare), pre-equilibrated with the protein buffer, was then run to remove excess unbound fluorophore. Protein concentration was determined by a Bradford assay. The efficiency of labeling (n^*) which corresponds to the ratio of moles of dye per mole of protein was determined after absorption measurements at the nanodrop (protein and label program, ThermoFisher Scientific) and using the following formula:

$$n^* = \frac{A_{max}}{\epsilon \times protein\ concentration\ (M)} \times dilution\ factor \quad [1]$$

Where A_{max} is the absorbance of the fluorescent protein at the wavelength maximum of the dye ($\lambda_{max} = 488\text{ nm}$ for Alexa488 and 568 nm for Alexa568) and ϵ is the fluorescent dye molar

extinction coefficient ($71,000 \text{ M}^{-1} \text{ cm}^{-1}$ and $91,300 \text{ M}^{-1} \text{ cm}^{-1}$ for Alexa488 and Alexa568 respectively).

3.2 Experimental studies with GUVs

3.2.1 Synthesis of giant unilamellar vesicles

3.2.1.1 Lipid reagents and GUV compositions

All lipids were from Avanti Polar Lipids. Phase separated GUVs contained Brain Sphingomyelin (BSM), Cholesterol and 1,2-dioleoyl-*sn*-glycero-3-phosphocholine (DOPC) at a molar ratio of 3:1:3 (Roux *et al.*, 2005) and were electroformed at 50°C to allow lipid mixing. The other GUVs tested were electroformed at room temperature. Lo vesicles and Ld vesicles were respectively composed of BSM : Cholesterol and DOPC : Cholesterol at 1:1 molar ratios (Roux *et al.*, 2005). The charged versions of Lo and Ld vesicles were composed of Cholesterol 3-sulfate instead of Cholesterol. To induce lipid packing defects, a 85% L- α -phosphatidylcholine (Egg, Chicken) (EggPC) : 15% 1,2-dioleoyl-*sn*-glycerol (DOG) (mol) mix was used. In control experiments, DOG was replaced by DOPC. In order to decrease the amount of lipid packing defects 30% (mol) of 1-stearoyl-2-docosahexaenoyl-*sn*-glycero-3-phosphoethanolamine (PUFA PE) was added to the previously mentioned DOG-containing mix, at the expense of EggPC. Control experiments were performed using 30% (mol) of 1-palmitoyl-2-oleoyl-*sn*-glycero-3-phosphoethanolamine (POPE) instead of PUFA PE.

Tube pulling experiments were performed using EggPC vesicles. To achieve adhesion between the GUV membrane and the streptavidin-coated beads, 0.035% (mol) of 1,2-distearoyl-*sn*-glycero-3-phosphoethanolamine-N-[biotinyl(polyethyleneglycol)-2000] (ammonium salt) (DSPE -PEG(2000)-Biotin) was added to the lipid mix.

GUVs were made fluorescent by adding 0.1% (mol) of the red-emitting dye TexasRedTM 1,2-Dihexadecanoyl-*sn*-glycero-3-phosphoethanolamine (triethylammonium salt) (TexasRed-DHPE) from Molecular Probes. The green-emitting dye β -BODIPYTM FL C₅-HPC (2-(4,4-Difluoro-5,7-Dimethyl-4-Bora-3a,4a-Diaza-s-Indacene-3-Pentanoyl)-1-Hexadecanoyl-*sn*-Glycero-3-Phosphocholine) from Molecular Probes was also used; mostly for calibration measurements (see 3.2.2.3).

3.2.1.2 Electroformation with ITO coated slides

GUVs were grown on conductive indium tin oxide (ITO) coated glass slides using the electroformation (EF) technique (Angelova *et al.*, 1992) (**Figure 3.5A**). 15 μL of a 0.5 mg/mL lipid mix was dried on pre-washed (water, ethanol, water, chloroform) ITO coated slides for a few minutes at 50°C and subsequently under vacuum for at least 2 h. The chamber is then assembled. Sealing wax (Vitrex, Denmark) is applied around the dried lipid films of two opposing ITO glass slides. The entire chamber is immobilized using two paper clips while 4 layers of Teflon tape on each side are used as a spacer (**Figure 3.5A**). The dried lipid films were then rehydrated in a sucrose solution (osmolarity between 100 and 430 mOsm, depending on the osmolarity of the protein buffer used for the experiments) and GUVs were grown for 3 h under a sinusoidal voltage (1.1 V, 10 Hz).

GUV growth was most of the time performed at room temperature except in the case of phase separation where it was performed at 50°C. In the latter, the sealing wax which is normally used to construct and isolate the chamber starts to melt which results in leakage of the sucrose solution. For this reason chambers were constructed using a hand-made PDMS chamber which is resistant to such temperatures.

3.2.1.3 Electroformation with platinum wires

The previously described EF method has the disadvantage to be restricted to growth buffers containing low levels of salt. In the case of lipid mixtures containing specific charged lipids (PI(4,5)P₂, PI(3)P), growth needed to be performed in presence of salt for stabilization purposes and the original EF method was not adapted. We thus used a more recently described method suitable for the use of buffers with higher concentrations of salt (Meleard *et al.*, 2009).

The EF chamber is made out of a block of Teflon of 5 mm thickness and 40 mm length, with three regularly spaced square wells of 8 x 8 mm (**Figure 3.5B**). The chamber is also perforated throughout its length by two narrow holes which are 3 mm apart from each other. Two platinum wires of 0.5 mm diameter (LS413074 Goodfellow, UK) are inserted into these holes, cross all three wells and are inserted in the hole on the opposite side of the chamber. These wires come out of the chamber by a few mm which allows us to later connect them to a function generator and to consequently build up an electric field inside the wells.

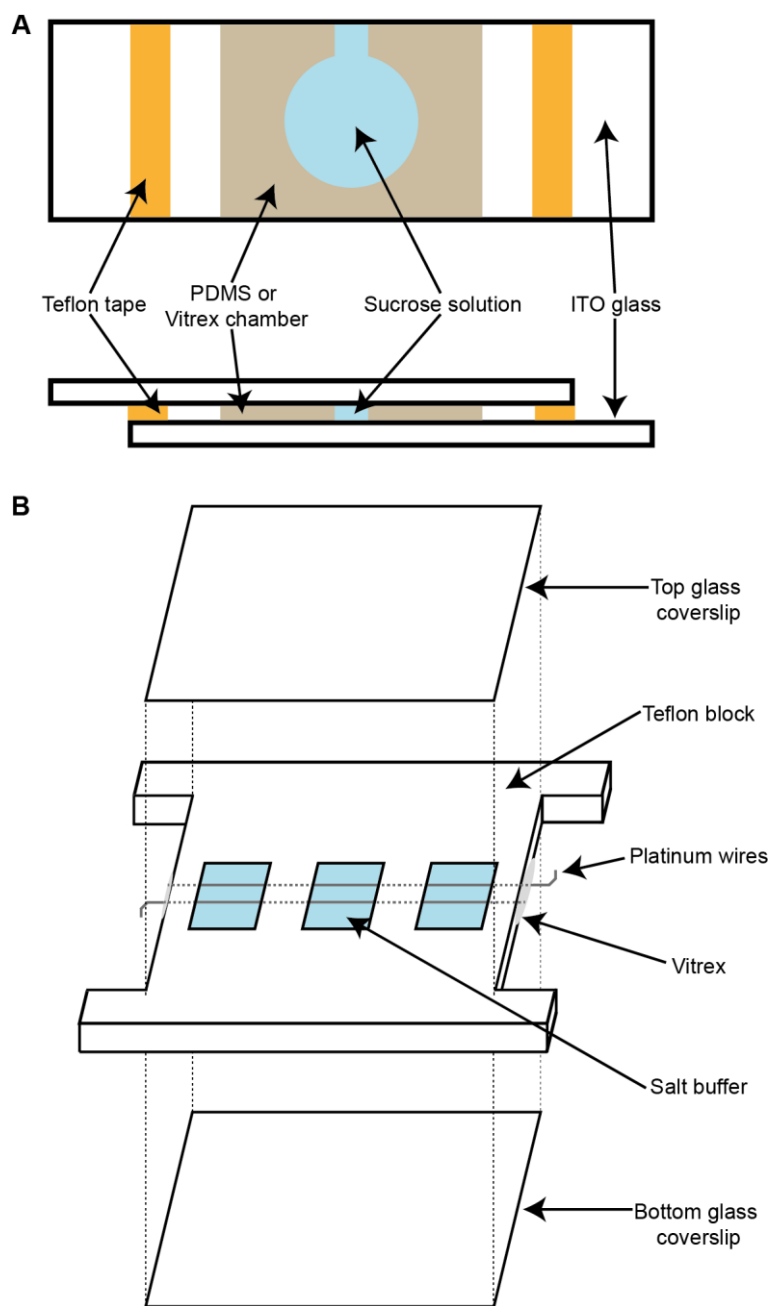


Figure 3.5: Schematic of GUV electroformation chambers. (A) Original electroformation using ITO coated slides. Two slides with dried lipid films are assembled a bit shifted from each other while sealing wax (Vitrex) or PDMS is used to isolate the chamber. 4 layers of Teflon tape on each side act as spacers and the chamber is immobilized using paper clips. (B) Electroformation under physiological conditions (high levels of salt). The chamber is made out of a block of Teflon with three identical wells that are sealed, at the top and the bottom of the chamber, by two glass coverslips. Lipids are applied on two platinum wires that cross the whole chamber and are connected to the generator on both extremities.

Around 5 μL of a 3 mg/mL lipid mixture was applied drop-by-drop on pre-washed wires (5 min. sonication steps in acetone, ethanol and water) and subsequent drying under high vacuum was performed.

The next step consists in the mounting of the EF chamber (**Figure 3.5B**). Sealing wax (Vitrex, Denmark) was applied on the side of the chamber to prevent leakage from the holes (from which the platinum wires come out). The bottom side of the chamber was closed using a glass coverslip fixed to the chamber by the anterior addition of vacuum grease (Dow Corning, USA). All the wells were filled with growth buffer and the chamber was completely sealed with a second glass coverslip. The chamber was connected to a generator through the extended platinum wires on the side and growth was performed at 4 °C overnight under sinusoidal voltage (0.35 V, 500 Hz). GUVs are then collected by pipetting directly next to the wires.

3.2.2 Generalities of the experimental approach

3.2.2.1 Experimental setup

As already mentioned, all experiments were performed *in vitro* using GUVs as controlled model systems and purified Golgi membranes. The experimental setup, which allowed us to perform the measurements (optical tweezer, necessary for tube pulling experiments) and optical acquisition at the same time, was originally developed by P. Bassereau's team at Institut Curie (Sorre, 2010; Sorre *et al.*, 2009) and was later adapted in our lab by David Guet, a previous PhD student (Guet, 2012) (**Figure 3.6**). The setup is originally based on a commercial Nikon eclipse Ti inverted microscope which was modified with the optional stage riser (Nikon), in order to create an extra port for epifluorescence microscopy (port #2). The confocal head consists in an AIR confocal system equipped with four laser lines (405 nm, 488 nm, 561 nm and 640 nm) and has two acquisition modes: Galvano and Resonant. Briefly, the first one allows an optimal signal to noise ratio and is more suited for fluorescence intensity measurements whereas the second one displays a higher scanning speed and thus allows the user to scan at a higher frame rate. In the scope of our experiments we always used the Galvano mode.

We also took advantage of an added DIC bright field visualization module (**Figure 3.6**) which allowed us to perform force measurements (calibration for tube pulling experiments) and helped us to easily find model membranes in the different experimental chambers (avoiding the use of the confocal module and fluorescence).

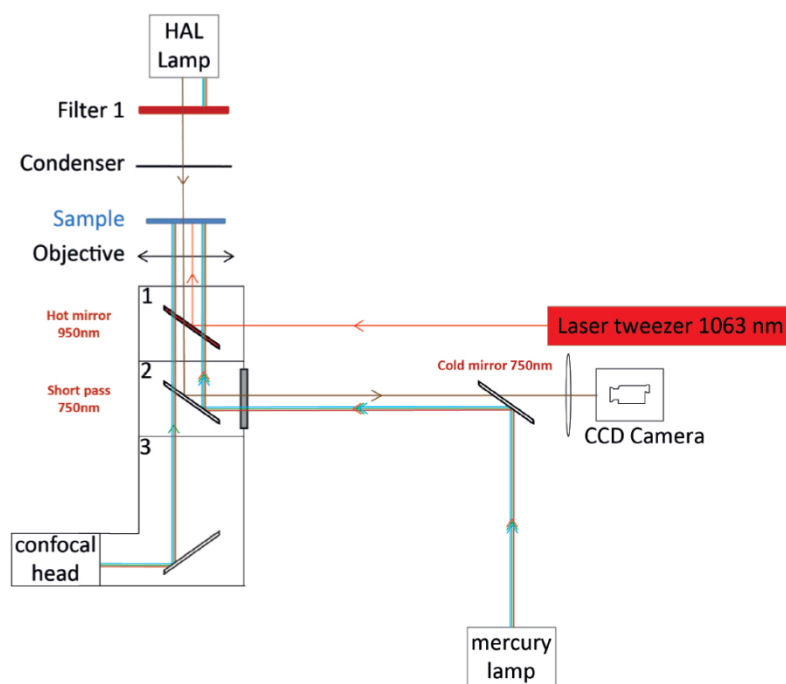


Figure 3.6: Schematic of the microscope experimental setup. The setup developed in the lab by D. Guet is composed of a confocal head which uses visible light (rainbow beam with simple arrow, port n°3), an optical tweezer which functions at 1063 nm (red beam, port n°1), a bright field visualization module which uses near infrared light (brown beam, port n°2) and finally epifluorescence mode (rainbow beam with triple arrows, port n°2). From (Guet, 2012).

Because the three modules (confocal microscopy, optical tweezers and DIC) are not usually compatible, the light spectrum was thereby split in three separate channels. Confocal fluorescence microscopy was performed in the visible range ($400 \text{ nm} < \lambda < 750 \text{ nm}$), optical trapping in the infra-red channel ($\lambda > 900 \text{ nm}$) and DIC was used in the near infra-red channel ($750 \text{ nm} < \lambda < 900 \text{ nm}$). Bright field imaging video was visualized using a Labview based custom software. Additional details about the setup can be found in D. Guet's thesis (Guet, 2012).

3.2.2.2 Measurement of fluorescence intensity

Many of the performed experiments required measurements of fluorescence intensities (**Figure 3.7**).

In chapter 4 and chapter 5, these were measured with the Fiji software using a rectangular selection (10 pixel width) including either the horizontal tube (for tube pulling experiments) or the GUV membrane and subsequent averaging along vertical lines (**Figure 3.7A**). All intensities were calculated after subtracting the noise level (intensity inside the vesicle) from the maximum of the fluorescence peak.

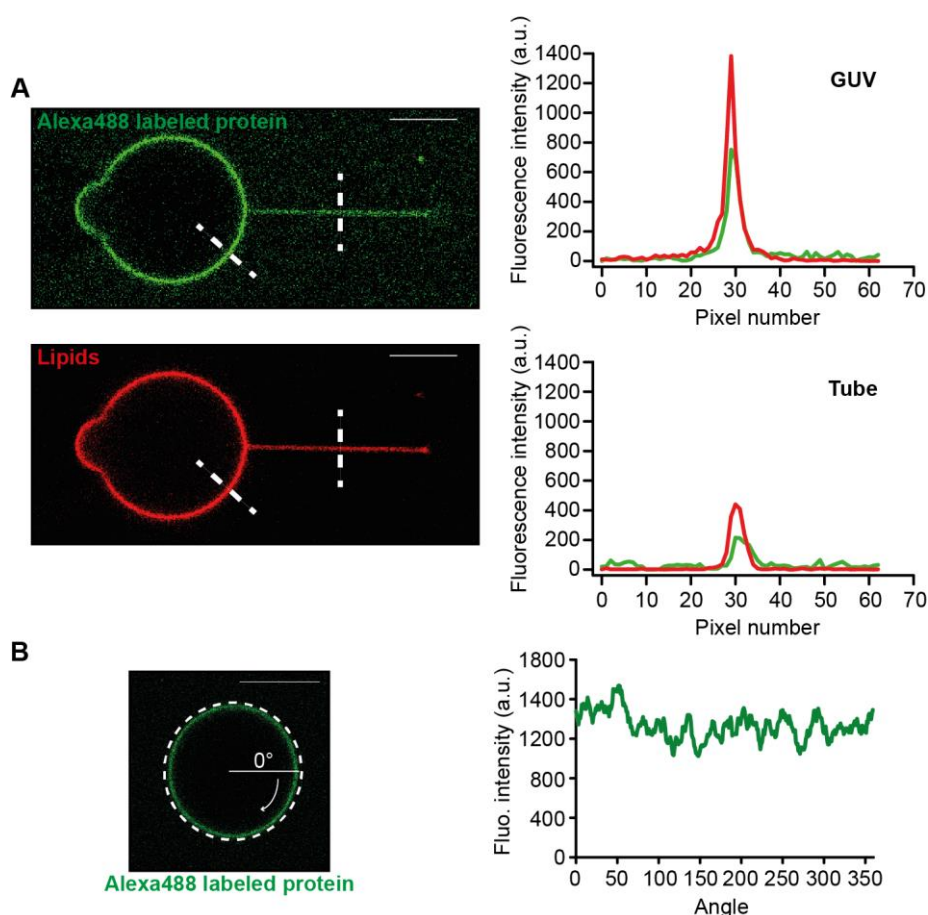


Figure 3.7: Measurements of fluorescence intensities. (A) The left images represent typical images obtained with tube pulling experiments. Each vertical line of the rectangular selection gives a plot of fluorescence intensity as a function of the pixel number along the line. The right panel of the figure shows the average plot of the rectangular selection. The maximum of the fluorescence peak is subtracted with the noise level (intensity inside the vesicle). (B) An oval selection is drawn around the vesicle and the oval profile plugin measures the pixel of highest intensity for each degree (360 in total). The plot on the right shows the fluorescence intensity values that were subtracted by the background (outside the vesicle) intensity value. (Scale bar: 10 μm).

In the case of chapter 6, fluorescence intensities were measured all over the vesicle with the Fiji software using the oval profile plugin (**Figure 3.7B**). An oval selection was drawn around the vesicle and the integrated oval profile plugin was set to measure the pixel of highest intensity for each degree (360° in total) of this oval selection. Because some experiments required the assessment of protein membrane binding, each intensity value was subtracted by the background intensity value outside the vesicle.

3.2.2.3 Measurement of protein density on the membrane

A standard measurement of fluorescence intensities is a good tool to assess and compare the binding or sorting of one labeled protein in different experimental GUV conditions. However, because the different proteins were labeled with various efficiencies, their binding to membranes could not be compared simply by using fluorescence intensity values.

Fluorescence intensities were thus converted into protein surface densities to overcome this issue and also to obtain more representative values of protein binding.

In order to convert fluorescence intensities into protein densities, we needed a calibration standard. In other words, we needed a fluorescent species that we could incorporate in GUVs at known densities. Fluorescence was thus calibrated using GUVs made of BodipyFL-C5-HPC (bodipyFL), a green fluorescent lipid. We synthesized pure EggPC GUVs with various molar ratios of bodipyFL and measured the fluorescence intensities on the membrane. BodipyFL surface density (Φ^{bodipyFL}) and the resulting fluorescence intensity on the membrane (I^{bodipyFL}) are related by:

$$\Phi^{\text{bodipyFL}} = A_{\text{gain}} I^{\text{bodipyFL}}(\text{gain}) \quad [2]$$

Where A_{gain} is the calibration coefficient at a given confocal photomultiplier tube detector (PMT) gain (same as the one used for protein experiments).

The bodipyFL surface density (Φ^{bodipyFL}) at each molar ratio was calculated by assuming that all the dye of the initial lipid mix was incorporated into the GUVs. The area per EggPC lipid is approximately 0.7 nm^2 (Nagle, 2000) which results in a number of lipid per μm^2 of $\frac{2 \times 10^6}{0.7} = 2.86 \cdot 10^6$ (where the factor 2 is to take both leaflets into account). The bodipyFL surface density was thus defined as: $\Phi^{\text{bodipyFL}} = 2.86 \cdot 10^6 x^{\text{bodipyFL}}$ (x^{bodipyFL} representing the molar ratio of the lipid dye).

Finally A_{gain} was determined using Eq. 2. A linear fit of bodipyFL fluorescence vs. bodipyFL area density plot gave the conversion constant (A_{gain}) (**Figure 3.8A**).

Proteins were labeled with the Alexa488 fluorophore and lipids with BodipyFL-C5-HPC, two fluorophores exhibiting different spectral properties. The calibration coefficient A_{gain} could thus not directly be used for the calculation of protein densities. To overcome this issue, the coefficient was corrected with the correction factor $F = I_{\text{bulk}}^{\text{A488}} / I_{\text{bulk}}^{\text{HPC}}$, i.e. the ratio of fluorescence intensities of Alexa488 and bodipyFL respectively at a given concentration in solution. Both

fluorescent signals in bulk scaled linearly with their concentration and F is defined as the ratio between the slopes of the Alexa488 linear fit and that of HPC (**Figure 3.8B**).

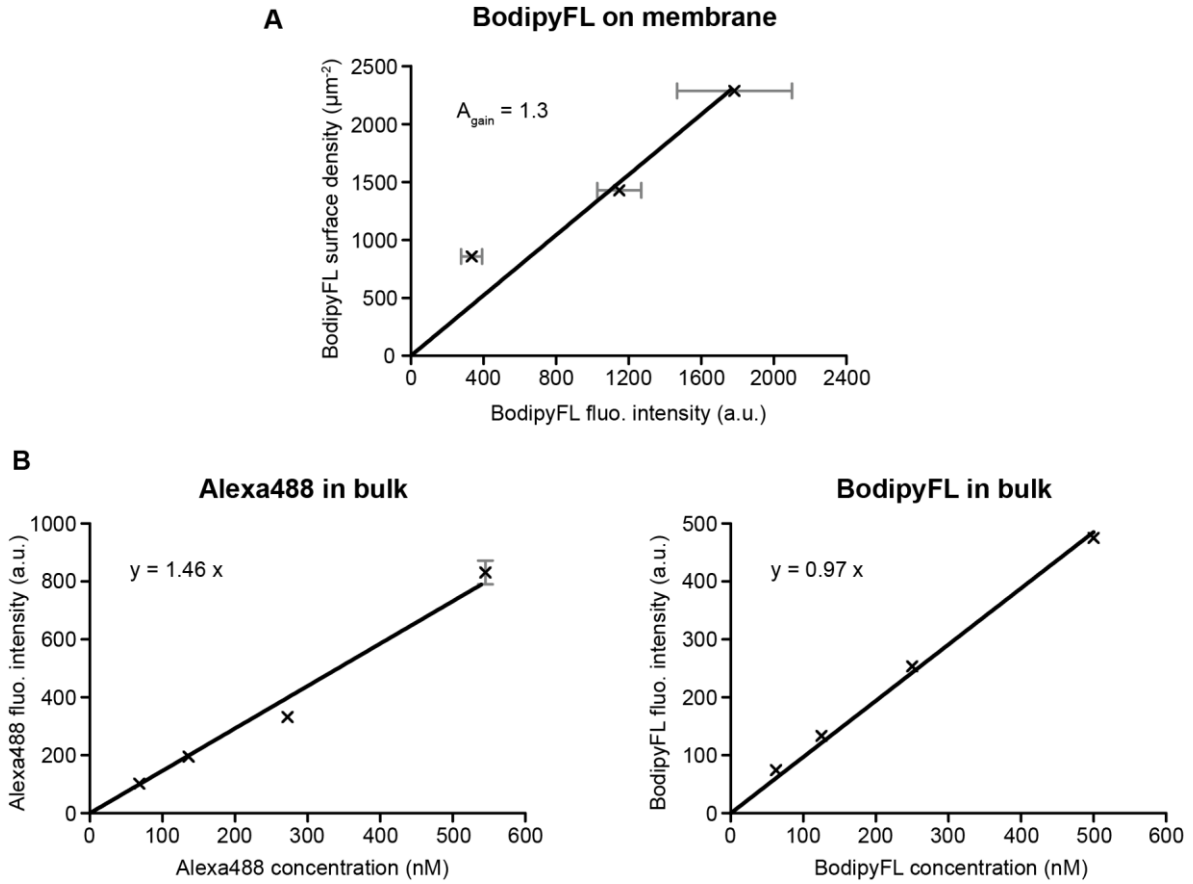


Figure 3.8: Green fluorescence calibration. (A) Determination of the proportionality constant A_{gain} by plotting the green lipid (here BodipyFL) surface density as a function of its fluorescence intensity (at a given PMT gain) and taking the slope of the resulting linear fit. Each point represents the average BodipyFL membrane fluorescent intensity of $N = 40$ GUVs at a given surface density. (B) Correction factor F determination. Fluorescent intensities of both green dyes are measured in solution at given concentrations. F is given by the ratio of left and right slopes.

Finally, as the bulk experiments were performed with Alexa488 alone, the correction factor needed to be adjusted with the number of fluorophores per protein. The protein labeling efficiency was thus taken into account by calculating the degree of labeling (n^*) of the protein using Eq. 1.

In the end, the protein density on the GUV membrane (Φ_v^{prot}) was defined by:

$$\Phi_v^{\text{prot}} = \frac{A_{\text{gain}}}{F \times n^*} \times I_v^{\text{prot}}(\text{gain}) \quad [3]$$

3.2.2.4 Lipid dependent protein recruitment experiments

In the simple case of protein recruitment to differently composed GUVs, a hand-made metal insert (gift from Phong Tran, Institut Curie, crafted by the university of Philadelphia) was used (**Figure 3.9**). A hand-made PDMS chamber with a 5 mm diameter hole in the middle was fixed to a pre-washed (water, ethanol, water) 22 x 40 mm glass coverslip, inserted and immobilized into the metal insert using two screws.

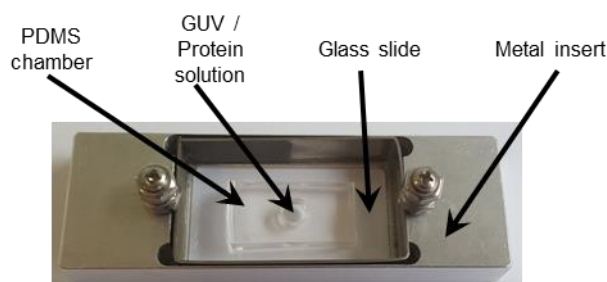


Figure 3.9: Hand-made PDMS chamber in metal insert. Studies of protein recruitment to GUVs of different compositions were always performed with this device.

The chamber was incubated with 35 μL of 0.5 mg/mL β -Casein (Sigma) for a couple of minutes to prevent adhesion of the GUV to the glass. The solution was removed and the chamber was washed using 50 μL protein buffer supplemented with 0.1 mg/mL β -Casein. After removal of the protein buffer, 1 or 2 μL of GUV solution and 2 μM proteins are added to the chamber in a total volume of 20 μL (completing to 20 μL with the previously used protein buffer).

3.2.3 Curvature sensing experiments with GUVs

The study of protein curvature sensing was performed by pulling a highly curved tube from a GUV and measuring the enrichment of the protein in the tube as compared to the GUV. In order to do so we used a setup originally developed by the Bassereau team (Institut Curie) and adapted in our lab by David Guet, a previous PhD student (Guet, 2012). Biotinylated GUVs are held on one side by a micropipette which is inserted into the experimental chamber. On their other side these biotinylated GUVs interact with streptavidin coated beads which are immobilized using an optical trap. By moving the micropipette away from the optical trap, the Biotin-streptavidin interaction allows to pull a highly curved tube. Subsequently, tube radius can be modulated by controlling the membrane tension through micropipette aspiration of the GUV (see “micropipette aspiration”

section). The sorting (or distribution) ratio of the protein between the highly curved tube and the flat GUV membrane can thus be measured for decreasing tube radii (or increasing tube curvatures). In the next sections the different components of the setup will be presented as well as the overall experiment and data analyses.

3.2.3.1 Experimental chamber

A 22 x 40 glass slide was cut in its length in two parts ($1/3$ and $2/3$ of the original glass slide) using a Retractable Diamond Scriber (Electron Microscopy Sciences). The two glass parts were washed (water, ethanol, water) and assembled on the microscope insert (**Figure 3.10**). More specifically, the larger glass part was fixed on the bottom side of two protruding StarFrost glass slides (themselves already fixed to the microscope insert) (Knittel Glass), using vacuum grease (Dow Corning, USA), while the smaller glass part is fixed on the upper part of the StarFrost glass slides.

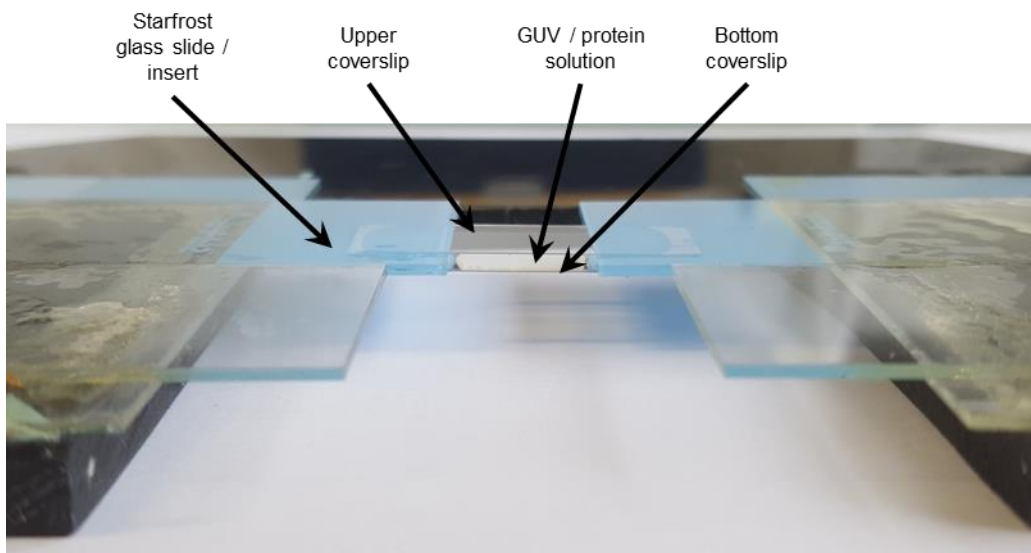


Figure 3.10: Experimental chamber for tube pulling experiments. This hand-made chamber has the particularity to be opened on the side allowing the insertion of the micropipette.

The chamber was incubated with 200 μL of 0.5 mg/mL β -Casein (Sigma) for a couple of minutes to prevent adhesion of the GUV to the glass. The solution was removed and the chamber was washed using 200 μL protein buffer supplemented with 0.1 mg/mL β -Casein. After removal of the protein buffer, 1 or 2 μL of GUV solution and 100-300 nM proteins were added to the chamber in a total volume of 200 μL (completing to 200 μL with the previously used protein buffer).

3.2.3.2 Micropipette aspiration

The micropipette aspiration technique is usually used to study the thermoelastic and mechanical properties of cells or synthetic vesicles. The micropipette is a key component of the tube pulling experimental setup as it allowed us to hold and manipulate GUVs and to control membrane tension (and consequently modulate the radius of the tube).

Micropipettes were made of borosilicate capillaries of 1 mm outer diameter and 0.58 mm inner diameter (Harvard Apparatus, UK). The forging of micropipettes is performed in two steps. First, an elongated tip is created on the capillary using a micropipette puller (P-2000, Sutter Instrument, USA). The latter pulls on both ends of the capillary while heating in the middle with a laser beam leading to the fabrication of two micropipettes with elongated tips that are closed at their end by the merged glass walls. Then, a smooth opening of 5-10 μm is generated at the tip of the micropipette using a microforge (MF-830, Narishige, Japan).

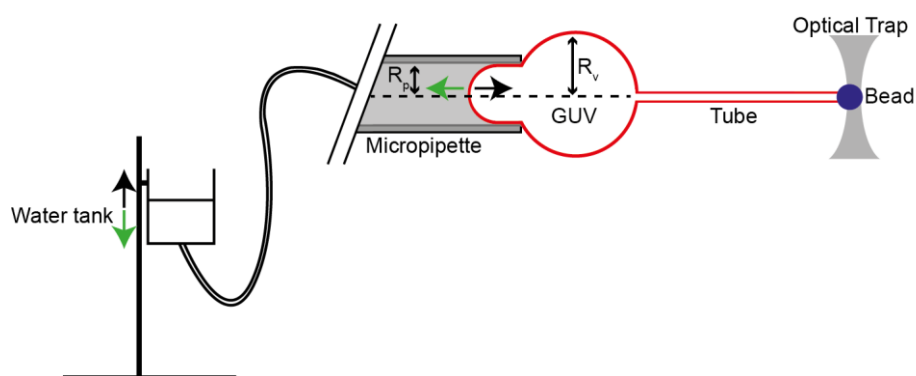


Figure 3.II: Tube pulling experimental setup. A biotinylated lipid-containing GUV is aspirated into a micropipette connected to a water tank of adjustable height which allows the control of membrane tension. A streptavidin coated bead is immobilized using an optical trap and a membrane tube is formed by the biotin-streptavidin interaction. Lowering of the water tank will lead to an increase in membrane tension and consequently a decrease of the tube radius. (Not to scale).

In order to control membrane tension, the micropipette, filled with protein buffer supplemented with 0.1 mg/mL β -Casein (to prevent adhesion of GUVs to the pipette), is connected to a water circuit which ends with a water reservoir of adjustable height (**Figure 3.II**).

The pipette is fixed to a mechanical micromanipulator which enables us to move it in three directions (x , y , z). The GUV is aspirated by decreasing the pressure inside the micropipette (by lowering the height of the water reservoir). Membrane tension is then proportional to the

pressure variation (ΔP) between the micropipette interior and exterior (the chamber) and can be calculated using the Young-Laplace equation (Evans and Rawicz, 1990):

$$\sigma = \frac{\Delta P R_p}{2\left(1 - \frac{R_p}{R_v}\right)} \quad [4]$$

Where R_p is the radius of the pipette and R_v is the radius of the vesicle

Consequently, in the case of tube pulling experiments, tube radius can be decreased by increasing membrane tension through stronger GUV aspiration.

3.2.3.3 Optical tweezers

Optical tweezers are micromanipulation tools used to manipulate micron-size particles very precisely. The optical trap was created by tightly focusing a laser beam with an objective of high numerical aperture. The trapped particle experiences a force in the piconewton range, referred to as a gradient force, which pushes it towards the laser focus where the light intensity is the highest. Optical trapping uses infrared light (1063 nm) which is less-invasive and thus has the advantage of causing limited damage to the sample.

An optical tweezer can function as a Hook spring which applies an elastic force on the bead. This force (f) is proportional to the displacement of the bead (x) from its equilibrium position at the trap center (x_0) and can thus be defined by:

$$f = k(x - x_0) \quad [5]$$

Where k is the trap stiffness.

In our experiments, the stiffness of the optical trap (k) at a given laser power needed to be measured (see next section). Charlotte Alibert, another PhD student in the lab, took care of this calibration.

Briefly, the chamber is filled with water containing micron-sized beads (around 3 μm diameter). One bead is trapped by the optical tweezers and the chamber is moved at a controlled velocity using a piezo-electric actuator (Mad City Labs, MCL-S02456).

The force applied on the bead can be calculated using Stokes' law:

$$f = 6\pi\eta r v \quad [6]$$

Where η is the viscosity of the fluid, r the radius of the bead and v the velocity of the fluid.

The displacement of the bead was assessed with the confocal microscope software (NIS Elements, Nikon) and analyzed using a home-made Matlab code to track the center of the bead.

The trap stiffness (k) at a given laser power was measured using Eq. 5. The force exerted by the trap is plotted as a function of the bead displacement and the resulting slope of the linear fit gives the stiffness value (at a given laser power).

Trap stiffness for other laser power values were also measured the same way. The trap stiffness was plotted as a function of the laser power and the slope of the linear fit gave the value of the trap stiffness per unit power: $K = 216.2 \pm 6 \text{ pN}/\mu\text{m}/\text{W}$.

3.2.3.4 Calibration and measurements of tube radii

As previously mentioned, GUV tension can be modulated through micropipette aspiration and consequently the tube radius can be varied (**Figure 3.II**). The tube radius can be measured in two ways.

First, the radius can be measured using the previously described equilibrium relation between the tube radius (R_{tube}), the force required to hold the tube (f) and the tension of the membrane (σ) (Derenyi *et al.*, 2002):

$$R_{\text{tube}} = \frac{f}{4\pi\sigma} \quad [7]$$

With f and σ that can respectively be deduced from Eq. 5 and Eq. 4.

However, when tube pulling experiments were performed in presence of proteins, the validity of this equation can be questioned, as the binding of peripheral proteins can change the properties of the membrane (such as membrane tension). Therefore, in the presence of proteins, the tube radius value was assessed with a second method, by measuring the intensity of lipid dye in the tube. Because the studied proteins were all labeled in green with Alexa488 or GFP dyes, we used a red lipid dye consisting of TexasRed-DHPE (Molecular Probes).

Fluorescence in the tube is proportional to the number of fluorophores per unit length and the number of fluorophores is logically proportional to the size of the tube. Thus the fluorescence of the tube is also proportional to its radius (R_{tube}).

The fluorescence of the tube at a given radius can however vary from one experiment to another and even from one GUV to another if the dye is not homogeneously distributed. The tube fluorescence will also be dependent on the type of fluorescent lipid used. For these reasons the fluorescence of the tube was normalized to that on the vesicle (I_{ves}) and tube radius was defined to be proportional to $\frac{I_{\text{tube}}}{I_{\text{ves}}}$:

$$R_{\text{tube}} = P_c \frac{I_{\text{tube}}}{I_{\text{ves}}} \quad [8]$$

Where P_c is the unknown proportionality constant (in nm).

P_c was calibrated and determined experimentally by using Eq. 8 in the absence of proteins. In this case, R_{tube} could be measured using Eq. 7 and the P_c value was consequently measured by plotting R_{tube} as a function of the $\frac{I_{\text{tube}}}{I_{\text{ves}}}$ ratio and taking the slope of the resulting linear fit (**Figure 3.12**). Measurements of tube radius and ratio of tube to vesicle fluorescence values were performed with several vesicles and P_c was determined to be 239 ± 10 nm.

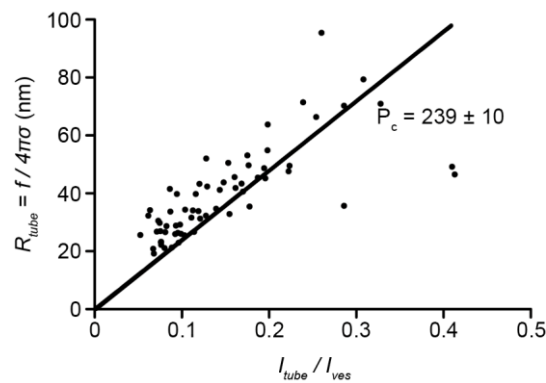


Figure 3.12: Determination of the proportionality constant between tube radius and fluorescence. Tube radius is measured using Eq. 7 and plotted as a function of its fluorescence intensity. Each point represents a GUV at a given membrane tension ($N = 10$ GUVs in total). P_c is determined using Eq. 8 by taking the slope of the resulting linear fit.

When looking at the calibration graph, the data seems very dispersed at high tube radii. This could be the result of two things: The GUV bilayer is asymmetrical (due to differences in inside and outside buffers) which can eventually lead to a spontaneous curvature (C_0) of the membrane. The impact of the spontaneous curvature will be higher on large tube radii and Eq. 7 would need to be modified by taking C_0 into account.

Another explanation is that this calibration is less reliable when the diameter of the tube gets closer to the thickness of the confocal volume.

3.2.3.5 Measurement of sorting ratio

In order to quantify protein sorting to the tube, the fluorescence intensity of the Alexa488 labeled protein (I_{protein}) was normalized by the intensity of the fluorescent lipid (TexasRed-DHPE, I_{lipid}) at

each tension step increase. The sorting ratio S corresponds to the ratio between the normalized protein intensity on the tube and the same normalized intensity on the GUV (Fig. S4B):

$$S = \frac{(I_{\text{protein}}/I_{\text{lipid}})_{\text{tube}}}{(I_{\text{protein}}/I_{\text{lipid}})_{\text{vesicle}}} \quad [9]$$

3.3 Experimental studies with purified Golgi membranes

3.3.1 Purification of Rat Liver Golgi stacks

Purified Golgi membranes were obtained by Hugo Bousquet (engineer in the lab) and Lena Oesterlin by following a previously described protocol (Slusarewicz *et al.*, 1994). It is important to note, that the purified membrane fraction is only enriched in Golgi membranes and does not consist of pure Golgi membranes. Final buffer consisted of 100 mM Potassium Phosphate pH 6.7, 5 mM MgCl₂, 250 mM Sucrose.

3.3.2 Experimental chamber

The chamber used for experiments with purified Golgi membranes was handmade (**Figure 3.B**).

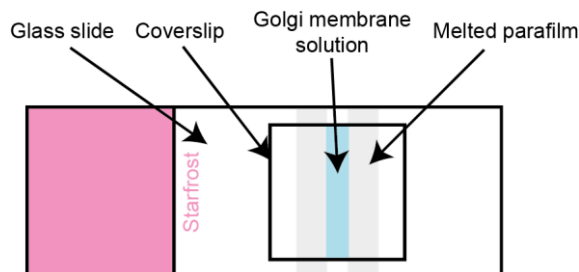


Figure 3.B: Experimental chamber for Golgi membranes studies. A glass coverslip is fixed to a Starfrost glass slide with melted parafilm in between. The parafilm acts as a spacer and also allows isolation of the chamber. This hand-made chamber has the advantage of working with small volumes (5 μ L).

A 22 x 22 mm coverslip was added on top of a 76 x 26 mm glass slide (Starfrost, Knittel glass) with two layers of sealing film (Parafilm) placed 1 cm apart from each other and acting as spacers. The mounted chamber was heated for 5 seconds on a heating and agitating device, which allowed the parafilm to melt and consequently to fix the coverslip to the glass.

3.3.3 Pulling tubes with kinesins

When using purified Golgi stacks as model membranes, protein sorting to tubular structures was monitored. Single tubes could be pulled out of immobilized Golgi membranes using the previously described optical tweezer setup. However, I took advantage of a previously described method (Roux *et al.*, 2002) consisting in Golgi membrane tubulation (can also be performed with GUVs) using purified kinesin motors (**Figure 3.14**). Briefly, biotinylated kinesin molecules are attached to biotin containing Golgi membranes through streptavidin (previously, small streptavidin coated beads were used) and tube formation occurs in presence of microtubules and ATP.

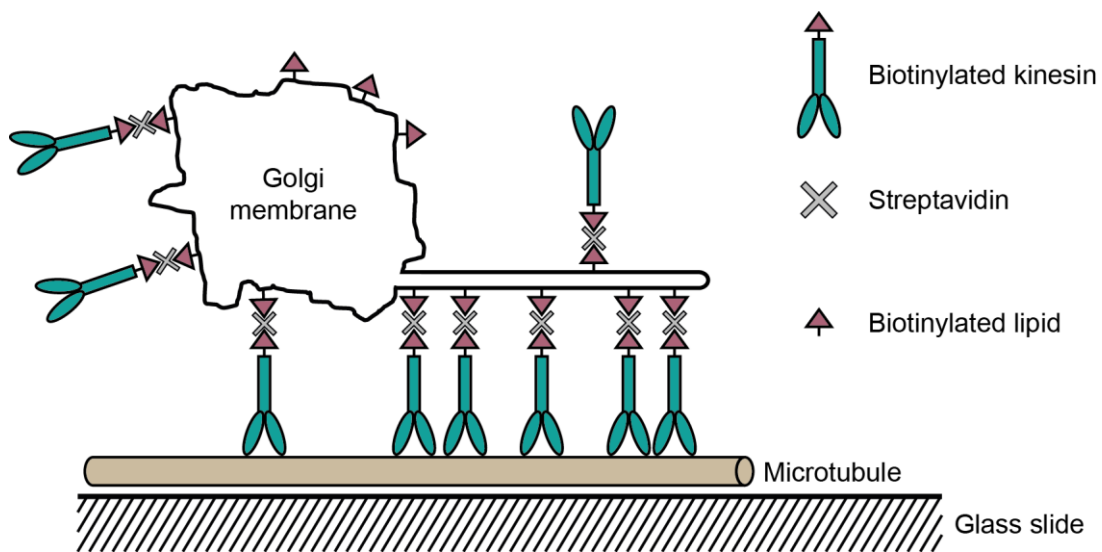


Figure 3.14: Tubulation of Golgi membranes mediated by kinesin motors. The chamber is coated with microtubules. Biotinylated kinesins and biotinylated Golgi membranes interact in presence of Streptavidin and ATP addition allows kinesins to move along microtubules and the subsequent pulling of membrane tubes.

3.3.3.1 Microtubule preparation

Microtubules were prepared from a tubulin solution (given to us by Jean-Baptiste Manneville, a researcher in the lab). A 50 μL aliquot of tubulin solution was incubated for 15 minutes at 37°C. 2 μL of 1 mM Taxol solution was added in order to stabilize the microtubules and the mix was incubated for 15 minutes at 37°C. The microtubule solution was then centrifuged for 17 minutes at 90000 rpm (TLA 120.2 rotor pre-heated at 37°C) and 37°C; and the pellet was resuspended in 50 μL IX BRB80 buffer (4X BRB80 buffer: 320 mM PIPES, 4 mM MgCl_2 , 4 mM EGTA pH 6.8)

supplemented with 30 μM Taxol. Microtubules were stored at room temperature and could be used one or two days after.

3.3.3.2 Experimental protocol

The experimental chamber was incubated with 5 μL of the previously prepared microtubule solution for 15 minutes in a humid chamber (with coverslip on the bottom so that microtubules can attach to the glass). To note, the direction of injection was always marked to make sure that all injections were performed on the same side of the chamber. The chamber was then incubated for 15 minutes with 5 μL solution of Imi Casein buffer (7 mg/mL β -Casein in 50 mM Imidazole pH 6.7, 50 mM NaCl, 2 mM EGTA, 1 mM MgCl_2), supplemented with 30 μM Taxol, to passivate the glass surface. The chamber is then washed with 5 μL solution of 5 μM DTT, 30 μM Taxol in Imi buffer.

On the side, 15 μL of 1.8 mg/mL purified biotinylated kinesin (Kinesin-₁₁₄₀₁-BCCP, see protein purification section) was incubated with 5 μL of 1 mg/mL Streptavidin solution (Sigma) on ice for at least 5 minutes. The chamber was then incubated with 5 μL of this kinesin / Streptavidin mix for 15 minutes in the humid chamber (coverslip down).

In parallel, purified Golgi membranes (4 μL) were incubated with 2 μM green or red labeled RAB protein and with an oppositely labeled lipid marker (red Bodipy TR C₅-ceramide complexed to BSA or green Bodipy FL C₅-ceramide complexed to BSA, both from Molecular Probes) for 20-30 minutes on ice (5 μL total reaction volume). Subsequently, 7.5 μL of motility buffer (In 100 μL total volume: 5 μM DTT, 30 μM Taxol, 2 mM ATP, 25 mM Glucose, 50 μL 2X Golgi membrane buffer, 3 μL Oxygen Scavenger*) and 1.25 μL of 0.2 mg/mL biotinylated lipids (Biotin-CAP-PE, Avanti Polar lipids) were added to the previous Golgi membrane mix.

Following its incubation with the kinesin / Streptavidin mix, the chamber was then injected with 5 μL of the Golgi membrane mix directly after motility buffer and biotinylated lipid addition.

After membranes have settled down to the bottom of the chamber and have interacted with microtubule-binding kinesins, they were visualized under the confocal microscope.

*Oxygen Scavenger: 50X stock with 9 mg Catalase (C9322, Sigma) and 18.5 mg Glucose Oxidase (G2133) in 100 μL Imi buffer.

3.3.4 Immunofluorescence on Golgi membranes

Golgi stacks were in reality only enriched in Golgi membranes but also contained other membrane types. In the course of our study, it became important to identify these different membranes. In order to do so, I adapted and modified the immunofluorescence protocol, usually used to identify different compartments of a cell.

First Golgi membranes needed to be immobilized at the bottom of the experimental chamber. The bottom side of the chamber was coated with Streptavidin by incubation with 0.25 mg/mL Streptavidin solution (1/4 dilution of a 1 mg/mL stock solution in Golgi membrane buffer) for 1 hour in a humid chamber (coverslip down). The chamber was then washed with Golgi membrane buffer (all injections are performed on the same side) to remove the excess unfixed Streptavidin, and incubated with a Golgi membrane – biotinylated lipid mix (5 μ L Golgi membrane solution + 1.5 μ L Biotin-CAP-PE from Avanti Polar lipids) for 30 minutes.

The chamber was subsequently filled with 2 μ M RAB proteins (dilution in Golgi membrane buffer) and washed 30 minutes later three times with Golgi membrane buffer. Fixation was then performed for 15 minutes using 4% paraformaldehyde (PFA, 16% stock diluted in Golgi membrane buffer) and the chamber was again washed two times with Golgi membrane buffer.

The chamber was incubated with Golgi membrane buffer supplemented with 0.2% (w/v) BSA for 15 minutes and finally injected with the primary antibody and, 1 hour later, with the secondary antibody (see **Table 3.2** for list of antibodies used). Several washing steps were performed after both incubations with antibodies using Golgi membrane buffer.

Table 3.2: List of primary and secondary antibodies used in this study.

Primary antibody	Species	Dilution	From	Secondary antibody	Fluorescent dye	Dilution
Anti-RAB11	Rabbit	1/100	Invitrogen	Anti-Rabbit	Far red Alexa647	1/400
Anti-RAB1 (ROF7)	Human	1/100	Recombinant antibodies platform, Institut Curie	Anti- Human	Red Cy3	1/400
Anti-GM130	Mouse	1/1000	BD Biosciences	Anti-Mouse	Far red Alexa647	1/400
Anti-EEA1	Goat	1/200	Santa Cruz Biotechnology	Anti-Goat	Red Cy3	1/400
Anti-ER	Mouse	1/1000	Perez team, Institut Curie	Anti-Mouse	Red Cy3	1/400

Chapter 4

4 Article: RAB proteins bind lipid packing defects

Title: Lipid packing defects and membrane charge control RAB GTPase recruitment

Running title: RAB proteins bind lipid packing defects

Guillaume Kulakowski^{a,b}, Hugo Bousquet^{a,b}, Jean-Baptiste Manneville^{a,b}, Patricia Bassereau^{b,c}, Bruno Goud^{a,b}, Lena K. Oesterlin^{a,b,1}

^aInstitut Curie, Paris Sciences et Lettres Research University, CNRS, UMR144, F-75005 Paris, France

^bSorbonne Universités, Université Pierre et Marie Curie, University Paris 06, CNRS, UMR 144, F-75005 Paris, France

^cLaboratoire Physico Chimie, Institut Curie, Paris Sciences et Lettres Research University, CNRS, UMR168, F-75005 Paris, France

¹**Corresponding author:**

Lena K. Oesterlin

Institut Curie, Paris Sciences et Lettres Research University, CNRS, UMR144, 26 rue d'Ulm, F-75005 Paris, France

Tel : +33 (0)1 56 24 64 06

E-mail : lena.oesterlin@curie.fr

Keywords: Membrane order, curvature sensing, lipid packing defects, prenylation, geranylgeranyl

Synopsis statement

Vesicular trafficking between intracellular compartments is regulated by many proteins such as RAB GTPases. Deciphering the molecular mechanisms governing RAB localization is thus critical to understand intracellular transport. We focused our study on the role of the physicochemical properties of membranes in the specific recruitment of RAB proteins. Using *in vitro* reconstitution, we demonstrate that a balance between electrostatic interactions and hydrophobic insertion of the RAB C-terminal prenyl group into lipid packing defects controls the recruitment of RAB proteins.

Abstract

Specific intracellular localization of RAB GTPases has been reported to be dependent on protein factors but the contribution of the membrane physicochemical properties to this process has been poorly described. Here, we show that three RAB proteins (RAB1/RAB5/RAB6) preferentially bind *in vitro* to disordered and curved membranes, and that this feature is uniquely dependent on their prenyl group. This implies RAB proteins can sense lipid packing defects induced by unsaturated conical-shaped lipids and curvature. Consistently, RAB recruitment increases with the amount of lipid packing defects, further indicating that these defects drive RAB membrane targeting. Membrane binding of RAB35 is also modulated by lipid packing defects but primarily dependent on negatively charged lipids. Our results suggest that a balance between hydrophobic insertion of the prenyl group into lipid packing defects and electrostatic interactions of the RAB C-terminal region with charged membranes tunes the specific intracellular localization of RAB proteins.

Introduction

RAB proteins are small GTPases of the RAS superfamily that are involved in many steps of transport inside the cell. There are over 60 RAB proteins in humans and they all localize to distinct membrane compartments. RAB proteins which oscillate between an active form (GTP-bound) and an inactive form (GDP-bound) can bind to membranes with the help of their prenyl group (geranylgeranyl group), a post-translational lipid modification at their C-terminal extremity. The RAB Escort Protein (REP), known to be involved in RAB prenylation, and the GDP Dissociation Inhibitor (GDI), known to bind to soluble RABs, are known to play key roles in both the delivery and the recycling of RAB proteins to and from membranes^(1,2) but cannot account for their specific intracellular localization. Until now, multiple studies have suggested that RAB specific membrane targeting could be mediated by protein factors such as Guanine nucleotide Exchange Factors (GEF), originally known to activate RABs by nucleotide exchange⁽³⁾, and GDI Displacement Factors (GDF), thought to influence the release of prenylated RAB proteins from GDI^(4,5). Extensive sequence analysis, domain swapping and mutagenesis studies of different RAB proteins have shown that specific domains are involved in RAB targeting to membranes. Pereira-Leal and coworkers⁽⁶⁾ identified five RAB family regions that distinguish RAB proteins from the other members of the RAS superfamily and four subfamily regions that stand to differentiate each RAB subfamily. Different combinations of mutations of these domains led to mislocalization of the RAB proteins suggesting that membrane specificity is also determined by specific RAB sequences⁽⁷⁾. The hypervariable region of RAB35 has also been shown to be determinant for proper membrane targeting⁽⁸⁾.

While protein-protein interaction has been widely studied to explain RAB specific membrane targeting, very little is known about the influence of the membrane itself. Diverging from the initial fluid mosaic model⁽⁹⁾, it is now known that membranes are crowded and heterogeneous environments with lipids and proteins diffusing laterally allowing the formation

of regions which vary in thickness and composition⁽¹⁰⁾. Due to specific lipid metabolism and selective transport, cellular membranes have heterogeneous lipid compositions with asymmetrical lipid compositions between the two leaflets⁽¹¹⁾. Because of their diversity, lipid membranes exhibit different physicochemical properties such as lipid order, bending rigidity or curvature. Lipid nanodomains have been shown to exist in biological membranes⁽¹²⁾ in a so-called 'raft phase' (or Liquid ordered Lo phase) enriched in saturated lipids, and in a non-raft phase (or Liquid disordered Ld phase), enriched in unsaturated lipids. Membrane curvature is also a key feature of intracellular membranes as most cellular organelles display regions of both low and high curvature. For example, the endoplasmic reticulum is formed of a complex network of interconnected flat sheets and highly curved tubules^(13,14), and endosomes display globular (low curvature) and tubular regions⁽¹⁵⁾.

In cellular membranes, specific membrane compositions or membrane curvature can induce the formation of defects in the arrangement of lipids. Indeed, membranes containing conical shaped lipids, such as phosphatidylethanolamine (PE) or diacylglycerols (DAG) will be less prone to have an ordered structure as compared to phosphatidylcholine (PC) membranes⁽¹⁶⁻¹⁸⁾. External constraints applied for instance by the cytoskeleton, protein coats, or insertion of amphipathic protein domains can force a lipid bilayer to bend⁽¹⁷⁻¹⁹⁾. In such a conformation the surface area of the lipid headgroup region of one monolayer is expanded whereas the hydrophobic region remains undisturbed. Biologically, lipid packing defects can be beneficial as they were shown to facilitate the folding of some transmembrane proteins and to be essential for binding to membranes of some peripheral proteins^(20,21). The varying amounts of packing defects could thus represent a key feature explaining why some membrane proteins are inserted into specific membrane areas.

In this work, we investigate the role of the physicochemical properties of membranes in the binding of RAB proteins using *in vitro* assays consisting of purified RAB proteins and giant unilamellar vesicles (GUVs) as model membranes of controlled lipid composition⁽²²⁾.

Results and discussion

Four RAB proteins, that localize to distinct membranes in cells, were chosen for our study: RAB1 and RAB6 which associate with pre-Golgi and Golgi/trans Golgi network membranes respectively, RAB5 which is present on early endosomes and RAB35 which mainly localizes to the plasma membrane⁽²³⁾ (see *SI Text*).

RAB6 specifically localizes to the Ld phase independently of its activation and prenylation state.

To test whether RAB proteins show specific recruitment to a given lipid phase, we investigated the recruitment of purified RAB proteins to GUVs exhibiting phase separation between Lo and Ld domains⁽²⁴⁾. GUVs were formed using a lipid mixture consisting of brain sphingomyelin (BSM), cholesterol and 1,2-dioleoyl-sn-glycero-3-phosphocholine

(DOPC) (3:1:3 molar ratio) ⁽²⁵⁾. No binding of unprenylated RAB proteins was observed on these membranes (Fig. S1) which is in good agreement with the commonly accepted view that RAB proteins are incorporated into biological membranes through their C-terminal geranylgeranyl groups ⁽²⁶⁾. Most RAB GTPases are diprenylated in the cell with the addition of two geranylgeranyl moieties on the two C-terminal cysteines ⁽²⁷⁾. The use of diprenylated proteins (Fig. S2A) is technically challenging due to the high affinity of the GDP-bound RAB for the REP ⁽²⁸⁾, which prevents binding to GUV membranes. Recruitment of diprenylated RAB6 to membranes exhibiting phase separation was however achieved through the use of additional protein factors (following a protocol detailed in Fig. S3) and clear segregation to the Ld phase was observed (Fig. S3A). Similar experiments were performed with monoprenylated GDP-bound RAB6 (Fig. S2B) and specific binding to Ld domains could also be observed in presence but also in absence of additional protein factors (Fig. S3B and Fig. 1A). To confirm these results, experiments were performed with GUVs composed of pure Ld phase (DOPC and cholesterol in a 1:1 molar ratio) or to GUVs composed of pure Lo phase (BSM and cholesterol in a 1:1 molar ratio) ⁽²⁵⁾. GDP-bound RAB6, independently of its mono- diprenylation status, was only recruited to Ld GUVs but not to Lo GUVs (Fig. S3 and Fig. 1B). Thus, RAB6 displayed similar membrane binding behavior on GUVs independently of its mono- or diprenylation status. Diprenylated RABs can only be activated by nucleotide exchange in the presence of membrane to avoid precipitation of the proteins; therefore preventing any measurement of the amount of active GTP-bound RABs in our system. For this reason we focused our study on monoprenylated RAB proteins.

The previous experiments were performed using GDP-bound (inactive) RAB6. However RAB proteins localize in the cytosol in their GDP-bound inactivated form and get activated (GTP-bound) by GEFs upon membrane incorporation ⁽²⁹⁾. As membrane bound RAB proteins are mostly active, we investigated the binding of RAB proteins in their GTP-bound form. Similarly to its GDP-bound form, monoprenylated GTP-bound RAB6 was only recruited to Ld domains on GUVs displaying phase separation (Fig. 1A) and recruitment was only observed on Ld vesicles but not on Lo vesicles (Fig. 1B); indicating that RAB6 specific binding was independent of its activation state. It should be noted that a quantitative comparison of fluorescence intensities is not feasible due to different prenylation and labeling efficiencies. As membrane-bound RAB proteins are mostly loaded with GTP in the cell and are known to fulfill their functions as such, only activated (GTP- or GppNHp-bound) RABs were used in the following experiments.

Some RAB proteins can undergo additional C-terminal modifications following geranylgeranylation, such as proteolysis and/or carboxyl methylation, depending on their prenylation motif ^(30,31). RAB carboxyl methylation, which consists in the addition of a carboxyl group to the exposed prenylated cysteine, was shown to enhance the hydrophobicity of the C-terminus and subsequently to increase membrane affinity ⁽³¹⁾. However, since the absence of methylation was shown to only affect the cycle of RAB membrane/cytosol partitioning, but not

their specific membrane localization ⁽³¹⁾, we did not investigate the potential effects of RAB carboxyl methylation in our *in vitro* experiments.

RAB proteins specifically localize to the Ld phase through their geranylgeranyl group.

Similarly to RAB6, monoprenylated and activated RAB1 and RAB5 segregated specifically to Ld domains on GUVs displaying phase separation (Fig. 1A) and recruitment was only observed on Ld vesicles but not on Lo vesicles (Fig. 1B).

We next investigated whether the prenyl group plays a direct role in the specific recruitment of RAB proteins to the Ld phase. For that purpose, we looked at the recruitment of glutathione S-transferase (GST) to which a CVIL prenylation motif was added at its C-terminus. The purified and fluorescently labeled protein was enzymatically monoprenylated using the same protocol than for the RAB proteins. As shown in Fig. 1, monoprenylated GST also specifically segregates to Ld domains. On the other hand, no recruitment of unprenylated GST could either be detected on Lo or Ld domains (Fig. S1), confirming that the prenyl group is required and sufficient for GST membrane insertion.

Altogether, the above results suggest that the recruitment of RAB proteins to Ld membranes is mediated by the geranylgeranyl moiety. The chemical structure of this C20 isoprenoid chain shows a high degree of unsaturation ("kinks" in the prenyl chain) (Fig. S2C), which might lead to preferential insertion of the geranylgeranyl moiety into Ld membranes. In agreement with this, it was recently shown that the unsaturated C15 isoprenoid farnesyl group, linked to the C-terminus of K-RAS4B spontaneously inserts into loosely packed bilayers consisting of unsaturated lipids (Ld phase) ⁽³²⁾. Preferential partitioning to flat Ld membranes was also observed for N-RAS proteins ⁽³³⁾. In contrast, the addition of a saturated C16 hydrocarbon chain palmitoyl group to transmembrane proteins mediates their dynamic targeting to raft-like Lo phases ⁽³⁴⁾. Thus, a likely hypothesis is that the high degree of unsaturation of the prenyl groups favors their insertion into Ld membranes.

RAB35 membrane recruitment is driven by both the charged hypervariable region and the prenyl group.

The great majority of RAB GTPases, including the previously tested RAB1, RAB5 and RAB6, are found associated with intracellular membranes ⁽²³⁾. RAB35 on the other hand, was shown to localize to intracellular endocytic compartments but also to the plasma membrane ⁽³⁵⁾. We thus wondered whether RAB35 membrane binding was governed by a similar mechanism. We first tested the recruitment of monoprenylated RAB35 to Lo and Ld GUVs. Unexpectedly, RAB35 was not recruited to either of these membranes (Fig. 2A), indicating that the prenyl group is not sufficient to drive RAB35 membrane insertion.

Endosomal and plasma membranes are known to be negatively charged due to the large amount of phosphoinositides and phosphatidyl-serine ⁽¹¹⁾, anionic lipids known to play major roles in signaling processes and membrane dynamics ^(36,37). RAB35 contains stretches of positively charged

residues at its C-terminal region, the last 20 amino acid region being the most charged as compared to that of the other RABs (Table S1). *In cellulo* studies have shown that this polybasic region is essential for targeting RAB35 to the plasma membrane⁽⁸⁾ indicating that RAB35 localization depends on electrostatic interactions between the negative charge of the inner leaflet of the plasma membrane and the positive charges of the RAB35 C-terminal region. To address the role of electrostatic interactions, we monitored the recruitment of RAB35 on negatively charged GUVs. The experiments were performed with anionic Lo and Ld GUVs by replacing cholesterol with negatively charged sulfate cholesterol (See *SI Text*). RAB35 binding was now observed on both Lo and Ld vesicles (Fig. 2A). These results confirm that RAB35 membrane recruitment is mediated by electrostatic interactions and clearly demonstrate that, in contrast to the other RAB proteins that we tested, RAB35 can also bind to Lo domains.

We then investigated whether the prenyl group is required for RAB35 membrane binding to negatively charged vesicles. No binding of unprenylated RAB35 to charged vesicles was observed (Fig. 2A), suggesting that both the electrostatic interactions and the prenyl group are necessary for RAB35 recruitment, but also that prenyl groups are able in some cases to interact with Lo membranes. Additionally, we quantified the area density of prenylated RAB35 (Φ_v) using Eq. 1 and observed a threefold increase in recruitment to Ld vesicles as compared to Lo vesicles (Fig. 2B). This is consistent with the previous observations that RAB proteins preferentially bind to Ld domains. Taken together, our results suggest that the membrane recruitment of C-terminally charged and prenylated RAB proteins is primarily dependent on the presence of anionic lipids. This specificity for negatively charged membranes gives the ability to RAB35 to overcome the exclusive binding of the prenyl group to Ld domains. This charge dependency is crucial for RAB35 interaction with negatively charged endosomal and plasma membranes. Interestingly, when comparing the charge of the last 20 amino acids of all human RAB proteins, we found that RAB23 and RAB35 display the highest positive charge (Table S1). RAB23 has also been shown to localize to the plasma membrane⁽³⁸⁾ suggesting that its specific recruitment to the plasma membrane might also be mediated by electrostatic interactions. Furthermore, in good agreement with this, previous studies demonstrated that the recruitment of proteins of the RAS family (K-RAS4B and RND3) to the plasma membrane can be modulated by electrostatic interactions between the positively charged C-terminus and anionic phospholipid headgroups^(39,40).

RAB proteins can sense membrane curvature through their prenyl group.

Most RAB proteins, for instance RAB1 or RAB6, are present on transport vesicles which typically have a diameter of 40-60 nm^(41,42) and can thus be regarded as curved membranes. We therefore investigated the influence of membrane curvature on RAB membrane recruitment. As a model, we used an optical tweezer setup to pull membrane tubes from EggPC GUVs (with additional 0.1% mol of TexasRed-DHPE lipids)

^(43,44) (Fig. S4A). RAB protein relative enrichment (or sorting) between the highly curved tube and the flat GUV membrane was imaged by confocal microscopy. Tuning membrane tension through micropipette aspiration of the GUV allows us to modulate the tube radius and to measure protein sorting for increasing curvature (up to $1/15 \text{ nm}^{-1}$). Biological membranes are two-dimensional surfaces with two principal curvatures $C_1 = 1/R_1$ and $C_2 = 1/R_2$ (with R_1 and R_2 referred to as the principal radii of curvature) along two perpendicular directions⁽⁴⁵⁾. The total curvature of the membrane is $C = C_1 + C_2$. In the case of a spherical vesicle of radius R , the membrane deforms equally in both directions leading to $C_1 = C_2 = 1/R$ and a total curvature $C_v = 2/R$. In the case of a cylindrical tube of radius R , which is curved only in one direction and flat in the other, $C_1 > 0$ and $C_2 = 0$ yielding a total curvature $C_t = 1/R$ ⁽⁴⁵⁾. A 15 nm radius tube will thus have the same curvature as a 30 nm radius intracellular transport vesicle⁽⁴²⁾, indicating that the typical curvatures in our experiments are biologically relevant.

Curvature sensing was assessed by calculating the sorting ratio (S) defined as the protein/lipid signal ratio on the tube divided by that observed on the GUV^(43,44) (Eq. 2 and Fig. S4B). When the tube radius was decreased (i.e. the curvature was increased), a clear enrichment of the proteins was detected in the tube region (Fig. 3A). Sorting was different among the studied RAB proteins, with a ratio increasing up to 5.5, 3 and 2.5 times at a 15 nm tube radius for RAB5, RAB6 and RAB1, respectively.

Because curvature sensing depends on the protein area density (Φ_v)⁽⁴⁴⁾, sorting values cannot be directly compared among RAB proteins. The protein density is coupled to membrane curvature through a protein curvature coupling coefficient (also called protein spontaneous curvature, C_p)⁽⁴⁴⁾. To quantitatively compare the sorting of RAB proteins with that of other proteins, we used the theoretical model previously developed by Sorre and coworkers⁽⁴⁴⁾ and the resulting equation: $S = 1 + 1/(R_t C_p \phi_v)$ where S is the sorting ratio, R_t is the tube radius, C_p is the effective spontaneous curvature of the protein and ϕ_v is the protein area fraction which is related to Φ_v by $\Phi_v = \rho \phi_v$ (ρ is the inverse of the area per protein). The intrinsic curvature radius of the protein C_p^{-1} can be determined by plotting $(S-1) \phi_v$ as a function of curvature ($1/R_t$) and taking the resulting slope of the linear fit (Fig. 3B). Φ_v was assessed using Eq. 1 and ρ was estimated by assuming that RAB proteins are spherical proteins of around 25 kDa with a corresponding average radius of 2 nm ($\rho = 1/12.6 \text{ nm}^{-2}$)⁽⁴⁶⁾. C_p^{-1} values were respectively $2.1 \pm 0.2 \text{ nm}$, $2.6 \pm 0.1 \text{ nm}$ and $1.5 \pm 0.1 \text{ nm}$ for RAB1, RAB5 and RAB6. The three RAB proteins display similar spontaneous curvatures, in the same range as what was obtained for Amphiphysin ($1.9 \pm 0.4 \text{ nm}$)⁽⁴⁴⁾, a known curvature sensor⁽⁴⁷⁾. However, Amphiphysin senses curvature both through its highly curved Bin/Amphiphysin/Rvs (BAR) domain and its N-terminal amphipathic helix^(47,48). Rab proteins interact with membranes through the hydrophobic insertion of their prenyl group into the bilayer while a few amino acid residues close to the prenylation site will be in proximity to the lipid headgroups. Thus, the geometry

of the inserted domain may be comparable to that of lipids with inverted conical shapes, such as lysophosphatidic acids (LPAs). LPAs generate local positive curvature and display a spontaneous curvature radius of 2 nm⁽⁴⁵⁾, a value close to those we obtained for RAB proteins.

We next investigated the contribution of the prenyl group to the sensitivity of RAB proteins for curved membranes using monoprenylated GST. As shown in Fig. 3A, a clear enrichment of monoprenylated GST in membrane tubes pulled from GUVs was observed (4 fold increase on tubes of 15 nm radius). The spontaneous curvature radius of monoprenylated GST was measured using the same model as above. We found $C_p^{-1} = 2.8 \pm 0.1$ nm, which is very similar to the values obtained for RAB proteins (Fig. 3B). This suggests that RAB curvature sensing is independent of the tertiary structure of the protein but, similarly to their preference for Ld membranes, depends on the geranylgeranyl moiety.

Prenylated proteins show preferences for lipid packing defects.

The Ld phase is characterized by the assembly of unsaturated lipids which are known to promote lipid packing defects⁽⁴⁹⁾. Membrane curvature was also shown to lead to the appearance of defects in the arrangement of lipids⁽⁴⁹⁾. To explain the preferential binding of RAB proteins to Ld membranes and their sensitivity to curvature, we hypothesized that RAB membrane recruitment is dependent on the presence of lipid packing defects in the bilayer.

To test this hypothesis, we performed recruitment experiments with GUVs containing 15% mol 1-2-dioleoyl-*sn*-glycerol (DOG), a conical-shaped lipid that was shown to induce the formation of packing defects similar to those found on positively curved membranes⁽⁵⁰⁾. Control GUVs containing lower amounts of lipid packing defects were composed of 15% mol DOPC cylindrical lipids (See *S/Text*). The membrane recruitment of all monoprenylated proteins was significantly increased in the presence of DOG (Fig. 4), i.e. in presence of higher amounts of lipid packing defects.

Unlike DOG, polyunsaturated fatty acids (PUFAs), such as 1-stearoyl-2-docosahexaenoyl-*sn*-glycero-3-phosphoethanolamine (PUFA PE), were shown to decrease the amount of lipid packing defects, especially in curved membranes⁽⁵¹⁾. We measured RAB and GST binding on GUVs composed of 30% mol PUFA PE and used as a control GUVs containing higher amounts of packing defects and composed of 30% mol 1-palmitoyl-2-oleoyl-*sn*-glycero-3-phosphoethanolamine (POPE) (See *S/Text*). We found that the membrane recruitment of geranylgeranylated proteins significantly decreases in the presence of PUFA PE (Fig. 5) i.e. when the amount of packing defects is decreased.

Altogether, the above results suggest that lipid packing defects are drivers of RAB membrane recruitment and that this lipid packing defect sensing is mediated by the C-terminal prenyl group.

Conclusions

It has been known for a long time that prenyl groups act as non-specific membrane anchors but our results, together with recently published data^(33,52),

highlight a role for prenyl groups (farnesyl and geranylgeranyl) in specific membrane domain targeting. Similarly to what we found with geranylgeranylated RAB proteins, farnesylated N-RAS preferentially binds to Ld domains on flat membranes and its differential membrane recruitment was shown to rely on the presence of lipid packing defects induced by curvature and specific lipid geometrical shapes^(33,52). A likely explanation is that prenyl groups are largely unsaturated and have a kinked structure allowing them to get preferentially inserted into membranes containing packing defects such as Ld or curved membranes.

This lipid-driven membrane binding mechanism sheds new light on how RAB GTPases could bind to membranes. Intracellular membranes are mainly composed of Ld phases⁽⁵³⁾, and many RAB proteins associate with highly curved transport vesicles^(41,42). Our hypothesis is that the addition of one or two geranylgeranyl moieties on all RAB proteins serves as a core mechanism to bind them to specific membrane domains displaying lipid packing defects, the specificity for a given compartment (ER, Golgi, endosomes) relying then on other mechanisms such as the presence of specific GEFs⁽³⁾.

An interesting variation to this theme is given by RAB35 which has a positively charged C-terminus and is mainly found at steady state associated with the plasma membrane and the endocytic compartments⁽³⁵⁾. We showed that RAB35 membrane recruitment is primarily dependent on the presence of negatively charged lipids which are also predominantly found on endosomal and plasma membranes⁽¹¹⁾. Even though lipid packing defects enhance RAB35 membrane affinity, they are not essential for membrane binding.

In conclusion, our work illustrates that the physicochemical properties of membranes, such as charge distribution and lipid packing defects, could be prime determinants of the localization of RAB proteins to cellular membranes.

Material and Methods

***In vitro* monoprenylation and diprenylation.** The prenylation reaction consists in the addition of one or two C20 geranylgeranyl moieties (Geranylgeranyl pyrophosphate, GGpp, Sigma) at the C-terminal extremity of the proteins. Prenylation was achieved either through monoprenylation (addition of one geranylgeranyl group) using purified Geranylgeranyl Transferase type 1 (GGTase1) (Fig. S2B) or diprenylation (addition of two geranylgeranyl groups) using the native prenylation machinery consisting of purified RAB Geranylgeranyl Transferase (RABGGTase or GGTase2) and RAB Escort Protein (REP) (Fig. S2A).

Monoprenylation reactions were performed at 25°C for 1.5 h with a molar ratio of 0.5:1:5 GGTase1, RAB and GGpp. Molar ratios for the diprenylation reaction were: 1:5:0.5:0.75 RABGGTase:GGpp: RAB:REP and the reaction was performed at 25°C for 4 h. To control efficient protein prenylation, NBD-Farnesyl pyrophosphate (Jena Bioscience), a C15 fluorescent analog of GeranylGeranyl pyro-phosphate, was used as described in⁽⁵⁴⁾.

Giant Unilamellar Vesicles. GUVs were grown on indium tin oxide coated (ITO) glass slides using the electroformation technique⁽⁵⁵⁾. 15 μ L of a 0.5 mg/mL lipid mix was dried on ITO coated slides for a few minutes at 50°C and subsequently under vacuum for at least 2 h. The dried lipid film was then rehydrated in a sucrose solution (osmolarity between 100 and 430 mOsm, depending on the osmolarity of the protein buffer used for the experiments) and GUVs were grown for 3 h under a sinusoidal voltage (1.1 V, 10 Hz). GUV growth was most of the time performed at room temperature except in the case of phase separation (see *SI Text*) where it was performed at 50°C.

Membrane tube pulling by optical tweezers. A highly curved membrane tube was pulled out from an EggPC containing GUV, aspirated in a micropipette to control its membrane tension, using 3.2 μ m diameter beads trapped in an optical tweezer as previously described in⁽⁴³⁾ (Fig. S4A). The membrane tension was increased in a stepwise fashion to decrease the tube radius and hence increase membrane curvature⁽⁴³⁾. The reaction buffer used was the one specific of the studied protein and was supplemented with 0.1 mg/mL β -Casein to prevent adhesion of the GUV to the glass. Membrane binding was studied using 100-300 nM final concentration of protein.

Measurement of protein density on the membrane. Protein density was assessed as previously described⁽⁴⁴⁾. Briefly, fluorescence was calibrated using GUVs made of EggPC lipids and BodipyFL-C5-HPC (HPC), a green fluorescent lipid, at various concentrations. The HPC area density on the GUV (Φ_v^{HPC}) can be calculated by assuming that the average area occupied by a single PC molecule is 0.7 nm²⁽⁵⁶⁾. The fluorescent intensity of this lipid on the GUV membrane was measured (I_v^{HPC} at a given confocal photomultiplier tube detector gain) for each area density. A linear fit of the fluorescence vs. area density plot gave the conversion constant (A_{gain}) ($\Phi_v^{HPC} = A_{gain} \times I_v^{HPC}$). Proteins were labeled with the Alexa488 fluorophore and lipids with BodipyFL-C5-HPC, two fluorophore exhibiting different spectral properties. Thus, we measured the correction factor $F = I_{bulk}^{A488} / I_{bulk}^{HPC}$, i.e. the ratio of fluorescence intensities of Alexa488 and HPC respectively at a given concentration in solution. Both fluorescent signals in bulk scaled linearly with their concentration and F is defined as the ratio between the slopes of the Alexa488 linear fit and that of HPC. The protein labeling efficiency was taken into account by calculating the degree of labeling (n^*) of the protein using Eq. **S1**. Protein density on the GUV membrane (Φ_v^{prot}) was thus given by:

$$\Phi_v^{prot} = \frac{A_{gain}}{F \times n^*} \times I_v^{prot} (gain) \quad [1]$$

Measurement of sorting ratio. In order to quantify protein sorting to the tube, the fluorescence intensity of the Alexa488 labeled protein ($I_{protein}$) was normalized by the intensity of the fluorescent lipid (TexasRed-DHPE, I_{lipid}) at each tension step increase. The sorting ratio S corresponds to the ratio between

the normalized protein intensity on the tube and the same normalized intensity on the GUV (Fig. S4B):

$$S = \frac{(I_{protein}/I_{lipid})_{tube}}{(I_{protein}/I_{lipid})_{vesicle}}$$

[2]

ACKNOWLEDGMENTS. We thank Roger Goody for providing the plasmids to express the prenylation machinery. Ahmed El Marjou is acknowledged for the purification of the REP protein. We thank Aymelt Itzen for critical reading of the manuscript. We thank Bruno Antony, Sandrine Etienne-Manneville and Jean-Claude Guillemot for stimulating discussions. We thank Ernesto Ambroggio, Maryam Alqabandi and Feng-Ching Tsai for their help with the fluorescence quantifications. We thank Mathieu Pinot for his technical assistance with the optical tweezer setup. This work was supported by an ERC (European Research Council) advanced grant (project 339847 'MYODYN'). The Goud team is a member of Labex CelTisPhyBio (11-LBX-038). L.K.O. was supported by a Marie Curie Intra European Fellowship (PIEF-GA-2012-326649).

The authors declare no conflict of interest.

References:

1. Alexandrov K, Horiuchi H, Steele-Mortimer O, Seabra MC, Zerial M. Rab escort protein-1 is a multifunctional protein that accompanies newly prenylated rab proteins to their target membranes. *EMBO J* 1994;13(22):5262-5273.
2. Alory C, Balch WE. Organization of the Rab-GDI/CHM superfamily: the functional basis for choroideremia disease. *Traffic* 2001;2(8):532-543.
3. Blumer J, Rey J, Dehmelt L, Mazel T, Wu YW, Bastiaens P, Goody RS, Itzen A. RabGEFs are a major determinant for specific Rab membrane targeting. *J Cell Biol* 2013;200(3):287-300.
4. Hutt DM, Da-Silva LF, Chang LH, Prosser DC, Ngsee JK. PRA1 inhibits the extraction of membrane-bound rab GTPase by GDI1. *J Biol Chem* 2000;275(24):18511-18519.
5. Sivars U, Aivazian D, Pfeffer SR. Yip3 catalyses the dissociation of endosomal Rab-GDI complexes. *Nature* 2003;425(6960):856-859.
6. Pereira-Leal JB, Seabra MC. The mammalian Rab family of small GTPases: definition of family and subfamily sequence motifs suggests a mechanism for functional specificity in the Ras superfamily. *J Mol Biol* 2000;301(4):1077-1087.
7. Ali BR, Wasmeier C, Lamoreux L, Strom M, Seabra MC. Multiple regions contribute to membrane targeting of Rab GTPases. *J Cell Sci* 2004;117(Pt 26):6401-6412.
8. Li F, Yi L, Zhao L, Itzen A, Goody RS, Wu YW. The role of the hypervariable C-terminal domain in Rab GTPases membrane targeting. *Proc Natl Acad Sci USA* 2014;111(7):2572-2577.
9. Singer SJ, Nicolson GL. The fluid mosaic model of the structure of cell membranes. *Science* 1972;175(4023):720-731.
10. Engelman DM. Membranes are more mosaic than fluid. *Nature* 2005;438(7068):578-580.
11. van Meer G, Voelker DR, Feigenson GW. Membrane lipids: where they are and how they behave. *Nat Rev Mol Cell Biol* 2008;9(2):112-124.
12. Lingwood D, Simons K. Lipid rafts as a membrane-organizing principle. *Science* 2010;327(5961):46-50.
13. Voeltz GK, Prinz WA. Sheets, ribbons and tubules - how organelles get their shape. *Nat Rev Mol Cell Biol* 2007;8:258-264.
14. Shibata Y, Hu J, Kozlov MM, Rapoport TA. Mechanisms shaping the membranes of cellular organelles. *Annu Rev Cell Dev Biol* 2009;25:329-354.
15. Sonnichsen B, De Renzis S, Nielsen E, Rietdorf J, Zerial M. Distinct membrane domains on endosomes in the recycling pathway visualized by multicolor imaging of Rab4, Rab5, and Rab11. *J Cell Biol* 2000;149(4):901-914.
16. Frolov VA, Shnyrova AV, Zimmerberg J. Lipid polymorphisms and membrane shape. *Cold Spring Harb Perspect Biol* 2011;3(11):a004747.
17. McMahon HT, Boucrot E. Membrane curvature at a glance. *J Cell Sci* 2015;128(6):1065-1070.
18. Graham TR, Kozlov MM. Interplay of proteins and lipids in generating membrane curvature. *Curr Opin Cell Biol* 2010;22(4):430-436.
19. Kozlov MM, Campelo F, Liska N, Chernomordik LV, Marrink SJ, McMahon HT. Mechanisms shaping cell membranes. *Curr Opin Cell Biol* 2014;29:53-60.
20. Antony B. Mechanisms of membrane curvature sensing. *Annu Rev Biochem* 2011;80:101-123.
21. Cui H, Lyman E, Voth GA. Mechanism of membrane curvature sensing by amphipathic helix containing proteins. *Biophys J* 2011;100(5):1271-1279.
22. Walde P, Cosentino K, Engel H, Stano P. Giant vesicles: preparations and applications. *ChemBioChem* 2010;11(7):848-865.
23. Hutagalung AH, Novick PJ. Role of Rab GTPases in membrane traffic and cell physiology. *Physiol Rev* 2011;91(1):119-149.
24. Baumgart T, Hess ST, Webb WW. Imaging coexisting fluid domains in biomembrane models coupling curvature and line tension. *Nature* 2003;425(6960):821-824.
25. Roux A, Cuvelier D, Nassoy P, Prost J, Bassereau P, Goud B. Role of curvature and phase transition in lipid sorting and fission of membrane tubules. *EMBO J* 2005;24(8):1537-1545.
26. Pechlivanis M, Kuhlmann J. Hydrophobic modifications of Ras proteins by isoprenoid groups and fatty acids - More than just membrane anchoring. *Biochim Biophys Acta* 2006;1764(12):1914-1931.
27. Gomes AQ, Ali BR, Ramalho JS, Godfrey RF, Barral DC, Hume AN, Seabra MC. Membrane targeting of Rab GTPases is influenced by the prenylation motif. *Mol Biol Cell* 2003;14(5):1882-1899.
28. Wu YW, Oesterlin LK, Tan KT, Waldmann H, Alexandrov K, Goody RS. Membrane targeting mechanism of Rab GTPases elucidated by semisynthetic protein probes. *Nat Chem Biol* 2010;6(7):534-540.
29. Stenmark H. Rab GTPases as coordinators of vesicle traffic. *Nat Rev Mol Cell Biol* 2009;10(8):513-525.
30. Smeland TE, Seabra MC, Goldstein JL, Brown MS. Geranylgeranylated Rab proteins terminating in Cys-Ala-Cys, but not Cys-Cys, are carboxyl-methylated by bovine brain membranes in vitro. *Proc Natl Acad Sci USA* 1994;91(22):10712-10716.
31. Leung KF, Baron R, Ali BR, Magee AI, Seabra MC. Rab GTPases containing a CAAX motif are processed post-geranylgeranylation by proteolysis and methylation. *J Biol Chem* 2007;282(2):1487-1497.
32. Jang H, Abraham SJ, Chavan TS, Hitchinson B, Khavrutskii L, Tarasova NI, Nussinov R, Gaponenko V. Mechanisms of membrane binding of small GTPase K-Ras4B farnesylated hypervariable region. *J Biol Chem* 2015;290(15):9465-9477.

Chapter 4: Article: RAB proteins bind lipid packing defects

33. Larsen JB, Jensen MB, Bhatia VK, Pedersen SL, Bjornholm T, Iversen L, Uline M, Szeleifer I, Jensen KJ, Hatzakis NS, Stamou D. Membrane curvature enables N-Ras lipid anchor sorting to liquid-ordered membrane phases. *Nat Chem Biol* 2015;11(3):192-194.
34. Levental I, Lingwood D, Grzybek M, Coskun U, Simons K. Palmitoylation regulates raft affinity for the majority of integral raft proteins. *Proc Natl Acad Sci USA* 2010;107(51):22050-22054.
35. Kouranti I, Sachse M, Arouche N, Goud B, Echard A. Rab35 regulates an endocytic recycling pathway essential for the terminal steps of cytokinesis. *Curr Biol* 2006;16(17):1719-1725.
36. Di Paolo G, De Camilli P. Phosphoinositides in cell regulation and membrane dynamics. *Nature* 2006;443(7112):651-657.
37. Raghupathy R, Anilkumar AA, Polley A, Singh PP, Yadav M, Johnson C, Suryawanshi S, Saikam V, Sawant SD, Panda A, Guo Z, Vishwakarma RA, Rao M, Mayor S. Transbilayer lipid interactions mediate nanoclustering of lipid-anchored proteins. *Cell* 2015;161(3):581-594.
38. Evans TM, Ferguson C, Wainwright BJ, Parton RG, Wicking C. Rab23, a negative regulator of hedgehog signaling, localizes to the plasma membrane and the endocytic pathway. *Traffic* 2003;4(12):869-884.
39. Gomez GA, Daniotti JL. Electrical properties of plasma membrane modulate subcellular distribution of K-Ras. *FEBS J* 2007;274(9):2210-2228.
40. Madigan JP, Bodemann BO, Brady DC, Dewar BJ, Keller PJ, Leitges M, Philips MR, Ridley AJ, Der CJ, Cox AD. Regulation of Rnd3 localization and function by protein kinase C alpha-mediated phosphorylation. *Biochem J* 2009;424(1):153-161.
41. McMahon HT, Boucrot E. Molecular mechanism and physiological functions of clathrin-mediated endocytosis. *Nat Rev Mol Cell Biol* 2011;12(8):517-533.
42. Takamori S, Holt M, Stenius K, Lemke EA, Grønborg M, Riedel D, Urlaub H, Schenck S, Brügger B, Ringler P, Müller SA, Rammner B, Gräter F, Hub JS, De Groot BL, Mieskes G, Moriyama Y, Klingauf J, Grubmüller H, Heuser J, Wieland F, Jahn R. Molecular anatomy of a trafficking organelle. *Cell* 2006;127(4):831-846.
43. Ambroggio E, Sorre B, Bassereau P, Goud B, Manneville JB, Antonny B. ArfGAP1 generates an Arf1 gradient on continuous lipid membranes displaying flat and curved regions. *EMBO J* 2010;29(2):292-303.
44. Sorre B, Callan-Jones A, Manzi J, Goud B, Prost J, Bassereau P, Roux A. Nature of curvature coupling of amphiphysin with membranes depends on its bound density. *Proc Natl Acad Sci USA* 2012;109(1):173-178.
45. Zimmerberg J, Kozlov MM. How proteins produce cellular membrane curvature. *Nat Rev Mol Cell Biol* 2006;7(1):9-19.
46. Erickson HP. Size and shape of protein molecules at the nanometer level determined by sedimentation, gel filtration, and electron microscopy. *Biol Proced Online* 2009;11:32-51.
47. Peter BJ, Kent HM, Mills IG, Vallis Y, Butler PJ, Evans PR, McMahon HT. BAR domains as sensors of membrane curvature: the amphiphysin BAR structure. *Science* 2004;303(5657):495-499.
48. Bhatia VK, Madsen KL, Bolinger PY, Kunding A, Hedegard P, Gether U, Stamou D. Amphipathic motifs in BAR domains are essential for membrane curvature sensing. *EMBO J* 2009;28(21):3303-3314.
49. Bigay J, Antonny B. Curvature, lipid packing, and electrostatics of membrane organelles: defining cellular territories in determining specificity. *Dev Cell* 2012;23(5):886-895.
50. Vamparys L, Gautier R, Vanni S, Bennett WF, Tieleman DP, Antonny B, Etchebest C, Fuchs PF. Conical lipids in flat bilayers induce packing defects similar to that induced by positive curvature. *Biophys J* 2013;104(3):585-593.
51. Pinot M, Vanni S, Pagnotta S, Lacas-Gervais S, Payet LA, Ferreira T, Gautier R, Goud B, Antonny B, Barelli H. Lipid cell biology. Polyunsaturated phospholipids facilitate membrane deformation and fission by endocytic proteins. *Science* 2014;345(6197):693-697.
52. Larsen JB, Kennard C, Pedersen SL, Jensen KJ, Uline MJ, Hatzakis NS, Stamou D. Membrane Curvature and Lipid Composition Synergize To Regulate N-Ras Anchor Recruitment. *Biophys J* 2017.
53. Niko Y, Didier P, Mely Y, Konishi G, Klymchenko AS. Bright and photostable push-pull pyrene dye visualizes lipid order variation between plasma and intracellular membranes. *Sci Rep* 2016;6:18870.
54. Dursina B, Reents R, Delon C, Wu Y, Kulharia M, Thutewohl M, Veligodsky A, Kalinin A, Evstifeev V, Ciobanu D, Szedlacsek SE, Waldmann H, Goody RS, Alexandrov K. Identification and specificity profiling of protein prenyltransferase inhibitors using new fluorescent phosphoisoprenoids. *J Am Chem Soc* 2006;128(9):2822-2835.
55. Angelova M, Soléau S, Méléard P, Faucon JF, Bothorel P. Preparation of giant vesicles by external AC electric fields. Kinetics and applications. *Prog Colloid Polym Sci* 1992;89:127-131.
56. Nagle JF, Tristram-Nagle S. Structure of lipid bilayers. *Biochim Biophys Acta* 2000;1469(3):159-195.

Figure legends:

Fig. 1. Monoprenylated proteins specifically bind to liquid disordered domains independently of their activation/inactivation status. Prenylated proteins (RAB1, RAB5, RAB6 and GST) were labeled with Alexa488 fluorophore and monoprenylated. All images show GTP- or GppNHp-bound RAB proteins except for RAB6 which was also GDP-bound. GUVs were incubated with 2 μ M protein. (A) GUV phase separation was achieved using a 3:1:3 (molar ratios) BSM:Cholesterol:DOPC lipid mixture. The Ld phase is marked with 0.1% (mol/mol) TexasRed-DHPE lipids whereas the Lo phase composed of saturated lipids is unlabeled. All tested proteins localize specifically to the Ld phase as shown by the merge images. (B) Lo and Ld GUVs were respectively composed of 1:1 (molar ratios) BSM:Cholesterol and DOPC:Cholesterol. Prenylated proteins were recruited to Ld vesicles but not to Lo vesicles. (Scale bar: 10 μ m).

Fig. 2. Negative charges allow binding of RAB35 to both Ld and Lo membranes with a significant preference for Ld domains. GUVs were incubated with 2 μ M GFP-tagged RAB35. Neutral Lo and Ld vesicles were formed using 1:1 (molar ratios) of BSM:Cholesterol and DOPC:Cholesterol respectively. Negatively charged Lo and Ld vesicles were formed by replacing Cholesterol with Cholesterol Sulfate. (A) Monoprenylated RAB35 was only recruited to charged Lo and Ld vesicles but not to neutral Ld vesicles. A clear preference for the Ld negatively charged membrane can be observed. Unprenylated RAB35 is not recruited to charged vesicles. (B) Quantification of GFP-RAB35 protein density (Φ_v) on charged Lo and Ld membranes. We observed a threefold increase in RAB35 recruitment on disordered membranes. (Scale bar: 10 μ m; *** = t-test, p-value < 0.0001).

Fig. 3. Prenylated proteins can sense membrane curvature. A highly curved membrane tube was pulled with optical tweezers from an EggPC GUV containing the fluorescent lipid marker TexasRed-DHPE (red) in the presence of 100-300 nM Alexa488 labeled monoprenylated proteins (RAB1, RAB5, RAB6 and GST). (A) The plots show the protein sorting ratios (Eq. 1) as a function of tube curvature ($1/R_{\text{tube}}$). Data was obtained from 10 (RAB1, GST) or 7 (RAB5, RAB6) independent experiments. Each dot represents one sorting measurement at a given tube radius. Each plot was fitted with a linear regression (black line). For all prenylated proteins, sorting increases when the curvature is increased (i.e. when the tube radius is decreased). (B) Same data as in A plotted as $(S-1)\phi_v$ as a function of curvature ($1/R_t$). Following the theoretical model from Sorre and coworkers⁽⁴⁴⁾, the sorting ratio S is given by $S = 1 + 1/(R_t C_p \phi_v)$ where R_t is the tube radius, C_p is the effective spontaneous curvature of the protein and ϕ_v is the protein area fraction. $(S-1)\phi_v$ is thus predicted to scale linearly with the tube curvature ($1/R_t$) with a slope C_p^{-1} . Each plot was fitted with a linear regression (black line) to measure the intrinsic curvature radius of the protein C_p^{-1} (in nm).

Fig. 4. Increasing amounts of lipid packing defects enhance RAB membrane binding. RAB1, RAB5, RAB6 and GST were labeled using Alexa488, monoprenylated and incubated with GUVs at 2 μ M final concentration. DOG containing GUVs with a high density of lipid packing defects were formed using an 85% EggPC: 15% DOG (mol/mol) mix. In control GUVs, DOPC replaced DOG. The right panel shows the quantification of protein density on the membrane (Φ_v) in both DOPC and DOG containing vesicles. We observed a significant increase in protein recruitment on GUVs with higher levels of lipid packing defects. (Scale bar: 10 μ m; *** = t-test, p-value < 0.0001; ** = t-test, p-value = 0.0006).

Fig. 5. Decreasing amounts of lipid packing defects reduce RAB membrane binding. RAB1, RAB5, RAB6 and GST were labeled using Alexa488, monoprenylated and incubated with GUVs at 2 μ M final concentration. PUFA PE containing GUVs with a low density of lipid packing defects were formed using a 55% EggPC : 15% DOG : 30% PUFA PE (mol/mol) mix. In control GUVs POPE replaced PUFA PE. The right panel represents the quantification of protein density on the membrane (Φ_v) in both POPE and PUFA PE containing vesicles. We observed a significant decrease in protein recruitment on GUVs with lower levels of lipid packing defects. (Scale bar: 10 μ m; *** = t-test, p-value < 0.0001).

Figure 1

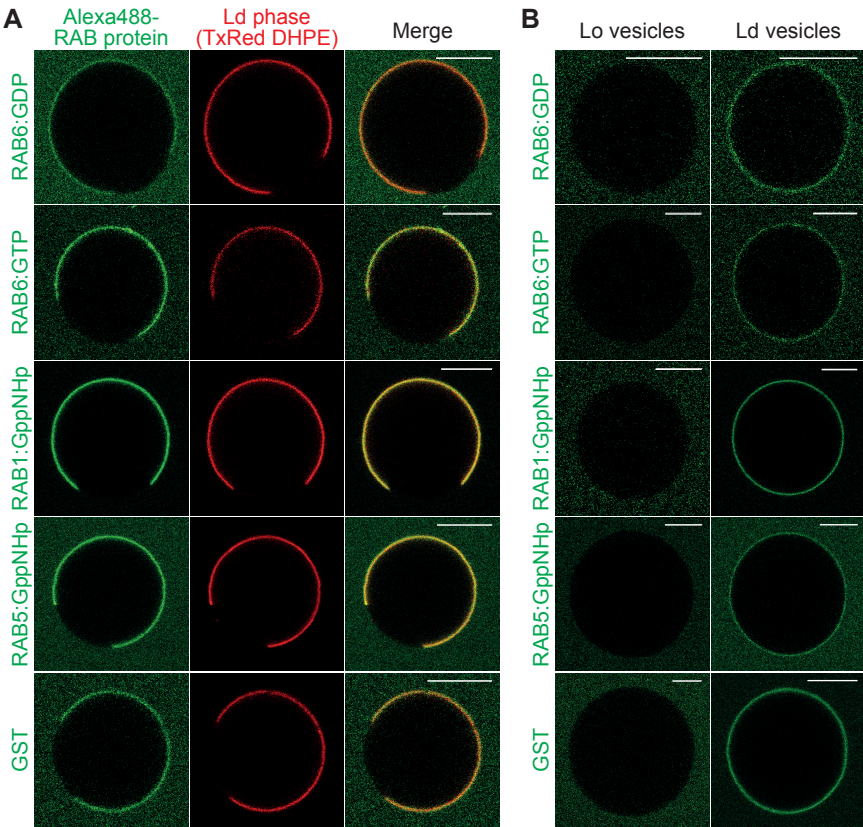


Figure 2

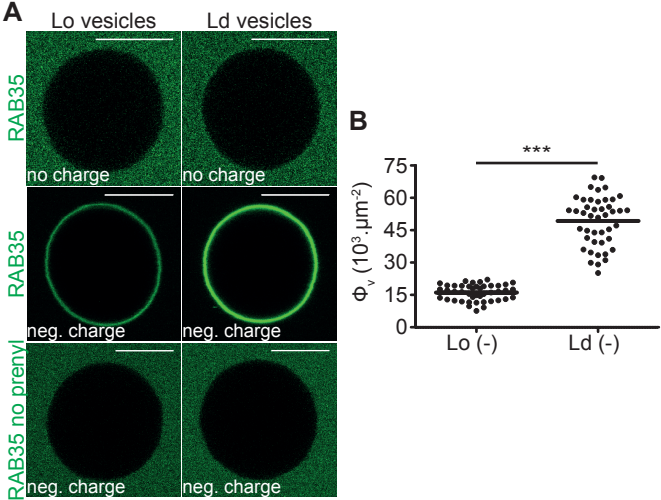


Figure 3

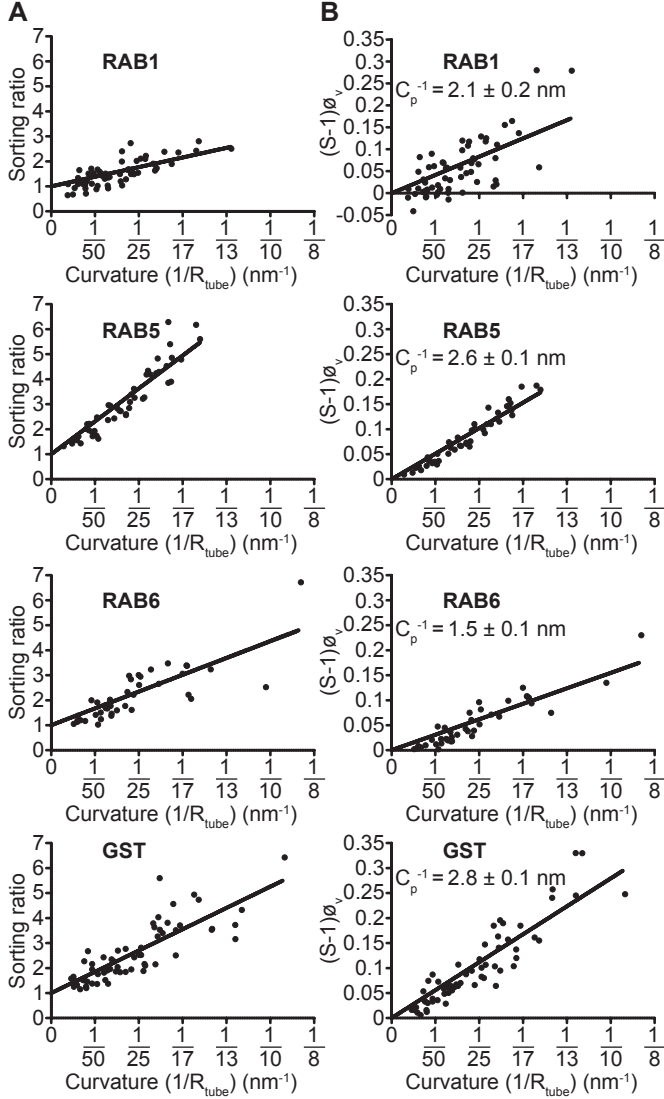


Figure 4

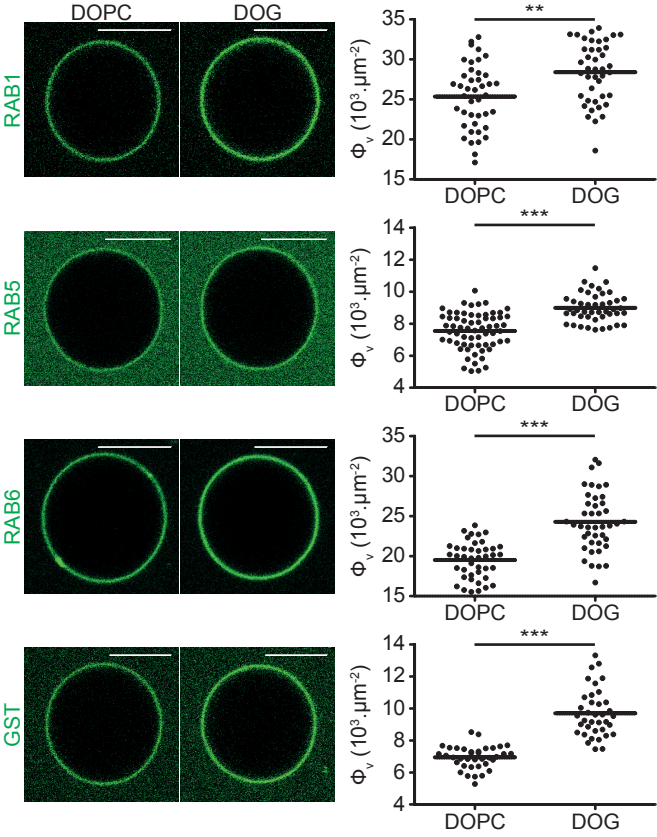
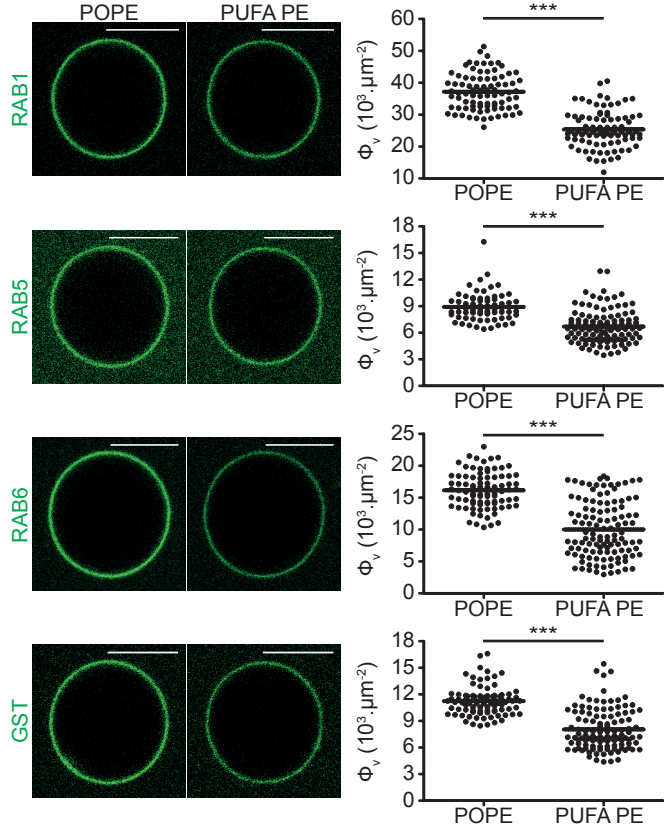


Figure 5



List of supplementary information

Supplementary text: Material and methods not necessary to understand the overall message of the paper, but required to reproduce the experiments.

Figure S1: Control experiment to demonstrate that RAB and GST proteins are only recruited to membranes if they are prenylated.

Figure S2: Graphic illustration of the different prenylation reactions performed in this study. This figure is mentioned at the beginning of the results and discussion section and can also be associated with the main material and methods section. It should allow the reader to better understand the protein modification reactions performed.

Figure S3: Control experiment to demonstrate why our study focused on the use of monoprenylated proteins rather than diprenylated proteins, which are most commonly found in the cell. This figure is mentioned in the first part of the results and discussion section and demonstrates that mono- and diprenylated RAB6 proteins are recruited to the same specific membrane domains.

Figure S4: Graphic illustration of the optical tweezer setup used to pull tubes from GUVs and of the quantification method used to assess protein enrichment to the tube. This figure is mentioned in the RAB curvature sensing section and can also be associated with the main material and methods section. It should help the reader to better understand the overall method used to study protein curvature sensing.

Table S1: Table showing the charge properties of the last 20 amino acids of all human RAB proteins. This figure is mentioned in the third part of the results and discussion section (on the study of RAB35 membrane recruitment). It will allow the reader to assess more easily the charge variations among the hypervariable domains of all RAB proteins and more specifically the higher positive charge of RAB35 and RAB23 as compared to the other RABs.

Supplementary text

Protein purification. Expression and purification of the prenyltransferases GGTase1 and RABGGTase were performed as described previously ⁽¹⁾. REP-1 was expressed in insect cells using a pFastBac vector and purified as in ⁽²⁾. RAB5A and codon optimized RAB1B were C-terminally modified, expressed and purified as described in ⁽³⁾. RAB6A, RAB35 and GST were also C-terminally modified with a CVIL motif (recognized by GGTase1 for monoprenylation) and were respectively expressed as a cleavable His6-fusion, His-GFP-fusion and GST-fusion constructs. RAB protein purification was performed at pH7.5 as previously described for RAB1B. GST purification was performed using Protino Glutathione Agarose 4B beads (Macherey Nagel). For RAB6A, residual His-tag was removed using a HisTrap HP column (GE Healthcare) and His₆-GFP-RAB35 was isolated as a fusion protein (no protease cleavage and no second affinity chromatography was required). Wild-Type RAB6A protein (RAB6A-WT) was purified the same way as the C-terminally modified RAB6A. His₆-mCherry-LidA_{aa201-583} was expressed and purified as previously described ⁽⁴⁾.

In vitro nucleotide exchange. Nucleotide exchange was induced chemically as described in ⁽⁵⁾. RAB6 was exchanged to GTP and GDP (Sigma Aldrich) and RAB1, RAB5, RAB35 were exchanged to GppNHP (Jena Bioscience), a non-hydrolysable analog of GTP. In order to measure the nucleotide bound state of the protein, an ion-paired reverse phase chromatography was performed as described in ⁽⁶⁾.

In vitro N-terminal labeling. The N-terminal labeling of the protein was performed using Alexa FluorTM 488 Sulfodichlorophenol ester (Alexa488 5-SDP ester, Molecular Probes). To ensure specific N-terminal labeling the reaction was performed at pH 7.5. The protein was incubated with a 4 fold molar excess of Alexa488 for 2 h at 25°C. A 250 fold molar excess of freshly prepared Hydroxylamine was added, for 1h at 25°C, to stop the reaction. A NAP column (GE Healthcare), pre-equilibrated with the protein buffer, was then run to remove excess unbound fluorophore. Protein concentration was determined by a Bradford assay. The efficiency of labeling (n) which corresponds to the ratio of moles of dye per mole of protein was determined after absorption measurements using the following formula:

$$n^* = \frac{A_{\max} \text{ of the labeled protein}}{\epsilon \times \text{protein concentration (M)}} \times \text{dilution factor}$$

[S1]

Where A_{\max} is the absorbance of the fluorescent protein at the wavelength maximum of the dye ($\lambda_{\max} = 488$ nm for Alexa488) and ϵ is the fluorescent dye molar extinction coefficient ($71,000 \text{ M}^{-1} \text{ cm}^{-1}$ for Alexa488).

Giant Unilamellar Vesicles: preparation and reagents. All lipids were from Avanti Polar Lipids. Phase separated GUVs contained Brain Sphingomyelin (BSM), Cholesterol and 1,2-dioleoyl-sn-glycero-3-phosphocholine (DOPC) at a molar ratio of 3:1:3 respectively ⁽⁷⁾ and were electroformed at 50°C

to allow lipid mixing. The other GUVs tested were electroformed at room temperature. Lo vesicles and Ld vesicles were respectively composed of BSM : Cholesterol and DOPC : Cholesterol at 1:1 molar ratios. The charged versions of Lo and Ld vesicles were composed of Cholesterol 3-sulfate instead of Cholesterol. To induce lipid packing defects, a 85% L- α -phosphatidylcholine (Egg, Chicken) (EggPC) : 15% 1-2-dioleoyl-sn-glycerol (DOG) (mol/mol) mix was used. In control experiments, DOG was replaced by DOPC. In order to decrease the amount of lipid packing defects 30% (mol/mol) of 1-stearoyl-2-docosahexaenoyl-sn-glycero-3-phosphoethanolamine (PUFA PE) was added to the previously mentioned DOG-containing mix, at the expense of EggPC. Control experiments were performed using 30% (mol/mol) of 1-palmitoyl-2-oleoyl-sn-glycero-3-phosphoethanolamine (POPE) instead of PUFA PE.

Tube pulling experiments were performed using EggPC vesicles. To achieve adhesion between the GUV membrane and the streptavidin-coated beads, 0.035% (mol/mol) of 1,2-distearoyl-sn-glycero-3-phosphoethanolamine-N-[biotinyl(poly-ethyleneglycol)-2000] (ammonium salt) (DSPE-PEG(2000)-Biotin) was added to the lipid mix (see also 'Membrane tube pulling by optical tweezers' section).

GUVs were made fluorescent by adding 0.1 (mol/mol) % of the red-emitting dye TexasRedTM 1,2-Dihexadecanoyl-sn-glycero-3-phosphoethanolamine (triethylammonium salt) (TexasRed-DHPE) from Molecular Probes.

Confocal microscopy. Confocal images were taken on a Nikon A1R microscope using a x100 objective. Green fluorescent dyes were excited with a 488 nm laser and red fluorescent dyes were excited with a 561 nm laser. Experiments were performed at room temperature (22°C). Images were quantified using the Fiji software ⁽⁸⁾.

Measurement of fluorescence intensities. Fluorescent intensities were measured using a rectangular selection including either the horizontal tube or the GUV membrane and subsequent averaging along vertical lines. All intensities were calculated after subtracting the noise level (intensity inside the vesicle) from the maximum of the fluorescence peak.

Supplementary references

1. Dursina B, Reents R, Delon C, Wu Y, Kulharia M, Thutewohl M, Veligodsky A, Kalinin A, Evstifeev V, Ciobanu D, Szedlacsek SE, Waldmann H, Goody RS, Alexandrov K. Identification and specificity profiling of protein prenyltransferase inhibitors using new fluorescent phosphoisoprenoids. *J Am Chem Soc* 2006;128(9):2822-2835.
2. Alexandrov K, Simon I, Yurchenko V, Iakovenko A, Rostkova E, Scheidig AJ, Goody RS. Characterization of the ternary complex between Rab7, REP-1 and Rab geranylgeranyl transferase. *Eur J Biochem* 1999;265(1):160-170.
3. Oesterlin LK, Goody RS, Itzen A. Posttranslational modifications of Rab proteins cause effective displacement of GDP dissociation inhibitor. *Proc Natl Acad Sci USA* 2012;109(15):5621-5626.
4. Schoebel S, Cichy AL, Goody RS, Itzen A. Protein LidA from Legionella is a Rab GTPase supereffector. *Proc Natl Acad Sci USA* 2011;108(44):17945-17950.
5. Muller MP, Peters H, Blumer J, Blankenfeldt W, Goody RS, Itzen A. The Legionella effector protein DrrA AMPylates the membrane traffic regulator Rab1b. *Science* 2010;329(5994):946-949.
6. Muller MP, Shkumatov AV, Oesterlin LK, Schoebel S, Goody PR, Goody RS, Itzen A. Characterization of enzymes from Legionella pneumophila involved in reversible adenylylation of Rab1 protein. *J Biol Chem* 2012;287(42):35036-35046.
7. Roux A, Cuvelier D, Nassoy P, Prost J, Bassereau P, Goud B. Role of curvature and phase transition in lipid sorting and fission of membrane tubules. *EMBO J* 2005;24(8):1537-1545.
8. Schindelin J, Arganda-Carreras I, Frise E, Kaynig V, Longair M, Pietzsch T, Preibisch S, Rueden C, Saalfeld S, Schmid B, Tinevez JY, White DJ, Hartenstein V, Eliceiri K, Tomancak P, Cardona A. Fiji: an open-source platform for biological-image analysis. *Nat Methods* 2012;9(7):676-682.
9. Wu YW, Oesterlin LK, Tan KT, Waldmann H, Alexandrov K, Goody RS. Membrane targeting mechanism of Rab GTPases elucidated by semisynthetic protein probes. *Nat Chem Biol* 2010;6(7):534-540.
10. Ambroggio E, Sorre B, Bassereau P, Goud B, Manneville JB, Antony B. ArfGAP1 generates an Arf1 gradient on continuous lipid membranes displaying flat and curved regions. *EMBO J* 2010;29(2):292-303.
11. Sorre B, Callan-Jones A, Manzi J, Goud B, Prost J, Bassereau P, Roux A. Nature of curvature coupling of amphiphysin with membranes depends on its bound density. *Proc Natl Acad Sci USA* 2012;109(1):173-178.

Supplementary figure and table legends

Fig. S1. Membrane recruitment of RAB proteins depends on the presence of the prenyl group. GUV phase separation was achieved by using a 3:1:3 (molar ratios) BSM:Cholesterol:DOPC lipid mixture. The Ld phase (made of of unsaturated lipids) was labelled with 0.1% (mol/mol) TexasRed-DHPE lipids (red) whereas the Lo phase (made of saturated lipids) was unlabeled. GUVs were incubated with 2 μ M Alexa488-labeled and unprenylated proteins. No membrane binding was observed with unprenylated proteins. (Scale bar: 10 μ m).

Fig. S2. Mechanisms of RAB prenylation. (A) Native diprenylation machinery consisting of a RAB protein with a double cysteine motif at its C-terminal extremity, the RAB Geranylgeranyl Transferase (RABGGTase, with two subunits α and β) and the RAB Escort Protein (REP). The RABGGTase transfers two geranylgeranyl groups on the double cysteine motif of the RAB protein, with the REP acting as a chaperone. (B) Monoprenylation of a RAB protein mediated by the Geranylgeranyl Transferase type 1 (two subunits α and β). The GGTase1 recognizes the CVIL motif at the C-terminus of the RAB protein (CAAX box) and transfers one geranylgeranyl group on the cysteine. (C) Structure of the geranylgeranyl pyrophosphate group. This lipid moiety has a C20 isoprenoid structure containing four unsaturations.

Fig. S3. Diprenylated and monoprenylated GDP-bound RAB6 are specifically recruited to disordered membranes. GUV phase separation was achieved by using a 3:1:3 (molar ratios) BSM:Cholesterol:DOPC lipid mixture. The Ld phase (made of of unsaturated lipids) was labelled with 0.1% (mol/mol) TexasRed-DHPE lipids (red) whereas the Lo phase (made of saturated lipids) was unlabeled. Lo and Ld GUVs were respectively composed of 1:1 (molar ratios) BSM:Cholesterol and DOPC:Cholesterol. Alexa488 labeled RAB6 proteins were used at a 2 μ M final concentration. *In vitro* diprenylation of RAB6 WT by both REP and the RABGGTase can only be performed if the RAB is inactive (i.e. GDP-bound). REP interacts with the RAB protein and then binds the RABGGTase in the presence of geranylgeranyl pyrophosphate. As the affinity of the RAB protein for the REP is very high (low nanomolar range)⁽⁹⁾, the RAB remains tightly bound to the complex even in the presence of membranes, thus preventing its recruitment. In order to overcome this issue and allow RAB recruitment, we added to the mixture a truncated version of the RAB6 supereffector from *Legionella pneumophila* LidA (LidA₂₀₁₋₅₈₃), which as an unusually high affinity for the RAB proteins in their GDP and GTP bound forms (respectively 4 nM and 30 pM affinities). As it was shown that LidA₂₀₁₋₅₈₃ covers an unusually large surface area of some RAB proteins⁽⁴⁾ and therefore shows overlapping binding sites with REP, it is possible to outcompete REP binding through the addition of this effector protein. By adding an equimolar concentration of LidA₂₀₁₋₅₈₃ and RAB:REP:RABGGTase (2 μ M) in the presence of membranes, we observed RAB membrane recruitment, confirming that LidA₂₀₁₋₅₈₃ outcompetes the RAB:REP:RABGGTase interaction. However, binding of RAB6 was also observed on Lo GUVs under these conditions. This is probably due to the dissociation of the RAB from the complex which forces the newly added hydrophobic prenyl groups to be in contact with the solvent. Therefore, because it is more energetically favorable, the RAB incorporates its prenyl group into the hydrophobic and more stable membrane environment. To prove this theory, we added GGTase1 to the experimental chamber (same molar ratios as for the monoprenylation reaction, see material and methods). Once LidA₂₀₁₋₅₈₃ has outcompeted the RAB:REP:RABGGTase interaction, GGTase1 (which does not have overlapping RAB binding sites with LidA₂₀₁₋₅₈₃) will interact with the prenyl group and shield it from the solvent. (A) In the presence of both LidA₂₀₁₋₅₈₃ and GGTase1, diprenylated RAB6 localizes specifically to the Ld phase on phase separated GUVs and to Ld vesicles. No recruitment is observed on Lo GUVs. (B) Monoprenylated GDP-bound RAB6 exhibits the same recruitment behavior in the presence of LidA₂₀₁₋₅₈₃ and GGTase1 as diprenylated RAB6. In the absence of LidA₂₀₁₋₅₈₃, monoprenylated GDP-bound RAB6 was also shown to bind specifically to Ld domains (Fig. 1) which demonstrates that this effector does not have any influence on the specific localization of RAB6 proteins. We conclude that RAB6 specifically binds to Ld domains independently of the quantity of prenyl groups. (Scale bar: 10 μ m).

Fig. S4. Pulling a tube from a GUV using an optical tweezer setup. (A) A biotin containing GUV was aspirated with a micropipette connected to a water reservoir which allows to control membrane tension. A bead coated with streptavidin was immobilized using an optical trap (highly focused infra-red laser beam)^(10,11). After addition of 100-300 nM of protein, a tube was pulled from the GUV through the interaction of the biotinylated lipids with the immobilized streptavidin coated bead. GUV tension was increased in a stepwise manner by decreasing the height of the water tank. 1 minute waiting time was required at each tension step increase to allow protein redistribution and sorting. (B) Vesicles were formed using EggPC lipids. Lipids were labelled using 0.1% (mol/mol) TexasRed-DHPE and 0.035% of DSPE-PEG(2000)-Biotin was added to the lipid mix to achieve adhesion between the GUV membrane and the streptavidin coated beads. At each tension step, confocal images of the green (protein) and red (lipid) channels were obtained and both fluorescence intensities were measured on the tube and on the GUV. The graphs represent the plots of intensities for both channels on the GUV and on the tube. Fluorescence intensities were calculated by subtracting the background noise (inside the vesicle) from the maximum of the fluorescence peak. The equation on the right defines the protein sorting ratio S as the protein/lipid signal ratio on the tube divided by that observed on the GUV. (Scale bar: 10 μ m).

Table S1. Charges at the RAB protein C-termini (last 20 amino acids). The charges of the last 20 amino acids of each RAB protein were calculated at a physiological pH (7.4) using a protein calculator tool (*Protein calculator*. [online] Available at: <http://protcalc.sourceforge.net/>). The amino acid residues colored in green are positively

Chapter 4: Article: RAB proteins bind lipid packing defects

charged whereas the red colored amino acids are negatively charged. RAB23 and RAB35 both display a highly positive C-terminus as compared to the other RAB proteins.

Figure S1

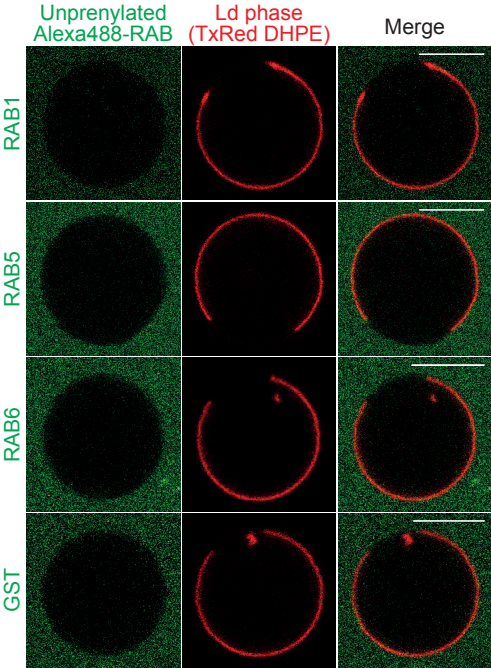


Figure S2

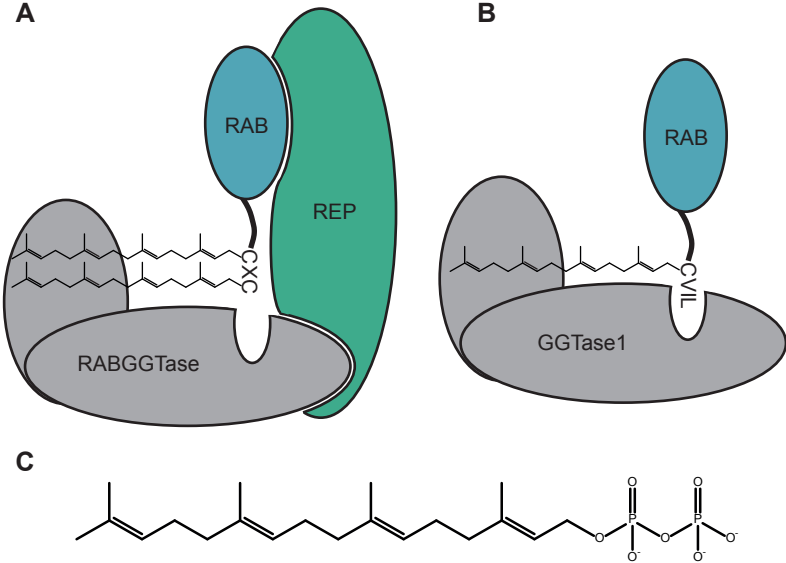


Figure S3

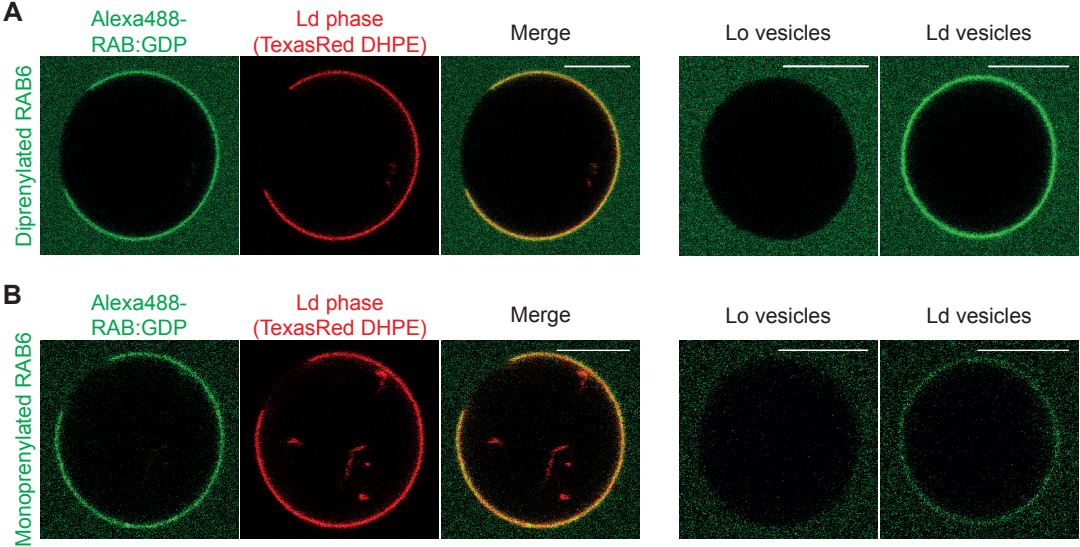


Figure S4

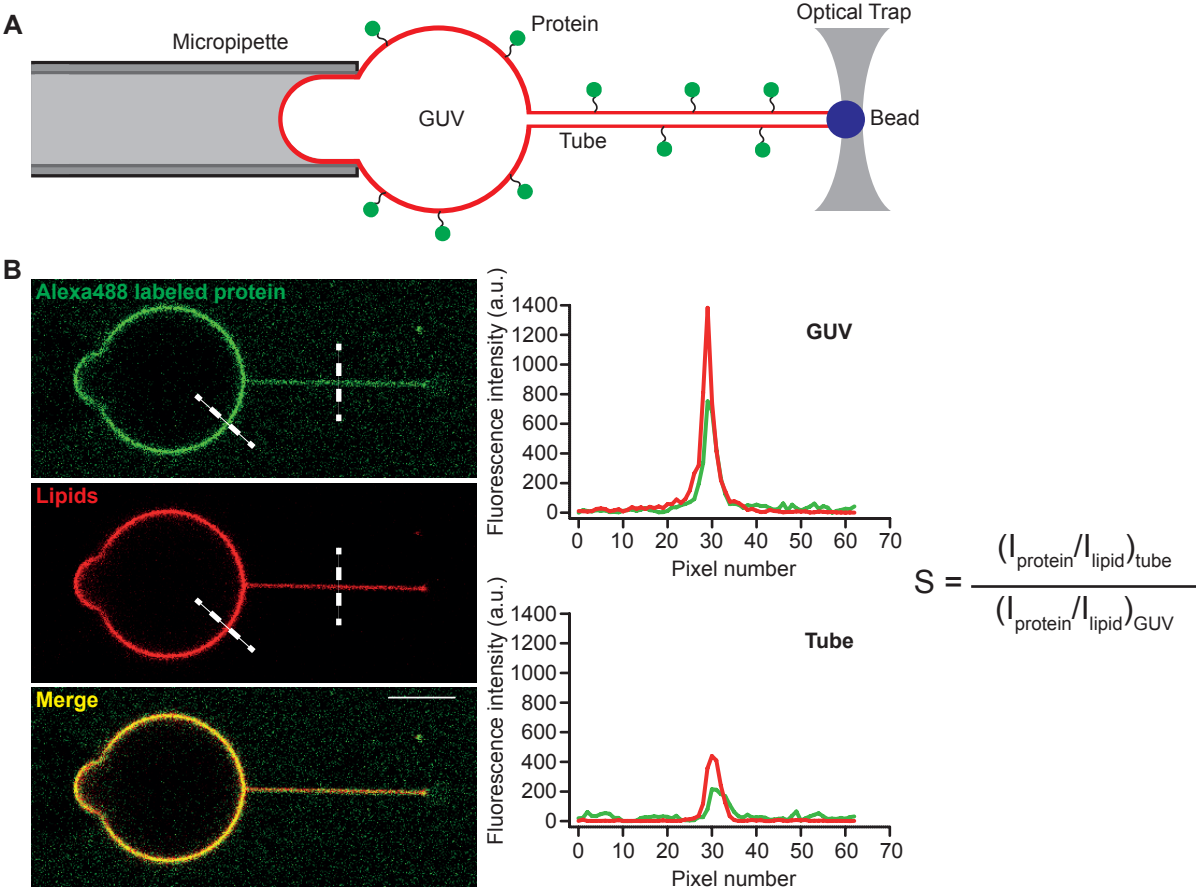


Table S1

RAB	Last 20 amino acid sequence	Number of positively charged amino acids (K, R, H)	Number of negatively charged amino acids (E, D)	Charge at pH 7.4
RAB1A	EKSNVKIQSTPVKQSGGGCC	3	1	1.6
RAB1B	ERP NLKIDSTPVKPAGGGCC	3	2	0.6
RAB2A	AATNATHAGNQGGQQAGGGC	1	0	-0.2
RAB2B	VGPSASQRNSRDI GSNNGCC	2	1	0.7
RAB3A	AKQGPQLSDQQVPPHQDCAC	2	2	-1.2
RAB3B	SSKNTRLSDTPPLLQQNCSC	2	1	0.7
RAB3C	AKQNTRLKETPPPPQPNCAC	3	1	1.6
RAB3D/RAB16	NGKGPVAGDAPAPQPSSCSC	1	1	-0.3
RAB4A	LRQLRSPRR AQAPNAQECGC	4	1	2.7
RAB4B	LRQLRQPRSAQAVAPQPCGC	3	0	2.7
RAB5A	GRGVDL TEPTQPTRNQCCSN	2	2	-0.3
RAB5B	SRGVDLHEQSQQNKSQCCSN	3	2	-0.2
RAB6A	IDIKLEKPEQFPVSEGGCSC	2	4	-2.3
RAB6A'	IDIKLEKPEQFPVSEGGCSC	2	4	-2.3
RAB6B	IDIKLDKPEPPASEGGCSC	2	4	-2.3
RAB6C	NLFPSLITFCNSSLLPVSWR	1	0	0.7
RAB7A	EPIKLDKNDRAKASAE SCSC	4	4	-0.4
RAB7B	ENHLTESIKLSPDQSRRC	4	3	-0.2
RAB8A	GVKITPDQQKRSSFFRCVLL	4	1	2.7
RAB8B	PVKITENRSKKT SFFRCSLL	5	1	3.7
RAB9A	LIQTDTVNLHRKPKPSSCC	4	1	1.8
RAB9B	CMLGHTIDLNSGSKAGSSCC	2	1	-0.3
RAB10	SENVDISSGGVGTGWKSKCC	2	2	-0.4
RAB11A	PIHVPPTTENKPKVQCCQNI	3	1	0.8
RAB11B	SVPPTTDGQKPNKLQCCQNL	2	1	0.6
RAB12	QPEPEIPPELPPPRPHVRCC	3	3	-1.2
RAB13	PPSTD LKTC DKKNTNKCSLG	4	2	1.6
RAB14	APQGGRLTSEFPQPREGCGC	2	2	-0.3
RAB15	LEEEEGKPEGPANSSKTCWC	2	5	-3.3

RAB17	GDAAVLNKGPARGAKCCAH	4	1	1.8
RAB18	LSHREEGQGGGACGGYCSVL	2	2	-1.2
RAB19	LDSSPVLMAQGPEKTHCTC	2	2	-1.2
RAB20	HTVDISSHKPPKRTRSGCCA	6	1	2.9
RAB21	QIIDDEPQAQTSGGGCCSSG	0	3	-3.3
RAB22A	SGGKGFKLRRQPEPKRSCC	6	1	4.6
RAB23	RPNKQRTKKNRNPFSSCSIP	6	0	5.7
RAB24	DKGVDLGQKPNPYFYSCCHH	4	2	-0.1
RAB25	SAQAGQEPGPGEKRACCISL	2	2	-0.3
RAB26	RFRLHDYVKREGRGASCCRP	7	2	3.8
RAB27A	NGHASTDQLSEEEKKGCACGC	3	3	-2.2
RAB27B	NGGNSGNLDCEKPPKCCIC	3	3	-0.4
RAB28	NQEPMSRTVNPPRSSMCAVQ	2	1	0.7
RAB29	LSTQGDYINLQTKSSSWSCC	1	1	-0.4
RAB30	SSPLPGEKGSISYLTCCNFN	1	1	-0.4
RAB31	GNGTIKVEKPTMQASRRCC	4	1	2.6
RAB32	VDKIKLDQETLRAENKSQCC	4	3	-0.4
RAB33A	GKVQKLEFPQEANSKTSCPC	3	2	0.6
RAB33B	PPDNGIILKPEPKPAMTCWC	2	2	-0.4
RAB34	NSDDSNLYLTASKKPTCCP	3	2	0.6
RAB35	QQQNDVVKLTKNKRRKRCC	7	1	5.6
RAB36	MEGSPPETQESKRPSLGGC	2	3	-1.3
RAB37	FQIRDYVESQKRSSCCSFM	4	2	1.6
RAB38	VVKPHLTSTKVASCSCGAKS	4	0	2.8
RAB39A	VPNTVHSSAAVKPRKECFC	4	3	-0.2
RAB39B	VPNVVHSSAAVVKERRCLC	4	3	-0.2
RAB41	EGTVEIELESFEEGNSYSY	1	6	-5.3
RAB42	HKTQIPRSPSRKQHSGPCQC	6	0	3.9
RAB43	SPDHIQLNSKDIGEGWCGC	2	3	-2.2

5 RAB4 and RAB11 binding requirements

5.1	Description of the <i>in vitro</i> approach.....	136
5.2	RAB4 and RAB11 recruitment to GUV membranes.....	137
5.2.1	RAB4 and RAB11 are not recruited to PC-containing membranes.....	137
5.2.2	RAB4 and RAB11 are not recruited to GUVs of various lipid composition.....	138
5.2.3	Membrane curvature has no effect on the recruitment of RAB4 and RAB11.....	140
5.3	RAB4 and RAB11 recruitment to purified Golgi fractions.....	141
5.3.1	RAB4 and RAB11 are positively recruited through their prenyl group	141
5.3.2	RAB4/RAB11 membrane recruitment does not depend on the presence of effector proteins.....	144
5.4	Monoprenylated RAB proteins are mislocalized to the same membrane structures.....	144
5.4.1	Monoprenylated RAB proteins localize to the same membrane structures.....	144
5.4.2	Monoprenylated RAB proteins do not localize to Golgi or recycling endosomal structures.....	146
5.5	Discussion.....	150

RAB proteins not only define organelle identity (Stenmark, 2009) but also form distinct domains on the same compartment (Barbero *et al.*, 2002; Sonnichsen *et al.*, 2000). RAB5 and RAB4 are segregated on early endosomes (Sonnichsen *et al.*, 2000), recycling endosomes are composed of two distinct RAB4 and RAB11 domains (Sonnichsen *et al.*, 2000), and late endosomes contain RAB7 and RAB9 domains (Barbero *et al.*, 2002). The formation of these domains is thought to be partially mediated by RAB effector proteins. The best example is given by Rabenosyn-5, a RAB5 effector, which binds PI(3)P on early endosomes (Nielsen *et al.*, 2000). It was also suggested that Rabenosyn-5 could promote, through its separate binding sites for RAB4 and RAB5, the formation and maintenance of distinct RAB domains on early endosomes (de Renzis *et al.*, 2002).

On the other hand, RAB4 and RAB11 preferentially localize to curved tubular structures, whereas RAB5 is predominantly found on globular and flatter structures (Sonnichsen *et al.*, 2000). This raises the possibility that the segregation of these RAB proteins into distinct domains could also be mediated by the physicochemical properties of membranes.

5.1 Description of the *in vitro* approach

In order to investigate the RAB4/RAB11 membrane binding requirements, I used an *in vitro* approach consisting of purified and prenylated RAB proteins, and giant unilamellar vesicles (GUVs) or purified Golgi fractions as model membranes.

Following purification, RAB proteins were exchanged to GTP/GppNHp (non-hydrolysable analog of GTP) or GDP using a chemically-induced reaction. Nucleotide exchange efficiency was then assessed by reverse-phase ion-pair chromatography. Of note, as membrane-bound RAB proteins are mostly loaded with GTP in the cell and are known to fulfill their functions as such, most experiments were performed using activated GTP/GppNHp-bound RABs.

RAB proteins were then fluorescently labeled at their N-terminus using Alexa fluorophores, and prenylated. Most RAB proteins, including RAB4 and RAB11 (but also RAB1, RAB5 and RAB6), are diprenylated (di-cysteine motif) in the cell by the joint action of the RAB escort protein (REP) and the RAB geranylgeranyl transferase (RABGGTase) (Alexandrov *et al.*, 1994; Seabra *et al.*, 1992). Diprenylation of RAB proteins could be achieved *in vitro* using purified REP and RABGGTase and geranylgeranyl pyrophosphate as a substrate. The particularity of this reaction is that REP only recognizes the GDP-bound form of RAB proteins (Seabra, 1996). Therefore, the nucleotide exchange to GTP can only be performed once proteins are diprenylated. Activation of diprenylated RAB proteins leads to the dissociation of the REP-RAB complex and to the subsequent exposure of the hydrophobic prenyl groups to the solvent, thereby causing protein precipitation. Protein precipitation can be avoided by activating diprenylated RABs in the presence of membranes, which allows stabilization of the hydrophobic prenyl groups; but consequently prevent any measurement of the amount of active GTP-bound RABs in the system. In order to overcome this issue, RAB proteins were monoprenylated using purified Geranylgeranyl transferase I (GGTaseI), which can catalyze the prenylation reaction in a nucleotide independent manner. AS GGTaseI recognizes the C-terminal mono-cysteine CAAX motif, RAB proteins were C-terminally modified to a CVIL motif.

More detailed information about this *in vitro* approach can be found in Chapter 3.

5.2 RAB4 and RAB11 recruitment to GUV membranes

5.2.1 RAB4 and RAB11 are not recruited to PC-containing membranes

Following RAB protein nucleotide exchange to GTP/GppNHp, N-terminal labeling with Alexa488 fluorophore, and monoprenylation, RAB recruitment to membranes was monitored using pure EggPC GUVs. Of note, this entire study started with the use of RAB1B, RAB5A and RAB6A (Chapter 4), which were all found to be effectively recruited to these EggPC-containing membranes. 2 μ M of RAB4A or RAB11A were incubated with pure EggPC vesicles (fluorescently labeled with 0.1% (mol) TexasRed-DHPE lipids). Surprisingly, no protein fluorescence was observed on the membrane in presence of either of these proteins (**Figure 5.1A**).

A 10% and 6.5% degree of labeling was quantified for Alexa488-RAB4A:GppNHp and Alexa488-RAB11A:GppNHp, respectively, which is in the same range as what was obtained for the effectively recruited Alexa488-RAB1B:GppNHp (5%). These measurements indicate that the absence of RAB4A/RAB11A membrane fluorescence intensity is not due to poor labeling efficiency, but probably the result of a lack of protein recruitment to the membrane.

To exclude the possibility that RAB proteins are not recruited because of ineffective prenylation, the efficiency of the GGTase1-mediated prenylation reaction was assessed using NBD-Farnesyl pyrophosphate, a C15 fluorescent analog of geranylgeranyl pyrophosphate (Chapter 3). The exposure of a polyacrylamide gel, loaded with RAB1B, RAB4A and RAB11A prenylation reactions, under a ChemiDoc imaging system, demonstrate that all these proteins are prenylated with comparable efficiencies (**Figure 5.1B**). This observation suggests that the absence of RAB4A / RAB11A membrane recruitment is not due to the absence of the prenyl group but rather due to the physicochemical properties of the membrane. These EggPC-containing GUV membranes might not display the appropriate characteristics necessary for RAB4A and RAB11A recruitment.

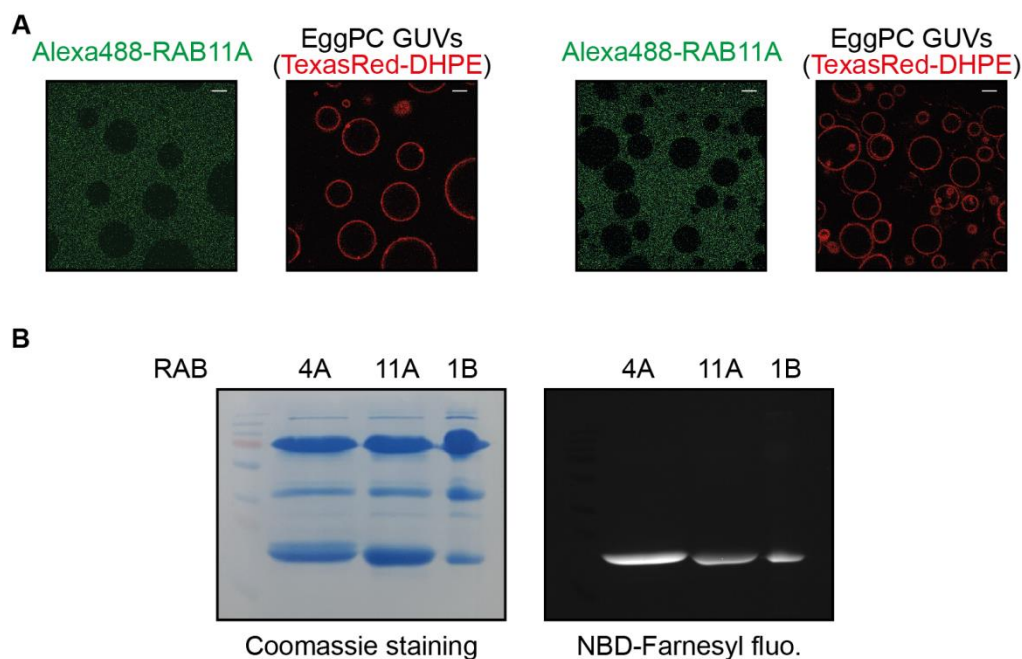


Figure 5.1: Monoprenylated RAB4A and RAB11A are not recruited to PC-containing vesicles. (A) 2 μ M monoprenylated Alexa488-labeled and GppNHp-bound RAB4A or RAB11A were incubated with EggPC-containing GUVs (labeled with 0.1% TexasRed-DHPE lipids). Proteins were not recruited to these membranes. (Scale bar = 10 μ m). (B) Prenylation efficiencies were assessed by performing monoprenylation reactions in the presence of NBD-Farnesyl pyrophosphate substrate (fluorescent analog of geranylgeranyl pyrophosphate). Monoprenylation reactions were performed on 5 μ g GppNHp-bound RAB4A, RAB11A and RAB1B (control) using GGTaseI and the NBD-Farnesyl pyrophosphate substrate. After 1h30 minutes, the prenylation reactions were loaded on an acrylamide gel and analyzed under a ChemiDoc imaging system. The observed fluorescent bands (right panel) correspond to proteins that underwent effective prenylation. The proteins on the gel are then revealed using coomassie blue staining. The two upper bands correspond to the two GGTaseI subunits and the lower band corresponds to the RAB proteins.

5.2.2 RAB4 and RAB11 are not recruited to GUVs of various lipid composition

The previous observations suggest that RAB4A and RAB11A membrane binding might require additional membrane factors (different lipid composition and/or structure) than RAB1B, RAB5A and RAB6A. I thus tested RAB4A and RAB11A recruitment to GUVs made of different lipid compositions. I investigated the binding of 2 μ M monoprenylated, Alexa488-labeled, GppNHp-bound RAB4A and RAB11A to negatively charged GUVs, endosomal-like GUVs with PI(3)P, brain total lipid extract-containing GUVs supplemented with PI(4,5)P₂, and vesicles exhibiting Lo and Ld phases. RAB4A and RAB11A were not recruited to any of these membranes (**Figure 5.2**).

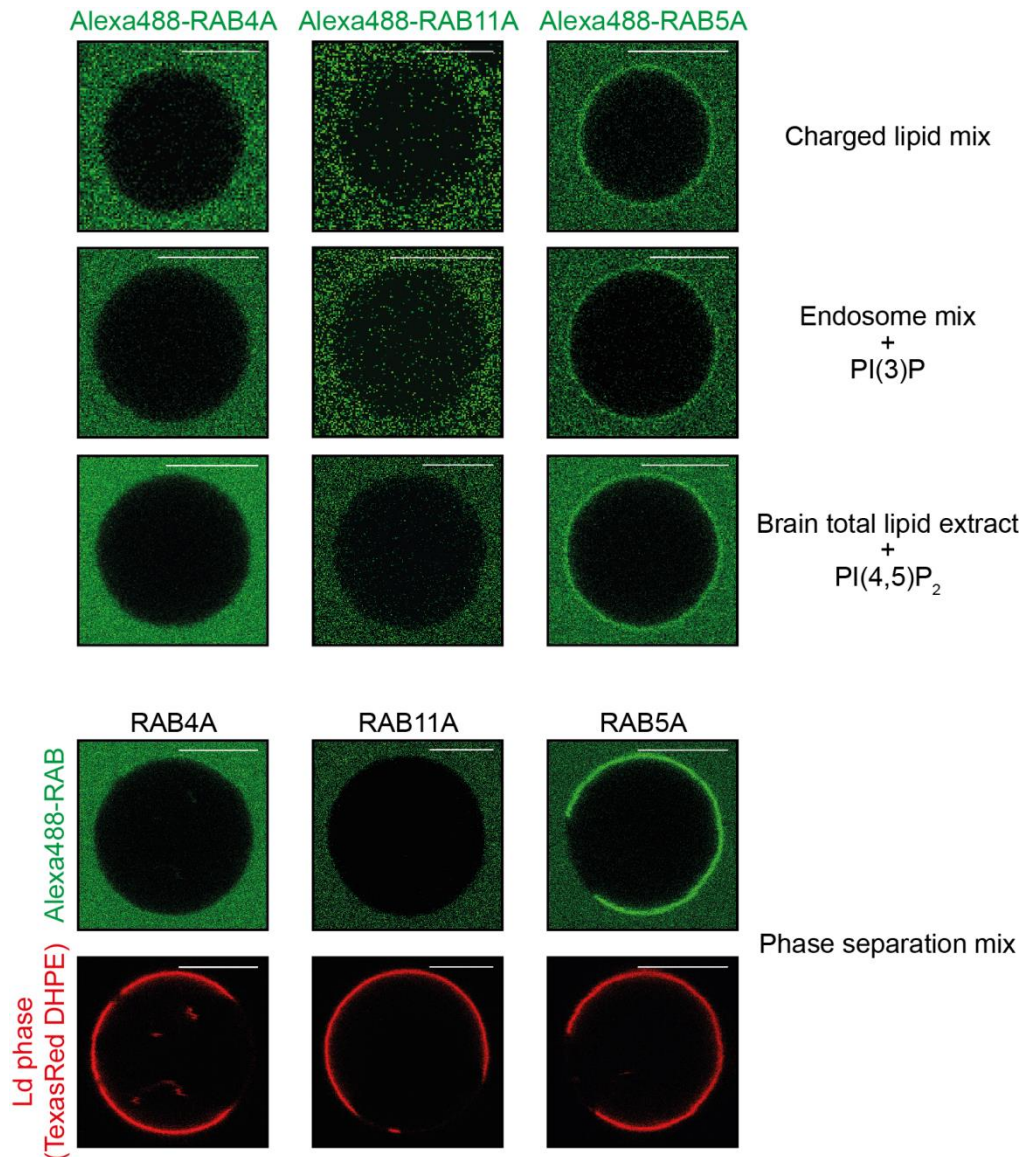


Figure 5.2: Monoprenylated RAB4A and RAB11A are not recruited to GUV membranes of various lipid composition. 2 μ M monoprenylated Alexa488-labeled and GppNHP-bound RAB4A, RAB11A or RAB5A (control) were incubated with charged GUVs, endosomal-like + PI(3)P GUVs, brain total lipid extract PI(4,5)P₂-containing GUVs and GUVs exhibiting Lo/Ld domains. In contrast to RAB5A, RAB4A and RAB11A were not recruited to these GUVs of different lipid composition. Charged lipid mix: 10% (mol) brain PS, 10% (mol) liver PI and 80% (mol) EggPC; Endosome mix + PI(3)P: 48% (mol) EggPC, 9% (mol) brain SM, 9% (mol) liver PI, 25% (mol) liver PE, 9% (mol) brain PS + 4% (mol) PI(3)P; Brain total lipid extract + PI(4,5)P₂: 9.6% (wt/wt) PC, 16.7% (wt/wt) PE, 1.6% (wt/wt) PI, 10.6% (wt/wt) PS, 2.8% (wt/wt) PA, 58.7% unknown + 6% (mol) PI(4,5)P₂; Phase separation mix: 43% (mol) DOPC, 14% (mol) Cholesterol, 43% (mol) brain SM, 0.1% (mol) TexasRed-DHPE. (Scale bar = 10 μ m).

In order to verify that the RAB4A and RAB11A absence of recruitment is not due to vesicle defects, I checked the binding of 2 μM monoprenylated Alexa488-labeled GppNHp-bound RAB5A to the same vesicles. RAB5A was found to be effectively recruited to all membrane types (**Figure 5.2**), thereby confirming that vesicles were in good shape. This clearly suggests that, in contrast to RAB5A, RAB4A and RAB11A require more demanding membrane parameters for their effective recruitment.

5.2.3 Membrane curvature has no effect on the recruitment of RAB4 and RAB11

RAB4 and RAB11 localize to tubular endosomal structures (Sonnichsen *et al.*, 2000). I thus thought that the absence of RAB4A and RAB11A recruitment to GUVs could reflect a high sensitivity to membrane curvature (GUVs have a 10 to 20 μm diameter and can therefore be considered as flat). As an example, ARFGAP is a known curvature sensor which was described to only bind to curved membranes displaying radii lower than 35nm (Ambroggio *et al.*, 2010). I thus wondered whether RAB4A and RAB11A might only be able to bind curved membranes.

In order to answer this question, I studied the recruitment of RAB4A and RAB11A to curved membrane structures by pulling tubes from an EggPC-containing GUV (labeled with 0.1% TexasRed-DHPE lipids), using the previously described optical tweezer setup (see Chapter 3) (**Figure 5.3**) (Ambroggio *et al.*, 2010; Sorre *et al.*, 2012).

This method allows the assessment of protein enrichment to the curved tube as compared to the “flat” vesicle. The holding of the vesicle with a micropipette connected to a water tank allows the control and variation of membrane tension, and consequently of tube curvature. 2 μM monoprenylated Alexa488-labeled GppNHp-bound RAB4A or RAB11A were incubated with TexasRed-DHPE-labeled EggPC GUVS. Membrane tubes were pulled and tube curvature was increased until rupture. Regardless of tube curvature, RAB4A and RAB11A were not recruited (**Figure 5.3**).

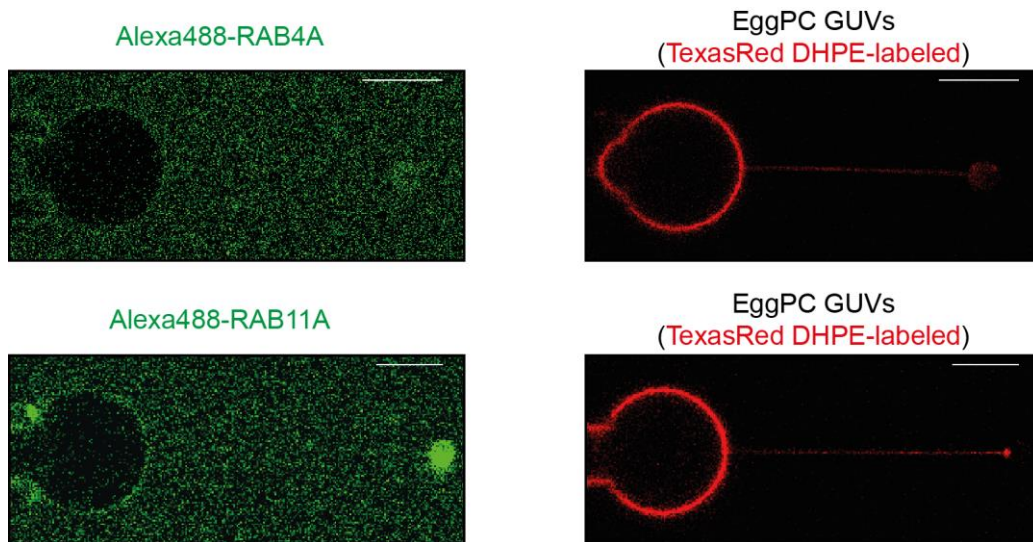


Figure 5.3: Monoprenylated RAB4A and RAB11A are not recruited to curved membranes. 2 μM monoprenylated Alexa488-labeled and GppNHp-bound RAB4A or RAB11A were incubated with EggPC-containing GUVs (labeled with 0.1% TexasRed-DHPE lipids and containing an extra 0.035% DSPE-PEG(2000)-Biotin) and 3.2 μm streptavidin-coated beads. Highly curved tubes were pulled from micropipette-aspirated GUVs using an optical tweezer setup. Protein enrichment to the tube was assessed for increasing tube curvature values. The displayed images show protein (green) and lipid (red) signals at 20 nm tube radius. RAB4A and RAB11A were not recruited to highly curved tubes. (Scale bar = 10 μm).

5.3 RAB4 and RAB11 recruitment to purified Golgi fractions

5.3.1 RAB4 and RAB11 are positively recruited through their prenyl group

As RAB4A and RAB11A were found not to be recruited to any of the tested GUVs, and as additional fluorescence studies using differently composed GUVs would have most certainly been time consuming and tedious, I made the decision to change the membrane model and to investigate the binding of these proteins to purified rat liver Golgi fractions. Electron microscopy analyses of these membrane fractions (purified in the lab by Hugo Bousquet and Lena Oesterlin) were performed by Ilse Hurbain (Graça Raposo lab, Institut Curie) and showed that the purified Golgi fractions were enriched in Golgi membranes but still contained other membrane types (Figure 5.4).

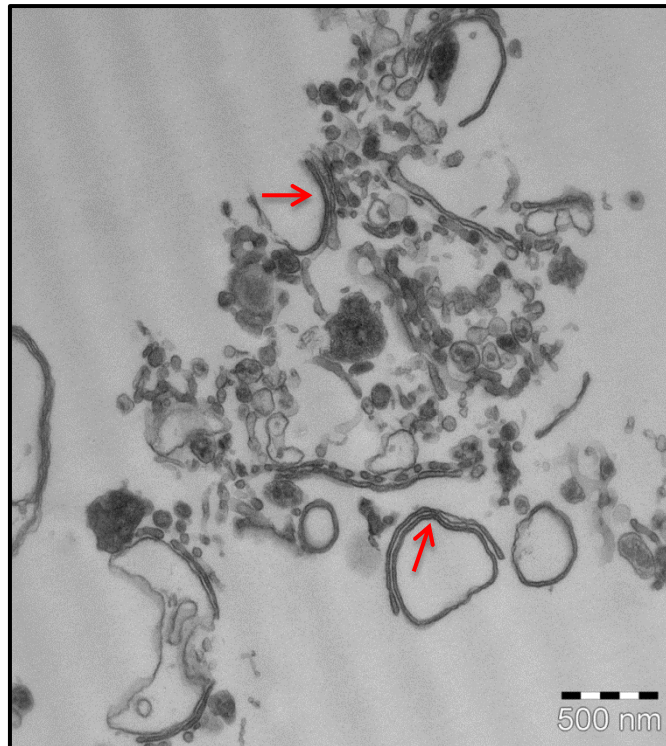


Figure 5.4: Electron microscopy analyses of the purified Golgi fractions. Red arrows indicate the Golgi stacks. From Ilse Hurbain (Graça Raposo's team, Institut Curie).

Purified Golgi fractions were identified by the addition of Rhodamine labeled WGA (wheat germ agglutinin, Vector labs) which interacts with N-acetylglucosamine sugars on the membrane.

Logically, I first checked the recruitment of RAB6A, a known Golgi-localized RAB protein (Antony *et al.*, 1992; Goud *et al.*, 1990), in order to verify that RAB proteins can effectively be recruited to purified Golgi fractions. 2 μ M monoprenylated Alexa488-labeled GTP-bound RAB6A was incubated in the presence of purified Rhodamine-WGA-labeled Golgi fractions (**Figure 5.5A**). Clear membrane recruitment of monoprenylated RAB6A was observed. I then investigated the binding of monoprenylated Alexa488-labeled and GppNHp-bound RAB4A and RAB11A (**Figure 5.5A**). Similarly to monoprenylated RAB6A, both monoprenylated RAB4A and RAB11A were found to be recruited to these Rhodamine-WGA-labeled membranes (**Figure 5.5A**).

In contrast, no binding to purified Golgi fractions was observed for unprenylated RAB6A, RAB4A and RAB11A (**Figure 5.5B**) which is in good agreement with the commonly accepted view that RAB proteins are incorporated into biological membranes through their C-terminal prenyl groups (Pechlivanis and Kuhlmann, 2006). The above observations highlight the fact that the prenyl group is absolutely required for membrane binding and that the previously observed absence of recruitment to GUV membranes was probably due to inadequate membrane composition (membrane lipids and/or proteins) and/or structure.

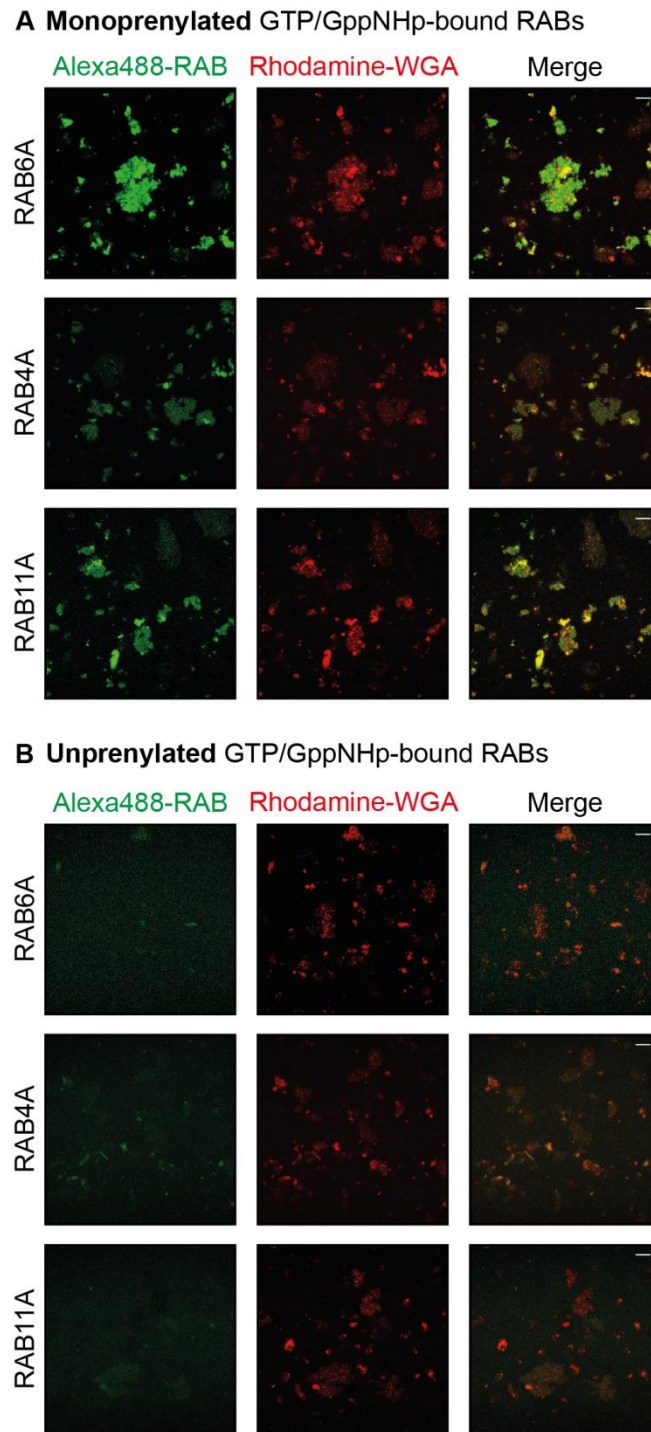


Figure 5.5: Monoprenylated and active RAB6A, RAB4A and RAB11A are recruited to purified Golgi fractions through their prenyl group. (A) 2 μ M monoprenylated Alexa488-labeled and GTP/GppNHp-bound RAB6A, RAB4A or RAB11A were incubated with purified Golgi fractions (labeled with Rhodamine WGA (Wheat Germ Agglutinin)). All monoprenylated and active RAB proteins were recruited to these membranes. (B) 2 μ M unprenylated Alexa488-labeled and GTP/GppNHp-bound RAB6A, RAB4A or RAB11A were incubated with purified Golgi fractions (labeled with Rhodamine WGA (Wheat Germ Agglutinin)). Unprenylated and active RAB proteins were not recruited to these membranes. (Scale bar = 10 μ m).

5.3.2 RAB4/RAB11 membrane recruitment does not depend on the presence of effector proteins

The previous observations indicate that the prenyl group is required for RAB4A / RAB11A membrane binding but does not exclude the possibility that other protein factors might be needed. One could imagine that membrane-bound proteins present on purified Golgi membranes, might also interact with prenylated RABs, therefore allowing their recruitment and stabilization on membranes. To address this point, I investigated the binding of inactive GDP-bound RAB proteins that cannot interact with effector proteins (**Figure 5.6**). RAB4A and RAB11A were both exchanged to GDP, prior to monoprenylation, and the nucleotide exchange efficiency was assessed by reverse phase ion-pair chromatography (see Chapter 3). Both proteins were exchanged to GDP with a 100% efficiency (not shown). 2 μ M monoprenylated Alexa488-labeled GDP-bound RAB4A and RAB11A were then incubated with purified Rhodamine-WGA-labeled Golgi fractions (**Figure 5.6A**). Both monoprenylated inactive RABs were found to be effectively recruited to these membranes. Consistently with results from the last section (5.3.1), no binding of unprenylated GDP-bound RAB4A and RAB11A proteins was observed on purified Golgi fractions (**Figure 5.6B**).

The effective membrane recruitment of these prenylated GDP-bound proteins suggests that RAB4A and RAB11A membrane binding does not require protein factors and is mostly dependent on prenyl group incorporation into membranes exhibiting specific lipid composition and/or structure.

5.4 Monoprenylated RAB proteins are mislocalized to the same membrane structures

5.4.1 Monoprenylated RAB proteins localize to the same membrane structures

While assessing the recruitment of monoprenylated Alexa488-labeled and GTP/GppNHp-bound RAB6A, RAB4A and RAB11A to purified Golgi fractions (**Figure 5.5A**), I noticed that it was not homogeneous, meaning that RAB4A and RAB11A seemed to preferentially localize to some

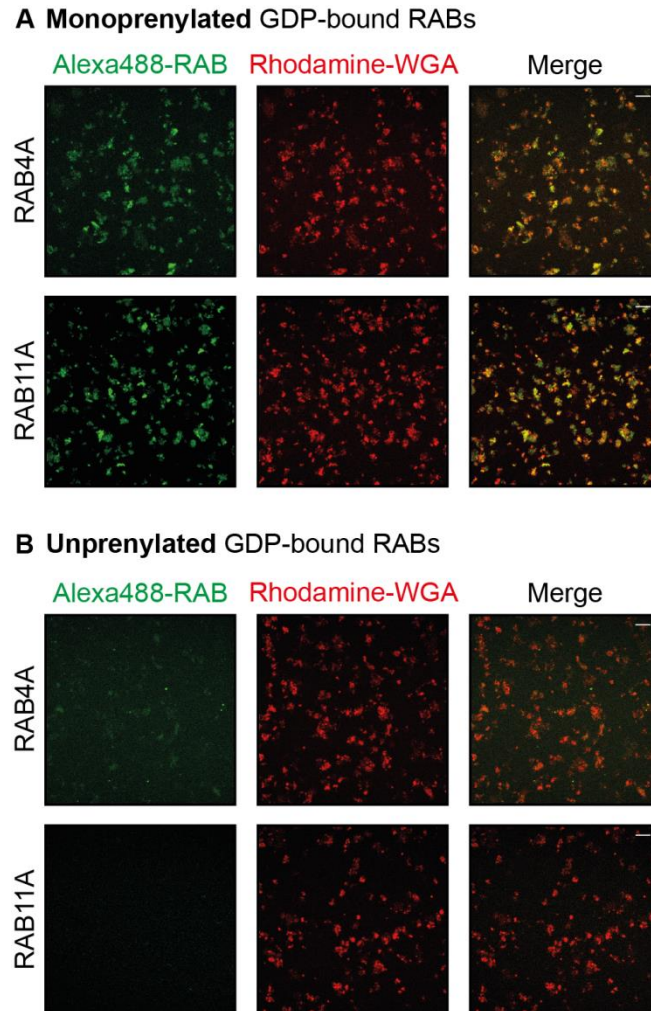


Figure 5.6: Monoprenylated and inactive RAB4A and RAB11A are recruited to purified Golgi fractions through their prenyl group. (A) 2 μ M monoprenylated Alexa488-labeled or GDP-bound RAB4A and RAB11A were incubated with purified Golgi fractions (labeled with Rhodamine WGA (Wheat Germ Agglutinin)). All monoprenylated and inactive RAB proteins were recruited to these membranes. (B) 2 μ M unprenylated Alexa488-labeled or GDP-bound RAB4A and RAB11A were incubated with purified Golgi fractions (labeled with Rhodamine WGA (Wheat Germ Agglutinin)). Unprenylated and inactive RAB proteins were not recruited to these membranes. (Scale bar = 10 μ m).

membrane structures. This was not very surprising, as these purified membrane fractions consisted of a mix of Golgi membranes and other membrane types. The three RAB proteins tested localize to specific compartments in the cell. RAB6A localizes to *medial-Golgi*, *trans-Golgi* and *trans-Golgi network* membranes (Antony *et al.*, 1992; Goud *et al.*, 1990); while RAB4A localizes to early endosomes (Van Der Sluijs *et al.*, 1991) and recycling endosomes (Trischler *et al.*, 1999); and RAB11A is found on recycling endosomes (Ullrich *et al.*, 1996) and *trans-Golgi network* membranes (Urbe *et al.*, 1993).

However, an interesting observation was made when 2 μM monoprenylated Alexa568-RAB4A:GppNHp and 2 μM monoprenylated Alexa488-RAB11A:GppNHp were added together to purified membrane fractions. Both proteins were found to specifically co-localize to the same membrane structures (**Figure 5.7A**). Similar experiments were performed in presence of 2 μM monoprenylated Alexa488-RAB6A:GTP and Alexa568-labeled GppNHp-bound RAB4A (**Figure 5.7B**) or RAB11A (**Figure 5.7C**). Surprisingly, RAB6A was also found to co-localize with both RAB4A and RAB11A. The above results suggest that, when using purified Golgi fractions as model membranes, monoprenylated RAB proteins might be localizing by default to the same membrane structures. This absence of specific localization could be due to the artificial system used. Purified Golgi fractions are missing soluble proteins, and probably also some membrane-bound proteins, which might be important for RAB specific membrane targeting. Another important particularity of this system consists in the use of mono-geranylgeranylated RAB proteins instead of the di-geranylgeranylated forms, which are usually found in cells. This will be further discussed in the last section of this chapter.

5.4.2 Monoprenylated RAB proteins do not localize to Golgi or recycling endosomal structures

The identification of these RAB4A, RAB6A and RAB11A positive membrane structures became important for two reasons: to identify the membrane type on which monoprenylated proteins seem to bind by default and to further characterize the RAB4A and RAB11A membrane binding requirements.

As RAB6A is known to specifically localize to *medial-Golgi*, *trans-Golgi* and *trans-Golgi network* membranes in cells (Antony *et al.*, 1992; Goud *et al.*, 1990), I started by investigating whether monoprenylated RAB proteins localize by default to Golgi structures.

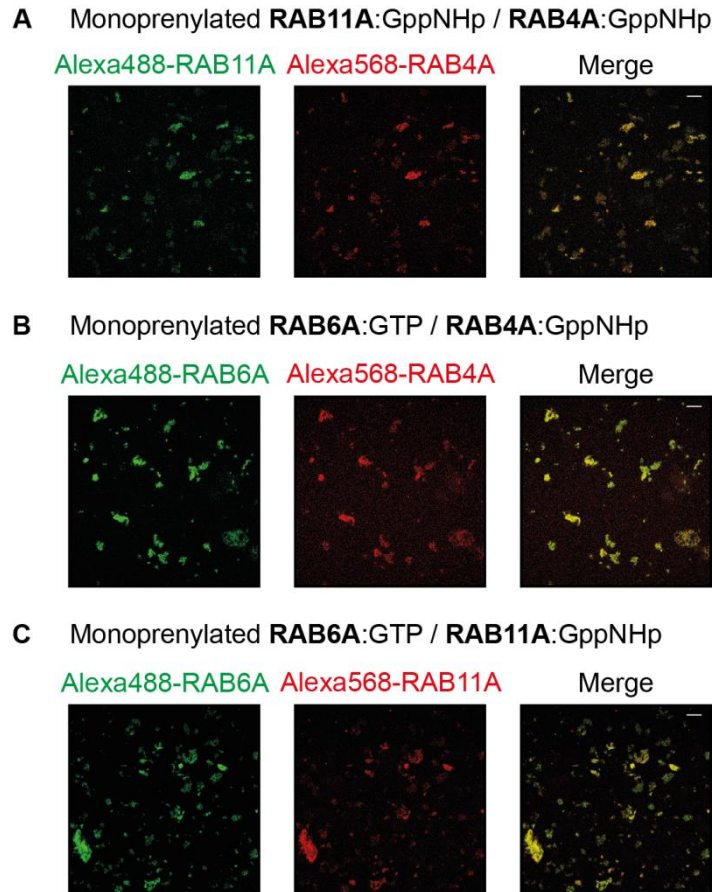


Figure 5.7: Monoprenylated RAB4A, RAB11A and RAB6A localize to the same membrane structures.

(A) 2 μ M monoprenylated GppNHp-bound Alexa488-RAB11A and Alexa568-RAB4A were incubated together with purified Golgi fractions. Both monoprenylated and active RAB proteins were found to co-localize to the same membrane structures. (B) 2 μ M monoprenylated Alexa488-RAB6A:GTP and Alexa568-RAB4A:GppNHp were incubated together with purified Golgi fractions. Both monoprenylated and active RAB proteins were found to co-localize to the same membrane structures. (C) 2 μ M monoprenylated Alexa488-RAB6A:GTP and Alexa568-RAB11A:GppNHp were incubated together with purified Golgi fractions. Both monoprenylated and active RAB proteins were found to co-localize to the same membrane structures. (Scale bar = 10 μ m).

Chapter 5: RAB4 and RAB11 binding requirements

I started by labeling specifically *trans*-Golgi and *trans*-Golgi network membranes using ATTO488-labeled α RAB6:GTP antibody (Adipogen). Simultaneously to the addition of α RAB6:GTP, 2 μ M monoprenylated Alexa568-labeled GppNHp-bound RAB4A or RAB11A were added. The membrane regions where both proteins were found to preferentially localize were negative for the Golgi marker α RAB6:GTP (**Figure 5.8A**). This was expected since RAB4A and RAB11A preferentially localize to endocytic compartments. However, because RAB6A was previously found to localize to the same membrane structures as RAB4A and RAB11A, the above results suggest that monoprenylated RAB6A does not localize to Golgi membranes *in vitro* and is therefore mislocalized.

Follow-up immunofluorescence experiments were performed using the *cis*-Golgi marker α -GM130 (anti-Golgi matrix protein 130) and monoprenylated Alexa488-labeled GppNHp-bound RAB11A (**Figure 5.8B**). Monoprenylated RAB11A was not found to co-localize with α -GM130 suggesting that monoprenylated proteins are not recruited to *cis*-Golgi membranes.

As RAB4A and RAB11A localize to recycling endosomes in cells (Trischler *et al.*, 1999; Ullrich *et al.*, 1996), I then checked whether monoprenylated RAB proteins might localize by default to endosomal structures.

By immunofluorescence, I labeled specifically recycling endosomal structures using an α -RAB11 antibody. Monoprenylated Alexa488-labeled GTP-bound RAB6A and α -RAB11 were added simultaneously (**Figure 5.8C**). Monoprenylated RAB6A did not seem to co-localize with the α -RAB11 antibody, indicating that monoprenylated RAB6A, and consequently monoprenylated RAB4A and RAB11A do not localize to recycling endosomal membranes. Monoprenylated RAB4A and RAB11A are therefore also mislocalized.

Other immunofluorescence studies were performed using an antibody targeted against the early endosomal marker EEAI and an antibody recognizing the ER. Unfortunately, poor membrane labeling was achieved when using these antibodies and no conclusive observations could be made.

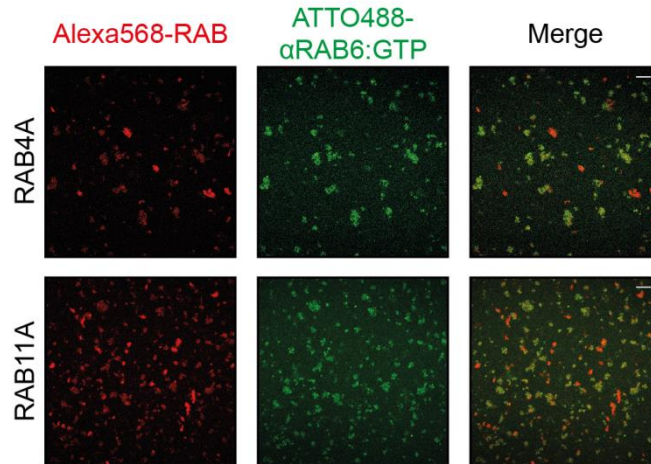
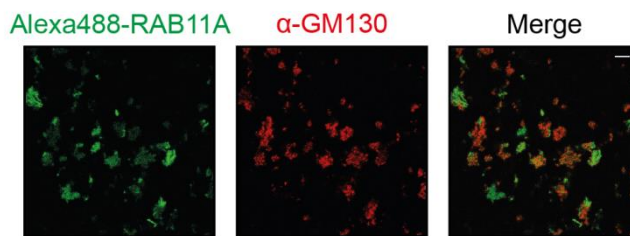
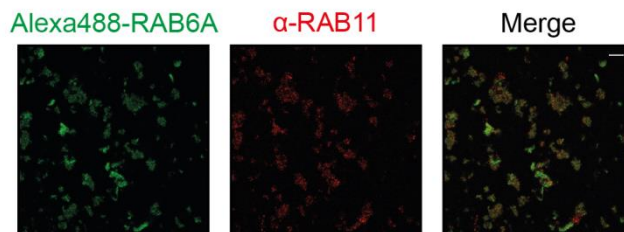
A Monoprenylated GppNHp-bound RABs + α RAB6:GTP**B Monoprenylated RAB11A:GppNHp + α GM130****C Monoprenylated RAB6A:GTP + α RAB11**

Figure 5.8: Monoprenylated RAB4A, RAB11A and RAB6A do not localize to Golgi or recycling endosomal structures. (A) 2 μ M monoprenylated Alexa568-labeled and GppNHp-bound RAB4A or RAB11A were incubated with the *medial-trans*-Golgi and *trans*-Golgi network marker Atto488-labeled α RAB6:GTP antibody in the presence of purified Golgi fractions. Both monoprenylated and active RAB proteins were found to preferentially localize to α RAB6:GTP antibody negative structures. (B) Immunofluorescence experiments were performed in presence of 2 μ M monoprenylated Alexa488-labeled and GppNHp-bound RAB11A and an antibody targeted against the *cis*-Golgi marker GM130 in the presence of purified Golgi fractions. Monoprenylated and active RAB11A was found to preferentially localize to α -GM130 antibody negative structures. (C) Immunofluorescence experiments were performed in presence of 2 μ M monoprenylated Alexa488-labeled and GTP-bound RAB6A and an antibody targeted against the recycling endosomal marker RAB11 in the presence of purified Golgi fractions. Monoprenylated and active RAB6A was found to preferentially localize to α -RAB11 antibody negative structures. (Scale bar = 10 μ m).

5.5 Discussion

In this chapter I showed that RAB4A and RAB11A were not directly recruited to PC-containing membranes. This led me to assume that the membrane binding requirements of these two proteins were much more specific. However, RAB4A and RAB11A were also not recruited to GUVS exhibiting distinct Lo/Ld phases and pulling of highly curved tubes did also not allow RAB4A/RAB11A membrane binding. The above results suggest that, in contrast to what was observed for RAB1B, RAB5A and RAB6A (Chapter 4), lipid packing defects, promoted by unsaturated lipids mainly found in Ld membranes and by membrane curvature (Bigay and Antony, 2012) are not sufficient to drive RAB4A and RAB11A membrane recruitment.

Although RAB4A/RAB11A and phosphoinositides were described to work synergistically through the recruitment of many common effectors (Campa and Hirsch, 2017; Jean and Kiger, 2012), RAB4A/RAB11A membrane insertion has never been shown, to my knowledge, to be primarily dependent on the presence of phosphoinositides. In addition, both proteins partially localize to recycling endosomes which exhibit only minor levels of PI(3,4,5)P₃ and PI(4,5)P₂ (Fields *et al.*, 2010; Thapa *et al.*, 2012). Finally, RAB4A and RAB11A display low levels of positive charges at their C-terminal extremity (see Figure SI, Chapter 4) as compared to RAB35, which was shown to only bind to negatively charged membranes (Chapter 4). However, in order not to exclude the possibility of charge dependency, I investigated the recruitment of RAB4A/RAB11A to PI(4,5)P₂ and to PI(3)P-containing GUVs. The observed absence of recruitment of these proteins suggest that negatively charged lipids are not sufficient to drive RAB4A/RAB11A membrane binding.

Interestingly, RAB4A and RAB11A were found to be recruited to purified Golgi fractions. This recruitment was shown to be both prenyl group dependent and nucleotide independent, thus confirming the commonly accepted view that the prenyl group is required for membrane binding (Pechlivanis and Kuhlmann, 2006) but also indicating that membrane binding does not require interactions with effector proteins. These findings suggest that RAB4A and RAB11A membrane incorporation is mainly dependent on the physicochemical properties of the membranes themselves and that recruitment to GUV membranes could be achieved if the appropriate membrane requirements are met.

I reasoned that RAB4A/RAB11A membrane recruitment could very well be due to a combination of multiple specific membrane features. As an example, α -Synuclein, a known curvature sensor, was described to only bind to curved and negatively charged membranes

(Pranke *et al.*, 2011). These Golgi membranes seemed to gather the necessary requirements for RAB4A/RAB11A binding. However, the direct assessment of the geometry (curvature) of RAB4A/RAB11A positive membranes proved to be very difficult due to the fact that these membranes tend to aggregate. The effect of membrane curvature on RAB recruitment was therefore investigated by using a previously described tube pulling approach (see Chapter 3) (Roux *et al.*, 2002). In this method, multiple tubes are pulled from Golgi membranes by using the force exerted by kinesin motors walking on microtubules; and relative protein enrichment to the tube can be estimated. These tube pulling experiments were performed in the presence of monoprenylated Alexa568-labeled RAB11A (**Figure 5.9A**) and Alexa488-labeled RAB6A (**Figure 5.9B**) but did not lead to any conclusive observations as the background protein fluorescence was very high.

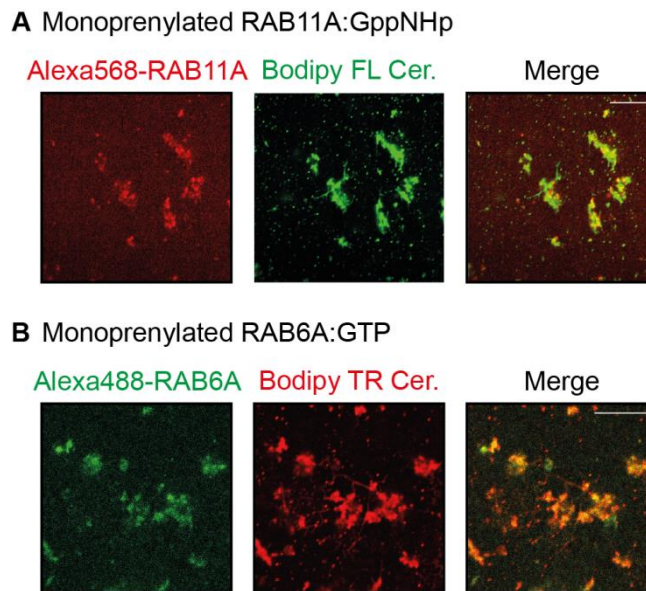


Figure 5.9: Study of RAB4A/RAB11A curvature sensing using purified Golgi fractions and kinesin motors. These experiments were performed using microtubule-coated chambers. Biotinylated kinesins interact with biotinylated Golgi membranes in the presence of streptavidin. Addition of an ATP-containing buffer allows kinesins to move on microtubules and to subsequently pull multiple tubes from Golgi membranes. (A) 2 μ M monoprenylated, Alexa568-labeled and GppNHp-bound RAB11A was incubated with purified Golgi fractions (labeled with Bodipy Fluorescein Ceramide) (B) 2 μ M monoprenylated, Alexa488-labeled and GTP-bound RAB6A was incubated with purified Golgi fractions (labeled with Bodipy TexasRed Ceramide). (Scale bar = 10 μ m).

When performing such experiments, pulled tubes are visualized under the microscope at a very close distance (2-3 μ m) from the coverslip. This high protein intensity background could have

Chapter 5: RAB4 and RAB11 binding requirements

thus been the result of non-specific interactions of the proteins with the solid glass surface. Although the coating of the glass with β -Casein was supposed to prevent such interactions, it proved not to be sufficient and clear background fluorescence could still be observed. In order to overcome this issue, the use of a polymer cushion, such as Polyethyleneglycol (PEG) (Wagner and Tamm, 2000), should be considered. Polymer cushions were originally used to increase the mobility of integral membrane proteins in supported planar lipid bilayers by preventing the non-specific interaction of the substrate-exposed protein domain with the hydrophilic substrate. PEGylated polymer cushions, which can prevent the non-specific binding of proteins to surfaces (Du *et al.*, 1997) may therefore also be used in the presence of purified Golgi membranes.

The use of synthetic vesicles, that allow a controlled lipid composition, seems however to be more favorable for such a study, as the properties of purified Golgi fractions are difficult to assess. Multiple combinations of membrane specific features (charge, curvature, etc.) could be achieved using synthetic vesicles and subsequent fluorescence studies by confocal microscopy. However, when visualizing protein binding by confocal microscopy, only one condition can be investigated at a time. Microscope studies of protein binding to GUVs exhibiting various physiochemical properties would therefore be time consuming and tedious.

In order to more rapidly assess the RAB4/RAB11 membrane binding properties, the use of the recently described high-throughput PLIF (protein-lipid interaction by fluorescence) method (Ceccato *et al.*, 2016) should be considered. This technique was originally developed to investigate the binding of proteins to liposomes containing specific phosphoinositide derivatives. I thought to adapt this method to my study, in order to probe the binding of RAB4A and RAB11A to liposomes exhibiting a wide range of different lipid compositions (**Figure 5.10**). This experimental approach consists as the following: GFP-tagged RAB proteins are incubated on anti-GFP antibody-coated 96-well plates with specific fluorescent liposome preparations. The level of lipids is then measured with a microplate reader by assessing the fluorescent signal intensity of bound liposomes. This sensitive experimental procedure, which is currently being optimized, would therefore allow the rapid screening of RAB-membrane interactions. Of note, influence of curvature could simultaneously be investigated by probing the binding to liposomes of decreasing sizes.

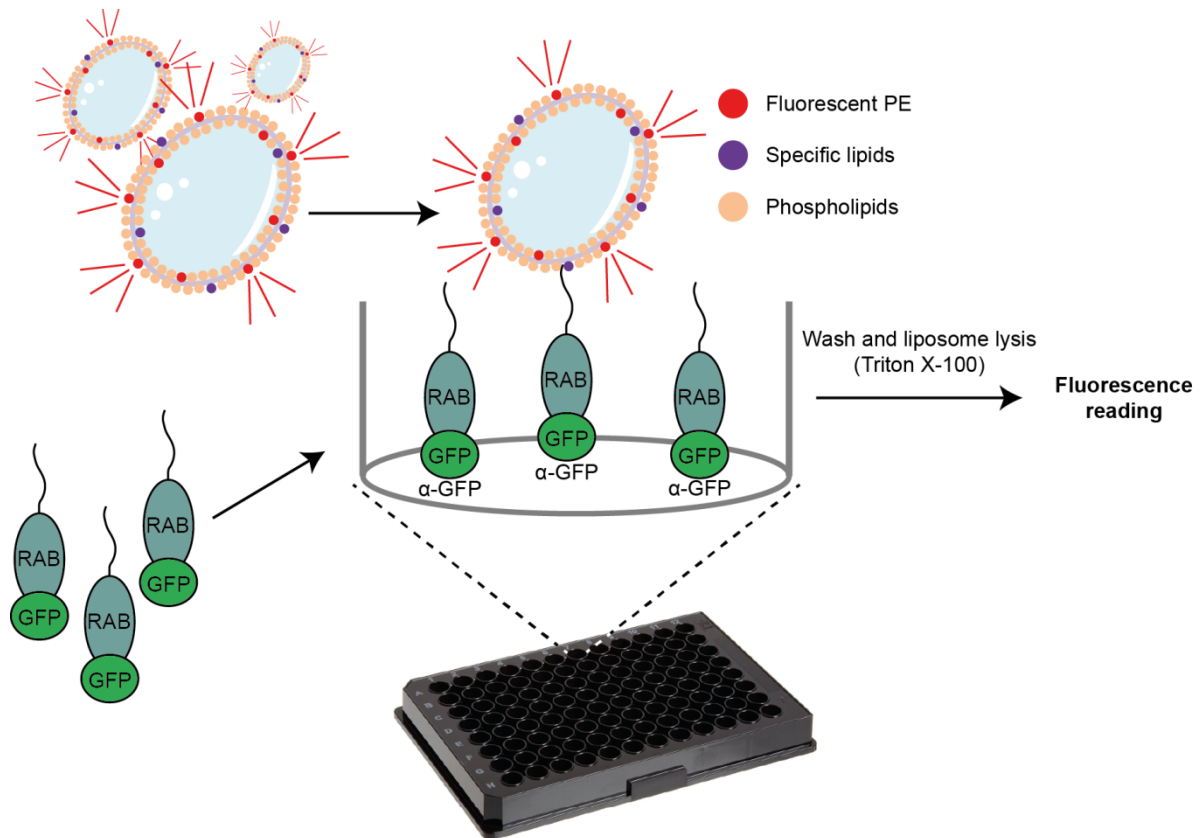


Figure 5.10: Description of the PLIF (protein-lipid interaction by fluorescence) assay adapted to my study. GFP-tagged RAB proteins are incubated on anti-GFP antibody-coated 96-well plates. Red-fluorescent liposomes are added in the wells with each well containing liposomes of specific size and/or lipid composition. The plate is put under agitation for 15 to 20 minutes to allow RAB-liposome interaction. The plate is then washed several times using the liposome buffer, in order to remove unbound liposomes, and incubated for 5 minutes under agitation with 1% triton solution (in PBS) to lyse the liposome solution. Levels of lipids are finally measured by assessing the fluorescent signal intensity of bound liposomes using a microplate reader. **Adapted from Ceccato, 2016.**

Chapter 5: RAB4 and RAB11 binding requirements

While performing recruitment experiments using purified Golgi fractions, I observed that both monoprenylated RAB4A and RAB11A, but also monoprenylated RAB6A, localized to the same membrane structures. These membrane structures were found to be negative for *cis*-Golgi, *medial*-Golgi, *trans*-Golgi, *trans*-Golgi network and recycling endosomal markers. Using purified membrane fractions, monoprenylated RAB4A, RAB11A and RAB6A are therefore all mislocalized to the same membrane structures.

Previous studies have shown that interactions with effectors could regulate the specific membrane targeting of RAB proteins (Aivazian *et al.*, 2006; Li *et al.*, 2014). When using purified Golgi fractions, one has to remember that this system does not contain soluble proteins and that some membrane-bound proteins might not be present as well due to the purification procedure. I therefore assumed that the absence of proper localization of RAB proteins in this *in vitro* system might be due to the absence of specific targeting factors.

The mislocalization of RAB proteins could also implicate the prenyl group. All my experiments were performed using monoprenylated (one geranylgeranyl group) RAB proteins, whereas most RABs, including RAB4, RAB6 and RAB11, were found to be diprenylated (two geranylgeranyl groups) in cells (Leung *et al.*, 2006). Studies showed that RAB5A and RAB27A mutants containing only one prenylatable cysteine were mistargeted to the ER and non-functional (Gomes *et al.*, 2003). This could be explained by the fact that decreasing the amount of prenyl groups might result in a loss of specific targeting information or in a decreased affinity for the target membrane.

Studies showed that YPT1 and SEC4 were mislocalized and not functional when mutated from a di-cysteine to a mono-cysteine motif (Calero *et al.*, 2003). In this same study, the interaction between mono-cysteine motif-containing YPT1 / SEC4 and YIPI, a protein known to only bind prenylated RAB proteins, was shown to be impaired; and loss of functional YIPI was described to impact YPT1 localization to the Golgi (Calero *et al.*, 2003). It was thus suggested that mislocalization of monoprenylated RAB proteins might be the result of an absence of interaction with specific targeting factors. However, contradicting results showed that inactivation or depletion of YIPI does not change YPT1 membrane association and localization (Barrowman *et al.*, 2003; Heidtman *et al.*, 2003), therefore implying that mislocalization of monoprenylated RAB proteins might result from other mechanisms.

Membrane targeting of mono- and diprenylated RABs could also be regulated by the lipid environment, for instance if monogeranylgeranylated RAB proteins exhibit lower affinity or are less stable in the target membranes than diprenylated RABs. *In vitro* studies using synthetic

vesicles have indeed suggested that proteins that possess two geranylgeranyl modifications have a half-life in the order of hours (Shahinian and Silviu, 1995) whereas monoprenylated proteins usually exhibit a half-life in the order of a second or less (Schroeder *et al.*, 1997). More recent *in vitro* studies demonstrated that, at a given membrane composition, membrane dissociation constant values of monofarnesylated N-RAS are generally higher than that of difarnesylated N-RAS proteins (Gohlke *et al.*, 2010). Monoprenylated RAB proteins could therefore dissociate faster from their target membranes and might consequently re-incorporate themselves into the most abundant cellular membrane, the ER.

Nevertheless, additional immunofluorescence experiments should be performed to confirm the identity of the RAB4A/RAB6A/RAB11A positive membrane structures. The use of a good anti-ER antibody now seems necessary in order to assess whether monoprenylated localize by default to ER membranes. Further investigations using the diprenylated versions of these RAB proteins should also be carried out in order to determine whether, when using purified Golgi fractions as model membranes, mono and diprenylated RABs localize differently.

6 RAB6-induced membrane tethering

6.1	Specificities of RAB6-induced membrane tethering	158
6.1.1	Vesicle tethering is a RAB6-specific effect.....	158
6.1.2	Vesicle tethering is nucleotide and concentration dependent	158
6.1.3	RAB6-induced vesicle tethering is mediated by a RAB-RAB dimerization in <i>trans</i>	161
6.1.4	The RAB-RAB interaction is dynamic	163
6.2	Involvement of the Switch regions	165
6.2.1	RAB6A mutant induces vesicle tethering	165
6.2.2	Unprenylated RAB6A does not interact with membrane-bound RAB6A	166
6.2.3	Bivalent α RAB:GTP antibodies promote vesicle tethering	168
6.2.4	Effect of monovalent RAB6 effector proteins	170
6.3	Discussion.....	174

Prior to my arrival to the lab, similar *in vitro* studies, using purified and prenylated RAB proteins and synthetic vesicles as model membranes, had led to the observation that vesicles tether in presence of monoprenylated and GTP-bound RAB6A. Part of my project consisted in investigating this process in greater detail.

As already mentioned in the previous chapter, RAB proteins were exchanged to GTP/GppNHp or GDP using a chemically-induced reaction, N-terminally labeled with Alexa fluorophores and monoprenylated using purified geranylgeranyl transferase I (GGTaseI). In contrast to the previous studies, the understanding of this particular tethering mechanism did not require the use of different membrane types but rather the use of different purified proteins. All experiments were thus performed using only EggPC GUVs.

6.1 Specificities of RAB6-induced membrane tethering

6.1.1 Vesicle tethering is a RAB6-specific effect

We have observed, by DIC and confocal microscope, vesicle tethering upon the addition of 2 μM monoprenylated Alexa488-RAB6:GTP (RAB6A and also RAB6A') (**Figure 6.1A**). In contrast, no vesicle tethering was observed in presence of identical concentrations of GppNHP-bound and monoprenylated Alexa488-RAB1B and Alexa488-RAB5A (**Figure 6.1B**), thus suggesting that vesicle tethering is a RAB6 specific effect.

This observation is partially consistent with previous studies (Lo *et al.*, 2011; Tamura and Mima, 2014) in the sense that RAB proteins can mediate liposome aggregation *in vitro* (these studies are discussed in detail in chapter 2). However, our results are also in conflict with these two studies as VPS21 (Lo *et al.*, 2011), the yeast RAB5 ortholog, and RAB5A (Tamura and Mima, 2014) but not RAB6A (Tamura and Mima, 2014) were shown to induce liposome tethering. An important difference between our experimental setups consists in the way of recruiting the proteins to the membranes. In the case of my study and similarly to what occurs in the cell, RAB proteins bound to membranes with their prenyl group whereas in their studies proteins were anchored to membranes using Histidine tagged proteins and Nickel-NTA containing liposomes. One could hypothesize that His-tagged and prenylated RAB proteins might display structural differences which could account for the differential tethering effects.

6.1.2 Vesicle tethering is nucleotide and concentration dependent

The tethering process seems to preferentially occur when the protein is in its active, GTP bound state but not when GDP-bound (**Figure 6.2A**). Additionally, a concentration threshold was roughly estimated simply by observing the frontier at which vesicles start to tether. I have identified a concentration threshold of 1.6 μM (**Figure 6.2B**). This concentration threshold is however not very representative as it might vary depending on the protein membrane density and thus on the protein prenylation efficiency but also on the affinity of the protein for the membrane. The measurement of a protein density threshold would therefore be more relevant and this should be further investigated. In relation to this, one could argue that the absence of

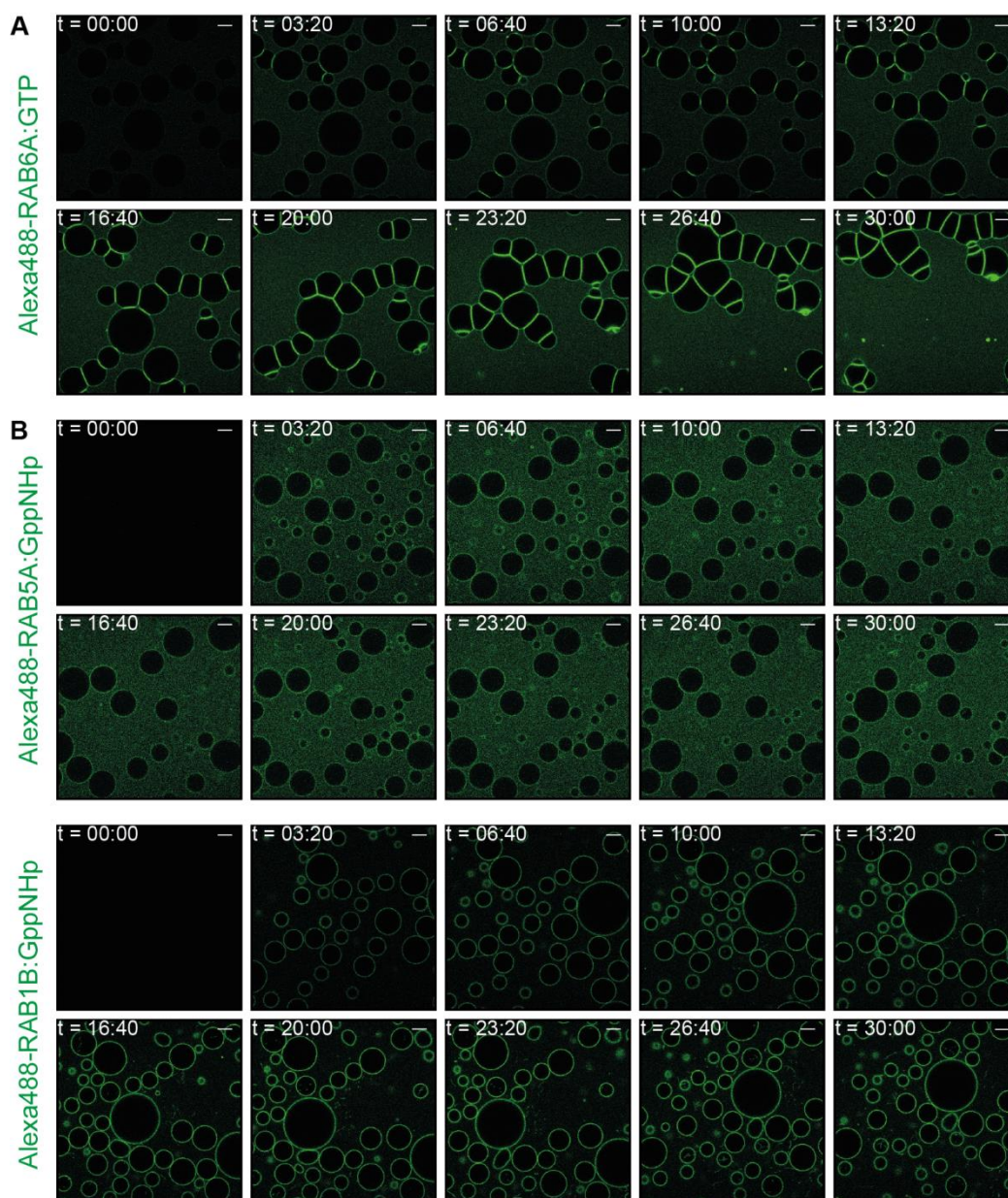


Figure 6.1: Vesicle tethering is a RAB6-specific effect. (A) Vesicle tethering was assessed over time (during 30 minutes), using a confocal microscope, in presence of 2 μ M monoprenylated Alexa488-RAB6A:GTP. RAB6 was added to the EggPC vesicle mix at t = 00:00. The same observation was made in the presence of the RAB6A' isoform (not shown) (B) The same experiments were carried out in presence of monoprenylated Alexa488-RAB5A:GppNHp or monoprenylated Alexa488-RAB1B:GppNHp and no vesicle tethering was observed. (Scale bar = 10 μ m).

Chapter 6: RAB6-induced membrane tethering

vesicle tethering with GDP-bound RAB6A could possibly simply be due to a decrease in membrane recruitment of the protein.

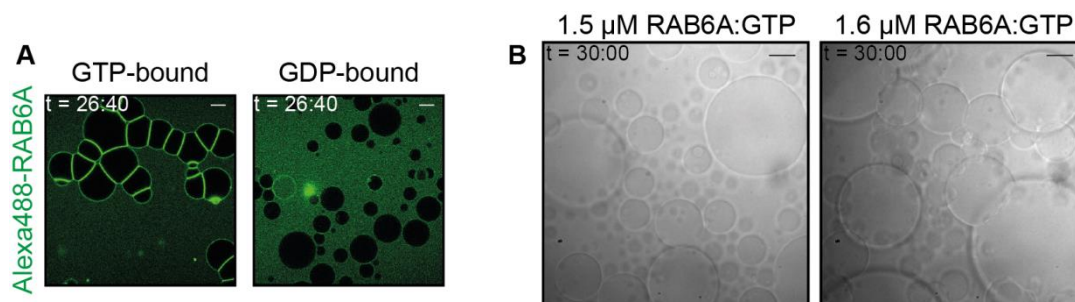


Figure 6.2: Vesicle tethering is nucleotide and concentration dependent. (A) Vesicle (pure EggPC) aggregation was assessed, using a confocal microscope, 26 minutes and 40 seconds after addition of 2 μM GTP-bound (left) and GDP-bound (right) monoprenylated Alexa488-RAB6A. No vesicle tethering was observed in presence of inactivated (GDP-bound) RAB6A. (B) Vesicle (pure EggPC) aggregation was assessed, using a DIC microscopy, 30 minutes after addition of various concentrations of monoprenylated RAB6A:GTP. Vesicle tethering was observed in presence of 1.6 μM RAB6A (right) but not after addition of 1.5 μM RAB6A (left). (Scale bar = 10 μM).

The study from Lo and coworkers showed that VPS21, the yeast RAB5 ortholog, is also able to tether vesicles (Lo *et al.*, 2011). This study demonstrates that tethering is GTP dependent and that it can consequently be regulated by GEFs and GAPs. In the case of RAB6, the impact of the nucleotide-bound state could be further investigated in a similar manner with the addition of known RAB6A GEFs or GAPs. Ric1-Rgpl was described to act as a RAB6 GEF (Pusapati *et al.*, 2012; Siniosoglou *et al.*, 2000) but no attempt was made to test it in our assay. On the other hand, no RAB6 GAPs have been clearly identified so far. Originally, TBC1D11/GAPCenA was proposed to act as a GAP for RAB6 (Cuif *et al.*, 1999) but this was later questioned by Barr and colleagues when GAP activity was only detected towards RAB4 but not RAB6 (Fuchs *et al.*, 2007).

A comparison of membrane recruitment of GDP-bound versus GTP-bound RAB6 (and other RABs) could nevertheless also be of interest for future studies. This will be further discussed in the last section of this chapter.

6.1.3 RAB6-induced vesicle tethering is mediated by a RAB-RAB dimerization in *trans*

The observation of vesicle tethering in confocal microscopy using Alexa488-labeled Rab6A (**Figure 6.1A**) gave the impression that the protein gets concentrated in the site of vesicle interaction. To further investigate this point, tethering of TexasRed-DHPE-labeled vesicles was induced by the addition of 2 μ M monoprenylated Alexa488-RAB6A:GTP; and lipid and protein enrichments at the interaction sites (as compared to the non-interacting regions) were assessed (**Figure 6.3A**). Quantification of fluorescence intensities of tethered vesicles showed that, whereas TexasRed DHPE lipids concentrate 2 times at the interaction site (because of the contact between two membranes), a 5 fold increase in Alexa488-RAB6A:GTP fluorescence intensity could be detected in the same region (**Figure 6.3A**). Cryo-electron microscopy analysis that were performed in collaboration with Daniel Levy's team (UMRI68, Institut Curie) showed clear protein densities of 5 ± 1 nm thickness at the interaction sites of the tethered vesicles whereas no protein densities could be observed in non-interacting regions (**Figure 6.3B**). Similarly to what was previously suggested with VPS21 (Lo *et al.*, 2011), we suggest a model in which the RAB6 proteins interact with the membrane through their C-terminal geranylgeranyl moiety and one RAB protein from one membrane would interact with one RAB from another membrane (**Figure 6.3C**).

In this model, based on the analysis of vesicle tethering by Cryo-EM, the average distance between the two opposing membranes is 10-12 nm with protein densities (RAB proteins) having a thickness of 5 ± 1 nm; and spaces between protein densities and vesicular membranes (corresponding to the length of the extended RAB6 C-termini) of 3.5 ± 0.5 nm. The structure of the YPTI/GDI complex (**Figure 6.4**) (Pylypenko *et al.*, 2006) indicates that, when in complex with GDI, YPTI has a core size of around 4.6 nm and a partially unresolved extended C-terminal tail that seems to be able to bridge distances of at least 4.3 nm; thus fitting nicely with my model. The reason why the C-terminal tail is partially unresolved resides in the fact that many C-terminal residues are flexible. However, the Cryo-EM analysis of vesicle tethering (**Figure 6.3B**) demonstrates that the 3.5 ± 0.5 nm space between protein densities and vesicular membranes is quite stable and conserved, thereby suggesting that, in such a configuration, the RAB6 C-terminal tail might no longer be flexible.

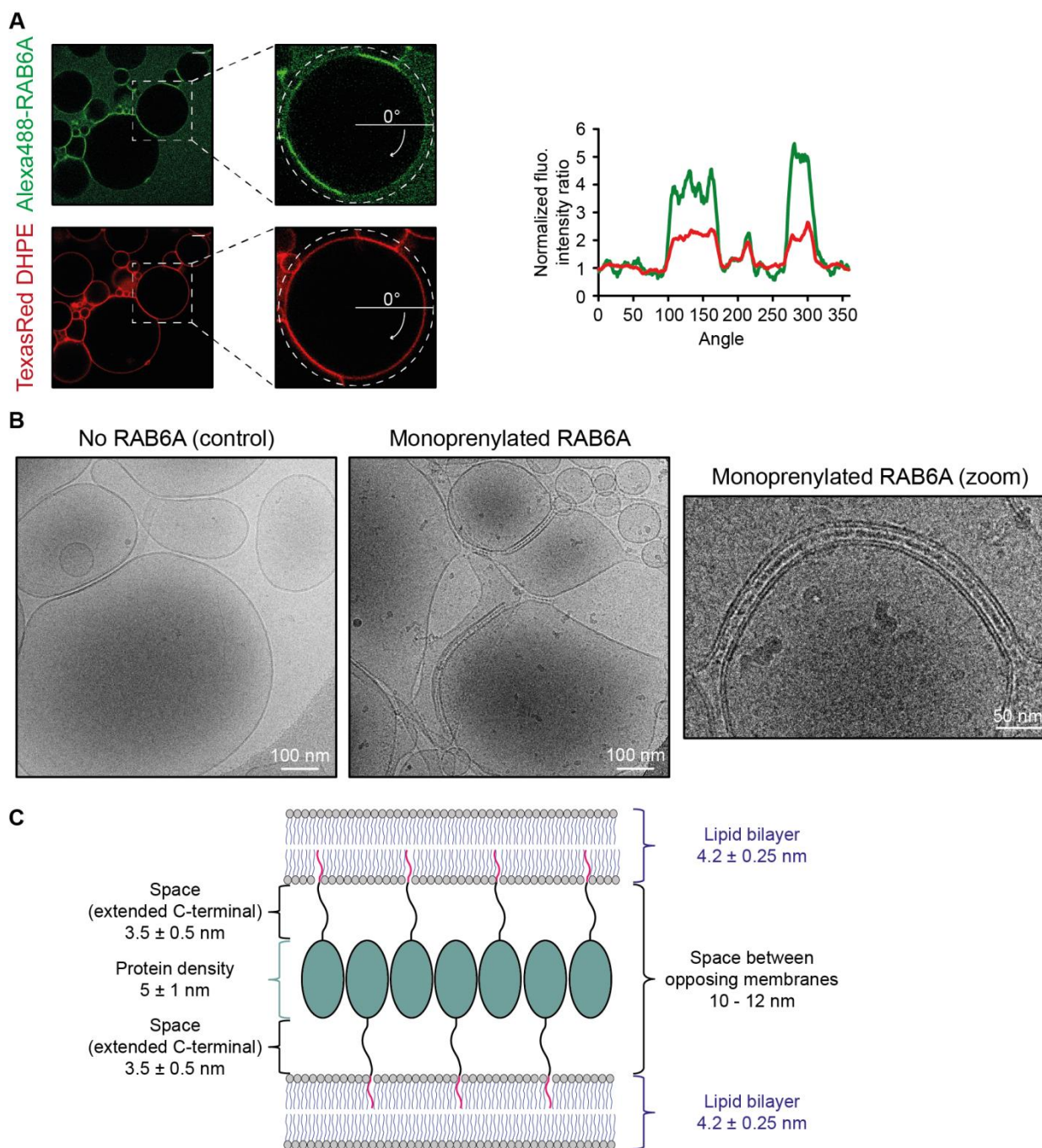


Figure 6.3: Vesicle tethering is induced by a RAB6-RAB6 dimerization in *trans*. (A) Quantification of fluorescence intensities of tethered vesicles. Vesicle (pure EggPC with 0.1% (mol/mol) TexasRed-DHPE lipids) tethering was induced with 2 μ M monoprenylated Alexa488-RAB6A:GTP. Fluorescence intensities of the protein (green channel) and lipids (red channel) were measured using the oval profile method (see Chapter 3). In order to assess the enrichment of the protein at the sites of vesicle interaction (plot on the right), each fluorescence intensity value was subtracted by the background and normalized to the average fluorescence intensity value of non-interacting regions. The normalized fluorescence intensity of the non-interacting regions therefore has approximately a value of 1. TexasRed DHPE lipids were found to concentrate 2 times at the interaction site (because of the contact between two membranes) whereas a 5

fold increase in Alexa488-RAB6A:GTP fluorescence intensity could be detected at the interacting regions. (Scale bar = 10 μm). (B) Vesicle (pure EggPC) aggregation was assessed, using cryo-electron microscopy (performed by Daniel Levy's team, Institut Curie), in presence and in absence of 23 μM monoprenylated RAB6A:GTP. Clear protein densities of 5 ± 1 nm thickness were detected between interacting vesicles only in presence of RAB6A. (C) Hypothetical model for RAB6-induced vesicle tethering. One RAB6 protein from one membrane interacts with another RAB6 protein from the opposing membrane. This dimerization induces the concentration of RAB6 proteins at the interaction sites and subsequent vesicle tethering.

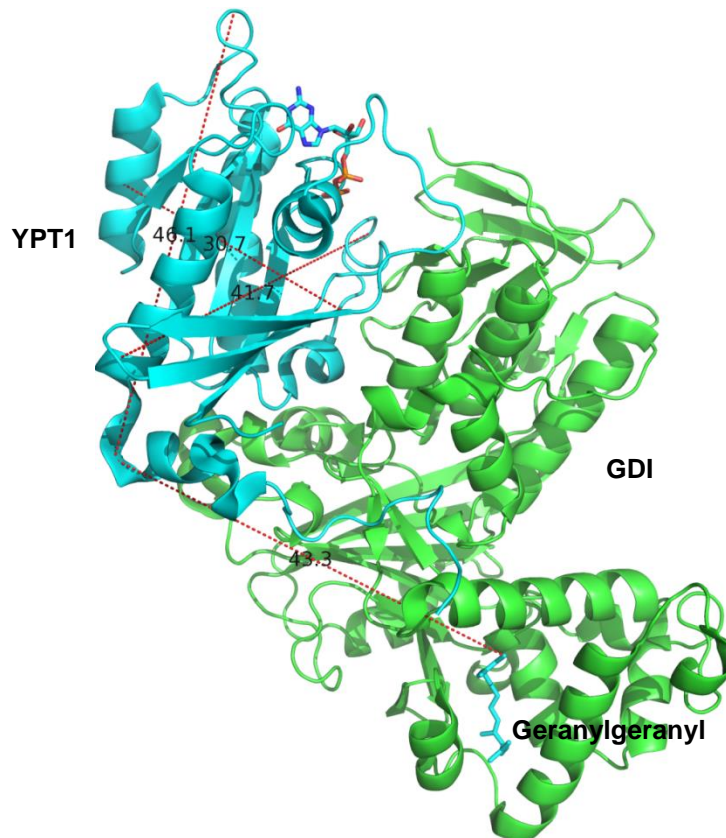


Figure 6.4: Structure of the YPT1:GDI complex. Ribbon representation of YPT1 (light blue) bound to GDI (green). The geranylgeranyl lipid anchor is shown. Distances are indicated in ångström. Adapted from (Pylypenko *et al.*, 2006).

6.1.4 The RAB-RAB interaction is dynamic

Protein densities visualized by Cryo-EM seemed to display a solid-like structure, as they were continuous and did not exhibit any apparent gaps. This suggested that strong and stable contacts are established between the dimerizing RAB6 proteins. I thus wondered how stable this interaction was. In order to investigate this point, I induced EggPC vesicle tethering with the addition of 2 μM red labeled RAB6A (monoprenylated Alexa568-RAB6A:GTP) and subsequently

to the formation of vesicle aggregates, an extra 2 μM of green labeled RAB6A (monoprenylated Alexa488-RAB6A:GTP) was added. The membrane recruitment of the green labeled RAB6 protein was assessed over time (**Figure 6.5A**). Interestingly, even though vesicle tethering had already occurred, the second RAB6 protein was rapidly recruited to the membrane and to the interaction sites (**Figure 6.5A**); and was also found to concentrate there (together with the first RAB6 protein) (**Figure 6.5B**). This suggests that the RAB6-RAB6 interaction is highly dynamic, therefore allowing a fast mixing of the proteins at the interface between two membranes.

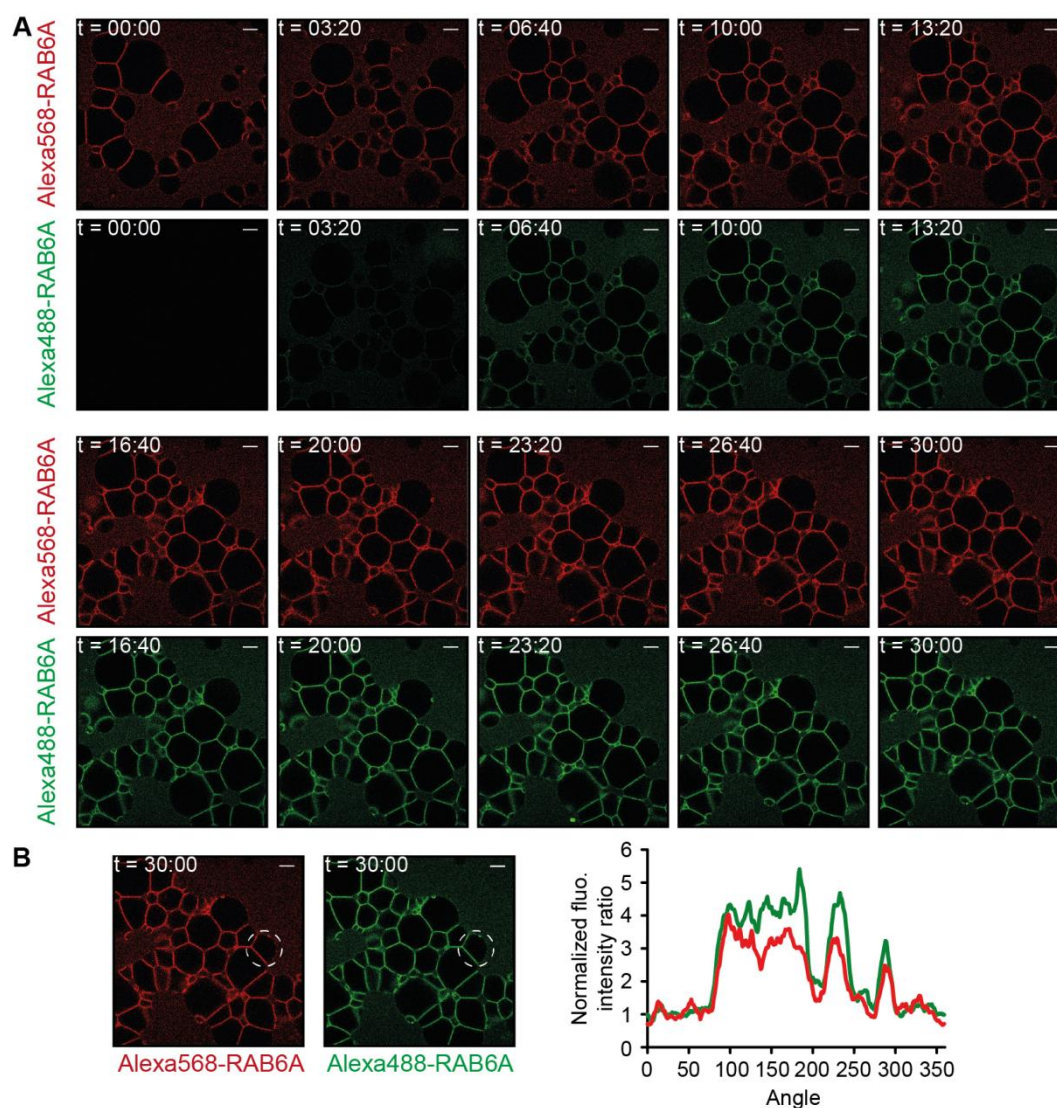


Figure 6.5: The RAB6-RAB6 interaction is dynamic. (A) Effect of the membrane incorporation of 2 μM monoprenylated Alexa488-RAB6A:GTP after vesicle tethering has occurred (achieved with previous addition of 2 μM monoprenylated Alexa568-RAB6A:GTP) was assessed over time (during 30 minutes), by confocal microscopy. Alexa488-RAB6A was added to the tethered EggPC vesicle / Alexa568-RAB6A mix at t = 00:00. (B) Respective enrichments of both labeled proteins at the interaction sites were quantified as in Figure 6.3A. Both proteins were found to concentrate between 3 and 5 times in these regions. (Scale bar = 10 μm).

6.2 Involvement of the Switch regions

6.2.1 RAB6A mutant induces vesicle tethering

To further understand the mechanism regulating RAB6-RAB6 dimerization, we searched for published crystal structures in which RAB6 is a dimer. One crystal structure of RAB6 from *Drosophila melanogaster* (DOI: 10.2210/pdb2y8e/pdb) was found to be crystalized as a dimer (**Figure 6.6**) (Walden *et al.*, 2011). The analysis of the dimer crystal structure by Olena Pylypenko (Anne Houdusse's lab, Institut Curie) revealed that the RAB6-RAB6 interaction might occur via β -sheet- β -sheet interactions (hydrogen bonds) and/or an aromatic ring interaction between tyrosines (at position 35) (**Figure 6.6**). To test this hypothesis, the aspartic acid (D) 49 residue, localized to the β -sheet structure and known to not be involved in interaction with effectors, and the tyrosine (Y) 35 residue were both mutated to arginine (R), a positively charged bulky residue which was expected to impede dimerization through repulsive electrostatic interactions.

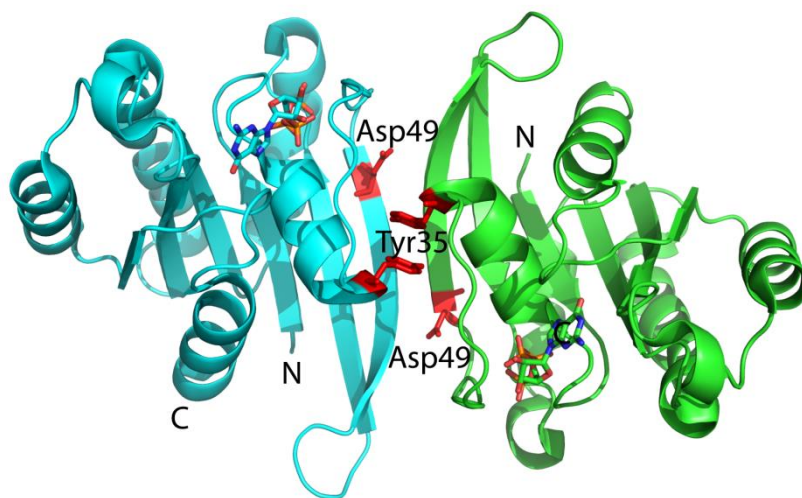


Figure 6.6: RAB6 dimer crystal structure. This published structure (DOI: 10.2210/pdb2y8e/pdb) was obtained with RAB6 from *Drosophila melanogaster*. Analysis of the crystal structure by Olena Pylypenko (Anne Houdusse's lab, Institut Curie) suggested that dimerization might be due to β -sheet- β -sheet interactions and/or interactions between tyrosine35 aromatic rings.

The mutated RAB6A protein (RAB6A-Y35R-D49R) was purified, exchanged to GTP, labeled and monoprenylated in a similar manner as non-mutated RAB6A. 2 μ M monoprenylated Alexa488-labeled GTP-bound RAB6A-Y35R-D49R was incubated in presence of EggPC-containing GUVs.

Vesicle tethering could still be observed in presence of mutated RAB6A; which suggests that the Y35 and D49 residues might not be involved in RAB6-RAB6 dimerization (**Figure 6.7A**).

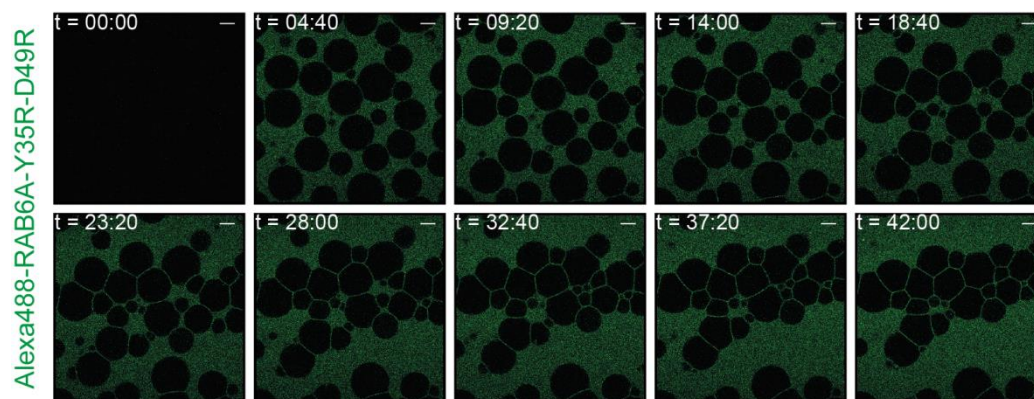


Figure 6.7: Vesicle tether in presence of RAB6A-Y35R-D49R. Vesicle tethering was assessed over time (during 42 minutes), using a confocal microscope, in presence of 2 μ M monoprenylated Alexa488-RAB6A-Y35R-D49R:GTP. Mutated RAB6 was added to the EggPC vesicle mix at $t = 00:00$. (Scale bar = 10 μ m).

An interesting observation was however made during the purification procedure, and more specifically during the gel filtration step. In the case of RAB5 and RAB6 but not of RAB1, clear protein dimerization could be observed when performing size-exclusion chromatography. However, during RAB6A-Y35R-D49R purification, no dimer complexes were obtained, suggesting that the double mutation might have prevented the formation of this complex in solution. The observation that RAB5 can aggregate in solution but not when bound to membranes and that conversely RAB6-Y35R-D49R induces vesicle tethering but does not aggregate in solution strongly suggests that these two types of oligomerization are not related and that RAB proteins might be able to oligomerize in different ways. This could partially account for the conflicting results with previously published data (Lo *et al.*, 2011; Tamura and Mima, 2014).

6.2.2 Unprenylated RAB6A does not interact with membrane-bound RAB6A

The already mentioned nucleotide specificity of vesicle tethering suggests that this interaction might involve the Switch regions. I therefore reasoned that, if the interaction involves the Switch regions, it would be possible to inhibit membrane tethering by out-competing the RAB-RAB interaction through the recruitment of unprenylated RAB6 or effector proteins.

First, I tried to out-compete this interaction by adding an excess of C-terminally truncated RAB6A (RAB6A₈₋₁₉₅) which cannot be prenylated. I started by monitoring whether RAB6A₈₋₁₉₅ could inhibit vesicle tethering. I induced EggPC vesicle tethering with the addition of 2 μ M monoprenylated GTP-bound RAB6A and subsequently to the formation of vesicle aggregates, I added a 10 fold molar excess of GTP-bound RAB6A₈₋₁₉₅. Surprisingly, vesicles were still found to tether (not shown). In another experiment, 2 μ M monoprenylated Alexa488-labeled GTP-bound RAB6A and a 10 fold molar excess of GTP-bound RAB6A₈₋₁₉₅ were added simultaneously. Vesicles were still aggregating and RAB6 was still found to concentrate at the interaction sites (**Figure 6.8A**), thereby indicating that addition of unprenylated RAB6A does not impede vesicle tethering.

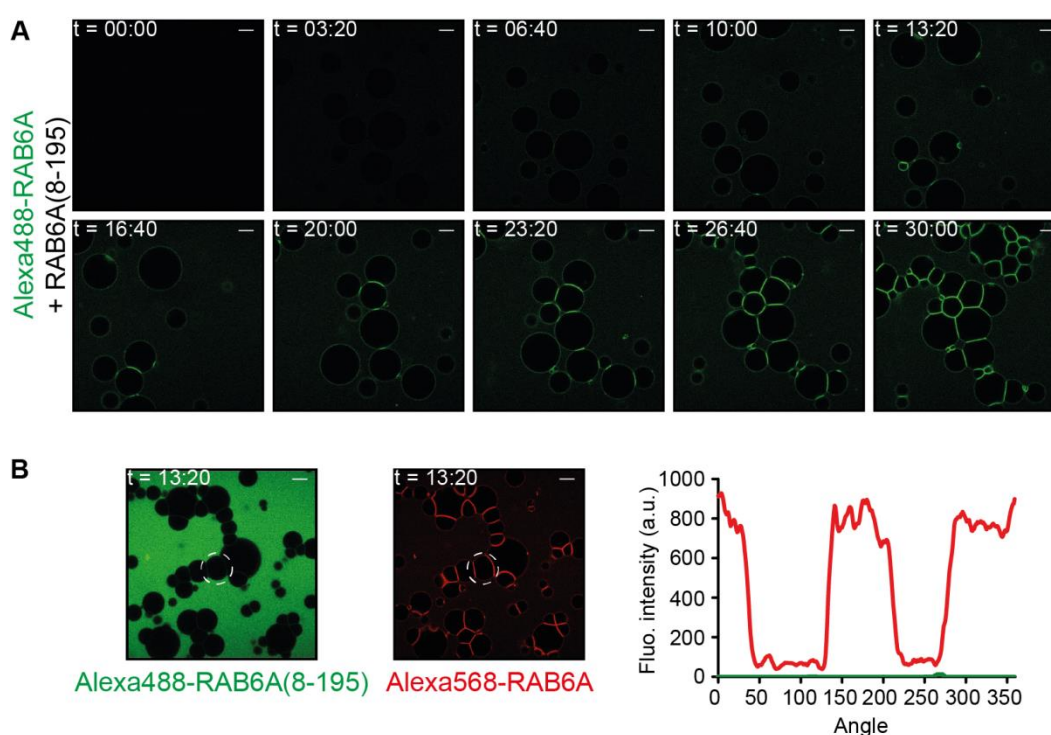


Figure 6.8: Unprenylated RAB6A does not compete with membrane-bound RAB6A. (A) 2 μ M monoprenylated Alexa488-RAB6A:GTP and a 10 fold molar excess of GTP-bound C-terminally truncated RAB6A (RAB6A₈₋₁₉₅) were added simultaneously (at $t = 00:00$). Vesicle aggregation was assessed over time (during 30 minutes), by confocal microscopy. RAB6A₈₋₁₉₅:GTP did not prevent RAB6A-induced vesicle tethering. (B) Equimolar amounts (2 μ M) of monoprenylated Alexa568-labeled GTP-bound RAB6A and Alexa488-labeled GTP-bound RAB6A₈₋₁₉₅ were added simultaneously. The membrane fluorescence intensities of each labeled protein were quantified, after vesicle tethering, using the oval profile method (see Chapter 3), and the obtained intensity values were subtracted by that of the background. Although Alexa568-labeled RAB6A was found to be recruited to the vesicular membrane and to concentrate at the interaction sites, Alexa488-labeled RAB6A₈₋₁₉₅ was not detected in any of these regions. (Scale bar = 10 μ m).

Chapter 6: RAB6-induced membrane tethering

In order to precisely investigate RAB6A₈₋₁₉₅ localization, RAB6A₈₋₁₉₅ was fluorescently labeled at its N-terminus with an Alexa488 fluorophore. Equimolar amounts (2 μ M) of monoprenylated Alexa568-labeled GTP-bound RAB6A and Alexa488-labeled GTP-bound RAB6A₈₋₁₉₅ were added simultaneously. Interestingly, RAB6A was positively recruited to the vesicles and concentrated at the interaction sites whereas RAB6A₈₋₁₉₅ was found to be completely excluded from all of these regions (**Figure 6.8B**); thereby indicating that RAB6A and RAB6A₈₋₁₉₅ cannot interact. The absence of interaction logically explains why vesicle tethering was not impaired but also strongly suggests that monoprenylated RAB6A might undergo conformational changes upon membrane binding, thereby preventing its interaction with unprenylated RAB6A.

Therefore, the previously described absence of liposome aggregation in presence of RAB6A (Tamura and Mima, 2014) could be explained by the fact that RAB6A membrane binding is mediated via a His tag-Nickel-NTA interaction which might not cause conformational changes necessary for RAB6 dimerization. The above results also imply that the RAB-mediated tethering effects previously described (Lo *et al.*, 2011; Tamura and Mima, 2014) and the RAB6 specific tethering effect described here might be a result of different mechanisms involving differently folded proteins.

6.2.3 Bivalent α RAB:GTP antibodies promote vesicle tethering

In order to out compete the RAB-RAB interaction, I investigated the effect of a green labeled anti-RAB6:GTP antibody (ATTO488- α RAB6:GTP, from Adipogen). The addition of a 20 fold molar excess ATTO488- α RAB6:GTP prior to, but also after, RAB6-induced vesicle tethering did not prevent or inhibit vesicle aggregation (**Figure 6.9A**). Interestingly, Alexa568-RAB6A and ATTO488- α RAB6:GTP were both found to concentrate, between 4 and 6 times, at the interaction sites (**Figure 6.9B**). The effect of α RAB6:GTP on vesicle tethering was also monitored by cryo-electron microscopy (again in collaboration with Daniel Levy's team) and clear protein densities could be detected at the interface between tethered vesicles (**Figure 6.9C**). The space between interacting membranes was also increased three times as compared to when α RAB6:GTP is not added to the GUV/RAB6 mix (**Figure 6.9C left** and **Figure 6.3B right**). This could be explained by the fact that the 110 kDa α RAB6:GTP is a bivalent (dimeric) antibody and can bind two RABs from different membranes and its recruitment to the interaction site would increase the space between the interacting vesicles (**Figure 6.9C right**).

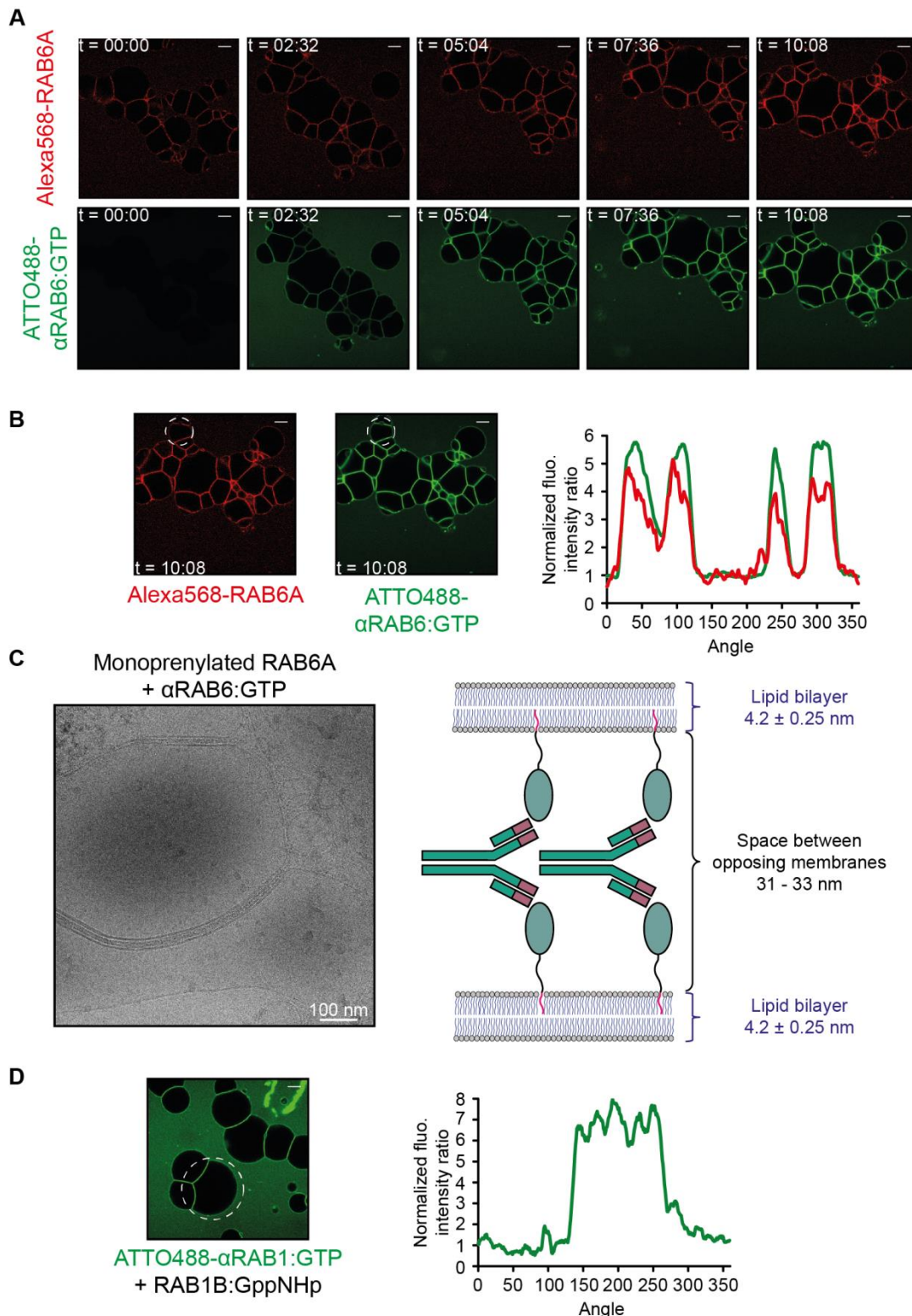


Figure 6.9: Bivalent α RAB:GTP antibodies promote vesicle tethering. (A) Effect of the addition of 40 μ M ATTO488- α RAB6:GTP after vesicle tethering has occurred (achieved with previous addition of 2 μ M monoprenylated Alexa568-RAB6A:GTP) was monitored over time (during 10 minutes), by confocal microscopy. ATTO488- α RAB6:GTP was added to the tethered EggPC vesicle / Alexa568-RAB6A mix at t = 00:00. (Scale bar = 10 μ m). (B) Respective enrichments of Alexa568-RAB6A:GTP and ATTO488- α RAB6:GTP at the interaction sites were quantified as in Figure 6.3A. Both were found to concentrate

Chapter 6: RAB6-induced membrane tethering

between 4 and 6 times in these regions. (Scale bar = 10 μm). (C) Vesicle (pure EggPC) aggregation was monitored, using cryo-electron microscopy (performed by Daniel Levy's team, Institut Curie), in the presence of 23 μM monoprenylated RAB6A:GTP and in the presence or absence of 40 μM $\alpha\text{RAB6:GTP}$ (see Figure 6.3B for the absence of $\alpha\text{RAB6:GTP}$). The thickness of the protein density was increased in presence of $\alpha\text{RAB6:GTP}$ leading to a 3 fold increase of the inter-membrane space thickness. Following these observations, a model (on the right), in which bivalent $\alpha\text{RAB6:GTP}$ binds two RABs from opposite membranes, is proposed. (D) Simultaneous addition of 2 μM monoprenylated RAB1B:GppNHp and a 20 fold excess of ATTO488- $\alpha\text{RAB1:GTP}$ induced vesicle tethering (left). Enrichment of ATTO488- $\alpha\text{RAB1:GTP}$ at the interaction sites (right) was quantified as in Figure 6.3A. ATTO488- $\alpha\text{RAB1:GTP}$ was found to concentrate between 6 and 8 times in these regions. (the ATTO488- $\alpha\text{RAB1:GTP}$ experiment was performed by Lena Oesterlin) (Scale bar = 10 μm).

According to this model, bivalent $\alpha\text{RAB6:GTP}$ should be expected to promote vesicle tethering. This hypothesis was confirmed with the observation that the addition of 40 μM bivalent anti-RAB1:GTP antibody (ATTO488- $\alpha\text{RAB1:GTP}$, courtesy of Adipogen) was able to promote vesicle tethering in presence of 2 μM monoprenylated RAB1B:GppNHp (**Figure 6.9D left**). Additionally, ATTO488- $\alpha\text{RAB1:GTP}$ was also found to concentrate at the interaction sites (**Figure 6.9D right**)

Interestingly, many RAB effector proteins are dimers that can interact with two RAB proteins (Oesterlin *et al.*, 2014). A tempting hypothesis would be that these effector dimers could promote, to some extent, tethering between two opposing membranes.

6.2.4 Effect of monovalent RAB6 effector proteins

As bivalent effectors seem to promote vesicle tethering, I then thought to inhibit the tethering by using monovalent effector proteins.

In relation to the previous section, I investigated the impact of the single-chain variable fragment of the $\alpha\text{RAB6:GTP}$ antibody (scFv). Addition of a 5 fold molar excess of purified $\alpha\text{RAB6:GTP}$ antibody (scFv) prior (**Figure 6.10A**), but also after RAB6-induced vesicle tethering, did not inhibit vesicle aggregation. When equimolar amounts (2 μM) of Alexa568-RAB6A:GTP and Alexa488- $\alpha\text{RAB6:GTP}$ (scFv) were added simultaneously, RAB6A was still found to concentrate around 5 times at the interaction site while $\alpha\text{RAB6:GTP}$ (scFv) was concentrated up to 2 times (**Figure 6.10B**). This suggests that the affinity of $\alpha\text{RAB6:GTP}$ (scFv) for RAB6A might be high enough to allow the formation of $\alpha\text{RAB6:GTP}$ (scFv)-RAB6A complexes at the interaction site but not sufficient to out-compete the RAB6-RAB6 dimerization.

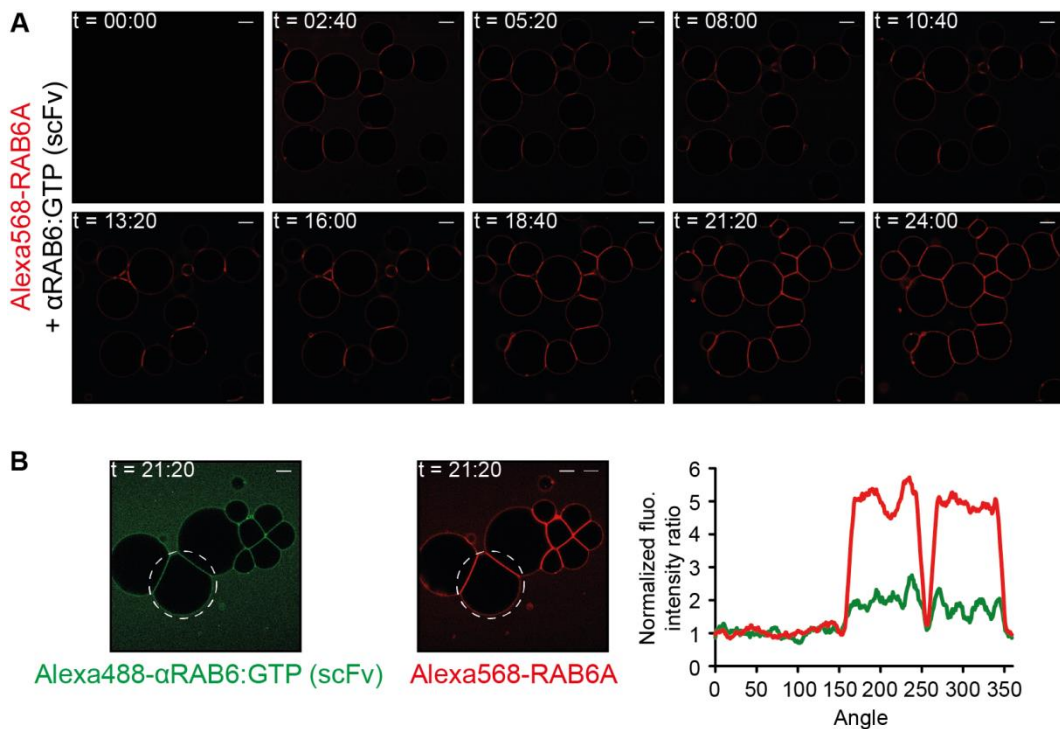


Figure 6.10: α RAB6:GTP (scFv) can access the interaction sites but does not inhibit vesicle tethering. 2 μ M monopenylyated Alexa568-RAB6A:GTP and a 5 fold molar excess of α RAB6:GTP (scFv) were added simultaneously (at t = 00:00). Vesicle aggregation was monitored over time (during 24 minutes), by confocal microscopy. α RAB6:GTP (scFv) did not prevent RAB6A-induced vesicle tethering. (B) Equimolar amounts (2 μ M) of monopenylyated Alexa568-RAB6A:GTP and Alexa488- α RAB6:GTP (scFv) were added simultaneously. Respective enrichments of Alexa568-RAB6A:GTP and Alexa488- α RAB6:GTP (scFv) at the interaction sites were quantified as in Figure 6.3A. RAB6A:GTP was found to concentrate around 5 times in these regions while only a two fold increase in recruitment was detected for α RAB6:GTP (scFv). (Scale bar = 10 μ m).

LidA from *Legionella pneumophila* is known to have a very high (picomolar) affinity for RAB6A, but also for RAB1B and RAB8A (Schoebel *et al.*, 2011). When equimolar amounts (2 μ M) of mCherry-LidA₂₀₁₋₅₈₃ (amino acids 201 to 583) and monopenylyated Alexa488-labeled GTP-bound RAB6A were added simultaneously, no vesicle tethering was observed (not shown). In a separate experiment, I induced EggPC vesicle tethering with the addition of 2 μ M monopenylyated GTP-bound RAB6A and subsequently to the formation of vesicle aggregates added a 2.5 fold molar excess of mCherry-LidA₂₀₁₋₅₈₃. Consistently with the previous experiment, the addition of LidA₂₀₁₋₅₈₃ led to a complete destruction of the tethering complex (Figure 6.IIA), and to the homogeneous redistribution of Alexa488-RAB6A:GTP over the GUV membrane (Figure 6.IIB). This suggests that monovalent effectors with a high affinity for RAB proteins are able to compete with the dimerization process.

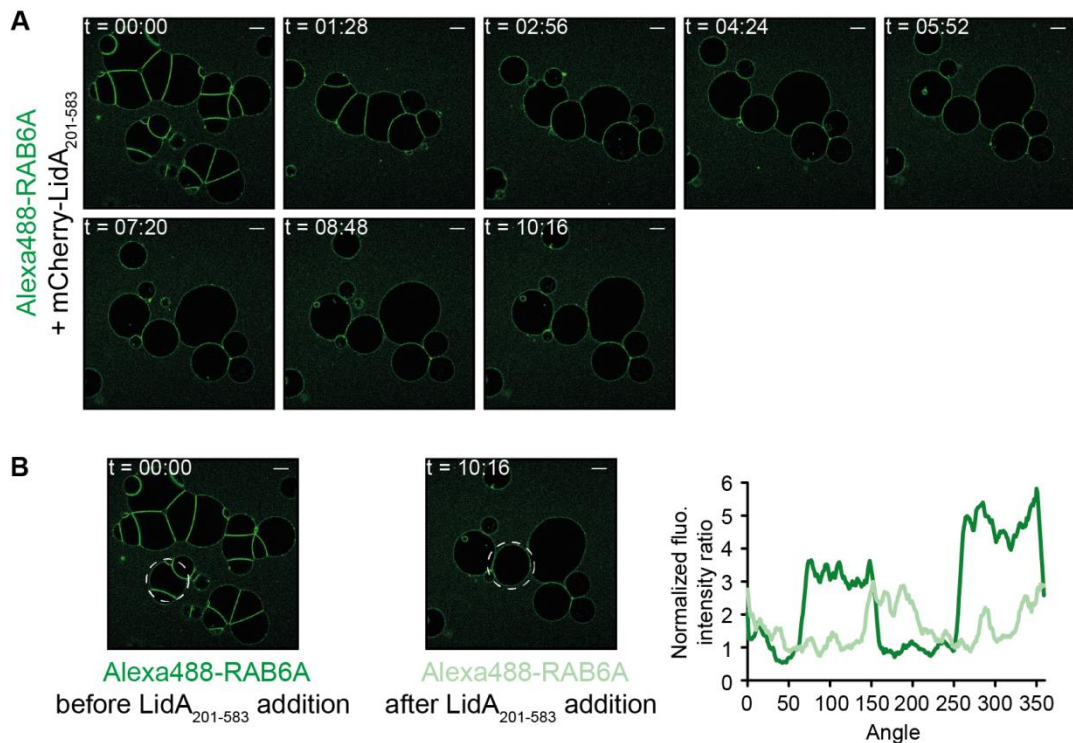


Figure 6.11: Inhibition of vesicle tethering by LidA₂₀₁₋₅₈₃. (A) Effect of the addition of 5 μM mCherry-LidA₂₀₁₋₅₈₃ after vesicle tethering has occurred (achieved with previous addition of 2 μM monoprenylated Alexa488-RAB6A:GTP) was monitored over time (during 10 minutes), by confocal microscopy. mCherry-LidA₂₀₁₋₅₈₃ was added to the tethered EggPC vesicle / Alexa488-RAB6A mix at $t = 00:00$. (B) Enrichment of Alexa488-RAB6A:GTP at the interaction sites, before ($t = 00:00$, green) and after ($t = 10:16$, light green) mCherry-LidA₂₀₁₋₅₈₃ addition, were quantified as in Figure 6.3A. Alexa488-RAB6A:GTP was found to concentrate less at the interaction sites after the addition of LidA₂₀₁₋₅₈₃. (Scale bar = 10 μm).

The OCRL protein (oculocerebrorenal syndrome of Lowe protein) is a known effector of several RAB GTPases, including RAB6 (Hyvola *et al.*, 2006). The study of the effect of OCRL on vesicle tethering gave rise to conflicting observations. I induced EggPC vesicle tethering with the addition of 2 μM monoprenylated GTP-bound RAB6A. Subsequently to the formation of vesicle aggregates, I added a 10 fold molar excess (20 μM) of either the mCherry-tagged RAB binding domain of OCRL (mCherry-OCRL₅₃₈₋₉₀₁) or the Alexa488-labeled OCRL₅₃₈₋₉₀₁. Although addition of mCherry-OCRL₅₃₈₋₉₀₁ seemed to partially impede the tethering, no alteration was observed after addition of Alexa488-labeled OCRL₅₃₈₋₉₀₁. When performing the same experiment using an untagged version of OCRL₅₃₈₋₉₀₁, the resulting effect was very similar to that obtained with mcherry-tagged OCRL₅₃₈₋₉₀₁. A likely explanation is that the Alexa488 fluorophore might somehow decrease the affinity of OCRL₅₃₈₋₉₀₁ for RAB6 thereby making it more difficult to inhibit vesicle tethering. In relation to this, when equimolar amounts (2 μM) of monoprenylated Alexa488-labeled GTP-bound RAB6A and mCherry-OCRL₅₃₈₋₉₀₁ were added simultaneously,

RAB6A was still found to concentrate around 5 times at the interaction site while mCherry-OCRL₅₃₈₋₉₀₁ concentrated up to 2 times (**Figure 6.12A**). Conversely, Alexa488-labeled OCRL₅₃₈₋₉₀₁, when added in equimolar amount, was found to be excluded from the interaction sites (**Figure 6.12B**).

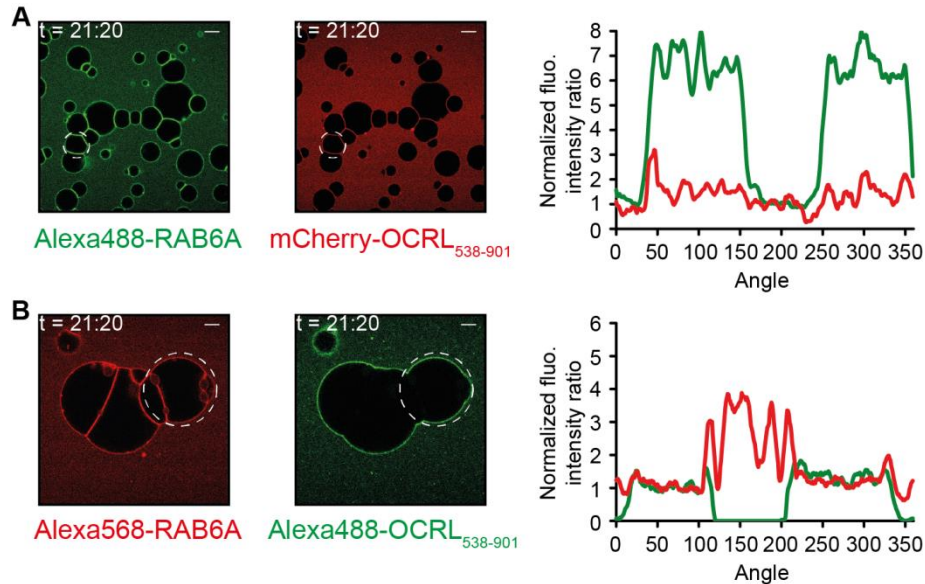


Figure 6.12: Effect of OCRL₅₃₈₋₉₀₁ on vesicle tethering. (A) RAB6-induced vesicle tethering was monitored after simultaneous addition of equimolar amounts (2 μ M) of monoprenylated Alexa488-labeled RAB6A:GTP and mCherry-OCRL₅₃₈₋₉₀₁, by confocal microscopy. Respective protein enrichments at the interaction sites were quantified as in Figure 6.3A. Alexa488-labeled RAB6A:GTP and mCherry-OCRL₅₃₈₋₉₀₁ were both found to concentrate at the interaction sites up to 7 and 2 times, respectively. (B) Same experiment as in (A) with Alexa568-labeled RAB6A:GTP and Alexa488-labeled OCRL₅₃₈₋₉₀₁. RAB6A:GTP was found to concentrate up to 4 times at the interaction sites whereas Alexa488-labeled OCRL₅₃₈₋₉₀₁ was found to be excluded from these regions. (Scale bar = 10 μ m).

These results suggest that Alexa488-OCRL₅₃₈₋₉₀₁ exhibits lower affinity towards RAB6A than mCherry-OCRL₅₃₈₋₉₀₁ and probably unlabeled OCRL₅₃₈₋₉₀₁. Due to its lower affinity for RAB6A, Alexa488-labeled OCRL₅₃₈₋₉₀₁ is not able to compete with the RAB-RAB interaction and to inhibit vesicle tethering. This decreased affinity for RAB6 might be due to the labeling reaction. This reaction consists in the covalent attachment of the Alexa488 fluorophore to the amine groups of the protein. We usually perform it at pH7.5 which should only allow labeling of the N-terminal amine group and not of the amine group-containing lysines (lower pKa of the N-terminal amine group). One possibility would be that the RAB-binding domain of OCRL (OCRL₅₃₈₋₉₀₁) was also labeled on some lysine residues, which led to a decreased affinity for RAB6.

Nevertheless, an excess of mcherry-tagged and untagged OCRL₅₃₈₋₉₀₁ was found to moderately inhibit vesicle tethering.

The effect of OCRL₅₃₈₋₉₀₁ on RAB6-induced vesicle tethering was found to be less strong than that of LidA₂₀₁₋₅₈₃. As already mentioned, LidA was shown to display a very high affinity (30 pM) towards RAB6 (Schoebel *et al.*, 2011) which is higher than what can be found for usual RAB effectors, including OCRL whose affinity for RAB6 was shown to be in the micromolar range (Hou *et al.*, 2011). LidA is therefore expected to out-compete the RAB6-RAB6 interaction much more effectively than OCRL.

6.3 Discussion

I have shown that activated GTP-bound RAB6 (A and A'), but not RAB1B or RAB5A, is able to tether vesicles *in vitro* without the need of any additional factors (such as tethering factors). We suggest that this tethering effect is mediated by RAB6-RAB6 dimerization in *trans*. This is partially consistent with previous studies showing that some RAB proteins can induce vesicle aggregation (Lo *et al.*, 2011; Tamura and Mima, 2014) and that such an effect is modulated by RAB-RAB interactions in their GTP-bound state (Lo *et al.*, 2011). However, in contrast to my work, these studies indicated that VPS21/RAB5A but not RAB6A are able to induce vesicle tethering. A difference between these studies and mine is the mean by which RAB proteins are anchored to membranes. RAB binding was previously achieved through the interaction of histidine-tagged proteins with Nickel-NTA-containing liposomes (Lo *et al.*, 2011; Tamura and Mima, 2014) whereas in my study RAB proteins were incorporated into membranes through their geranylgeranyl group. The observation that unprenylated RAB6 was not membrane localized in the presence of monoprenylated RAB6 indicate that the prenylated and non-prenylated proteins do not interact with each other. We therefore suggest that monoprenylated RAB6 undergoes conformational changes upon membrane insertion of its prenyl group, which only allows its interaction with another monoprenylated and membrane-bound RAB6 protein. As the previously mentioned studies used RAB proteins anchored to membranes through a histidine tag, we hypothesize that their proteins might not undergo similar changes in conformation and thereby that the RAB-RAB interactions possibly involve different sequence regions.

One can argue that my study mostly relies on qualitative measurements of vesicle tethering by confocal microscopy. More quantitative analyses of liposome aggregation, using

dynamic light scattering (Lo *et al.*, 2011) or turbidity assays (Tamura and Mima, 2014), should be performed in order to confirm these observations.

RAB proteins are thought to drive membrane tethering through the recruitment of tethering factors (coiled-coil tethers and multisubunit tethering complexes) (Brocker *et al.*, 2010; Cai *et al.*, 2007a). Our results suggest that some RAB proteins, including RAB6, might also operate in concert with these conventional effector proteins to directly drive membrane recognition.

As mentioned in chapter 2, tethering events also occur during the formation of membrane contact sites (MCSs) allowing the transfer of material, such as lipids, between organelles (Jackson *et al.*, 2016; Phillips and Voeltz, 2016). ER-Golgi contact sites have been described to be mostly promoted by a variety of lipid transfer proteins which contain a pleckstrin homology (PH) domain, allowing their binding to Golgi-localized PI(4)P lipids, and an FFAT motif (diphenylalanine in an acidic tract) that can interact with the ER-localized VAP-A protein (vesicle-associated membrane protein-associated protein A). Among them, the oxysterol-binding protein (OSBP), which mediates the transfer of both cholesterol and PI(4)P between the ER and the Golgi, was also shown to bind ARF1 at the Golgi membrane (Mesmin *et al.*, 2013). Of note, a construct consisting of the PH domain, the coiled-coil region and the FFAT motif of OSBP (PH-FFAT) was sufficient to promote and stabilize ER-Golgi contact sites in HeLa cells (Mesmin *et al.*, 2013).

Prior to my arrival, it was found by Cathy Jackson's team (Institut Jacques Monod) that GBF1 (Golgi-specific brefeldin A-resistance guanine nucleotide exchange factor 1), a known *cis*-Golgi localized GEF for ARF1 (Zhao *et al.*, 2002), interacts with RAB6. This interaction was first assessed by co-immunoprecipitation/mass spectrometry analyses and subsequently confirmed by Stephanie Miserey-Lenkei (Bruno Goud's lab, Institut Curie) by yeast two hybrid. Later on, Cathy Jackson's team also identified VAP-A as a potential GBF1 interacting protein by immunoprecipitation. They subsequently observed, using a proximity ligation assay, that both proteins co-localize at PH-FFAT stabilized contact sites in HeLa cells. Altogether, the above results raise the interesting possibility that RAB6 might also localize to ER-Golgi contact sites and might participate in membrane tethering. Further experiments are needed to test this hypothesis.

Part of my work consisted in investigating the effect of RAB6 effector recruitment on RAB6-induced vesicle tethering. Because this effect seemed to be dependent on the nucleotide bound state of the protein, I assumed that effector proteins might be able to out-compete the RAB6-RAB6 interaction. Experiments performed in the presence of bivalent α RAB:GTP antibodies

Chapter 6: RAB6-induced membrane tethering

strongly suggest that, instead of impairing vesicle aggregation, they can promote vesicle tethering through their interaction with two RAB proteins from distinct membranes. This suggests that effector proteins containing two or more RAB binding sites might be able to promote tethering between two membranes. In relation to this, one could make a distinction between dimeric RAB effector proteins (Oesterlin *et al.*, 2014) that would rather promote homotypic fusion (interaction with two proteins of the same RAB subfamily) and effector proteins that have the ability to interact with different RAB proteins and thereby would rather drive heterotypic fusion. A striking example of such an effector is the Golgi-localized coiled-coil tethering factor GCC185 which associates as a dimer and can therefore bind two RAB proteins (Oesterlin *et al.*, 2014). Although a direct interaction between GCC185 and RAB6 is controversial (Burguete *et al.*, 2008; Houghton *et al.*, 2009), GCC185 also contains multiple other RAB binding-sites which have been suggested to be necessary for the maintenance of Golgi stack morphology (Hayes *et al.*, 2009). Another tethering factor Rabenosyn-5, which possesses separate RAB4 and RAB5 binding sites, was suggested to connect distinct domains in *cis* on early endosomes (de Renzis *et al.*, 2002) and could possibly also mediate to some extent membrane interaction in *trans*.

In contrast, monomeric effector proteins containing only one RAB6 binding site did not promote vesicle aggregation but, as expected, seemed to rather compete with the RAB-RAB interaction. This competition was more or less efficient, likely depending on their affinities for RAB6. Both α RAB6:GTP (scFv) and OCRL were found to localize at the interaction sites, and OCRL was able to moderately impair vesicle tethering. Their effective recruitment to the interaction sites suggests that both effectors exhibit an affinity towards RAB6 that is high enough to take advantage of the high dynamics of the RAB-RAB interaction but not sufficient to completely impair dimerization. An increased concentration of OCRL might eventually result in a complete inhibition of the vesicle tethering process. However, if the required concentration is too high, impairment of this process might not be experimentally achievable. These results suggest that the RAB6-RAB6 affinity might be higher than that of OCRL-RAB6 which was previously described to be in the low micromolar range (3.7 μ M) (Hou *et al.*, 2011).

Many human RAB6 effectors were described to have low micromolar to high nanomolar affinities towards RAB6 (Oesterlin *et al.*, 2014), suggesting that they might not always be able to compete with RAB6-RAB6 dimerization. I thus investigated the effect of LidA, a protein translocated by *Legionella pneumophila* into the host cytosol at the beginning of infection which was shown to interact with RAB1, RAB6 and RAB8 (Machner and Isberg, 2006) with an extremely high (picomolar) affinity (Schoebel *et al.*, 2011). Interestingly, no vesicle aggregation was observed after simultaneous addition of RAB6 and LidA; and the addition of LidA to previously tethered

vesicles seemed to impair the stability of vesicle aggregates. This suggests that LidA, due to its high affinity for RAB6, might out-compete the RAB6-RAB6 interaction, thereby inhibiting homotypic membrane tethering. LidA was previously shown to interfere with the early steps of the secretory pathway (Derre and Isberg, 2005). This was suggested to be mediated by its interaction with GTP but also GDP-bound RAB1 (Machner and Isberg, 2006). In addition, LidA was shown to exhibit similar properties towards GTP- and GDP-bound RAB6 (Schoebel *et al.*, 2011), which strongly suggests that it can also interfere with RAB6-mediated trafficking events, including RAB6-induced membrane tethering.

Our study raised the question of the influence of the nucleotide bound state of RAB proteins on their recruitment to membranes. All members of the RAS superfamily of proteins are activated by GEFs upon membrane binding. GDP to GTP exchange was extensively described to be crucial for interaction with effector proteins. In the case of ARF1, GTP binding was also shown to allow the displacement of its N-terminal amphipathic from the core of the protein and its subsequent availability for membrane anchorage (Antonny *et al.*, 1997). Additionally, H-RAS was shown to be first targeted to lipid rafts at the plasma membrane and then laterally redistributed to disordered membranes upon activation (Prior *et al.*, 2001). This process was suggested to rely on conformational changes of the H-RAS N-terminal domain, coincident with GTP binding, which could be transmitted to the lipid anchor. To my knowledge, no such mechanisms were described for RAB proteins. RABs do not possess N-terminal amphipathic helices and were observed to preferentially localize to disordered membranes independently of their nucleotide-bound state (see Chapter 4). This point should however be further investigated.

Concluding remarks

In this study, we have managed for the first time to incorporate prenylated RABs into artificial membranes. My PhD project started with the study of the RAB6-induced membrane tethering, a phenomenon which had just been observed before my arrival to the lab. I have confirmed that RAB6, but not RAB1 or RAB5, is able to promote by itself, and in a GTP-dependent manner, vesicle tethering. We believe that prenylated RAB6 is able to interact in *trans* with itself and thereby promotes homotypic membrane tethering. This suggests that RAB6 might regulate, in concert with tethering factors or lipid transfer proteins, membrane recognition and tethering events during lipid and protein transport processes.

The main part of my project consisted in investigating the membrane binding properties necessary for the effective recruitment of prenylated RAB GTPases.

RAB1, RAB5 and RAB6 were all found to only localize to Ld membrane domains and to preferentially bind to curved membranes; and this seemed to occur independently of the nucleotide-bound state and the number of geranylgeranyl groups. We demonstrated that the specific recruitment of RAB1, RAB5 and RAB6 is primarily dependent on the hydrophobic insertion of the prenyl group into lipid packing defects. We therefore showed that, in accordance with recently published data on farnesylated N-RAS proteins (Larsen *et al.*, 2015; Larsen *et al.*, 2017), prenyl groups do not only act as non-specific anchors but are also involved in specific membrane targeting. This lipid-driven mechanism might partially explain how RAB proteins could bind to intracellular membranes which are mainly found in a disordered state (Niko *et al.*, 2016), and associate with highly curved transport carriers.

Although the membrane incorporation of the prenyl group was shown to be sufficient for RAB1, RAB5 and RAB6 membrane binding, it was proven not to be the case for other RABs.

The membrane recruitment of RAB35, known to localize in cells to the endocytic compartments and the plasma membrane (Kouranti *et al.*, 2006), was shown to be primarily dependent on the presence of negatively charged lipids. This observation is consistent with previous studies (Heo *et al.*, 2006; Li *et al.*, 2014) demonstrating that RAB35 plasma membrane localization is regulated by the interaction of its C-terminal positively charged hypervariable region with negatively charged phosphoinositides. Although lipid packing defects were shown to enhance RAB35 membrane affinity, they were not essential for membrane binding. RAB23,

Concluding remarks

another plasma membrane-localized RAB protein (Evans *et al.*, 2003), also displays a C-terminal polybasic hypervariable region, thereby suggesting that its specific recruitment to the plasma membrane might also be mediated by electrostatic interactions. As many other intracellular compartments are enriched in specific phosphoinositide derivatives, known to be involved in various cellular signaling processes, electrostatic interactions might also mediate the recruitment of other RAB proteins.

RAB4 and RAB11 were effectively recruited to purified Golgi fractions in an effector-independent manner. However membrane charges, but also lipid packing defects, promoted by unsaturated lipids or membrane curvature, were not sufficient to promote RAB4 and RAB11 recruitment to synthetic vesicles. Altogether, this suggests that RAB4 and RAB11 require more demanding membrane physicochemical properties. Possibly, RAB4 and RAB11 effective membrane binding might require a combination of multiple membrane features, such as charge and curvature. This could be rapidly investigated using a “protein-lipid interaction by fluorescence” assay (Ceccato *et al.*, 2016).

Most studies so far have identified protein factors, such as GEFs, as being responsible for the targeting of RAB proteins to specific intracellular membranes. This study sheds new light on the important role of the physicochemical properties of membranes in mediating the recruitment of RAB proteins. An important question however remains. What is the relative involvement of each of these mechanisms? One could argue that because RAB1, RAB5 and RAB6 can all sense lipid packing defects via their prenyl group, the specificity of localization to a given compartment would then rather rely on protein-mediated mechanisms. However, RAB35 only binds to negatively charged membranes and RAB4/RAB11 membrane binding appears much more specific, suggesting that protein factors and properties of membranes are equally important for the regulation of RAB specific membrane targeting. This matter generates an exciting area for future investigations. An increased complexity of the *in vitro* system, through the addition of other membrane-bound proteins such as GEFs or lipid-binding effector proteins, could offer an interesting new way to better understand how RAB proteins are specifically localized.

References

- Aivazian D, Serrano RL, Pfeffer S. 2006. TIP47 is a key effector for Rab9 localization. *The Journal of cell biology* 173: 917-926
- Alexandrov K, Horiuchi H, Steele-Mortimer O, Seabra MC, Zerial M. 1994. Rab escort protein-1 is a multifunctional protein that accompanies newly prenylated rab proteins to their target membranes. *EMBO Journal* 13: 5262-5273
- Alexandrov K, Simon I, Yurchenko V, Iakovenko A, Rostkova E, Scheidig AJ, Goody RS. 1999. Characterization of the ternary complex between Rab7, REP-1 and Rab geranylgeranyl transferase. *European Journal of Biochemistry* 265: 160-170
- Ali BR, Seabra MC. 2005. Targeting of Rab GTPases to cellular membranes. *Biochemical Society Transactions* 33: 652-656
- Ali BR, Wasmeier C, Lamoreux L, Strom M, Seabra MC. 2004. Multiple regions contribute to membrane targeting of Rab GTPases. *Journal of Cell Science* 117: 6401-6412
- Alory C, Balch WE. 2001. Organization of the Rab-GDI/CHM superfamily: the functional basis for choroideremia disease. *Traffic* 2: 532-543
- Ambroggio E, Sorre B, Bassereau P, Goud B, Manneville JB, Antonny B. 2010. ArfGAP1 generates an Arf1 gradient on continuous lipid membranes displaying flat and curved regions. *EMBO Journal* 29: 292-303
- Andres DA, Seabra MC, Brown MS, Armstrong SA, Smeland TE, Cremers FP, Goldstein JL. 1993. cDNA cloning of component A of Rab geranylgeranyl transferase and demonstration of its role as a Rab escort protein. *Cell* 73: 1091-1099
- Angelova M, Soléau S, Méléard P, Faucon JF, Bothorel P. 1992. Preparation of giant vesicles by external AC electric fields. Kinetics and applications. *Progress in Colloid and Polymer Science* 89: 127-131
- Anitei M, Hoflack B. 2011. Bridging membrane and cytoskeleton dynamics in the secretory and endocytic pathways. *Nature Cell Biology* 14: 11-19
- Antonny B. 2006. Membrane deformation by protein coats. *Current Opinion in Cell Biology* 18: 386-394
- Antonny B. 2011. Mechanisms of membrane curvature sensing. *Annual Review of Biochemistry* 80: 101-123
- Antonny B, Beraud-Dufour S, Chardin P, Chabre M. 1997. N-terminal hydrophobic residues of the G-protein ADP-ribosylation factor-1 insert into membrane phospholipids upon GDP to GTP exchange. *Biochemistry* 36: 4675-4684
- Antony C, Cibert C, Geraud G, Santa Maria A, Maro B, Mayau V, Goud B. 1992. The small GTP-binding protein rab6p is distributed from medial Golgi to the trans-Golgi network as determined by a confocal microscopic approach. *Journal of Cell Science* 103 (Pt 3): 785-796

References

- Aridor M, Bannykh SI, Rowe T, Balch WE. 1995. Sequential coupling between COPII and COPI vesicle coats in endoplasmic reticulum to Golgi transport. *The Journal of cell biology* 131: 875-893
- Babst M. 2011. MVB vesicle formation: ESCRT-dependent, ESCRT-independent and everything in between. *Current Opinion in Cell Biology* 23: 452-457
- Bagatolli L, Sunil Kumar PB. 2009. Phase behavior of multicomponent membranes: Experimental and computational techniques. *Soft Matter* 5: 3234-3248
- Bagatolli LA. 2006. To see or not to see: lateral organization of biological membranes and fluorescence microscopy. *Biochimica et biophysica acta* 1758: 1541-1556
- Bailly E, McCaffrey M, Touchot N, Zahraoui A, Goud B, Bornens M. 1991. Phosphorylation of two small GTP-binding proteins of the Rab family by p34cdc2. *Nature* 350: 715-718
- Barbacid M. 1987. ras genes. *Annual Review of Biochemistry* 56: 779-827
- Barbero P, Bittova L, Pfeffer SR. 2002. Visualization of Rab9-mediated vesicle transport from endosomes to the trans-Golgi in living cells. *The Journal of cell biology* 156: 511-518
- Barbieri MA, Roberts RL, Mukhopadhyay A, Stahl PD. 1996. Rab5 regulates the dynamics of early endosome fusion. *Biocell : official journal of the Sociedades Latinoamericanas de Microscopia Electronica et al* 20: 331-338
- Bardin S, Miserey-Lenkei S, Hurbain I, Garcia-Castillo D, Raposo G, Goud B. 2015. Phenotypic characterisation of RAB6A knockout mouse embryonic fibroblasts. *Biology of the Cell* 107: 427-439
- Barr F, Lambright DG. 2010. Rab GEFs and GAPs. *Current Opinion in Cell Biology* 22: 461-470
- Barrowman J, Novick P. 2003. Three Yips for Rab recruitment. In *Nat Cell Biol* Vol. 5, pp 955-956. England
- Barrowman J, Wang W, Zhang Y, Ferro-Novick S. 2003. The Yiplp.Yiflp complex is required for the fusion competence of endoplasmic reticulum-derived vesicles. *The Journal of biological chemistry* 278: 19878-19884
- Baumgart T, Hess ST, Webb WW. 2003. Imaging coexisting fluid domains in biomembrane models coupling curvature and line tension. *Nature* 425: 821-824
- Baumgart T, Hunt G, Farkas ER, Webb WW, Feigenson GW. 2007. Fluorescence probe partitioning between Lo/Ld phases in lipid membranes. *Biochimica et biophysica acta* 1768: 2182-2194
- Beck R, Sun Z, Adolf F, Rutz C, Bassler J, Wild K, Sinning I, Hurt E, Brugger B, Bethune J, Wieland F. 2008. Membrane curvature induced by Arf1-GTP is essential for vesicle formation. *Proceedings of the National Academy of Sciences of the United States of America* 105: 11731-11736
- Bell RM, Ballas LM, Coleman RA. 1981. Lipid topogenesis. *Journal of Lipid Research* 22: 391-403
- Benmerah A. 2004. Endocytosis: signaling from endocytic membranes to the nucleus. *Current biology : CB* 14: R314-316

- Beranger F, Paterson H, Powers S, de Gunzburg J, Hancock JF. 1994. The effector domain of Rab6, plus a highly hydrophobic C terminus, is required for Golgi apparatus localization. *Molecular and Cellular Biology* 14: 744-758
- Bhatia VK, Madsen KL, Bolinger PY, Kunding A, Hedegard P, Gether U, Stamou D. 2009. Amphipathic motifs in BAR domains are essential for membrane curvature sensing. *EMBO Journal* 28: 3303-3314
- Bielli A, Thornqvist PO, Hendrick AG, Finn R, Fitzgerald K, McCaffrey MW. 2001. The small GTPase Rab4A interacts with the central region of cytoplasmic dynein light intermediate chain-1. *Biochemical and Biophysical Research Communications* 281: 1141-1153
- Bigay J, Antonny B. 2012. Curvature, lipid packing, and electrostatics of membrane organelles: defining cellular territories in determining specificity. *Developmental Cell* 23: 886-895
- Bigay J, Casella JF, Drin G, Mesmin B, Antonny B. 2005. ArfGAP1 responds to membrane curvature through the folding of a lipid packing sensor motif. *EMBO Journal* 24: 2244-2253
- Bigay J, Gounon P, Robineau S, Antonny B. 2003. Lipid packing sensed by ArfGAP1 couples COPI coat disassembly to membrane bilayer curvature. *Nature* 426: 563-566
- Blumer J, Rey J, Dehmelt L, Mazel T, Wu YW, Bastiaens P, Goody RS, Itzen A. 2013. RabGEFs are a major determinant for specific Rab membrane targeting. *Journal of Cell Biology* 200: 287-300
- Bock JB, Matern HT, Peden AA, Scheller RH. 2001. A genomic perspective on membrane compartment organization. *Nature* 409: 839-841
- Bonifacino JS. 2014. Vesicular transport earns a Nobel. *Trends in Cell Biology* 24: 3-5
- Bonifacino JS, Glick BS. 2004. The mechanisms of vesicle budding and fusion. *Cell* 116: 153-166
- Bonifacino JS, Rojas R. 2006. Retrograde transport from endosomes to the trans-Golgi network. *Nature reviews Molecular cell biology* 7: 568-579
- Boucrot E, Pick A, Camdere G, Liska N, Evergren E, McMahon HT, Kozlov MM. 2012. Membrane fission is promoted by insertion of amphipathic helices and is restricted by crescent BAR domains. *Cell* 149: 124-136
- Brocker C, Engelbrecht-Vandre S, Ungermann C. 2010. Multisubunit tethering complexes and their role in membrane fusion. *Current biology : CB* 20: R943-952
- Brown WJ, Chambers K, Doody A. 2003. Phospholipase A2 (PLA2) enzymes in membrane trafficking: mediators of membrane shape and function. *Traffic (Copenhagen, Denmark)* 4: 214-221
- Brugger B, Sandhoff R, Wegehingel S, Gorgas K, Malsam J, Helms JB, Lehmann WD, Nickel W, Wieland FT. 2000. Evidence for segregation of sphingomyelin and cholesterol during formation of COPI-coated vesicles. *The Journal of cell biology* 151: 507-518
- Bucci C, Lutcke A, Steele-Mortimer O, Olkkonen VM, Dupree P, Chiariello M, Bruni CB, Simons K, Zerial M. 1995. Co-operative regulation of endocytosis by three Rab5 isoforms. *FEBS Letters* 366: 65-71

References

- Bucci C, Parton RG, Mather IH, Stunnenberg H, Simons K, Hoflack B, Zerial M. 1992. The small GTPase rab5 functions as a regulatory factor in the early endocytic pathway. *Cell* 70: 715-728
- Bucher P, Fischer A, Luisi PL, Oberholzer T, Walde P. 1998. Giant vesicles as biochemical compartments: the use of microinjection techniques. *Langmuir* 14: 2712-2721
- Burguete AS, Fenn TD, Brunger AT, Pfeffer SR. 2008. Rab and Arl GTPase family members cooperate in the localization of the golgin GCC185. *Cell* 132: 286-298
- Bustelo XR, Sauzeau V, Berenjano IM. 2007. GTP-binding proteins of the Rho/Rac family: regulation, effectors and functions in vivo. *BioEssays : news and reviews in molecular, cellular and developmental biology* 29: 356-370
- Cabrera M, Ungermann C. 2013. Guanine nucleotide exchange factors (GEFs) have a critical but not exclusive role in organelle localization of Rab GTPases. *The Journal of biological chemistry* 288: 28704-28712
- Cai H, Reinisch K, Ferro-Novick S. 2007a. Coats, tethers, Rabs, and SNAREs work together to mediate the intracellular destination of a transport vesicle. *Developmental Cell* 12: 671-682
- Cai H, Yu S, Menon S, Cai Y, Lazarova D, Fu C, Reinisch K, Hay JC, Ferro-Novick S. 2007b. TRAPPI tethers COPII vesicles by binding the coat subunit Sec23. *Nature* 445: 941-944
- Calero M, Chen CZ, Zhu W, Winand N, Havas KA, Gilbert PM, Burd CG, Collins RN. 2003. Dual prenylation is required for Rab protein localization and function. *Molecular Biology of the Cell* 14: 1852-1867
- Campa CC, Hirsch E. 2017. Rab11 and phosphoinositides: A synergy of signal transducers in the control of vesicular trafficking. *Advances in biological regulation* 63: 132-139
- Campelo F, McMahon HT, Kozlov MM. 2008. The hydrophobic insertion mechanism of membrane curvature generation by proteins. *Biophysical Journal* 95: 2325-2339
- Capraro BR, Yoon Y, Cho W, Baumgart T. 2010. Curvature sensing by the epsin N-terminal homology domain measured on cylindrical lipid membrane tethers. *Journal of the American Chemical Society* 132: 1200-1201
- Carney DS, Davies BA, Horazdovsky BF. 2006. Vps9 domain-containing proteins: activators of Rab5 GTPases from yeast to neurons. *Trends in Cell Biology* 16: 27-35
- Carroll KS, Hanna J, Simon I, Krise J, Barbero P, Pfeffer SR. 2001. Role of Rab9 GTPase in facilitating receptor recruitment by TIP47. *Science (New York, NY)* 292: 1373-1376
- Carvalho K, Lemiere J, Faqir F, Manzi J, Blanchoin L, Plastino J, Betz T, Sykes C. 2013. Actin polymerization or myosin contraction: two ways to build up cortical tension for symmetry breaking. *Philosophical transactions of the Royal Society of London Series B, Biological sciences* 368: 20130005
- Casey PJ, Seabra MC. 1996. Protein prenyltransferases. *The Journal of biological chemistry* 271: 5289-5292

- Cauvin C, Rosendale M, Gupta-Rossi N, Rocancourt M, Larraufie P, Salomon R, Perrais D, Echard A. 2016. Rab35 GTPase Triggers Switch-like Recruitment of the Lowe Syndrome Lipid Phosphatase OCRL on Newborn Endosomes. *Current biology : CB* 26: 120-128
- Ceccato L, Chicanne G, Nahoum V, Pons V, Payraastre B, Gaits-Iacovoni F, Viaud J. 2016. PLIF: A rapid, accurate method to detect and quantitatively assess protein-lipid interactions. *Science signaling* 9: rs2
- Cevc G. 1991. How membrane chain-melting phase-transition temperature is affected by the lipid chain asymmetry and degree of unsaturation: an effective chain-length model. *Biochemistry* 30: 7186-7193
- Chavrier P, Gorvel JP, Stelzer E, Simons K, Gruenberg J, Zerial M. 1991. Hypervariable C-terminal domain of rab proteins acts as a targeting signal. *Nature* 353: 769-772
- Chavrier P, Parton RG, Hauri HP, Simons K, Zerial M. 1990. Localization of low molecular weight GTP binding proteins to exocytic and endocytic compartments. *Cell* 62: 317-329
- Chen PI, Schauer K, Kong C, Harding AR, Goud B, Stahl PD. 2014. Rab5 isoforms orchestrate a "division of labor" in the endocytic network; Rab5C modulates Rac-mediated cell motility. *PLoS one* 9: e90384
- Chen SH, Chen S, Tokarev AA, Liu F, Jedd G, Segev N. 2005. Ypt31/32 GTPases and their novel F-box effector protein Rcy1 regulate protein recycling. *Molecular Biology of the Cell* 16: 178-192
- Cheney PP, Weisgerber AW, Feuerbach AM, Knowles MK. 2017. Single Lipid Molecule Dynamics on Supported Lipid Bilayers with Membrane Curvature. *Membranes* 7
- Cherfils J, Zeghouf M. 2013. Regulation of small GTPases by GEFs, GAPs, and GDIs. *Physiological Reviews* 93: 269-309
- Cheung PY, Limouse C, Mabuchi H, Pfeffer SR. 2015. Protein flexibility is required for vesicle tethering at the Golgi. *eLife* 4
- Christoforidis S, Miaczynska M, Ashman K, Wilm M, Zhao L, Yip SC, Waterfield MD, Backer JM, Zerial M. 1999. Phosphatidylinositol-3-OH kinases are Rab5 effectors. *Nature Cell Biology* 1: 249-252
- Cormont M, Bortoluzzi MN, Gautier N, Mari M, van Obberghen E, Le Marchand-Brustel Y. 1996. Potential role of Rab4 in the regulation of subcellular localization of Glut4 in adipocytes. *Molecular and Cellular Biology* 16: 6879-6886
- Cui H, Lyman E, Voth GA. 2011. Mechanism of membrane curvature sensing by amphipathic helix containing proteins. *Biophysical Journal* 100: 1271-1279
- Cuif MH, Possmayer F, Zander H, Bordes N, Jollivet F, Couedel-Courteille A, Janoueix-Lerosey I, Langsley G, Bornens M, Goud B. 1999. Characterization of GAPCenA, a GTPase activating protein for Rab6, part of which associates with the centrosome. *The EMBO journal* 18: 1772-1782
- Cuvelier D, Derenyi I, Bassereau P, Nassoy P. 2005. Coalescence of membrane tethers: experiments, theory, and applications. *Biophysical Journal* 88: 2714-2726

References

- Dambournet D, Machicoane M, Chesneau L, Sachse M, Rocancourt M, El Marjou A, Formstecher E, Salomon R, Goud B, Echard A. 2011. Rab35 GTPase and OCRL phosphatase remodel lipids and F-actin for successful cytokinesis. *Nature Cell Biology* 13: 981-988
- Dar S, Kamerkar SC, Pucadyil TJ. 2017. Use of the supported membrane tube assay system for real-time analysis of membrane fission reactions. *Nature protocols* 12: 390-400
- de Renzis S, Sonnichsen B, Zerial M. 2002. Divalent Rab effectors regulate the sub-compartmental organization and sorting of early endosomes. *Nature Cell Biology* 4: 124-133
- Del Nery E, Miserey-Lenkei S, Falguieres T, Nizak C, Johannes L, Perez F, Goud B. 2006. Rab6A and Rab6A' GTPases play non-overlapping roles in membrane trafficking. *Traffic (Copenhagen, Denmark)* 7: 394-407
- Demchenko AP, Mely Y, Duportail G, Klymchenko AS. 2009. Monitoring biophysical properties of lipid membranes by environment-sensitive fluorescent probes. *Biophysical Journal* 96: 3461-3470
- Deneka M, van der Sluijs P. 2002. 'Rab'ing up endosomal membrane transport. In *Nature cell biology* Vol. 4, pp E33-35. England
- Derenyi I, Julicher F, Prost J. 2002. Formation and interaction of membrane tubes. *Physical review letters* 88: 238101
- Derre I, Isberg RR. 2005. LidA, a translocated substrate of the Legionella pneumophila type IV secretion system, interferes with the early secretory pathway. *Infection and Immunity* 73: 4370-4380
- Desnoyers L, Anant JS, Seabra MC. 1996. Geranylgeranylation of Rab proteins. *Biochemical Society Transactions* 24: 699-703
- Devaux PF. 1991. Static and dynamic lipid asymmetry in cell membranes. *Biochemistry* 30: 1163-1173
- Devaux PF, Herrmann A, Ohlwein N, Kozlov MM. 2008. How lipid flippases can modulate membrane structure. *Biochimica et biophysica acta* 1778: 1591-1600
- Di Paolo G, De Camilli P. 2006. Phosphoinositides in cell regulation and membrane dynamics. *Nature* 443: 651-657
- Dimova R, Aranda S, Bezlyepkina N, Nikolov V, Riske KA, Lipowsky R. 2006. A practical guide to giant vesicles. Probing the membrane nanoregime via optical microscopy. *Journal of physics Condensed matter : an Institute of Physics journal* 18: S1151-S1176
- Dirac-Svejstrup AB, Sumizawa T, Pfeffer SR. 1997. Identification of a GDI displacement factor that releases endosomal Rab GTPases from Rab-GDI. *The EMBO journal* 16: 465-472
- Donaldson JG, Jackson CL. 2011. ARF family G proteins and their regulators: roles in membrane transport, development and disease. *Nature reviews Molecular cell biology* 12: 362-375
- Drin G, Antonny B. 2010. Amphipathic helices and membrane curvature. *FEBS Letters* 584: 1840-1847

- Drin G, Casella JF, Gautier R, Boehmer T, Schwartz TU, Antony B. 2007. A general amphipathic alpha-helical motif for sensing membrane curvature. *Nature Structural & Molecular Biology* 14: 138-146
- Drin G, Morello V, Casella JF, Gounon P, Antony B. 2008. Asymmetric tethering of flat and curved lipid membranes by a golgin. *Science (New York, NY)* 320: 670-673
- Du H, Chandaroy P, Hui SW. 1997. Grafted poly-(ethylene glycol) on lipid surfaces inhibits protein adsorption and cell adhesion. *Biochimica et biophysica acta* 1326: 236-248
- Dubuke ML, Munson M. 2016. The Secret Life of Tethers: The Role of Tethering Factors in SNARE Complex Regulation. *Frontiers in cell and developmental biology* 4: 42
- Dumas JJ, Zhu Z, Connolly JL, Lambright DG. 1999. Structural basis of activation and GTP hydrolysis in Rab proteins. *Structure (London, England : 1993)* 7: 413-423
- Dursina B, Reents R, Delon C, Wu Y, Kulharia M, Thutewohl M, Veligodsky A, Kalinin A, Evstifeev V, Ciobanu D, Szedlacsek SE, Waldmann H, Goody RS, Alexandrov K. 2006. Identification and specificity profiling of protein prenyltransferase inhibitors using new fluorescent phosphoisoprenoids. *Journal of the American Chemical Society* 128: 2822-2835
- Duve C. 1975. Exploring cells with a centrifuge. *Science (New York, NY)* 189: 186-194
- Eberth A, Ahmadian MR. 2009. In vitro GEF and GAP assays. *Current protocols in cell biology* Chapter 14: Unit 14 19
- Echard A, Jollivet F, Martinez O, Lacapere JJ, Rousselet A, Janoueix-Lerosey I, Goud B. 1998. Interaction of a Golgi-associated kinesin-like protein with Rab6. *Science (New York, NY)* 279: 580-585
- Echard A, Opdam FJ, de Leeuw HJ, Jollivet F, Savelkoul P, Hendriks W, Voorberg J, Goud B, Franssen JA. 2000. Alternative splicing of the human Rab6A gene generates two close but functionally different isoforms. *Molecular Biology of the Cell* 11: 3819-3833
- El-Amraoui A, Schonn JS, Kussel-Andermann P, Blanchard S, Desnos C, Henry JP, Wolfrum U, Darchen F, Petit C. 2002. MyRIP, a novel Rab effector, enables myosin VIIa recruitment to retinal melanosomes. *EMBO reports* 3: 463-470
- Engelman DM. 2005. Membranes are more mosaic than fluid. *Nature* 438: 578-580
- Erickson HP. 2009. Size and shape of protein molecules at the nanometer level determined by sedimentation, gel filtration, and electron microscopy. *Biological Procedures Online* 11: 32-51
- Evans E, Rawicz W. 1990. Entropy-driven tension and bending elasticity in condensed-fluid membranes. *Physical review letters* 64: 2094-2097
- Evans TM, Ferguson C, Wainwright BJ, Parton RG, Wicking C. 2003. Rab23, a negative regulator of hedgehog signaling, localizes to the plasma membrane and the endocytic pathway. *Traffic* 4: 869-884
- Faini M, Beck R, Wieland FT, Briggs JA. 2013. Vesicle coats: structure, function, and general principles of assembly. *Trends in Cell Biology* 23: 279-288

References

- Farnsworth CC, Kawata M, Yoshida Y, Takai Y, Gelb MH, Glomset JA. 1991. C terminus of the small GTP-binding protein smg p25A contains two geranylgeranylated cysteine residues and a methyl ester. *Proceedings of the National Academy of Sciences of the United States of America* 88: 6196-6200
- Feigenson GW. 2006. Phase behavior of lipid mixtures. *Nature Chemical Biology* 2: 560-563
- Ferguson SM, De Camilli P. 2012. Dynamin, a membrane-remodelling GTPase. *Nature reviews Molecular cell biology* 13: 75-88
- Fields IC, King SM, Shteyn E, Kang RS, Folsch H. 2010. Phosphatidylinositol 3,4,5-trisphosphate localization in recycling endosomes is necessary for AP-1B-dependent sorting in polarized epithelial cells. *Molecular Biology of the Cell* 21: 95-105
- Ford MG, Mills IG, Peter BJ, Vallis Y, Praefcke GJ, Evans PR, McMahon HT. 2002. Curvature of clathrin-coated pits driven by epsin. *Nature* 419: 361-366
- Frolov VA, Shnyrova AV, Zimmerberg J. 2011. Lipid polymorphisms and membrane shape. *Cold Spring Harbor Perspectives in Biology* 3: a004747
- Frost A, Unger VM, De Camilli P. 2009. The BAR domain superfamily: membrane-molding macromolecules. *Cell* 137: 191-196
- Fuchs E, Haas AK, Spooner RA, Yoshimura S, Lord JM, Barr FA. 2007. Specific Rab GTPase-activating proteins define the Shiga toxin and epidermal growth factor uptake pathways. *The Journal of cell biology* 177: 1133-1143
- Fukuda M. 2011. TBC proteins: GAPs for mammalian small GTPase Rab? *Bioscience reports* 31: 159-168
- Fukuda M, Kanno E, Ishibashi K, Itoh T. 2008. Large scale screening for novel rab effectors reveals unexpected broad Rab binding specificity. *Molecular & cellular proteomics : MCP* 7: 1031-1042
- Futerman AH, Riezman H. 2005. The ins and outs of sphingolipid synthesis. *Trends in Cell Biology* 15: 312-318
- Galea G, Bexiga MG, Panarella A, O'Neill ED, Simpson JC. 2015. A high-content screening microscopy approach to dissect the role of Rab proteins in Golgi-to-ER retrograde trafficking. *Journal of Cell Science* 128: 2339-2349
- Gallala HD, Sandhoff K. 2011. Biological function of the cellular lipid BMP-BMP as a key activator for cholesterol sorting and membrane digestion. *Neurochemical Research* 36: 1594-1600
- Gallop JL, Jao CC, Kent HM, Butler PJ, Evans PR, Langen R, McMahon HT. 2006. Mechanism of endophilin N-BAR domain-mediated membrane curvature. *The EMBO journal* 25: 2898-2910
- Gallwitz D, Donath C, Sander C. 1983. A yeast gene encoding a protein homologous to the human c-has/bas proto-oncogene product. *Nature* 306: 704-707
- Gilman AG. 1987. G proteins: transducers of receptor-generated signals. *Annual Review of Biochemistry* 56: 615-649

- Gohlke A, Triola G, Waldmann H, Winter R. 2010. Influence of the lipid anchor motif of N-ras on the interaction with lipid membranes: a surface plasmon resonance study. *Biophysical Journal* 98: 2226-2235
- Goksu EI, Vanegas JM, Blanchette CD, Lin WC, Longo ML. 2009. AFM for structure and dynamics of biomembranes. *Biochimica et biophysica acta* 1788: 254-266
- Goldenring JR, Shen KR, Vaughan HD, Modlin IM. 1993. Identification of a small GTP-binding protein, Rab25, expressed in the gastrointestinal mucosa, kidney, and lung. *The Journal of biological chemistry* 268: 18419-18422
- Gomes AQ, Ali BR, Ramalho JS, Godfrey RF, Barral DC, Hume AN, Seabra MC. 2003. Membrane targeting of Rab GTPases is influenced by the prenylation motif. *Molecular Biology of the Cell* 14: 1882-1899
- Gomez GA, Daniotti JL. 2007. Electrical properties of plasma membrane modulate subcellular distribution of K-Ras. *FEBS Journal* 274: 2210-2228
- Goni FM, Alonso A, Bagatolli LA, Brown RE, Marsh D, Prieto M, Thewalt JL. 2008. Phase diagrams of lipid mixtures relevant to the study of membrane rafts. *Biochimica et biophysica acta* 1781: 665-684
- Goody RS, Hofmann-Goody W. 2002. Exchange factors, effectors, GAPs and motor proteins: common thermodynamic and kinetic principles for different functions. *European biophysics journal : EBJ* 31: 268-274
- Goud B, Zahraoui A, Tavitian A, Saraste J. 1990. Small GTP-binding protein associated with Golgi cisternae. *Nature* 345: 553-556
- Graham TR, Kozlov MM. 2010. Interplay of proteins and lipids in generating membrane curvature. *Current Opinion in Cell Biology* 22: 430-436
- Grigoriev I, Splinter D, Keijzer N, Wulf PS, Demmers J, Ohtsuka T, Modesti M, Maly IV, Grosveld F, Hoogenraad CC, Akhmanova A. 2007. Rab6 regulates transport and targeting of exocytotic carriers. *Developmental Cell* 13: 305-314
- Guet D. 2012. Architecture of the Golgi apparatus and membrane trafficking probed by intracellular optical micromanipulation. PhD Thesis, Université Paris 6 - Pierre et Marie Curie,
- Gulyas G, Radvanszki G, Matuska R, Balla A, Hunyady L, Balla T, Varnai P. 2017. Plasma membrane phosphatidylinositol 4-phosphate and 4,5-bisphosphate determine the distribution and function of K-Ras4B but not H-Ras proteins. *The Journal of biological chemistry*
- Guo Z, Wu YW, Das D, Delon C, Cramer J, Yu S, Thuns S, Lupilova N, Waldmann H, Brunsveld L, Goody RS, Alexandrov K, Blankenfeldt W. 2008. Structures of RabGGTase-substrate/product complexes provide insights into the evolution of protein prenylation. *The EMBO journal* 27: 2444-2456
- Gurel PS, Hatch AL, Higgs HN. 2014. Connecting the cytoskeleton to the endoplasmic reticulum and Golgi. *Current biology : CB* 24: R660-672
- Gurkan C, Lapp H, Alory C, Su AI, Hogenesch JB, Balch WE. 2005. Large-scale profiling of Rab GTPase trafficking networks: the membrane. *Molecular Biology of the Cell* 16: 3847-3864

References

- Hales CM, Vaerman JP, Goldenring JR. 2002. Rab11 family interacting protein 2 associates with Myosin Vb and regulates plasma membrane recycling. *The Journal of biological chemistry* 277: 50415-50421
- Hammer JA, 3rd, Wu XS. 2002. Rabs grab motors: defining the connections between Rab GTPases and motor proteins. *Current Opinion in Cell Biology* 14: 69-75
- Hammond AT, Heberle FA, Baumgart T, Holowka D, Baird B, Feigenson GW. 2005. Crosslinking a lipid raft component triggers liquid ordered-liquid disordered phase separation in model plasma membranes. *Proceedings of the National Academy of Sciences of the United States of America* 102: 6320-6325
- Hanson PI, Roth R, Morisaki H, Jahn R, Heuser JE. 1997. Structure and conformational changes in NSF and its membrane receptor complexes visualized by quick-freeze/deep-etch electron microscopy. *Cell* 90: 523-535
- Hatzakis NS, Bhatia VK, Larsen J, Madsen KL, Bolinger PY, Kunding AH, Castillo J, Gether U, Hedegard P, Stamou D. 2009. How curved membranes recruit amphipathic helices and protein anchoring motifs. *Nature Chemical Biology* 5: 835-841
- Haubruck H, Prange R, Vorgias C, Gallwitz D. 1989. The ras-related mouse ypt1 protein can functionally replace the YPT1 gene product in yeast. *The EMBO journal* 8: 1427-1432
- Haucke V. 2005. Phosphoinositide regulation of clathrin-mediated endocytosis. *Biochemical Society Transactions* 33: 1285-1289
- Hayes GL, Brown FC, Haas AK, Nottingham RM, Barr FA, Pfeffer SR. 2009. Multiple Rab GTPase binding sites in GCC185 suggest a model for vesicle tethering at the trans-Golgi. *Molecular Biology of the Cell* 20: 209-217
- Heerklotz H. 2002. Triton promotes domain formation in lipid raft mixtures. *Biophysical Journal* 83: 2693-2701
- Heidtmann M, Chen CZ, Collins RN, Barlowe C. 2003. A role for Yiplp in COPII vesicle biogenesis. *The Journal of cell biology* 163: 57-69
- Heinrich V, Waugh RE. 1996. A piconewton force transducer and its application to measurement of the bending stiffness of phospholipid membranes. *Annals of Biomedical Engineering* 24: 595-605
- Henriksen J, Rowat AC, Brief E, Hsueh YW, Thewalt JL, Zuckermann MJ, Ipsen JH. 2006. Universal behavior of membranes with sterols. *Biophysical Journal* 90: 1639-1649
- Henriksen JR, Ipsen JH. 2004. Measurement of membrane elasticity by micro-pipette aspiration. *The European physical journal E, Soft matter* 14: 149-167
- Heo WD, Inoue T, Park WS, Kim ML, Park BO, Wandless TJ, Meyer T. 2006. PI(3,4,5)P3 and PI(4,5)P2 lipids target proteins with polybasic clusters to the plasma membrane. *Science (New York, NY)* 314: 1458-1461
- Hill E, Clarke M, Barr FA. 2000. The Rab6-binding kinesin, Rab6-KIFL, is required for cytokinesis. *The EMBO journal* 19: 5711-5719

- Hochmuth RM, Mohandas N, Blackshear PL, Jr. 1973. Measurement of the elastic modulus for red cell membrane using a fluid mechanical technique. *Biophysical Journal* 13: 747-762
- Hochmuth RM, Wiles HC, Evans EA, McCown JT. 1982. Extensional flow of erythrocyte membrane from cell body to elastic tether. II. Experiment. *Biophysical Journal* 39: 83-89
- Hoepfner S, Severin F, Cabezas A, Habermann B, Runge A, Gillooly D, Stenmark H, Zerial M. 2005. Modulation of receptor recycling and degradation by the endosomal kinesin KIF16B. *Cell* 121: 437-450
- Holopainen JM, Angelova MI, Soderlund T, Kinnunen PK. 2002. Macroscopic consequences of the action of phospholipase C on giant unilamellar liposomes. *Biophysical Journal* 83: 932-943
- Hoogenraad CC, Popa I, Futai K, Martinez-Sanchez E, Wulf PS, van Vlijmen T, Dortland BR, Oorschot V, Govers R, Monti M, Heck AJ, Sheng M, Klumperman J, Rehmann H, Jaarsma D, Kapitein LC, van der Sluijs P. 2010. Neuron specific Rab4 effector GRASP-1 coordinates membrane specialization and maturation of recycling endosomes. *PLoS Biology* 8: e1000283
- Horgan CP, Hanscom SR, Jolly RS, Futter CE, McCaffrey MW. 2010. Rab11-FIP3 links the Rab11 GTPase and cytoplasmic dynein to mediate transport to the endosomal-recycling compartment. *Journal of Cell Science* 123: 181-191
- Horgan CP, McCaffrey MW. 2011. Rab GTPases and microtubule motors. *Biochemical Society Transactions* 39: 1202-1206
- Horger KS, Estes DJ, Capone R, Mayer M. 2009. Films of agarose enable rapid formation of giant liposomes in solutions of physiologic ionic strength. *Journal of the American Chemical Society* 131: 1810-1819
- Horiuchi H, Lippe R, McBride HM, Rubino M, Woodman P, Stenmark H, Rybin V, Wilm M, Ashman K, Mann M, Zerial M. 1997. A novel Rab5 GDP/GTP exchange factor complexed to Rabaptin-5 links nucleotide exchange to effector recruitment and function. *Cell* 90: 1149-1159
- Hou X, Hagemann N, Schoebel S, Blankenfeldt W, Goody RS, Erdmann KS, Itzen A. 2011. A structural basis for Lowe syndrome caused by mutations in the Rab-binding domain of OCRL1. *The EMBO journal* 30: 1659-1670
- Houghton FJ, Chew PL, Lodeho S, Goud B, Gleeson PA. 2009. The localization of the Golgin GCC185 is independent of Rab6A/A' and Arl1. *Cell* 138: 787-794
- Hsieh WT, Hsu CJ, Capraro BR, Wu T, Chen CM, Yang S, Baumgart T. 2012. Curvature sorting of peripheral proteins on solid-supported wavy membranes. *Langmuir : the ACS journal of surfaces and colloids* 28: 12838-12843
- Hsu C, Morohashi Y, Yoshimura S, Manrique-Hoyos N, Jung S, Lauterbach MA, Bakhti M, Gronborg M, Mobius W, Rhee J, Barr FA, Simons M. 2010. Regulation of exosome secretion by Rab35 and its GTPase-activating proteins TBC1D10A-C. *The Journal of cell biology* 189: 223-232
- Huang J, Birmingham CL, Shahnazari S, Shiu J, Zheng YT, Smith AC, Campellone KG, Heo WD, Gruenheid S, Meyer T, Welch MD, Ktistakis NT, Kim PK, Klionsky DJ, Brumell JH. 2011. Antibacterial autophagy occurs at PI(3)P-enriched domains of the endoplasmic reticulum and requires Rab1 GTPase. *Autophagy* 7: 17-26

References

- Hurley JH, Boura E, Carlson LA, Rozycki B. 2010. Membrane budding. *Cell* 143: 875-887
- Hutagalung AH, Novick PJ. 2011. Role of Rab GTPases in membrane traffic and cell physiology. *Physiological Reviews* 91: 119-149
- Hutt DM, Da-Silva LF, Chang LH, Prosser DC, Ngsee JK. 2000. PRA1 inhibits the extraction of membrane-bound rab GTPase by GDII. *Journal of Biological Chemistry* 275: 18511-18519
- Hyvola N, Diao A, McKenzie E, Skippen A, Cockcroft S, Lowe M. 2006. Membrane targeting and activation of the Lowe syndrome protein OCRL1 by rab GTPases. *The EMBO journal* 25: 3750-3761
- Ikonen E. 2008. Cellular cholesterol trafficking and compartmentalization. *Nature reviews Molecular cell biology* 9: 125-138
- Inaba T, Kishimoto T, Murate M, Tajima T, Sakai S, Abe M, Makino A, Tomishige N, Ishitsuka R, Ikeda Y, Takeoka S, Kobayashi T. 2016. Phospholipase C β 1 induces membrane tubulation and is involved in caveolae formation. *Proceedings of the National Academy of Sciences of the United States of America* 113: 7834-7839
- Ipsen JH, Karlstrom G, Mouritsen OG, Wennerstrom H, Zuckermann MJ. 1987. Phase equilibria in the phosphatidylcholine-cholesterol system. *Biochimica et biophysica acta* 905: 162-172
- Israelachvili JN. 1992. Intermolecular and surface forces. *Academic Press, London*
- Itoh T, De Camilli P. 2006. BAR, F-BAR (EFC) and ENTH/ANTH domains in the regulation of membrane-cytosol interfaces and membrane curvature. *Biochimica et biophysica acta* 1761: 897-912
- Jackson CL, Bouvet S. 2014. Arfs at a glance. *Journal of Cell Science* 127: 4103-4109
- Jackson CL, Walch L, Verbavatz JM. 2016. Lipids and Their Trafficking: An Integral Part of Cellular Organization. *Developmental Cell* 39: 139-153
- Jacobson K, Mouritsen OG, Anderson RG. 2007. Lipid rafts: at a crossroad between cell biology and physics. *Nature Cell Biology* 9: 7-14
- Jahn R, Scheller RH. 2006. SNAREs--engines for membrane fusion. *Nature reviews Molecular cell biology* 7: 631-643
- Jang H, Abraham SJ, Chavan TS, Hitchinson B, Khavrutskii L, Tarasova NI, Nussinov R, Gaponenko V. 2015. Mechanisms of membrane binding of small GTPase K-Ras4B farnesylated hypervariable region. *Journal of Biological Chemistry* 290: 9465-9477
- Jao CC, Hegde BG, Chen J, Haworth IS, Langen R. 2008. Structure of membrane-bound alpha-synuclein from site-directed spin labeling and computational refinement. *Proceedings of the National Academy of Sciences of the United States of America* 105: 19666-19671
- Jean S, Kiger AA. 2012. Coordination between RAB GTPase and phosphoinositide regulation and functions. *Nature reviews Molecular cell biology* 13: 463-470
- Jena BP. 2008. Assembly and disassembly of SNAREs in membrane fusion. *Methods in cell biology* 90: 157-182

- Jensen MB, Bhatia VK, Jao CC, Rasmussen JE, Pedersen SL, Jensen KJ, Langen R, Stamou D. 2011. Membrane curvature sensing by amphipathic helices: a single liposome study using alpha-synuclein and annexin B12. *The Journal of biological chemistry* 286: 42603-42614
- Joberty G, Tavitian A, Zahraoui A. 1993. Isoprenylation of Rab proteins possessing a C-terminal CaaX motif. *FEBS Letters* 330: 323-328
- Johannes L, Popoff V. 2008. Tracing the retrograde route in protein trafficking. *Cell* 135: 1175-1187
- Jones S, Newman C, Liu F, Segev N. 2000. The TRAPP complex is a nucleotide exchanger for Ypt1 and Ypt31/32. *Molecular Biology of the Cell* 11: 4403-4411
- Jordens I, Fernandez-Borja M, Marsman M, Dusseljee S, Janssen L, Calafat J, Janssen H, Wubbolts R, Neefjes J. 2001. The Rab7 effector protein RILP controls lysosomal transport by inducing the recruitment of dynein-dynactin motors. *Current biology : CB* 11: 1680-1685
- Kalin S, Hirschmann DT, Buser DP, Spiess M. 2015. Rabaptin5 is recruited to endosomes by Rab4 and Rabex5 to regulate endosome maturation. *Journal of Cell Science* 128: 4126-4137
- Kamena F, Diefenbacher M, Kilchert C, Schwarz H, Spang A. 2008. Ypt1p is essential for retrograde Golgi-ER transport and for Golgi maintenance in *S. cerevisiae*. *Journal of Cell Science* 121: 1293-1302
- Karnoub AE, Weinberg RA. 2008. Ras oncogenes: split personalities. *Nature reviews Molecular cell biology* 9: 517-531
- Khosravi-Far R, Clark GJ, Abe K, Cox AD, McLain T, Lutz RJ, Sinensky M, Der CJ. 1992. Ras (CXXX) and Rab (CC/CXC) prenylation signal sequences are unique and functionally distinct. *The Journal of biological chemistry* 267: 24363-24368
- Kim HM, Jeong BH, Hyon JY, An MJ, Seo MS, Hong JH, Lee KJ, Kim CH, Joo T, Hong SC, Cho BR. 2008. Two-photon fluorescent turn-on probe for lipid rafts in live cell and tissue. *Journal of the American Chemical Society* 130: 4246-4247
- Klemm RW, Ejsing CS, Surma MA, Kaiser HJ, Gerl MJ, Sampaio JL, de Robillard Q, Ferguson C, Proszynski TJ, Shevchenko A, Simons K. 2009. Segregation of sphingolipids and sterols during formation of secretory vesicles at the trans-Golgi network. *The Journal of cell biology* 185: 601-612
- Klinkert K, Echard A. 2016. Rab35 GTPase: A Central Regulator of Phosphoinositides and F-actin in Endocytic Recycling and Beyond. *Traffic (Copenhagen, Denmark)* 17: 1063-1077
- Klymchenko AS, Kreder R. 2014. Fluorescent probes for lipid rafts: from model membranes to living cells. *Chemistry & Biology* 21: 97-113
- Kobayashi T, Beuchat MH, Chevallier J, Makino A, Mayran N, Escola JM, Lebrand C, Cosson P, Gruenberg J. 2002. Separation and characterization of late endosomal membrane domains. *The Journal of biological chemistry* 277: 32157-32164
- Koster G, VanDuijn M, Hofs B, Dogterom M. 2003. Membrane tube formation from giant vesicles by dynamic association of motor proteins. *Proceedings of the National Academy of Sciences of the United States of America* 100: 15583-15588

References

- Kouranti I, Sachse M, Arouche N, Goud B, Echard A. 2006. Rab35 regulates an endocytic recycling pathway essential for the terminal steps of cytokinesis. *Current Biology* 16: 1719-1725
- Kozlov MM, Campelo F, Liska N, Chernomordik LV, Marrink SJ, McMahon HT. 2014. Mechanisms shaping cell membranes. *Current Opinion in Cell Biology* 29: 53-60
- Krauss M, Jia JY, Roux A, Beck R, Wieland FT, De Camilli P, Haucke V. 2008. Arf1-GTP-induced tubule formation suggests a function of Arf family proteins in curvature acquisition at sites of vesicle budding. *The Journal of biological chemistry* 283: 27717-27723
- Krawczyk M, Leimgruber E, Seguin-Estevez Q, Dunand-Sauthier I, Barras E, Reith W. 2007. Expression of RAB4B, a protein governing endocytic recycling, is co-regulated with MHC class II genes. *Nucleic Acids Research* 35: 595-605
- Kwok R, Evans E. 1981. Thermoelasticity of large lecithin bilayer vesicles. *Biophysical Journal* 35: 637-652
- Lai F, Stubbs L, Artzt K. 1994. Molecular analysis of mouse Rab11b: a new type of mammalian YPT/Rab protein. *Genomics* 22: 610-616
- Lai YC, Kondapalli C, Lehneck R, Procter JB, Dill BD, Woodroof HI, Gourlay R, Peggie M, Macartney TJ, Corti O, Corvol JC, Campbell DG, Itzen A, Trost M, Muqit MM. 2015. Phosphoproteomic screening identifies Rab GTPases as novel downstream targets of PINK1. *The EMBO journal* 34: 2840-2861
- Larsen JB, Jensen MB, Bhatia VK, Pedersen SL, Bjornholm T, Iversen L, Uline M, Szleifer I, Jensen KJ, Hatzakis NS, Stamou D. 2015. Membrane curvature enables N-Ras lipid anchor sorting to liquid-ordered membrane phases. *Nature Chemical Biology* 11: 192-194
- Larsen JB, Kennard C, Pedersen SL, Jensen KJ, Uline MJ, Hatzakis NS, Stamou D. 2017. Membrane Curvature and Lipid Composition Synergize To Regulate N-Ras Anchor Recruitment. *Biophysical Journal*
- Lazar T, Gotte M, Gallwitz D. 1997. Vesicular transport: how many Ypt/Rab-GTPases make a eukaryotic cell? *Trends in Biochemical Sciences* 22: 468-472
- Lazzarino DA, Blier P, Mellman I. 1998. The monomeric guanosine triphosphatase rab4 controls an essential step on the pathway of receptor-mediated antigen processing in B cells. *The Journal of experimental medicine* 188: 1769-1774
- Leduc C, Campas O, Zeldovich KB, Roux A, Jolimaitre P, Bourel-Bonnet L, Goud B, Joanny JF, Bassereau P, Prost J. 2004. Cooperative extraction of membrane nanotubes by molecular motors. *Proceedings of the National Academy of Sciences of the United States of America* 101: 17096-17101
- Lee MC, Orci L, Hamamoto S, Futai E, Ravazzola M, Schekman R. 2005. Sar1p N-terminal helix initiates membrane curvature and completes the fission of a COPII vesicle. *Cell* 122: 605-617
- Lee MT, Mishra A, Lambright DG. 2009. Structural mechanisms for regulation of membrane traffic by rab GTPases. *Traffic (Copenhagen, Denmark)* 10: 1377-1389
- Leung KF, Baron R, Ali BR, Magee AI, Seabra MC. 2007. Rab GTPases containing a CAAX motif are processed post-geranylgeranylation by proteolysis and methylation. *Journal of Biological Chemistry* 282: 1487-1497

- Leung KF, Baron R, Seabra MC. 2006. Thematic review series: lipid posttranslational modifications. geranylgeranylation of Rab GTPases. *Journal of Lipid Research* 47: 467-475
- Levental I, Lingwood D, Grzybek M, Coskun U, Simons K. 2010. Palmitoylation regulates raft affinity for the majority of integral raft proteins. *Proceedings of the National Academy of Sciences, USA* 107: 22050-22054
- Levental KR, Levental I. 2015. Giant plasma membrane vesicles: models for understanding membrane organization. *Current topics in membranes* 75: 25-57
- Levin RS, Hertz NT, Burlingame AL, Shokat KM, Mukherjee S. 2016. Innate immunity kinase TAK1 phosphorylates Rab1 on a hotspot for posttranslational modifications by host and pathogen. *Proceedings of the National Academy of Sciences of the United States of America* 113: E4776-4783
- Li F, Yi L, Zhao L, Itzen A, Goody RS, Wu YW. 2014. The role of the hypervariable C-terminal domain in Rab GTPases membrane targeting. *Proceedings of the National Academy of Sciences, USA* 111: 2572-2577
- Lichtenberg D, Goni FM, Heerklotz H. 2005. Detergent-resistant membranes should not be identified with membrane rafts. *Trends in Biochemical Sciences* 30: 430-436
- Liewen H, Meinhold-Heerlein I, Oliveira V, Schwarzenbacher R, Luo G, Wadle A, Jung M, Pfreundschuh M, Stenner-Liewen F. 2005. Characterization of the human GARP (Golgi associated retrograde protein) complex. *Experimental Cell Research* 306: 24-34
- Lifshitz I, Slyozov V. 1961. The kinetics of precipitation from supersaturated solid solution. *Journal of physics and chemistry of solids* 19: 35-50
- Limozin L, Barmann M, Sackmann E. 2003. On the organization of self-assembled actin networks in giant vesicles. *The European physical journal E, Soft matter* 10: 319-330
- Lindsay AJ, Jollivet F, Horgan CP, Khan AR, Raposo G, McCaffrey MW, Goud B. 2013. Identification and characterization of multiple novel Rab-myosin Va interactions. *Molecular Biology of the Cell* 24: 3420-3434
- Lingwood D, Simons K. 2010. Lipid rafts as a membrane-organizing principle. *Science (New York, NY)* 327: 46-50
- Lippe R, Miaczynska M, Rybin V, Runge A, Zerial M. 2001. Functional synergy between Rab5 effector Rabaptin-5 and exchange factor Rabex-5 when physically associated in a complex. *Molecular Biology of the Cell* 12: 2219-2228
- Liu J, Sun Y, Oster GF, Drubin DG. 2010. Mechanochemical crosstalk during endocytic vesicle formation. *Current Opinion in Cell Biology* 22: 36-43
- Lo SY, Brett CL, Plemel RL, Vignali M, Fields S, Gonen T, Merz AJ. 2011. Intrinsic tethering activity of endosomal Rab proteins. *Nature Structural & Molecular Biology* 19: 40-47
- London E. 2002. Insights into lipid raft structure and formation from experiments in model membranes. *Current Opinion in Structural Biology* 12: 480-486
- Longo GS, Schick M, Szeleifer I. 2009. Stability and liquid-liquid phase separation in mixed saturated lipid bilayers. *Biophysical Journal* 96: 3977-3986

References

- Los DA, Murata N. 2004. Membrane fluidity and its roles in the perception of environmental signals. *Biochimica et biophysica acta* 1666: 142-157
- Lowe M. 2005. Structure and function of the Lowe syndrome protein OCRLI. *Traffic (Copenhagen, Denmark)* 6: 711-719
- Lozano MM, Liu Z, Sunnick E, Janshoff A, Kumar K, Boxer SG. 2013. Colocalization of the ganglioside G(M1) and cholesterol detected by secondary ion mass spectrometry. *Journal of the American Chemical Society* 135: 5620-5630
- Lundmark R, Doherty GJ, Vallis Y, Peter BJ, McMahon HT. 2008. Arf family GTP loading is activated by, and generates, positive membrane curvature. *The Biochemical journal* 414: 189-194
- Lurick A, Gao J, Kuhlee A, Yavavli E, Langemeyer L, Perz A, Raunser S, Ungermann C. 2017. Multivalent Rab interactions determine tether-mediated membrane fusion. *Molecular Biology of the Cell* 28: 322-332
- M'Baye G, Mely Y, Duportail G, Klymchenko AS. 2008. Liquid ordered and gel phases of lipid bilayers: fluorescent probes reveal close fluidity but different hydration. *Biophysical Journal* 95: 1217-1225
- Machner MP, Isberg RR. 2006. Targeting of host Rab GTPase function by the intravacuolar pathogen *Legionella pneumophila*. *Developmental Cell* 11: 47-56
- Madigan JP, Bodemann BO, Brady DC, Dewar BJ, Keller PJ, Leitges M, Philips MR, Ridley AJ, Der CJ, Cox AD. 2009. Regulation of Rnd3 localization and function by protein kinase C alpha-mediated phosphorylation. *Biochemical Journal* 424: 153-161
- Mallard F, Tang BL, Galli T, Tenza D, Saint-Pol A, Yue X, Antony C, Hong W, Goud B, Johannes L. 2002. Early/recycling endosomes-to-TGN transport involves two SNARE complexes and a Rab6 isoform. *The Journal of cell biology* 156: 653-664
- Marat AL, Dokainish H, McPherson PS. 2011. DENN domain proteins: regulators of Rab GTPases. *The Journal of biological chemistry* 286: 13791-13800
- Marie M, Dale HA, Sannerud R, Saraste J. 2009. The function of the intermediate compartment in pre-Golgi trafficking involves its stable connection with the centrosome. *Molecular Biology of the Cell* 20: 4458-4470
- Marquardt D, Heberle FA, Greathouse DV, Koeppe RE, Standaert RF, Van Oosten BJ, Harroun TA, Kinnun JJ, Williams JA, Wassall SR, Katsaras J. 2016. Lipid bilayer thickness determines cholesterol's location in model membranes. *Soft Matter* 12: 9417-9428
- Martinez O, Goud B. 1998. Rab proteins. *Biochimica et biophysica acta* 1404: 101-112
- Masuda M, Mochizuki N. 2010. Structural characteristics of BAR domain superfamily to sculpt the membrane. *Seminars in Cell & Developmental Biology* 21: 391-398
- Masuda M, Takeda S, Sone M, Ohki T, Mori H, Kamioka Y, Mochizuki N. 2006. Endophilin BAR domain drives membrane curvature by two newly identified structure-based mechanisms. *The EMBO journal* 25: 2889-2897

- Matanis T, Akhmanova A, Wulf P, Del Nery E, Weide T, Stepanova T, Galjart N, Grosveld F, Goud B, De Zeeuw CI, Barnekow A, Hoogenraad CC. 2002. Bicaudal-D regulates COPI-independent Golgi-ER transport by recruiting the dynein-dynactin motor complex. *Nature Cell Biology* 4: 986-992
- Matesic LE, Yip R, Reuss AE, Swing DA, O'Sullivan TN, Fletcher CF, Copeland NG, Jenkins NA. 2001. Mutations in Mlph, encoding a member of the Rab effector family, cause the melanosome transport defects observed in leaden mice. *Proceedings of the National Academy of Sciences of the United States of America* 98: 10238-10243
- Matsuo H, Chevallier J, Mayran N, Le Blanc I, Ferguson C, Faure J, Blanc NS, Matile S, Dubochet J, Sadoul R, Parton RG, Vilbois F, Gruenberg J. 2004. Role of LBPA and Alix in multivesicular liposome formation and endosome organization. *Science (New York, NY)* 303: 531-534
- Mattila PK, Lappalainen P. 2008. Filopodia: molecular architecture and cellular functions. *Nature reviews Molecular cell biology* 9: 446-454
- Maxfield FR, McGraw TE. 2004. Endocytic recycling. *Nature reviews Molecular cell biology* 5: 121-132
- McBride HM, Rybin V, Murphy C, Giner A, Teasdale R, Zerial M. 1999. Oligomeric complexes link Rab5 effectors with NSF and drive membrane fusion via interactions between EEA1 and syntaxin 13. *Cell* 98: 377-386
- McCullough J, Clippinger AK, Talledge N, Skowrya ML, Saunders MG, Naismith TV, Colf LA, Afonine P, Arthur C, Sundquist WI, Hanson PI, Frost A. 2015. Structure and membrane remodeling activity of ESCRT-III helical polymers. *Science (New York, NY)* 350: 1548-1551
- McMahon HT, Boucrot E. 2011. Molecular mechanism and physiological functions of clathrin-mediated endocytosis. *Nature Reviews: Molecular Cell Biology* 12: 517-533
- McMahon HT, Boucrot E. 2015. Membrane curvature at a glance. *Journal of Cell Science* 128: 1065-1070
- McMahon HT, Gallop JL. 2005. Membrane curvature and mechanisms of dynamic cell membrane remodelling. *Nature* 438: 590-596
- Medkova M, France YE, Coleman J, Novick P. 2006. The rab exchange factor Sec2p reversibly associates with the exocyst. *Molecular Biology of the Cell* 17: 2757-2769
- Melchior F. 2001. Ran GTPase cycle: oOne mechanism -- two functions. *Current biology : CB* 11: R257-260
- Meleard P, Bagatolli LA, Pott T. 2009. Giant unilamellar vesicle electroformation from lipid mixtures to native membranes under physiological conditions. *Methods in Enzymology* 465: 161-176
- Mesmin B, Bigay J, Moser von Filseck J, Lacas-Gervais S, Drin G, Antonny B. 2013. A four-step cycle driven by PI(4)P hydrolysis directs sterol/PI(4)P exchange by the ER-Golgi tether OSBP. *Cell* 155: 830-843

References

- Mesmin B, Drin G, Levi S, Rawet M, Cassel D, Bigay J, Antonny B. 2007. Two lipid-packing sensor motifs contribute to the sensitivity of ArfGAP1 to membrane curvature. *Biochemistry* 46: 1779-1790
- Mesmin B, Maxfield FR. 2009. Intracellular sterol dynamics. *Biochimica et biophysica acta* 1791: 636-645
- Miaczynska M, Pelkmans L, Zerial M. 2004. Not just a sink: endosomes in control of signal transduction. *Current Opinion in Cell Biology* 16: 400-406
- Michaelson D, Ali W, Chiu VK, Bergo M, Silletti J, Wright L, Young SG, Philips M. 2005. Postprenylation CAAX processing is required for proper localization of Ras but not Rho GTPases. *Molecular Biology of the Cell* 16: 1606-1616
- Mills IG, Urbe S, Clague MJ. 2001. Relationships between EEA1 binding partners and their role in endosome fusion. *Journal of Cell Science* 114: 1959-1965
- Mim C, Unger VM. 2012. Membrane curvature and its generation by BAR proteins. *Trends in Biochemical Sciences* 37: 526-533
- Miserey-Lenkei S, Chalancon G, Bardin S, Formstecher E, Goud B, Echard A. 2010. Rab and actomyosin-dependent fission of transport vesicles at the Golgi complex. *Nature Cell Biology* 12: 645-654
- Miserey-Lenkei S, Couedel-Courteille A, Del Nery E, Bardin S, Piel M, Racine V, Sibarita JB, Perez F, Bornens M, Goud B. 2006. A role for the Rab6A' GTPase in the inactivation of the Mad2-spindle checkpoint. *The EMBO journal* 25: 278-289
- Morrison HA, Dionne H, Rusten TE, Brech A, Fisher WW, Pfeiffer BD, Celniker SE, Stenmark H, Bilder D. 2008. Regulation of early endosomal entry by the Drosophila tumor suppressors Rabenosyn and Vps45. *Molecular Biology of the Cell* 19: 4167-4176
- Mukherjee S, Maxfield FR. 2000. Role of membrane organization and membrane domains in endocytic lipid trafficking. *Traffic (Copenhagen, Denmark)* 1: 203-211
- Muller MP, Goody RS. 2017. Molecular control of Rab activity by GEFs, GAPs and GDI. *Small GTPases*: 1-17
- Muller MP, Peters H, Blumer J, Blankenfeldt W, Goody RS, Itzen A. 2010. The Legionella effector protein DrrA AMPylates the membrane traffic regulator Rab1b. *Science (New York, NY)* 329: 946-949
- Muller MP, Shkumatov AV, Oesterlin LK, Schoebel S, Goody PR, Goody RS, Itzen A. 2012. Characterization of enzymes from Legionella pneumophila involved in reversible adenylylation of Rab1 protein. *Journal of Biological Chemistry* 287: 35036-35046
- Mulligan K, Brownholland D, Carnini A, Thompson DH, Johnston LJ. 2010. AFM investigations of phase separation in supported membranes of binary mixtures of POPC and an eicosanyl-based bisphosphocholine bolalipid. *Langmuir : the ACS journal of surfaces and colloids* 26: 8525-8533
- Murray DH, Jahnel M, Lauer J, Avellaneda MJ, Brouilly N, Cezanne A, Morales-Navarrete H, Perini ED, Ferguson C, Lupas AN, Kalaidzidis Y, Parton RG, Grill SW, Zerial M. 2016. An endosomal tether undergoes an entropic collapse to bring vesicles together. *Nature* 537: 107-111

- Muthusamy BP, Natarajan P, Zhou X, Graham TR. 2009. Linking phospholipid flippases to vesicle-mediated protein transport. *Biochimica et biophysica acta* 1791: 612-619
- Nagano F, Sasaki T, Fukui K, Asakura T, Imazumi K, Takai Y. 1998. Molecular cloning and characterization of the noncatalytic subunit of the Rab3 subfamily-specific GTPase-activating protein. *The Journal of biological chemistry* 273: 24781-24785
- Nagle JF, Tristram-Nagle S. 2000. Structure of lipid bilayers. *Biochimica et Biophysica Acta (BBA)* 1469: 159-195
- Neuman KC, Block SM. 2004. Optical trapping. *The Review of scientific instruments* 75: 2787-2809
- Nielsen E, Christoforidis S, Uttenweiler-Joseph S, Miaczynska M, Dewitte F, Wilm M, Hoflack B, Zerial M. 2000. Rabenosyn-5, a novel Rab5 effector, is complexed with hVPS45 and recruited to endosomes through a FYVE finger domain. *The Journal of cell biology* 151: 601-612
- Nielsen E, Severin F, Backer JM, Hyman AA, Zerial M. 1999. Rab5 regulates motility of early endosomes on microtubules. *Nature Cell Biology* 1: 376-382
- Niko Y, Didier P, Mely Y, Konishi G, Klymchenko AS. 2016. Bright and photostable push-pull pyrene dye visualizes lipid order variation between plasma and intracellular membranes. *Scientific reports* 6: 18870
- Nizak C, Monier S, del Nery E, Moutel S, Goud B, Perez F. 2003. Recombinant antibodies to the small GTPase Rab6 as conformation sensors. *Science (New York, NY)* 300: 984-987
- Nomura F, Honda M, Takeda S, Inaba T, Takiguchi K, Itoh TJ, Ishijima A, Umeda T, Hotani H. 2002. Morphological and topological transformation of membrane vesicles. *Journal of biological physics* 28: 225-235
- Nottingham RM, Pfeffer SR. 2009. Defining the boundaries: Rab GEFs and GAPs. *Proceedings of the National Academy of Sciences of the United States of America* 106: 14185-14186
- Novick P, Medkova M, Dong G, Hutagalung A, Reinisch K, Grosshans B. 2006. Interactions between Rabs, tethers, SNAREs and their regulators in exocytosis. *Biochemical Society Transactions* 34: 683-686
- Oesterlin LK, Goody RS, Itzen A. 2012. Posttranslational modifications of Rab proteins cause effective displacement of GDP dissociation inhibitor. *Proceedings of the National Academy of Sciences, USA* 109: 5621-5626
- Oesterlin LK, Pylypenko O, Goud B. 2014. *Effectors of Rab GTPases: Rab binding specificity and their role in coordination of Rab function and localization*, Springer International Publishing.
- Ohvo-Rekila H, Ramstedt B, Leppimaki P, Slotte JP. 2002. Cholesterol interactions with phospholipids in membranes. *Progress in lipid research* 41: 66-97
- Ohya T, Miaczynska M, Coskun U, Lommer B, Runge A, Drechsel D, Kalaidzidis Y, Zerial M. 2009. Reconstitution of Rab- and SNARE-dependent membrane fusion by synthetic endosomes. *Nature* 459: 1091-1097

References

- Opdam FJ, Echard A, Croes HJ, van den Hurk JA, van de Vorstenbosch RA, Ginsel LA, Goud B, Fransen JA. 2000. The small GTPase Rab6B, a novel Rab6 subfamily member, is cell-type specifically expressed and localised to the Golgi apparatus. *Journal of Cell Science* 113 (Pt 15): 2725-2735
- Ortiz D, Medkova M, Walch-Solimena C, Novick P. 2002. Ypt32 recruits the Sec4p guanine nucleotide exchange factor, Sec2p, to secretory vesicles; evidence for a Rab cascade in yeast. *The Journal of cell biology* 157: 1005-1015
- Ostermeier C, Brunger AT. 1999. Structural basis of Rab effector specificity: crystal structure of the small G protein Rab3A complexed with the effector domain of rabphilin-3A. *Cell* 96: 363-374
- Owen DM, Magenau A, Williamson D, Gaus K. 2012. The lipid raft hypothesis revisited--new insights on raft composition and function from super-resolution fluorescence microscopy. *BioEssays : news and reviews in molecular, cellular and developmental biology* 34: 739-747
- Palade G. 1975. Intracellular aspects of the process of protein synthesis. *Science (New York, NY)* 189: 867
- Paulick MG, Bertozzi CR. 2008. The glycosylphosphatidylinositol anchor: a complex membrane-anchoring structure for proteins. *Biochemistry* 47: 6991-7000
- Pautot S, Frisken BJ, Weitz DA. 2003. Production of unilamellar vesicles using an inverted emulsion. *Langmuir* 19: 2870-2879
- Pechlivanis M, Kuhlmann J. 2006. Hydrophobic modifications of Ras proteins by isoprenoid groups and fatty acids--More than just membrane anchoring. *Biochimica et Biophysica Acta (BBA)* 1764: 1914-1931
- Pereira-Leal JB, Seabra MC. 2000. The mammalian Rab family of small GTPases: definition of family and subfamily sequence motifs suggests a mechanism for functional specificity in the Ras superfamily. *Journal of Molecular Biology* 301: 1077-1087
- Pereira-Leal JB, Seabra MC. 2001. Evolution of the Rab family of small GTP-binding proteins. *Journal of Molecular Biology* 313: 889-901
- Perez-Victoria FJ, Bonifacino JS. 2009. Dual roles of the mammalian GARP complex in tethering and SNARE complex assembly at the trans-golgi network. *Molecular and Cellular Biology* 29: 5251-5263
- Peter BJ, Kent HM, Mills IG, Vallis Y, Butler PJ, Evans PR, McMahon HT. 2004. BAR domains as sensors of membrane curvature: the amphiphysin BAR structure. *Science (New York, NY)* 303: 495-499
- Pfeffer SR. 2005. Structural clues to Rab GTPase functional diversity. *The Journal of biological chemistry* 280: 15485-15488
- Phillips MJ, Voeltz GK. 2016. Structure and function of ER membrane contact sites with other organelles. *Nature reviews Molecular cell biology* 17: 69-82
- Pike LJ. 2006. Rafts defined: a report on the Keystone Symposium on Lipid Rafts and Cell Function. In *J Lipid Res* Vol. 47, pp 1597-1598. United States

- Pinot M, Vanni S, Pagnotta S, Lacas-Gervais S, Payet LA, Ferreira T, Gautier R, Goud B, Antonny B, Barelli H. 2014. Lipid cell biology. Polyunsaturated phospholipids facilitate membrane deformation and fission by endocytic proteins. *Science (New York, NY)* 345: 693-697
- Plutner H, Cox AD, Pind S, Khosravi-Far R, Bourne JR, Schwaninger R, Der CJ, Balch WE. 1991. Rab1b regulates vesicular transport between the endoplasmic reticulum and successive Golgi compartments. *The Journal of cell biology* 115: 31-43
- Pomorski TG, Nylander T, Cardenas M. 2014. Model cell membranes: discerning lipid and protein contributions in shaping the cell. *Advances in colloid and interface science* 205: 207-220
- Pontani LL, van der Gucht J, Salbreux G, Heuvingh J, Joanny JF, Sykes C. 2009. Reconstitution of an actin cortex inside a liposome. *Biophysical Journal* 96: 192-198
- Pranke IM, Morello V, Bigay J, Gibson K, Verbavatz JM, Antonny B, Jackson CL. 2011. alpha-Synuclein and ALPS motifs are membrane curvature sensors whose contrasting chemistry mediates selective vesicle binding. *The Journal of cell biology* 194: 89-103
- Preuss D, Mulholland J, Franzusoff A, Segev N, Botstein D. 1992. Characterization of the *Saccharomyces* Golgi complex through the cell cycle by immunoelectron microscopy. *Molecular Biology of the Cell* 3: 789-803
- Prevost C, Zhao H, Manzi J, Lemichez E, Lappalainen P, Callan-Jones A, Bassereau P. 2015. IRSp53 senses negative membrane curvature and phase separates along membrane tubules. *Nature Communications* 6: 8529
- Prior IA, Harding A, Yan J, Sluimer J, Parton RG, Hancock JF. 2001. GTP-dependent segregation of H-ras from lipid rafts is required for biological activity. *Nature Cell Biology* 3: 368-375
- Pusapati GV, Luchetti G, Pfeffer SR. 2012. Ricl-Rgp1 complex is a guanine nucleotide exchange factor for the late Golgi Rab6A GTPase and an effector of the medial Golgi Rab33B GTPase. *The Journal of biological chemistry* 287: 42129-42137
- Pylypenko O, Rak A, Durek T, Kushnir S, Dursina BE, Thomae NH, Constantinescu AT, Brunsveld L, Watzke A, Waldmann H, Goody RS, Alexandrov K. 2006. Structure of doubly prenylated Ypt1:GDI complex and the mechanism of GDI-mediated Rab recycling. *The EMBO journal* 25: 13-23
- Raghupathy R, Anilkumar AA, Polley A, Singh PP, Yadav M, Johnson C, Suryawanshi S, Saikam V, Sawant SD, Panda A, Guo Z, Vishwakarma RA, Rao M, Mayor S. 2015. Transbilayer lipid interactions mediate nanoclustering of lipid-anchored proteins. *Cell* 161: 581-594
- Raiborg C, Wenzel EM, Pedersen NM, Olsvik H, Schink KO, Schultz SW, Vietri M, Nisi V, Bucci C, Brech A, Johansen T, Stenmark H. 2015. Repeated ER-endosome contacts promote endosome translocation and neurite outgrowth. *Nature* 520: 234-238
- Rawicz W, Olbrich KC, McIntosh T, Needham D, Evans E. 2000. Effect of chain length and unsaturation on elasticity of lipid bilayers. *Biophysical Journal* 79: 328-339
- Rawicz W, Smith BA, McIntosh TJ, Simon SA, Evans E. 2008. Elasticity, strength, and water permeability of bilayers that contain raft microdomain-forming lipids. *Biophysical Journal* 94: 4725-4736

References

- Rink J, Ghigo E, Kalaidzidis Y, Zerial M. 2005. Rab conversion as a mechanism of progression from early to late endosomes. *Cell* 122: 735-749
- Rivera-Molina FE, Novick PJ. 2009. A Rab GAP cascade defines the boundary between two Rab GTPases on the secretory pathway. *Proceedings of the National Academy of Sciences of the United States of America* 106: 14408-14413
- Rojas AM, Fuentes G, Rausell A, Valencia A. 2012. The Ras protein superfamily: evolutionary tree and role of conserved amino acids. *The Journal of cell biology* 196: 189-201
- Roland JT, Lapierre LA, Goldenring JR. 2009. Alternative splicing in class V myosins determines association with Rab10. *The Journal of biological chemistry* 284: 1213-1223
- Roth TF, Porter KR. 1964. Yolk Protein Uptake in the Oocyte of the Mosquito *Aedes Aegypti*. L. *The Journal of cell biology* 20: 313-332
- Roux A, Cappello G, Cartaud J, Prost J, Goud B, Bassereau P. 2002. A minimal system allowing tubulation with molecular motors pulling on giant liposomes. *Proceedings of the National Academy of Sciences of the United States of America* 99: 5394-5399
- Roux A, Cuvelier D, Nassoy P, Prost J, Bassereau P, Goud B. 2005. Role of curvature and phase transition in lipid sorting and fission of membrane tubules. *EMBO Journal* 24: 1537-1545
- Roux A, Koster G, Lenz M, Sorre B, Manneville JB, Nassoy P, Bassereau P. 2010. Membrane curvature controls dynamin polymerization. *Proceedings of the National Academy of Sciences of the United States of America* 107: 4141-4146
- Saarikangas J, Zhao H, Pykalainen A, Laurinmaki P, Mattila PK, Kinnunen PK, Butcher SJ, Lappalainen P. 2009. Molecular mechanisms of membrane deformation by I-BAR domain proteins. *Current biology : CB* 19: 95-107
- Sacher M, Barrowman J, Wang W, Horecka J, Zhang Y, Pypaert M, Ferro-Novick S. 2001. TRAPP I implicated in the specificity of tethering in ER-to-Golgi transport. *Molecular Cell* 7: 433-442
- Salminen A, Novick PJ. 1987. A ras-like protein is required for a post-Golgi event in yeast secretion. *Cell* 49: 527-538
- Saraste J, Lahtinen U, Goud B. 1995. Localization of the small GTP-binding protein rab1p to early compartments of the secretory pathway. *Journal of Cell Science* 108 (Pt 4): 1541-1552
- Sasaki T, Kikuchi A, Araki S, Hata Y, Isomura M, Kuroda S, Takai Y. 1990. Purification and characterization from bovine brain cytosol of a protein that inhibits the dissociation of GDP from and the subsequent binding of GTP to smg p25A, a ras p21-like GTP-binding protein. *The Journal of biological chemistry* 265: 2333-2337
- Satoh A, Wang Y, Malsam J, Beard MB, Warren G. 2003. Golgin-84 is a rab1 binding partner involved in Golgi structure. *Traffic (Copenhagen, Denmark)* 4: 153-161
- Satoh AK, O'Tousa JE, Ozaki K, Ready DF. 2005. Rab11 mediates post-Golgi trafficking of rhodopsin to the photosensitive apical membrane of *Drosophila* photoreceptors. *Development (Cambridge, England)* 132: 1487-1497

- Scherfeld D, Kahya N, Schwille P. 2003. Lipid dynamics and domain formation in model membranes composed of ternary mixtures of unsaturated and saturated phosphatidylcholines and cholesterol. *Biophysical Journal* 85: 3758-3768
- Schindelin J, Arganda-Carreras I, Frise E, Kaynig V, Longair M, Pietzsch T, Preibisch S, Rueden C, Saalfeld S, Schmid B, Tinevez JY, White DJ, Hartenstein V, Eliceiri K, Tomancak P, Cardona A. 2012. Fiji: an open-source platform for biological-image analysis. *Nature Methods* 9: 676-682
- Schmid SL, Sorkin A, Zerial M. 2014. Endocytosis: Past, present, and future. *Cold Spring Harbor Perspectives in Biology* 6: a022509
- Schoebel S, Cichy AL, Goody RS, Itzen A. 2011. Protein LidA from Legionella is a Rab GTPase supereffector. *Proceedings of the National Academy of Sciences, USA* 108: 17945-17950
- Schoebel S, Oesterlin LK, Blankenfeldt W, Goody RS, Itzen A. 2009. RabGDI displacement by DrrA from Legionella is a consequence of its guanine nucleotide exchange activity. *Molecular Cell* 36: 1060-1072
- Schroeder H, Leventis R, Rex S, Schelhaas M, Nagele E, Waldmann H, Silvius JR. 1997. S-Acylation and plasma membrane targeting of the farnesylated carboxyl-terminal peptide of N-ras in mammalian fibroblasts. *Biochemistry* 36: 13102-13109
- Seabra MC. 1996. Nucleotide dependence of Rab geranylgeranylation. Rab escort protein interacts preferentially with GDP-bound Rab. *The Journal of biological chemistry* 271: 14398-14404
- Seabra MC, Coudrier E. 2004. Rab GTPases and myosin motors in organelle motility. *Traffic (Copenhagen, Denmark)* 5: 393-399
- Seabra MC, Goldstein JL, Sudhof TC, Brown MS. 1992. Rab geranylgeranyl transferase. A multisubunit enzyme that prenylates GTP-binding proteins terminating in Cys-X-Cys or Cys-Cys. *The Journal of biological chemistry* 267: 14497-14503
- Seabra MC, Reiss Y, Casey PJ, Brown MS, Goldstein JL. 1991. Protein farnesyltransferase and geranylgeranyltransferase share a common alpha subunit. *Cell* 65: 429-434
- Segev N, Mulholland J, Botstein D. 1988. The yeast GTP-binding YPT1 protein and a mammalian counterpart are associated with the secretion machinery. *Cell* 52: 915-924
- Seu KJ, Cambrea LR, Everly RM, Hovis JS. 2006. Influence of lipid chemistry on membrane fluidity: tail and headgroup interactions. *Biophysical Journal* 91: 3727-3735
- Sezgin E, Sadowski T, Simons K. 2014. Measuring lipid packing of model and cellular membranes with environment sensitive probes. *Langmuir : the ACS journal of surfaces and colloids* 30: 8160-8166
- Sezgin E, Schwille P. 2012. Model membrane platforms to study protein-membrane interactions. *Molecular Membrane Biology* 29: 144-154
- Shahinian S, Silvius JR. 1995. Doubly-lipid-modified protein sequence motifs exhibit long-lived anchorage to lipid bilayer membranes. *Biochemistry* 34: 3813-3822
- Shan J, Yuan L, Budman DR, Xu HP. 2002. WTH3, a new member of the Rab6 gene family, and multidrug resistance. *Biochimica et biophysica acta* 1589: 112-123

References

- Shapiro AD, Pfeffer SR. 1995. Quantitative analysis of the interactions between prenyl Rab9, GDP dissociation inhibitor- α , and guanine nucleotides. *The Journal of biological chemistry* 270: 11085-11090
- Sheff DR, Daro EA, Hull M, Mellman I. 1999. The receptor recycling pathway contains two distinct populations of early endosomes with different sorting functions. *The Journal of cell biology* 145: 123-139
- Shibata Y, Hu J, Kozlov MM, Rapoport TA. 2009. Mechanisms shaping the membranes of cellular organelles. *Annual Review of Cell and Developmental Biology* 25: 329-354
- Shibata Y, Voss C, Rist JM, Hu J, Rapoport TA, Prinz WA, Voeltz GK. 2008. The reticulon and DPI/Yoplp proteins form immobile oligomers in the tubular endoplasmic reticulum. *The Journal of biological chemistry* 283: 18892-18904
- Shin HW, Hayashi M, Christoforidis S, Lacas-Gervais S, Hoepfner S, Wenk MR, Modregger J, Uttenweiler-Joseph S, Wilm M, Nystuen A, Frankel WN, Solimena M, De Camilli P, Zerial M. 2005. An enzymatic cascade of Rab5 effectors regulates phosphoinositide turnover in the endocytic pathway. *The Journal of cell biology* 170: 607-618
- Short B, Haas A, Barr FA. 2005. Golgins and GTPases, giving identity and structure to the Golgi apparatus. *Biochimica et biophysica acta* 1744: 383-395
- Short B, Preisinger C, Schaletzky J, Kopajtich R, Barr FA. 2002. The Rab6 GTPase regulates recruitment of the dynactin complex to Golgi membranes. *Current biology : CB* 12: 1792-1795
- Silvius JR, del Giudice D, Lafleur M. 1996. Cholesterol at different bilayer concentrations can promote or antagonize lateral segregation of phospholipids of differing acyl chain length. *Biochemistry* 35: 15198-15208
- Silvius JR, l'Heureux F. 1994. Fluorimetric evaluation of the affinities of isoprenylated peptides for lipid bilayers. *Biochemistry* 33: 3014-3022
- Simons K, Ikonen E. 1997. Functional rafts in cell membranes. *Nature* 387: 569-572
- Simonsen A, Gaullier JM, D'Arrigo A, Stenmark H. 1999. The Rab5 effector EEA1 interacts directly with syntaxin-6. *The Journal of biological chemistry* 274: 28857-28860
- Simonsen A, Lippe R, Christoforidis S, Gaullier JM, Brech A, Callaghan J, Toh BH, Murphy C, Zerial M, Stenmark H. 1998. EEA1 links PI(3)K function to Rab5 regulation of endosome fusion. *Nature* 394: 494-498
- Simpson JC, Wellenreuther R, Poustka A, Pepperkok R, Wiemann S. 2000. Systematic subcellular localization of novel proteins identified by large-scale cDNA sequencing. *EMBO reports* 1: 287-292
- Singer SJ, Nicolson GL. 1972. The fluid mosaic model of the structure of cell membranes. *Science (New York, NY)* 175: 720-731
- Siniossoglou S, Peak-Chew SY, Pelham HR. 2000. Ric1p and Rg1p form a complex that catalyses nucleotide exchange on Ypt6p. *The EMBO journal* 19: 4885-4894

- Sinka R, Gillingham AK, Kondylis V, Munro S. 2008. Golgi coiled-coil proteins contain multiple binding sites for Rab family G proteins. *The Journal of cell biology* 183: 607-615
- Sivars U, Aivazian D, Pfeffer SR. 2003. Yip3 catalyses the dissociation of endosomal Rab-GDI complexes. *Nature* 425: 856-859
- Slusarewicz P, Nilsson T, Hui N, Watson R, Warren G. 1994. Isolation of a matrix that binds medial Golgi enzymes. *The Journal of cell biology* 124: 405-413
- Smeland TE, Seabra MC, Goldstein JL, Brown MS. 1994. Geranylgeranylated Rab proteins terminating in Cys-Ala-Cys, but not Cys-Cys, are carboxyl-methylated by bovine brain membranes in vitro. *Proceedings of the National Academy of Sciences, USA* 91: 10712-10716
- Sonnichsen B, De Renzis S, Nielsen E, Rietdorf J, Zerial M. 2000. Distinct membrane domains on endosomes in the recycling pathway visualized by multicolor imaging of Rab4, Rab5, and Rab11. *Journal of Cell Biology* 149: 901-914
- Sorre B. 2010. Role of membrane curvature in intracellular trafficking. PhD Thesis, Université Paris 7 - Denis Diderot,
- Sorre B, Callan-Jones A, Manneville JB, Nassoy P, Joanny JF, Prost J, Goud B, Bassereau P. 2009. Curvature-driven lipid sorting needs proximity to a demixing point and is aided by proteins. *Proceedings of the National Academy of Sciences of the United States of America* 106: 5622-5626
- Sorre B, Callan-Jones A, Manzi J, Goud B, Prost J, Bassereau P, Roux A. 2012. Nature of curvature coupling of amphiphysin with membranes depends on its bound density. *Proceedings of the National Academy of Sciences, USA* 109: 173-178
- Sprong H, van der Sluijs P, van Meer G. 2001. How proteins move lipids and lipids move proteins. *Nature reviews Molecular cell biology* 2: 504-513
- Stachowiak JC, Schmid EM, Ryan CJ, Ann HS, Sasaki DY, Sherman MB, Geissler PL, Fletcher DA, Hayden CC. 2012. Membrane bending by protein-protein crowding. *Nature Cell Biology* 14: 944-949
- Stenmark H. 2009. Rab GTPases as coordinators of vesicle traffic. *Nature Reviews: Molecular Cell Biology* 10: 513-525
- Suda Y, Kurokawa K, Hirata R, Nakano A. 2013. Rab GAP cascade regulates dynamics of Ypt6 in the Golgi traffic. *Proceedings of the National Academy of Sciences of the United States of America* 110: 18976-18981
- Suvorova ES, Duden R, Lupashin VV. 2002. The Sec34/Sec35p complex, a Ypt1p effector required for retrograde intra-Golgi trafficking, interacts with Golgi SNAREs and COPI vesicle coat proteins. *The Journal of cell biology* 157: 631-643
- Szmodis AW, Blanchette CD, Longo ML, Orme CA, Parikh AN. 2010. Thermally induced phase separation in supported bilayers of glycosphingolipid and phospholipid mixtures. *Biointerphases* 5: 120-130
- Sztul E, Lupashin V. 2006. Role of tethering factors in secretory membrane traffic. *American journal of physiology Cell physiology* 290: C11-26

References

- Tafesse FG, Huitema K, Hermansson M, van der Poel S, van den Dikkenberg J, Uphoff A, Somerharju P, Holthuis JC. 2007. Both sphingomyelin synthases SMS1 and SMS2 are required for sphingomyelin homeostasis and growth in human HeLa cells. *The Journal of biological chemistry* 282: 17537-17547
- Takahashi S, Kubo K, Waguri S, Yabashi A, Shin HW, Katoh Y, Nakayama K. 2012. Rab11 regulates exocytosis of recycling vesicles at the plasma membrane. *Journal of Cell Science* 125: 4049-4057
- Takamori S *et al.* 2006. Molecular anatomy of a trafficking organelle. *Cell* 127: 831-846
- Tamura N, Mima J. 2014. Membrane-anchored human Rab GTPases directly mediate membrane tethering in vitro. *Biology open* 3: 1108-1115
- Tanigawa G, Orci L, Amherdt M, Ravazzola M, Helms JB, Rothman JE. 1993. Hydrolysis of bound GTP by ARF protein triggers uncoating of Golgi-derived COP-coated vesicles. *The Journal of cell biology* 123: 1365-1371
- Thapa N, Sun Y, Schramp M, Choi S, Ling K, Anderson RA. 2012. Phosphoinositide signaling regulates the exocyst complex and polarized integrin trafficking in directionally migrating cells. *Developmental Cell* 22: 116-130
- Thoma NH, Iakovenko A, Goody RS, Alexandrov K. 2001a. Phosphoisoprenoids modulate association of Rab geranylgeranyltransferase with REP-1. *The Journal of biological chemistry* 276: 48637-48643
- Thoma NH, Iakovenko A, Kalinin A, Waldmann H, Goody RS, Alexandrov K. 2001b. Allosteric regulation of substrate binding and product release in geranylgeranyltransferase type II. *Biochemistry* 40: 268-274
- Tierney KJ, Block DE, Longo ML. 2005. Elasticity and phase behavior of DPPC membrane modulated by cholesterol, ergosterol, and ethanol. *Biophysical Journal* 89: 2481-2493
- Tisdale EJ, Bourne JR, Khosravi-Far R, Der CJ, Balch WE. 1992. GTP-binding mutants of rab1 and rab2 are potent inhibitors of vesicular transport from the endoplasmic reticulum to the Golgi complex. *The Journal of cell biology* 119: 749-761
- Touchot N, Chardin P, Tavitian A. 1987. Four additional members of the ras gene superfamily isolated by an oligonucleotide strategy: molecular cloning of YPT-related cDNAs from a rat brain library. *Proceedings of the National Academy of Sciences of the United States of America* 84: 8210-8214
- Trahey M, Hay JC. 2010. Transport vesicle uncoating: it's later than you think. *F1000 biology reports* 2: 47
- Trajkovic K, Hsu C, Chiantia S, Rajendran L, Wenzel D, Wieland F, Schwille P, Brugger B, Simons M. 2008. Ceramide triggers budding of exosome vesicles into multivesicular endosomes. *Science (New York, NY)* 319: 1244-1247
- Trischler M, Stoorvogel W, Ullrich O. 1999. Biochemical analysis of distinct Rab5- and Rab11-positive endosomes along the transferrin pathway. *Journal of Cell Science* 112 (Pt 24): 4773-4783
- Ullrich O, Reinsch S, Urbe S, Zerial M, Parton RG. 1996. Rab11 regulates recycling through the pericentriolar recycling endosome. *The Journal of cell biology* 135: 913-924

- Urbe S, Huber LA, Zerial M, Tooze SA, Parton RG. 1993. Rab11, a small GTPase associated with both constitutive and regulated secretory pathways in PC12 cells. *FEBS Letters* 334: 175-182
- Valente C, Polishchuk R, De Matteis MA. 2010. Rab6 and myosin II at the cutting edge of membrane fission. In *Nature cell biology* Vol. 12, pp 635-638. England
- Vallis Y, Wigge P, Marks B, Evans PR, McMahon HT. 1999. Importance of the pleckstrin homology domain of dynamin in clathrin-mediated endocytosis. *Current biology : CB* 9: 257-260
- Vamparys L, Gautier R, Vanni S, Bennett WF, Tieleman DP, Antonny B, Etchebest C, Fuchs PF. 2013. Conical lipids in flat bilayers induce packing defects similar to that induced by positive curvature. *Biophysical Journal* 104: 585-593
- van der Sluijs P, Hull M, Huber LA, Male P, Goud B, Mellman I. 1992a. Reversible phosphorylation--dephosphorylation determines the localization of rab4 during the cell cycle. *The EMBO journal* 11: 4379-4389
- van der Sluijs P, Hull M, Webster P, Male P, Goud B, Mellman I. 1992b. The small GTP-binding protein rab4 controls an early sorting event on the endocytic pathway. *Cell* 70: 729-740
- Van Der Sluijs P, Hull M, Zahraoui A, Tavitian A, Goud B, Mellman I. 1991. The small GTP-binding protein rab4 is associated with early endosomes. *Proceedings of the National Academy of Sciences of the United States of America* 88: 6313-6317
- van Meer G, Lisman Q. 2002. Sphingolipid transport: rafts and translocators. *The Journal of biological chemistry* 277: 25855-25858
- van Meer G, Vaz WL. 2005. Membrane curvature sorts lipids. Stabilized lipid rafts in membrane transport. *EMBO reports* 6: 418-419
- van Meer G, Voelker DR, Feigenson GW. 2008. Membrane lipids: where they are and how they behave. *Nature Reviews: Molecular Cell Biology* 9: 112-124
- Vanni S, Vamparys L, Gautier R, Drin G, Etchebest C, Fuchs PF, Antonny B. 2013. Amphipathic lipid packing sensor motifs: probing bilayer defects with hydrophobic residues. *Biophysical Journal* 104: 575-584
- Veatch SL, Keller SL. 2003. Separation of liquid phases in giant vesicles of ternary mixtures of phospholipids and cholesterol. *Biophysical Journal* 85: 3074-3083
- Veatch SL, Keller SL. 2005. Seeing spots: complex phase behavior in simple membranes. *Biochimica et biophysica acta* 1746: 172-185
- Verkleij AJ, Zwaal RF, Roelofsen B, Comfurius P, Kastelijn D, van Deenen LL. 1973. The asymmetric distribution of phospholipids in the human red cell membrane. A combined study using phospholipases and freeze-etch electron microscopy. *Biochimica et biophysica acta* 323: 178-193
- Vetter IR, Wittinghofer A. 2001. The guanine nucleotide-binding switch in three dimensions. *Science (New York, NY)* 294: 1299-1304
- Voeltz GK, Prinz WA. 2007. Sheets, ribbons and tubules - how organelles get their shape. *Nature Reviews: Molecular Cell Biology* 8: 258-264

References

- Voeltz GK, Prinz WA, Shibata Y, Rist JM, Rapoport TA. 2006. A class of membrane proteins shaping the tubular endoplasmic reticulum. *Cell* 124: 573-586
- Votteler J, Sundquist WI. 2013. Virus budding and the ESCRT pathway. *Cell host & microbe* 14: 232-241
- Wagner ML, Tamm LK. 2000. Tethered polymer-supported planar lipid bilayers for reconstitution of integral membrane proteins: silane-polyethyleneglycol-lipid as a cushion and covalent linker. *Biophysical Journal* 79: 1400-1414
- Walde P, Cosentino K, Engel H, Stano P. 2010. Giant vesicles: preparations and applications. *ChemBioChem* 11: 848-865
- Walden M, Jenkins HT, Edwards TA. 2011. Structure of the *Drosophila melanogaster* Rab6 GTPase at 1.4 Å resolution. *Acta crystallographica Section F, Structural biology and crystallization communications* 67: 744-748
- Walser PJ, Ariotti N, Howes M, Ferguson C, Webb R, Schwudke D, Leneva N, Cho KJ, Cooper L, Rae J, Floetenmeyer M, Oorschot VM, Skoglund U, Simons K, Hancock JF, Parton RG. 2012. Constitutive formation of caveolae in a bacterium. *Cell* 150: 752-763
- Wang W, Sacher M, Ferro-Novick S. 2000. TRAPP stimulates guanine nucleotide exchange on Ypt1p. *The Journal of cell biology* 151: 289-296
- Waugh R, Evans EA. 1979. Thermoelasticity of red blood cell membrane. *Biophysical Journal* 26: 115-131
- Weinberger A, Tsai FC, Koenderink GH, Schmidt TF, Itri R, Meier W, Schmatko T, Schroder A, Marques C. 2013. Gel-assisted formation of giant unilamellar vesicles. *Biophysical Journal* 105: 154-164
- Wesolowska O, Michalak K, Maniewska J, Hendrich AB. 2009. Giant unilamellar vesicles - a perfect tool to visualize phase separation and lipid rafts in model systems. *Acta Biochimica Polonica* 56: 33-39
- White J, Johannes L, Mallard F, Girod A, Grill S, Reinsch S, Keller P, Tzschaschel B, Echard A, Goud B, Stelzer EH. 1999. Rab6 coordinates a novel Golgi to ER retrograde transport pathway in live cells. *The Journal of cell biology* 147: 743-760
- Wilson AL, Erdman RA, Castellano F, Maltese WA. 1998. Prenylation of Rab8 GTPase by type I and type II geranylgeranyl transferases. *Biochemical Journal* 333 (Pt 3): 497-504
- Wollert T, Hurley JH. 2010. Molecular mechanism of multivesicular body biogenesis by ESCRT complexes. *Nature* 464: 864-869
- Wollert T, Patel A, Lee YL, Provance DW, Jr., Vought VE, Cosgrove MS, Mercer JA, Langford GM. 2011. Myosin5a tail associates directly with Rab3A-containing compartments in neurons. *The Journal of biological chemistry* 286: 14352-14361
- Wood WG, Igbavboa U, Muller WE, Eckert GP. 2011. Cholesterol asymmetry in synaptic plasma membranes. *Journal of Neurochemistry* 116: 684-689

- Wu M, Wang T, Loh E, Hong W, Song H. 2005. Structural basis for recruitment of RILP by small GTPase Rab7. *The EMBO journal* 24: 1491-1501
- Wu YW, Oesterlin LK, Tan KT, Waldmann H, Alexandrov K, Goody RS. 2010. Membrane targeting mechanism of Rab GTPases elucidated by semisynthetic protein probes. *Nature Chemical Biology* 6: 534-540
- Wu YW, Tan KT, Waldmann H, Goody RS, Alexandrov K. 2007. Interaction analysis of prenylated Rab GTPase with Rab escort protein and GDP dissociation inhibitor explains the need for both regulators. *Proceedings of the National Academy of Sciences of the United States of America* 104: 12294-12299
- Yoshihisa T, Barlowe C, Schekman R. 1993. Requirement for a GTPase-activating protein in vesicle budding from the endoplasmic reticulum. *Science (New York, NY)* 259: 1466-1468
- Young J, Menetrey J, Goud B. 2010. RAB6C is a retrogene that encodes a centrosomal protein involved in cell cycle progression. *Journal of Molecular Biology* 397: 69-88
- Young J, Stauber T, del Nery E, Vernos I, Pepperkok R, Nilsson T. 2005. Regulation of microtubule-dependent recycling at the trans-Golgi network by Rab6A and Rab6A'. *Molecular Biology of the Cell* 16: 162-177
- Zahraoui A, Touchot N, Chardin P, Tavitian A. 1989. The human Rab genes encode a family of GTP-binding proteins related to yeast YPT1 and SEC4 products involved in secretion. *The Journal of biological chemistry* 264: 12394-12401
- Zerial M, McBride H. 2001. Rab proteins as membrane organizers. *Nature reviews Molecular cell biology* 2: 107-117
- Zhang FL, Casey PJ. 1996. Protein prenylation: molecular mechanisms and functional consequences. *Annual Review of Biochemistry* 65: 241-269
- Zhao X, Lasell TK, Melancon P. 2002. Localization of large ADP-ribosylation factor-guanine nucleotide exchange factors to different Golgi compartments: evidence for distinct functions in protein traffic. *Molecular Biology of the Cell* 13: 119-133
- Zhen Y, Stenmark H. 2015. Cellular functions of Rab GTPases at a glance. *Journal of Cell Science* 128: 3171-3176
- Zimmerberg J, Kozlov MM. 2006. How proteins produce cellular membrane curvature. *Nature Reviews: Molecular Cell Biology* 7: 9-19
- Zoppino FC, Militello RD, Slavin I, Alvarez C, Colombo MI. 2010. Autophagosome formation depends on the small GTPase Rab1 and functional ER exit sites. *Traffic (Copenhagen, Denmark)* 11: 1246-1261

Abstract

RAB GTPases are major regulators of vesicular trafficking and localize to specific compartments. Deciphering the molecular mechanisms governing RAB localization is thus critical to understand intracellular transport processes. We have managed, for the first time, to incorporate purified and prenylated RABs into artificial membranes. By doing so, we observed that RAB6, but not RAB1 or RAB5, is able to promote by itself vesicle tethering. We believe that RAB6 is able to interact in *trans* with itself and to consequently drive homotypic membrane tethering. In the main part of this study, we investigated the physicochemical membrane requirements necessary for RAB recruitment. RAB1, RAB5 and RAB6 were all found to only localize to disordered membrane domains and to preferentially bind to curved membranes. We demonstrated that this specific recruitment of RAB1, RAB5 and RAB6 is primarily dependent on the hydrophobic insertion of their prenyl group into lipid packing defects. In contrast, RAB35 recruitment was primarily dependent on the presence of negatively charged lipids and was found to be modulated, to a lesser extent, by lipid packing defects. Although RAB4 and RAB11 were effectively recruited to purified Golgi fractions, in an effector-independent manner, membrane charges and lipid packing defects were not sufficient to promote their recruitment to synthetic vesicles; suggesting that RAB4 and RAB11 require more demanding membrane physicochemical properties. Our work demonstrates that the properties of membranes are critical for the regulation of RAB specific membrane targeting.

Résumé

Les RAB GTPases sont des régulateurs majeurs du trafic vésiculaire et sont localisées sur des compartiments spécifiques. L'identification des processus moléculaires régulant la localisation des RAB est donc cruciale afin de comprendre les mécanismes de transport intracellulaire. Nous sommes parvenus, pour la première fois, à incorporer des protéines RAB purifiées et prénylées dans des membranes artificielles. Nous avons tout d'abord observé que RAB6 est capable de promouvoir une agrégation de vésicules, phénomène qui n'est pas observé avec RAB1 et RAB5. Nous suggérons un modèle dans lequel RAB6 interagit en *trans* avec lui-même et par conséquent induit un accolement de membranes. La partie principale de cette étude consistait à identifier les propriétés physicochimiques des membranes requises pour le recrutement des protéines RAB. Nous avons observé que RAB1, RAB5 et RAB6 se lient préférentiellement à des membranes désordonnées et courbées, phénomène qui s'explique par l'insertion du groupement prenyl hydrophobe au niveau de défauts d'agencement de lipides. En revanche, le recrutement de RAB35 requiert la présence de lipides chargés négativement et peut être modulé, dans une moindre mesure, par les défauts d'agencement lipidique. Bien que RAB4 et RAB11 soient recrutées sur des fractions de Golgi purifiées, les charges membranaires et les défauts d'agencement lipidique ne sont pas suffisants pour permettre leur recrutement sur des vésicules synthétiques. Cela suggère que le recrutement de RAB4 et RAB11 nécessite des propriétés membranaires plus complexes. Nos travaux démontrent que les propriétés membranaires sont cruciales pour la localisation spécifique des protéines RAB.